

**Transition Metal Catalysts for Hydrogen Storage and Carbon
Dioxide Activation**

A Dissertation

Presented to the Faculty of the Graduate School

of

Yale University

In Candidacy for the Degree of

Doctor of Philosophy

by

Elizabeth Anne Bielinski

Dissertation Director: Nilay Hazari

May 2015

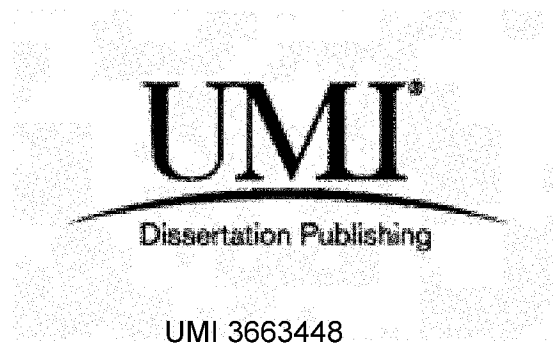
UMI Number: 3663448

All rights reserved

INFORMATION TO ALL USERS

The quality of this reproduction is dependent upon the quality of the copy submitted.

In the unlikely event that the author did not send a complete manuscript and there are missing pages, these will be noted. Also, if material had to be removed, a note will indicate the deletion.

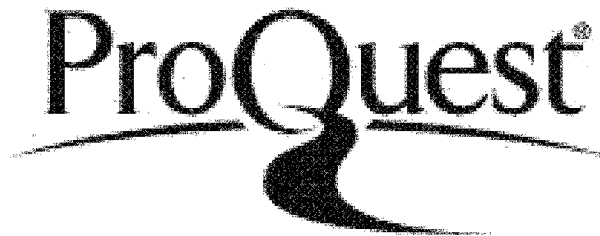


UMI 3663448

Published by ProQuest LLC 2015. Copyright in the Dissertation held by the Author.

Microform Edition © ProQuest LLC.

All rights reserved. This work is protected against unauthorized copying under Title 17, United States Code.



ProQuest LLC
789 East Eisenhower Parkway
P.O. Box 1346
Ann Arbor, MI 48106-1346

Abstract

Transition Metal Catalysts for Hydrogen Storage and Carbon Dioxide Activation

Elizabeth A. Bielinski

2015

This dissertation describes the synthesis of a series of transition metal compounds and their reactivity with hydrogen and carbon dioxide for application in reversible hydrogen storage in organic molecules. Chapter 1 is a review of hydrogen storage molecules and discusses each from the perspectives of safety, availability, and environmental impact. Heterogeneous and homogeneous catalysts for dehydrogenation of these molecules are also discussed here. In Chapter 2, a family of PNP pincer-supported iron compounds is investigated by Mössbauer spectroscopy and magnetic circular dichroism with the goal of elucidating the degree of solution-state flexibility of the PNP pincer ligand. Chapter 3 expands on this family of PNP pincer-supported iron compounds with the synthesis of several new compounds through reaction with hydrogen and carbon dioxide. Furthermore, these compounds are shown to be highly active catalysts for formic acid dehydrogenation in the presence of a Lewis acid co-catalyst. The action of the Lewis acid co-catalyst is further demonstrated in Chapter 4, where PNP pincer-supported iron compounds are used as catalysts for aqueous-phase methanol dehydrogenation. Chapter 5 describes the synthesis, characterization and reactivity of a family of palladium and nickel compounds supported by allyl, cyclopentadienyl, and indenyl ligands. These compounds are shown to react with simple electrophiles, although they do not show the desired reactivity with carbon dioxide.

© 2015 by Elizabeth Bielinski

All rights reserved.

Acknowledgements

First, I must thank my advisor Professor Nilay Hazari, for his support and insight over the last five years. I also thank him for allowing me the opportunity to explore my interests outside of lab, and for supporting my passion for teaching and outreach. Additionally, the members of my committee Professors Robert Crabtree, Patrick Holland, and Gary Brudvig have been tirelessly supportive, and offered excellent suggestions every time I hit a roadblock. Finally, I must thank Professor Wesley Bernskoetter, who has become like a second advisor to me. His humor, positive outlook, and seemingly encyclopedic knowledge of the negative aspects of New Jersey have kept me laughing and motivated. I am also greatly indebted to him and all his students for welcoming me into their lab on numerous occasions as I performed experiments and finished up measurements for projects.

I have had the great fortune to spend my five years at Yale with a fantastic group of friends and coworkers. The members of the Hazari lab have become my second family, and I am grateful to each and every one for their friendship. Joy Farnaby trained me in lab, taught me to be patient and careful, and was always willing to answer questions, no matter how silly. I had the pleasure of sharing an office with Damian Hruszkewycz, and learned from his detail-oriented and rigorous manner in the lab. I also thank him for teaching me Ukrainian history, for expanding my musical horizons, and making me laugh almost daily. Louise Guard and Hee Won Suh have been my partners in crime and I thank them for sticking by me even when I thought grad school was going to be too hard. I'm especially grateful to Louise for her patience, tireless optimism and willingness to proofread every document I've ever written. I was fortunate to work with outstanding undergraduate students, Matthew Ambler, Cassie Pan and Jocelyn Legere. They taught me more about teaching and mentoring than they realize, and I thank them for their hard work and friendship.

Graduate school is a hard journey, one that I would not have survived if not for the love and support of my friends and family. My New Haven contingent, Shane, Naomi, Kinnon, and Danielle always knew when to give hugs, wine and a night out. They made New Haven my home, and I am so grateful to have them in my life. My trifecta of strong women, the sisters I never had: Meredith, Tessa, and Candice are the three best friends I could ever ask for. Each came into my life during a particularly formative time, and they have stuck around to forge the most wonderful family imaginable. Mark, my better half, partner in life and

in science, has shown me that no matter where life takes you, its always better to do it with your best buddy at your side; life is just better when I'm with you. It is nearly impossible to express my love and gratitude to my mother. When people tell me I look like you, sound like you, act like you, it is the greatest compliment in the world. There is no one I'd rather aspire to be.

Finally, I dedicate this work to the memory my grandfather, William R. Stalker. He was my greatest inspiration and my hero from the day I was born, and I hope this work lives up to his great legacy.

Table of Contents

List of Figures, Schemes and Tables	vii
Chapter 1: Hydrogen Storage and the Search for an Alternative Energy Vector	1
I. Thesis Prospectus	1
II. Introduction	1
III. Hydrogen as an energy vector	2
IV. Conclusions	17
V. References	18
Chapter 2: Synthesis and Spectroscopic Investigation of PNP-Supported Fe Compounds	24
I. Introduction	24
II. Results and Discussion	25
III. Conclusions	34
IV. Experimental Details	35
V. Acknowledgments	38
VI. References	38
Chapter 3: Lewis Acid-Assisted Formic Acid Dehydrogenation Using a Pincer-Supported Iron Compound	42
I. Introduction	42
II. Results and Discussion	43
III. Conclusions	52
IV. Experimental Details	53
V. Acknowledgements	62
VI. References	63
Chapter 4: Base-Free Methanol Dehydrogenation Using a Pincer-Supported Iron Compound and Lewis Acid Co-Catalyst	67
I. Introduction	67
II. Results and Discussion	69
III. Conclusions	88
IV. Experimental Details	89
V. Acknowledgements	100
VI. References	100
Chapter 5: Synthesis, Characterization, and Reactivity of NHC-Supported Ni and Pd Compounds Bearing Combinations of Allyl, Cyclopentadienyl, and Indenyl Ligands	104
I. Introduction	104
II. Results and Discussion	106
III. Conclusions	124
IV. Experimental Details	125
V. Acknowledgements	133
VI. References	133

List of Figures and Tables

Figure 1.01	Combustion of H ₂ in a proton-exchange membrane (PEM) fuel cell	3
Figure 1.02	Effect of doping on dehydrogenation temperature of complex metal hydrides	5
Figure 1.03	Stepwise dehydrogenation of ammonia borane (AB) and related cyclic borane compounds	6
Scheme 1.01	Dehydrogenation of Bis-BN cyclohexane catalyzed by Ru(Cl) ₂ (NH ₂ CH ₂ CH ₂ P(^t Bu) ₂) ₂ .	7
Scheme 1.02	Reversible (de)hydrogenation of 2-methylquinoline catalyzed by Cp*Ir catalyst	10
Scheme 1.03	Hydrogenation of 2-methylquinoline catalyzed by an NHC-Ir catalyst	11
Scheme 1.04	Representative examples of Fe-catalyzed (de)hydrogenation of N-heterocycles	11
Table 1.01	Selected homogeneous transition metal catalysts for FA dehydrogenation	14
Table 1.02	Homogeneous transition metal catalysts for aqueous-phase MeOH dehydrogenation to CO ₂ and H ₂	17
Figure 2.01	Synthesis of ^R PN ^H P-Supported Fe Compounds	25
Figure 2.02	ORTEP of 1a ^{spy} and 1a ^{tbp}	27
Figure 2.03	ORTEP of 1c and structural overlay of 1a ^{spy} with 1c	28
Figure 2.04	80K ⁵⁷ Fe Mössbauer data of 1a , 1b , and 1c	29
Figure 2.05	5K, 7T NIR MCD Spectra of (^R PN ^H P)FeCl ₂ compounds	30
Figure 2.06	Ligand field energies in idealized 5C, high spin, S = 2 Fe(II) compounds in either square pyramidal or trigonal bipyramidal geometries	31
Figure 2.07	5K, variable-field NIR MCD spectra of a frozen glass sample of 1a	33
Figure 2.08	5K, 7T NIR MCD peak fit analysis of frozen solution glass samples of 1a and 1c	34
Scheme 3.01	Synthesis and reactivity of 5-coordinate Fe amido species	44
Figure 3.01	ORTEP of 1a and 1b	44
Table 3.01	FA dehydrogenation using 1a , 1b , 2a , and 2b	45
Scheme 3.02	Proposed mechanism of FA dehydrogenation	46
Scheme 3.03	Effect of additives on decarboxylation of 2 under H ₂ and N ₂	47
Table 3.02	Base Screening for FA dehydrogenation catalyzed by 2a and 2b	47
Scheme 3.04	DFT calculated pathway for the decarboxylation of 2a	48
Table 3.03	LA screening for FA dehydrogenation using 2a/2b	49
Table 3.04	Effect of LA loading on FA dehydrogenation catalyzed by 2a	50
Table 3.05	Quantitative poisoning of FA dehydrogenation catalyzed by 2a	50
Table 3.06	Optimization of catalytic dehydrogenation of FA using 2a	51
Scheme 3.05	Proposed mechanism of β-hydride elimination in the absence and presence of LA	51
Table 3.07	Application of LA assistance in FA dehydrogenation using Beller's system	52
Figure 3.02	Variable temperature ¹ H NMR spectra of the hydride region of the reaction between 1a and H ₂ (1 atm)	58
Figure 3.03	¹ H NOESY/EXSY NMR spectrum (400 MHz) of 3a/3a' (τ = 1s)	58
Figure 3.04	¹ H NMR spectrum of (^{Cy} PN ^H P)Fe(CO)H ₂ (3b)	60
Figure 3.05	³¹ P{ ¹ H} NMR spectrum of (^{Cy} PN ^H P)Fe(CO)H ₂ (3b)	60
Scheme 4.01	Reaction of C with base to generate 1a	68
Scheme 4.02	Summary of previous reaction reactions catalyzed by 1a , 1b , 2a , and 2b	69
Scheme 4.03	Proposed stepwise pathway for aqueous-phase MeOH dehydrogenation to CO ₂ and H ₂	70
Table 4.01	Solvent screen for MeOH dehydrogenation catalyzed by 1b	71
Table 4.02	Dilution study of MeOH dehydrogenation catalyzed by 1b	71
Figure 4.01	ORTEP of (^{Cy} PN ^H P)Fe(CO) ₂	72
Table 4.03	Catalyst optimization for MeOH dehydrogenation	72
Figure 4.02	Effect of Lewis acid on MeOH dehydrogenation in the absence of water catalyzed by 1b	73
Scheme 4.04	Stoichiometric reactions of 1b with methanol and/or water	75
Scheme 4.05	Proposed stepwise pathway for MeOH dehydrogenation in the absence of water	75

Scheme 4.06	Proposed pathway for stoichiometric reaction of one equivalent of MeOH and water with 1b	76
Table 4.04	LA screening for aqueous phase MeOH dehydrogenation using 1b	77
Table 4.05	Screening of LAs with low catalyst loading for MeOH dehydrogenation in the presence of water	78
Table 4.06	Effect of amount of LA on MeOH dehydrogenation in the presence of water	78
Table 4.07	Effect of MeOH:H ₂ O ratio on MeOH dehydrogenation in the presence of water using 1b	79
Table 4.08	Screening of catalysts for MeOH dehydrogenation in the presence of water	80
Scheme 4.07	Possible pathway for MeOH dehydrogenation via 1,2-addition and β -hydride elimination	82
Scheme 4.08	Calculated lowest free energy pathway for MeOH dehydrogenation (A)	82
Scheme 4.09	Comparison of computed pathways for loss of H ₂ from A4	83
Figure 4.03	Impact of applied pressure on the reaction free energy for the conversion of A4 to A1 and one equivalent of H ₂ at two temperatures	84
Scheme 4.10	Calculated pathways for conversion of formaldehyde and water into methanediol (B)	85
Scheme 4.11	Calculated lowest free energy pathway for methanediol dehydrogenation (C)	86
Scheme 4.12	Formic acid dehydrogenation: Lowest free energy pathways in the absence and presence of LA (D)	88
Figure 4.04	Burette set up used to collect H ₂ for catalytic MeOH dehydrogenation	92
Figure 4.05	¹ H NMR spectra at different temperatures from the reaction of 1b with 1 eq MeOH at -80°C	93
Figure 4.06	³¹ P{ ¹ H} NMR spectra at different temperatures from the reaction of 1b with 1 eq MeOH at -80°C	94
Figure 4.07	² H NMR spectra at different temperatures from the reaction of 1b with 1 eq CD ₃ OD at -75°C	95
Figure 4.08	³¹ P{ ¹ H} NMR spectrum of crude mixture from the reaction of 1b with 1 eq MeOH after heating at 50°C for 40 min	96
Figure 4.09	¹ H NMR spectrum of organic products vacuum transferred from the reaction of 1b with 1 eq MeOH	96
Figure 4.10	¹ H NMR spectrum from the reaction of 1 eq MeOH and 1 eq H ₂ O with 1b	97
Figure 4.11	³¹ P{ ¹ H} NMR spectrum from the reaction of 1 eq MeOH and 1 eq H ₂ O with 1b	98
Figure 5.01	Depictions of the two most common binding modes of allyl ligands	104
Scheme 5.01	Reaction of compounds of the type (η^1 -2-methylallyl)(η^3 -2-methylallyl)M(L) with CO ₂ .	105
Figure 5.02	Ni and Pd complexes with combinations of allyl, Cp, and indenyl ligands	106
Scheme 5.02	Synthesis of ^{CpAll} Pd and ^{CpAll} Ni	107
Figure 5.03	ORTEP of ^{CpAll} Pd and ^{CpAll} Ni	109
Scheme 5.03	Synthesis of ^{CpCp} Ni and ^{CpCp} Pd	112
Figure 5.04	ORTEP of ^{CpCp} Ni and ^{CpCp} Pd	114
Scheme 5.04	Synthesis of ^{IndCl} Pd and ^{IndAll} Pd	115
Figure 5.05	Numbering scheme of indenyl ligand	115
Figure 5.06	ORTEP of ^{IndCl} Pd	116
Figure 5.07	ORTEP of ^{IndAll} Pd	118
Scheme 5.05	Attempted synthesis of ^{IndCl} Ni and ^{IndAll} Ni	119
Scheme 5.06	Synthesis of ^{IndCp} Pd and ^{IndCp} Ni	119
Scheme 5.07	Synthesis of ^{IndInd} Pd	120
Figure 5.08	ORTEP of ^{IndInd} Pd	121
Table 5.01	Summary of reactivity of species prepared in this work with acid (2,6-lutidinium chloride)	122
Table 5.02	Summary of reactivity of species prepared in this work with triphenylcarbenium chloride.	123

Chapter 1: Hydrogen Storage and the Search for an Alternative Energy Vector

I. Thesis Prospectus

This thesis is an investigation into iron (Fe) catalyzed dehydrogenation of the liquid organic molecules formic acid and methanol, primarily for their use as hydrogen storage molecules. This chapter describes the growing need for an energy vector to replace fossil fuels, gives an overview of current technologies for using hydrogen as an energy vector, and describes several hydrogen storage molecules of interest. Chapter 2 describes the synthesis of a series of pincer-supported Fe compounds and the investigation of pincer flexibility in solution using magnetic circular dichroism (MCD) and Mössbauer spectroscopy. Chapter 3 focuses on the use of several pincer-supported Fe compounds as highly active catalysts for formic acid (FA) dehydrogenation and highlights the discovery of Lewis acids as co-catalysts for this reaction. The utility of the Lewis acid co-catalysts is extended to Fe-catalyzed methanol (MeOH) dehydrogenation in Chapter 4. Chapter 5 describes the synthesis of a family of palladium (Pd) and nickel (Ni) compounds supported by combinations of allyl, cyclopentadienyl (Cp) and indenyl (Ind) ligands and investigates their reactivity with simple electrophiles.

II. Introduction

Beginning in the year 1769, when James Watt patented a highly efficient steam engine, global demand for fossil fuels has grown steadily, with the world demand for coal increasing 800-fold between 1769 and 2006.¹ In 2013 the worldwide energy consumption reached 16 terawatts (TW), much of which was obtained from fossil fuels (oil, coal and natural gas).² Furthermore, this demand is projected to increase to 27.6 TW by 2050 and 43 TW by 2100.³ Coincident with the increased burning of fossil fuels is the emission of carbon dioxide (CO₂), a known greenhouse gas; atmospheric levels of CO₂ are now in excess of 380 ppm, a significant increase from 210-300 ppm where they had remained for the past 420,000 years.⁴ This increase in atmospheric levels of CO₂ (as well as other greenhouse gases produced from fossil fuel burning) has contributed to a temperature increase of 0.8°C since 1880, increasing the melting rate of Arctic ice, killing coral reefs and disrupting a host of other ecosystems.⁵ In addition to the environmental impact

of burning fossil fuels, there are a variety of geopolitical and economic arguments against their continued use. While the natural reserves of fossil fuels are not set to be expended in the near future (current estimates allow for 50-150 years of oil reserves and 1,000-2,000 years of coal, shale and tar sands reserves)^{3a} it is certainly true that the majority of these reserves are concentrated in a portion of the world with significant political unrest. Furthermore, even if foreign relations with countries controlling the vast supply of fossil fuels remain cordial, this does nothing to ensure the price of such fuels will be appropriate for usage at our current rate and economic state.^{1,3,6}

Creating an energy economy based on non-fossil fuels requires that the new energy vector (method of storage and transport) be cheap, abundant, environmentally benign, and free from geopolitical entanglement. Much research has focused on the use of solar power via solar cells^{3a,7} and other renewable energy sources like nuclear power,⁸ water,⁹ wind,¹⁰ and geothermal energy.^{8b,11} While these energy vectors fulfill several requirements, such as environmental safety and abundance, the greatest barrier to implementation, aside from cost, is the need to store and transport energy. Many renewable energy sources, particularly solar and wind, are not only intermittent, but also lack a vehicle for storage and transport, decreasing their utility for long-range applications. It has long been suggested that storing energy in chemical bonds, particularly in the bonds of molecular hydrogen (H_2), would create a vector by which energy can be stored, transported and selectively released for use.^{3b,6,12} This chapter will focus on the implementation of a hydrogen economy, focusing on the barriers associated with this energy vector, as well as recent advances in hydrogen storage molecules and catalysts for their selective dehydrogenation.

III. Hydrogen as an energy vector

The potential of H_2 to act as a clean fuel lies in the fact that its combustion with oxygen produces only water as a byproduct. In this combustion, H_2 releases three times greater chemical energy per unit mass than any other chemical fuel (142 MJ/kg for H_2 compared to 47 MJ/kg for liquid hydrocarbons).^{3b,13} When burned with only oxygen, the subsequent mixture will contain nothing but water vapor; however, when burned in air the mixtures can contain various nitrogen and oxygen compounds of the general formula NO_x .¹³ More importantly, H_2 can be used as a source of protons and electrons in proton-exchange membrane (PEM) fuel cells¹⁴ (Figure 1.01). PEM fuel cells can generate electrical energy with efficiencies

upwards of 50%, far surpassing the limits set on traditional internal combustion engines by the Carnot cycle.^{6,13}

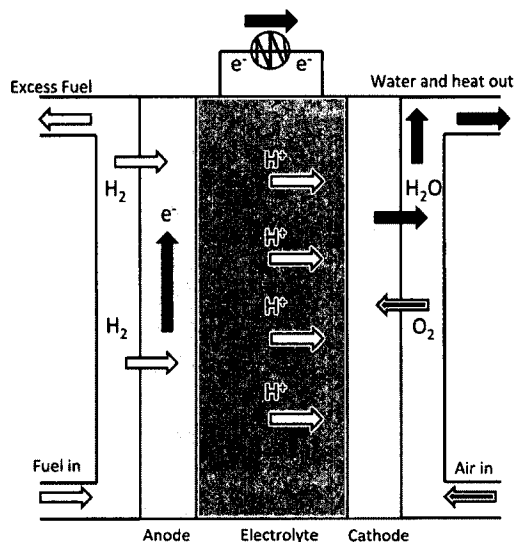


Figure 1.01. Combustion of H₂ in a proton-exchange membrane (PEM) fuel cell.

While hydrogen is one of the most abundant elements on Earth, less than 1% occurs in its molecular form as H₂ gas;¹⁵ most hydrogen is tied up in the chemical bonds of water, hydrocarbons, and biomass.¹³ The lack of abundant molecular H₂ is a significant barrier to its use as an energy vector. Although it is possible to produce H₂ by using sunlight to split water in a photovoltaic cell,^{7a} the vast majority (48 million metric tons per annum) of H₂ is still produced from steam reforming (SMR) of fossil fuels (Eq 1) or through the water gas shift (WGS) reaction (Eq 2).¹⁵ Despite being a complicated, non-renewable, multi-step catalytic process, SMR is the most popular industrial method for H₂ production and will remain so as long as the cost of natural gas is low to moderate. A more detailed analysis of renewable H₂ production can be found in the review by Fierro et al.¹⁵ This thesis will deal exclusively with the problems of H₂ storage and release.



In addition to the need for a renewable method of H₂ production, the potential H₂ economy encounters a large barrier in terms of storage, transport, and selective release. For example, fueling a car simply on the energy generated from electrochemical combustion of H₂ in a PEM fuel cell would require 4kg of H₂, which would occupy a volume of 45m³ at room temperature and atmospheric pressure.^{13,16} It is possible to

carry the same amount of H₂ in a compressed form, but this would require outfitting cars with specialized carbon fiber-reinforced tanks capable of holding pressures of up to 700 bar (10,000 psi). Furthermore, significant energy is lost during the compression process and any analysis of the use of cryogenic H₂ must weigh the potential H₂ lost to boil-off against the inherent safety concerns associated with carrying such a volume of a highly-flammable gas.¹⁶ H₂ has very high diffusivity and burns with an invisible flame, which increases the risks associated with leaks in a storage system.¹³

To avoid the complications associated with transporting large quantities of H₂ gas, it has been proposed to reversibly store H₂ absorbed onto solids or in the chemical bonds of another molecule. Absorption-based storage of H₂ involves the use of single-walled nanotubes¹⁷ (SWNTs) or metal-organic frameworks (MOFs).¹⁸ These methods have shown great promise, but the overall utility suffers due to lack of complete and easy reversibility, as well as overall quantity of H₂ stored.¹³ Storage in chemical bonds encompasses a variety of metal hydrides and salts, ammonia borane, hydrazine, N-heterocycles, and liquid organics such as formic acid and methanol. Given the appropriate catalyst, these hydrogen storage molecules (HSM) can be decomposed to release hydrogen suitable for combustion in a PEM fuel cell, or direct use in other applications. It is also important to address the production of byproducts of dehydrogenation, their environmental impact, and their potential for use in regeneration of the H₂ storage molecule. Each of these approaches, along with the barriers to application and further considerations, is discussed below.

a) Hydrogen storage in metal hydrides

H₂ storage in metal hydrides of compounds such as LaNi₅, Mg₂Ni and MgH₂ has been studied extensively.¹⁹ However, these compounds incorporate elements of high molecular weight, and as such, the percent H₂ by weight is low and far beneath the standards set by the Department of Energy (DOE).^{13,16} Another important metric is the “operating pressure/temperature (P/T) window”, the conditions at which the metal hydride favorably releases H₂. The range that would be appropriate for energy applications (for example, use in cars) lies between 1-10 atm and 25-120°C.¹⁶ Metal hydrides of LaNi₅, Mg₂Ni and MgH₂ have P/T operating windows far outside this range (>300°C), making them unlikely candidates for favorable, reversible H₂ storage.

More recently, Group I and II salts of $[\text{AlH}_4]^-$, $[\text{NH}_2]^-$, and $[\text{BH}_4]^-$ (“complex hydrides”) have received attention for H_2 storage (Figure 1.02a).^{16,19c} These compounds also have unfavorable kinetic barriers to reversible (de)hydrogenation, but work by Bogdanovic and Schwickardi²⁰ showing that NaAlH_4 doped with Ti underwent solid state dehydrogenation at 150°C has renewed interest in metal hydrides as HSM. Similar effects have been seen using zirconium and vanadium chlorides as dopants, which have also reduced the time required for hydrogenation by a factor of 2. However, these materials suffer from poor stability over the course of repeated dehydrogenation/hydrogenation cycling.^{19c} Doping effects have also been studied on LiNH_2 , which undergoes dehydrogenation as shown in Figure 1.02b. In the absence of Mg doping, LiNH_2 undergoes dehydrogenation beginning at 277°C . As the concentration of Mg is increased, the dehydrogenation temperature lowers to 100°C ,^{19c} well within an appropriate P/T operating window. Finally, alkali metal and alkaline-earth metal borohydrides contain the highest percent H_2 by mass. LiBH_4 releases H_2 upon melting at 280°C .^{19c} However, there is limited research on their behavior as H_2 storage molecules due to their inherent instability.

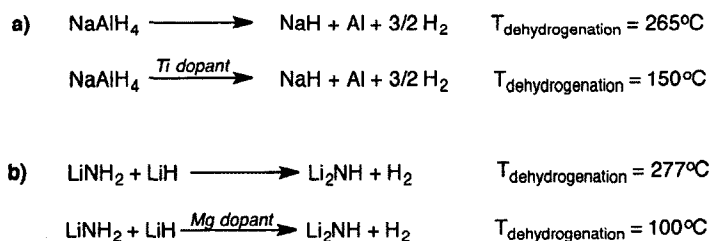


Figure 1.02. Effect of doping on dehydrogenation temperature of complex metal hydrides.

Additional concerns surrounding metal hydrides focus on safety and implementation. Metal hydrides, in particular $[\text{AlH}_4]^-$, are highly water sensitive and storage vessels must be developed to exclude water. Furthermore, regeneration of metal hydrides will most certainly require “off-board” recharging⁶ and in the recharging process itself, metal hydrides suffer from incomplete rehydrogenation.^{6,19c}

b) Ammonia Borane

A particularly exciting molecule, ammonia borane (AB) boasts 19.6% by weight H_2 (Figure 1.03).^{16,21} There are a variety of homogeneous, transition metal catalysts,²² as well as acid catalysts,²³ that are capable of dehydrogenating AB at temperatures and pressures relevant for use in every day application. AB dehydrogenation is proposed to proceed through a 3-step process, each releasing one equivalent of H_2

(Figure 1.03a).^{21b} In the first step, AB is dehydrogenated to release 1 equivalent of H₂ and an N-B byproduct of the general formula (H₂N-BH₂)_x, of which cyclotriborazane (Figure 1.03b) is an example. The second step releases another equivalent of H₂ and byproducts such as borazine (HN-BH)_x. Finally, the remaining equivalent of H₂ is released to give boron nitride. This complete dehydrogenation releases 3 equivalents of H₂. However, there is currently no broadly applicable method by which AB can be regenerated from boron nitride.²⁴ There is one DFT-directed study suggesting that it might be possible to regenerate AB from polyborazylene, a polymer of borazine formed under extended heating.²⁵ While this would allow for cycling of hydrogen storage and release, it is only possible to regenerate AB from polyborazylene, not boron nitride. As such, the total weight percent H₂ released drops to 13.06%, or two-thirds of the initial theoretical yield. Ramachandran and co-workers have reported Ru-catalyzed solvolysis of AB to yield [NH₄][B(OMe)₄], which can be treated with NH₄Cl and LiAlH₄ to regenerate AB.²⁶ However, there has been no report of recycling Al(OMe)₄ back to LiAlH₄, a necessary step to create a catalytic cycle.

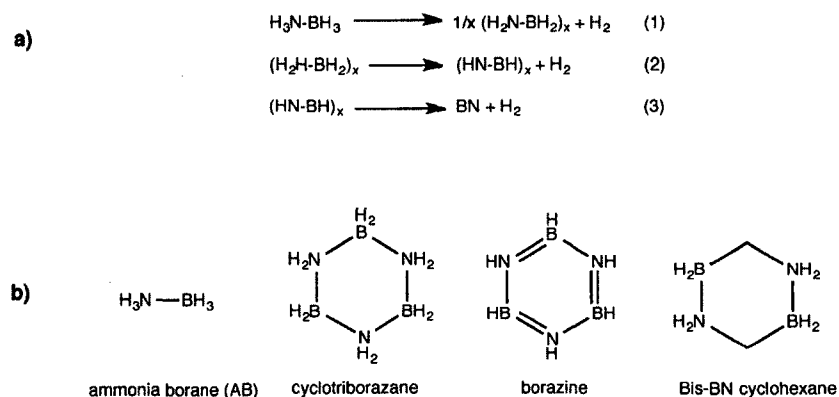
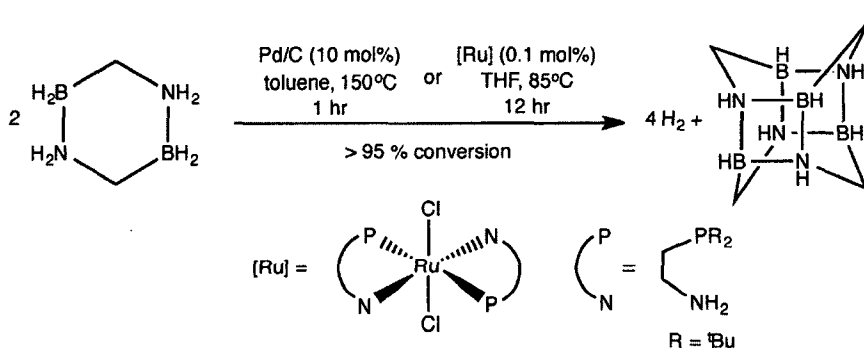


Figure 1.03. a) Stepwise dehydrogenation of ammonia borane (AB) b) AB and related cyclic borane compounds.

Other boron hydride systems have also been investigated, most recently Bis-BN cyclohexane (Figure 1.03b).²⁷ Unlike AB and its derivatives, Bis-BN cyclohexane is kinetically stable in both solution and the solid state at 150°C, which is attractive if H₂ storage is needed for long periods of time under more extreme conditions. Both heterogeneous and homogeneous catalysts are capable of dehydrogenating Bis-BN cyclohexane to release its 4.8% hydrogen. Pd/C mediates the dehydrogenation at 120°C to give 75% conversion, but higher temperatures (150°C) were required to achieve conversion >95%. Even more

impressive, when subjected to 5 mol% $\text{Ru}(\text{Cl})_2(\text{NH}_2\text{CH}_2\text{CH}_2\text{PR}_2)_2$ ($\text{R} = \text{}^t\text{Bu}$), Bis-BN cyclohexane undergoes dehydrogenation at room temperature in 15 min, yielding >95% conversion of Bis-BN cyclohexane. At more elevated temperatures, 65°C , only 0.5 mol% catalyst was required to give the same conversion (Scheme 1.01). While these results are certainly promising, Bis-BN cyclohexane suffers from similar problems to AB. The synthesis of Bis-BN requires 5 steps, including reduction with LiAlH_4 , and two steps involving significant amounts of strong acids. Furthermore, in addition to H_2 , dehydrogenation of Bis-BN cyclohexane produces boron, carbon, nitrogen-containing cage structures (Scheme 1.01). These were found to be highly crystalline, but no methods for regeneration Bis-BN cyclohexane are currently known.



Scheme 1.01. Dehydrogenation of Bis-BN cyclohexane catalyzed by $\text{Ru}(\text{Cl})_2(\text{NH}_2\text{CH}_2\text{CH}_2\text{P}(\text{}^t\text{Bu}_2))_2$.

c) Hydrazine

Anhydrous hydrazine is a colorless, oily liquid at room temperature and has H_2 content of 12.5% by weight.²⁸ It has been widely used as a propellant in rocket propulsion and in automobile air bags, as a blowing agent in polymer synthesis, and as a starting material for many pesticide syntheses.²⁹ In its anhydrous form, hydrazine undergoes decomposition by one of two processes; incomplete decomposition (Eq 3) releases 4 equivalents of NH_3 and no H_2 gas, while complete decomposition (Eq 4) releases 2 equivalents of H_2 along with N_2 .²⁸⁻²⁹



Selectivity for complete over incomplete dehydrogenation is of importance if hydrazine is to be used for H₂ storage. While it is possible to further dehydrogenate NH₃ to H₂, this requires temperatures >400°C, a significant and unnecessary increase from 30-80°C where a variety of reported catalysts effect complete decomposition to produce high yields of H₂.^{28,30} Despite its high H₂ content and production of only N₂ as a byproduct of decomposition, hydrazine is extremely toxic and explodes on contact with metal surfaces, although supported metal surfaces (such as supported nanoparticles) do not show this behavior.²⁹ Hydrazine is toxic to bacteria, algae and marine wildlife.²⁹ Additionally, it is not permissible to dispose of hydrazine in wastewater, and any water contaminated with hydrazine must be collected and treated with NaClO or H₂O₂, as well as assessed for possible NH₃ contamination as a result of incomplete decomposition.²⁹ Because of its toxicity and explosive nature, anhydrous hydrazine has received less attention than hydrous hydrazine as a possible H₂ storage molecule. Nonetheless, SiO₂-supported Ni, Pd, and Pt catalysts have shown activity for H₂ production (with 90% selectivity for H₂) at 50°C.³¹ Increasing the temperature results in a decrease in selectivity, until H₂ is once again the favored product at temperatures >400°C. As was described above, this suggests competition between Eq (3) and Eq (4) and highlights the power of temperature control over selectivity.

With safety in mind, research has focused more on the use of hydrous hydrazine (H₂NNH₂•H₂O), which does not exhibit the same explosive qualities as its anhydrous counterpart. Nanoparticles (NPs) of Fe, Co; Ni, Cu, Ru, Rh, Ir, Pt and Pd have been investigated for activity toward dehydrogenation of hydrous hydrazine.³² Of these, Rh-based NPs were found to be the most active and selective (44% selectivity) for dehydrogenation at 25°C. This selectivity could be improved to give 100% at 25°C by the addition of Ni at a Rh:Ni ratio of 4:1.³³ While these selectivities and conditions are impressive and appropriate for application in fuel cells, the use of expensive and rare noble metals, especially Rh, is not ideal. Qiang and co-workers extended their work with Rh NPs to first row transition metals and reported the use of Ni-Fe NPs at 70°C to give 81% selectivity for H₂ release.³⁴ This selectivity could be increased 100% by the addition of NaOH. It was suggested that NaOH acted to basify the catalyst surface, thus decreasing the favorability for the formation of basic NH₃. Ni-Fe NPs in other ratios (Ni₃Fe and NiFe₃) showed lower selectivities for H₂ production, 89% and 71% respectively, and were not affected by the addition of base.

However, base addition did increase selectivity of Ni₄₅Pt₅₅ (61% to 86%) and Ni₅₀Ir₅₀ (7% to 95%) NPs, indicating it may be a more universal promoter than previously thought.³⁴

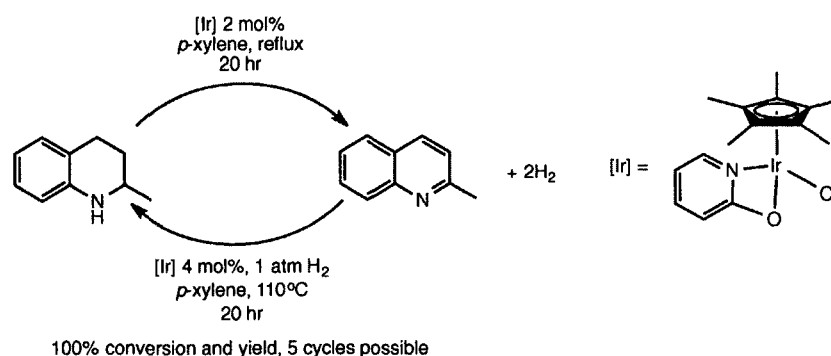
Although these NP systems show high selectivity at low temperature, they all require the use of surfactants such as hexadecyltrimethylammonium bromide (CTAB) to allow for high dispersion and an increased surface area. Surfactants can often decrease the overall catalytic performance of NPs as they compete with NPs for open sites on the supporting surface, make preparation of NPs difficult, and often require inert atmospheres for processing.³⁵ In 2015, Jiang and co-workers reported the one-step, 10-minute, surfactant-free synthesis of Ni_{0.6}Fe_{0.4}Mo NPs. These NPs exhibit excellent catalytic activity and show 100% selectivity for H₂ production from hydrous hydrazine at 50°C.³⁵ Furthermore, these particles could be recycled through at least 3 iterations of hydrazine dehydrogenation with no loss in activity or selectivity. Combining the knowledge of how to safely work with hydrous hydrazine with simplified syntheses of surfactant-free, non-noble metal NPs opens doors for future work on hydrazine dehydrogenation. However, it still remains to be seen if hydrazine generation from N₂ and H₂ is possible, as this would be necessary to create a renewable cycle for H₂ storage.²⁸

d) N-Heterocycles

N-heterocycles represent a promising HSM due to their increased safety and stability as compared to metal hydrides and AB, as well as ease of transport and distribution using existing infrastructure.⁶ Additionally, liquid fuels would not require the engineering of sophisticated high-pressure, low-temperature fuel tanks, as would be required for use of gaseous H₂.¹⁶ Furthermore, their direct dehydrogenation would produce only organic byproducts that could feasibly be regenerated in an off-board recharging station.⁶ However, N-heterocycles do not contain a high percent H₂ by weight (typically 6-8% compared to AB 19.6%). In addition, only the hydrogen released from the N-heterocycle is combusted to generate energy, whereas in gasoline, the hydrogen and carbon are both combusted. This translates to an N-heterocycle fuel producing only 17% of the energy content of a comparable gasoline fuel.⁶ However, maintaining the carbon framework means no CO₂ is produced as a result of combustion; this is certainly positive given the detrimental environmental effects of CO₂. Finally, the retained carbon framework presents the opportunity for direct regeneration of the fuel, creating a closed, carbon-neutral cycle.

For some time, it had been assumed that reversible (de)hydrogenation of organic compounds was not possible, due to unfavorable energetics, both thermodynamic and kinetic.⁶ The few examples reported required temperatures in excess 375°C to release H₂ from cyclohexane. However, it is possible to define a temperature, T_d, at which ΔG = 0. At T_d, the entropy created by release of H₂ offsets the unfavorable enthalpy. Furthermore, when using N-heterocycles rather than all-carbon systems, T_d can be lowered significantly.^{6,36} Crabtree and co-workers reported computational results showing the ring size, number and placement of nitrogens in the N-heterocycle can drastically change the energetics of dehydrogenation.³⁶ Specifically, five-membered rings with nitrogen in the 1 and 3 positions show the most significant thermodynamic driving force for dehydrogenation.

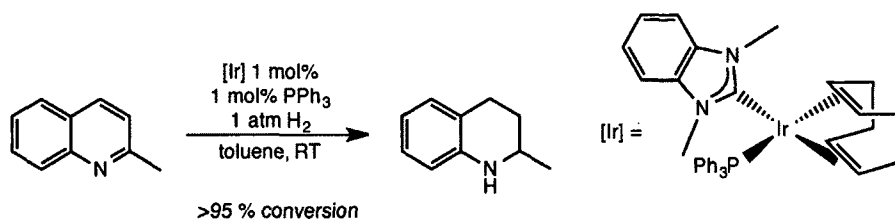
Using this information, many groups have designed homogeneous catalysts for the (de)hydrogenation of N-heterocycles.³⁷ In order for N-heterocycles to act as HSM, reversibility under moderate conditions is required. In 2009, Fujita and co-workers reported the first homogeneous system for reversible (de)hydrogenation of N-heterocycles using a Cp*Ir catalyst (Scheme 1.02).^{37c} Using 2 mol% catalyst in refluxing *p*-xylene, they were able to obtain 100% conversion and 100% yield of a variety of quinoline derivatives. Furthermore, the reverse reaction could be carried out with 4 mol% catalyst under 1 atm H₂ at 110°C, again in 100% conversion and yield. To fully demonstrate the utility of this system, Fujita and co-workers were able to perform 5 consecutive dehydrogenation/hydrogenation cycles with only 2% loss in yield by the fifth cycle.



Scheme 1.02. Reversible (de)hydrogenation of 2-methylquinoline catalyzed by Cp*Ir catalyst.

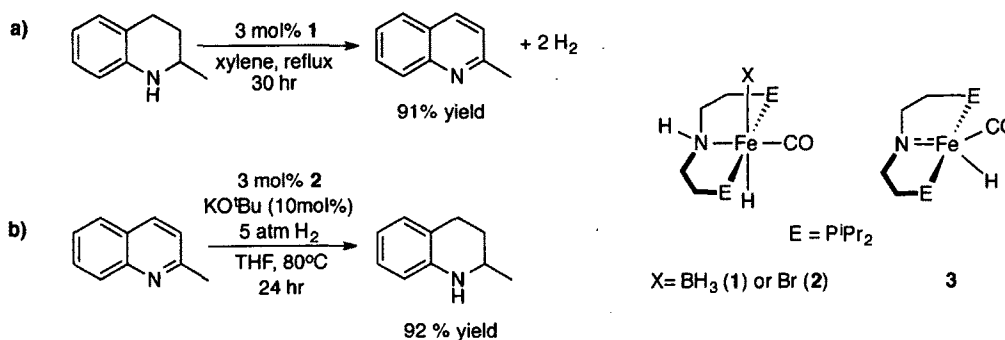
Following this excellent discovery, Crabtree and co-workers reported an Ir catalyst capable of hydrogenating a wide variety of quinoline derivatives, with high yields and selectivity, at room temperature

and only 1 atm H₂ (Scheme 1.03).^{37a} While this system did not explore reversibility, it demonstrates the remarkable activity of homogeneous catalysts and set the groundwork for future work toward applicable reversible H₂ storage in N-heterocycles.



Scheme 1.03. Hydrogenation of 2-methylquinoline catalyzed by an NHC-Ir catalyst.

More recently, Jones and co-workers reported the first Fe-based catalyst for reversible N-heterocycle (de)hydrogenation.^{37b} At catalyst loadings of 3 mol%, 100% conversion was seen for catalytic dehydrogenation of 1,2,3,4-tetrahydroquinoline. Isolated yields in excess of 60% were seen for a variety of N-heterocycles, including methylindoline and piperidine derivatives, of which a representative example is shown in Scheme 1.04a. The reversibility of this reaction was demonstrated by subjecting the related unsaturated N-heterocycles to 3 mol% catalyst and low pressures of H₂ (representative example shown in Scheme 1.04b). The addition of base was required when using catalyst **2** and the mechanism of action was determined to be the formation of the active species, **3**. Catalyst **1** was able to undergo thermal loss of BH₄ to generate this active species *in-situ* in the absence of base. Furthermore, isolated samples of **3** were found to give comparable catalytic activity. The reactivity of these and related Fe compounds will be further discussed in relation to dehydrogenation of FA (Chapter 3) and MeOH (Chapter 4).

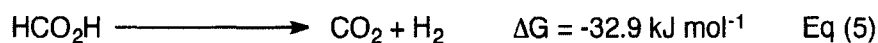


Scheme 1.04. Representative examples of Fe-catalyzed (de)hydrogenation of N-heterocycles.

e) **Liquid organics: formic acid and methanol**

i. **Formic Acid**

Formic acid (FA) was first proposed as an HSM in 1978 by Bloom and co-workers.³⁸ In particular, they noted that FA was easily formed from the electrocatalytic reduction of CO₂,³⁹ and thus offered a convenient way to utilize CO₂ in the search for alternative energy vectors.³⁸ Since this original report, there have been many subsequent reports of CO₂ reduction to FA, using both electrocatalytic, heterogeneous⁴⁰ as well as thermal, homogeneous⁴¹ transition metal catalysts. Furthermore, it has recently been shown that FA can be generated renewably from biomass.⁴² The dehydrogenation of FA is thermodynamically favored, and releases one equivalent of H₂ of sufficient purity for direct use in PEM fuel cells⁴³ (Eq 5).



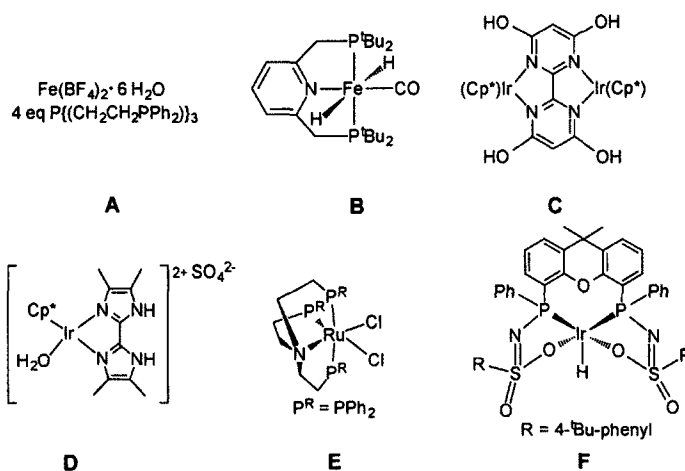
The DOE has set criteria such that by the year 2015, any potential HSM must contain 9% by weight H₂.⁶ FA is 4.8% by weight H₂ and falls below this, arguably ambitious, standard. Furthermore, FA is a corrosive acid, which, in concentrated amounts, can cause significant burns to skin and mucous membranes of humans and animals.⁴⁴ It is dangerous if ingested in large amounts (*vide infra*), although arguably no more toxic than ingesting large quantities of gasoline.⁴⁴ FA is approved by the Food and Drug Administration (FDA) to be used as a food additive and many FA derivatives are used as sweeteners and artificial flavors. Additionally, many biological processes are capable of clearing FA from the body and the half-life of FA in human blood plasma is a mere 45 min.⁴⁴ Overall, FA is considered to be generally non-toxic, stable, and easily transportable using current infrastructure. In addition, its dehydrogenation is favorable at moderate temperatures and ambient pressure, a feature that is not true of other H₂ storage molecules such as metal hydrides and AB.^{19c,21a,43}

Heterogeneous catalysts for FA dehydrogenation have been known since 1930, although most of these systems were not designed with hydrogen storage in mind, and required high temperatures to release significant amounts of H₂.⁴⁵ Additionally, this lack of optimization led to high yields of CO formation, a known poisoning agent of PEM fuel cells.⁴³ More recent work has focused on the use of Al₂O₃-supported Au nanoparticles. These particles have shown good selectivity for FA dehydrogenation and produce very

little CO at temperatures around 80°C, comparable to homogenous systems (*vide infra*).⁴⁶ The use of noble metals such as Ir, Pd, Pt, Ru and Rh on activated carbon surfaces highlights some of the shortcomings of heterogeneous FA dehydrogenation.⁴⁷ Under similar conditions to those used on Au nanoparticles, these metals give moderate selectivities for FA dehydrogenation. However, they also produce a significant amount of CO. The addition of water and increased temperatures (>220°C) improved selectivity and decreased CO production. However, the addition of water makes these materials unsuitable for use in fuel cells and the elevated temperatures make their application impractical.⁴³ Heterogeneous catalysts are of great interest in systems where the separation of the catalyst from the product mixture is important for high yields and purity. Selective release of H₂ for use in transportation certainly falls into this category, but the need for elevated temperatures and the poor selectivity of many heterogeneous catalysts has hindered their application in these systems.

The earliest work on FA dehydrogenation using homogenous catalysts focused on noble metals, in particular ruthenium (Ru) and iridium (Ir). In 1967 Coffey described the activity of IrH₂Cl(PPh₃)₃ which gave a turnover frequency (TOF) of 1187 hr⁻¹ and turnover numbers (TON) of up to 10,000.⁴⁸ However, this reaction required temperatures of greater than 100°C and the addition of excess phosphine ligand to achieve such rapid turnover and extended catalyst life. It was not until 1998 that another homogenous system of similar activity was reported. Puddephatt and co-workers reported the use of a Ru dimer, [Ru₂(μ-CO)(CO)₄(μ-dppm)₂] (dppm = diphenylphosphinomethane), for FA decomposition which gave a TON of 500 after 20 minutes.⁴⁹ Following these initial discoveries, a variety of Ru and Ir catalysts showing high activity (TON often >350,000) were reported by Fujita⁵⁰ (Table 1.01 C), Himeda⁵¹ (Table 1.01 D), Beller⁵² (Table 1.01 E), and Reek⁵³ (Table 1.01 F).

Table 1.01. Selected homogeneous transition metal catalysts for FA dehydrogenation.



Catalyst	TOF (h ⁻¹) ^a	TON	Yield (%)	Reaction Conditions	Reference
A	5,390	92,417	1	4 eq ligand	80°C, PC ^e Beller ⁵⁴
B	Not given	100,000	100	50 mol% NEt ₃	40°C, dioxane Milstein ⁵⁵
C	228,000 ^b	308,000 ^c	-	1:1 HCO ₂ H:NaCO ₂ H	90°C Fujita ^{50b}
D	34,000 ^b	10,000	100	Aqueous HCO ₂ H	80°C Himeda ⁵¹
E	902	10,000	100	11:10 HCO ₂ H:OctNMe ₂	80°C Beller ^{52b}
F	3,092 ^d	10,000	10	Toluene	85°C Reek ⁵³

^aMeasured after the first hour, ^bMeasured after the first 10 min, ^cPerformed at 80°C, ^dMeasured after 12-35% conversion achieved. ^ePC = propylene carbonate

There are only two examples of first row transition metal catalysts for FA dehydrogenation, both utilizing Fe. In 2011, Beller and co-workers reported the first Fe-based catalyst for FA dehydrogenation using Fe(BF₄)₂·6H₂O and 4 equivalents of the ligand PP₃ (tris[(2-diphenylphosphino)ethyl]phosphine) to achieve a TON of 92,000 (Table 1.01 A).⁵⁴ Three years later, Milstein and co-workers reported a pincer-supported Fe catalyst that, with the addition of 50 mol% NEt₃, achieved TON of 100,000 (Table 1.01 B).⁵⁵ While these catalysts show high activity at moderate temperatures (40-80°C), overall reaction times are very long (on the order of days) and TOF and TON do not come close to those achieved with noble metal catalysts.

A common problem with many of these systems remains the need for added base, often in large excess, or complicated ligands that often contained a pendant base.^{50b,53} In systems requiring base,^{52b,55-56} amine bases such as triethylamine (NEt₃) and di-methyl-octylamine (OctNMe₂) are most common. It has long been known that NEt₃ forms 3:1 adducts with FA to give “activated FA”.⁵⁷ These NEt₃:FA adducts are highly reactive reducing agents and are often used in organic chemistry as an *in-situ* source of hydrogen.⁵⁷⁻

⁵⁸ Whether this is the action of the added base in FA dehydrogenation is still unknown, although research presented in Chapter 3 delves further into this topic.

If FA is to be a useful H₂ storage molecule, highly active catalysts for dehydrogenation must be made from cheap, abundant, non-toxic metals. Furthermore, they must be used in combination with simple, easily synthesized or commercially available supporting ligands, preferably in the absence of expensive and potentially dangerous additives.

ii. Methanol

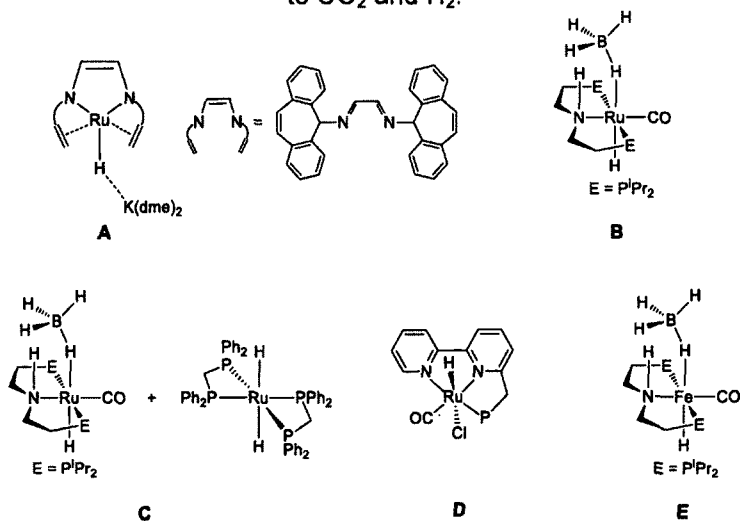
Methanol is one of the most important industrial chemicals in the world, with worldwide consumption reaching nearly 50 million metric tons in 2011.⁵⁹ Nearly 85% of this methanol is converted to other industrial products such as formaldehyde, methyl tert-butyl ether (MTBE), and acetic acid.⁵⁹ Since the 1920s, methanol has been used as a fuel in the highly specialized Otto engines of racing cars and airplanes.⁶⁰ However, despite the decrease in emissions of NO_x, hydrocarbons and CO, Otto engines produce a significant amount of formaldehyde.⁵⁹ As such, direct use of methanol as a fuel is no more environmentally or health conscious than the use of fossil fuels.

The use of methanol as an HSM is attractive for reasons beyond its 12.3% by weight H₂ content. Methanol is non-corrosive and readily biodegraded by the enzyme alcohol dehydrogenase, which is found in most microorganisms that inhabit the soil.⁵⁹ It has been determined that methanol poses no significant environmental threat as accumulation in the atmosphere, water or ground would be negated by the action of alcohol dehydrogenase.⁵⁹ However, methanol does pose a significant threat to human life, if consumed in excess. Methanol poisoning, first reported in 1855,⁶¹ occurs when methanol is degraded in the body to FA. In the presence of folic acid, this FA can be further degraded to harmless CO₂ and H₂O.⁶² However, folic acid in this amount is not generally present in the human body, and excessive methanol absorption can lead to FA build up and ultimately poisoning. Despite these health concerns, methanol is still of great interest as an HSM because it is already produced and transported worldwide on an enormous scale. The required infrastructure and safety measures to avoid ill effects to humans have already been developed, tested and proven effective. A true barrier to the use of methanol as a H₂ storage molecule lies in the fact that is

currently produced from steam reforming of natural gas and/or the use of WGS reaction.⁵⁹ This is a non-sustainable and environmentally detrimental method of production. Renewable and environmentally-benign production of methanol is an enormous area of research and has seen marginal success in homogeneous systems,⁶³ with significant progress greatly needed to make methanol dehydrogenation a renewable hydrogen production cycle.

The earliest report of methanol dehydrogenation was in 1985 when Saito and co-workers reported the use of $[\text{Ru}_2(\text{OAc})_4\text{Cl}]$ in combination with PPh_3 to produce formaldehyde and methyl formate as well as H_2 with a TOF of 0.59 hr^{-1} .⁶⁴ In 2013, Grützmacher⁶⁵ reported a Ru catalyst (Table 1.02, A) with the complicated trop₂dad ligand which is capable of storing several equivalents of H_2 . Using this catalyst it was possible to achieve yields of H_2 of 90% from the dehydrogenation of 1:1 MeOH:H₂O. More importantly, Grützmacher's catalyst is active in the absence of base, which is not true of the Ru-based system subsequently reported by Beller.⁶⁶ Beller's pincer-supported Ru catalyst (Table 1.02, B) achieved unprecedented TONs, but suffered from low yields and the requirement for 8M KOH. However, in 2014 Beller reported a bicatalytic Ru system that was capable of base-free MeOH dehydrogenation (Table 1.02, C). This system also suffered from low yields and TON. Milstein also reported a pincer-support Ru catalyst capable aqueous phase methanol dehydrogenation (Table 1.02, D).⁶⁷ As with Grützmacher's catalyst, this Ru complex was dependent on the action of the ligand to reversibly add H_2 . However, Milstein's catalyst required addition of base. The only example of a first row transition metal catalyst was reported in 2013 when Beller described the use of an Fe catalyst (Table 1.02, E).⁶⁸ Again, this catalyst required significant amounts of 8M KOH for activity and gave only a 6% yield of H_2 from a 4:1 MeOH:H₂O mixture. Chapter 4 outlines a new advance allowing for base-free methanol dehydrogenation using an Fe catalyst.

Table 1.02. Homogeneous transition metal catalysts for aqueous-phase MeOH dehydrogenation to CO₂ and H₂.



Catalyst	Ratio MeOH:H ₂ O	Solvent	Additive	TON	Yield (%)	Reference
A	1:1 MeOH:H ₂ O	THF	-	540	90	Grützmacher ⁶⁵
B	4:1 MeOH:H ₂ O	Neat	8M KOH	350,000	27	Beller ^{66b}
C	4:1 MeOH:H ₂ O	Triglyme	-	4200	26	Beller ^{66a}
D	1:1 MeOH:H ₂ O	Toluene	KOH	28,000	77	Milstein ⁶⁷
E	4:1 MeOH:H ₂ O	Neat	8M KOH	9800	6	Beller ⁶⁸

IV. Conclusions

The implementation of an environmentally-benign, renewable energy vector is essential for the continued evolution of our global economy; H₂ is a possible energy vector that produces only H₂O as a byproduct. However, the safety concerns associated with H₂ gas necessitate the development of reversible hydrogen storage molecules. Many of the proposed HSM discussed above must overcome similar problems including lack of renewable sources of starting materials or regeneration of the spent fuel, selectivity for H₂ over fuel cell-poisoning side products, toxicity of the energy vector, or production of environmentally harmful side products. Much research has focused on mitigating these ill effects as well as producing highly active catalysts composed of cheap and abundant materials. This thesis will focus exclusively on the use of Fe-based catalysts for the dehydrogenation of FA and methanol. FA and methanol are among the safest HSM in terms of environmental and health effects, ease of transport, and overall reactivity with transition metal catalysts. Furthermore, both are industrially important chemicals, which increases the demand for the development of renewable syntheses. The following chapters will contain detailed discussions of syntheses of Fe-based catalysts, optimization of catalytic conditions for FA and methanol dehydrogenation, as well as

a discussion of the application of Lewis acid co-catalysts for catalytic enhancement.

V. References

- 1) MacKay, D. J. *Sustainable Energy- Without The Hot Air*; UIT Cambridge Ltd.: Cambridge, England, 2009.
- 2) DOE Annual Energy Outlook, available at <http://www.eia.doe.gov/oiaf/aeo/>.
- 3) (a) Lewis, N. S.; Nocera, D. G. *Proc. Natl. Acad. Sci. USA* **2006**, *103*, 15729; (b) Crabtree, G. W.; Dresselhaus, M. S.; Buchanan, M. V. *Phys. Today* **2004**, *57*, 39.
- 4) Petit, J. R.; Jouzel, J.; Raynaud, D.; Barkov, N. I.; Barnola, J. M.; Basile, I.; Bender, M.; Chappellaz, J.; Davis, M.; Delaygue, G.; Delmotte, M.; Kotlyakov, V. M.; Legrand, M.; Lipenkov, V. Y.; Lorius, C.; Pepin, L.; Ritz, C.; Saltzman, E.; Stievenard, M. *Nature* **1999**, *399*, 429.
- 5) Field, C. B.; Barros, V., R.; Dokken, D. J.; Mach, K. J.; Mastrandrea, M. D.; Bilir, T. E.; Cahatterjee, M.; Ebi, K. L.; Estrada, Y. O.; Genova, R. C.; Girma, B.; Kissel, E. S.; Levy, A. N.; MacCracken, S.; Mastrandrea, P. R.; White, L. L. *Climate Change 2014: Impacts, Adaptation, and Vulnerability. Part A: Global and Sectoral Aspects. Contribution of Working Group II to the Fifth Assessment Report of the Intergovernmental Panel on Climate Change*, IPCC, 2014.
- 6) Crabtree, R. H. *Energy Environ. Sci.* **2008**, *1*, 134.
- 7) (a) Grätzel, M. *Nature* **2001**, *414*, 338; (b) Bard, A. J.; Fox, M. A. *Acc. Chem. Res.* **1995**, *28*, 141; (c) Maeda, K.; Domen, K. *J. Phys. Chem. Lett.* **2010**, *1*, 2655; (d) Ni, M.; Leung, M. K. H.; Leung, D. Y. C.; Sumathy, K. *Renew. Sust. Energ. Rev.* **2006**, *11*, 401; (e) Walter, M. G.; Warren, E. L.; McKone, J. R.; Boettcher, S. W.; Mi, Q.; Santori, E. A.; Lewis, N. S. *Chem. Rev.* **2010**, *110*, 6446.
- 8) (a) Balat, M. *Int. J. Hydrogen Energy* **2008**, *33*, 4013; (b) Jacobson, M. Z. *Energy Environ. Sci.* **2009**, *2*, 148; (c) Naterer, G.; Suppiah, S.; Lewis, M.; Gabriel, K.; Dincer, I.; Rosen, M. A.; Fowler, M.; Rizvi, G.; Easton, E. B.; Ikeda, B. M.; Kaye, M. H.; Lu, L.; Pioro, I.; Spekkens, P.; Tremaine, P.; Mostaghimi, J.; Avsec, J.; Jiang, J. *Int. J. Hydrogen Energy* **2009**, *34*, 2901; (d) Zinkle, S. J.; Was, G. S. *Acta Mater.* **2013**, *61*, 735.
- 9) (a) Rosenberg, D. M.; Berkes, F.; Bodaly, R. A.; Hecky, R. E.; Kelly, C. A.; Rudd, J. W. M. *Environ. Rev.* **1997**, *5*, 27; (b) Sims, R. E. H. *MRS Bull.* **2008**, *33*, 389; (c) Tarnay, D. S. *Int. J. Hydrogen Energy* **1985**, *10*, 577.

- 10) (a) Ackermann, T.; Soder, L. *Renew. Sust. Energ. Rev.* **2000**, *4*, 315; (b) Knopper, L. D.; Ollson, C. A. *Environ. Health* **2011**, *10*, 78; (c) Moriarty, P.; Honnery, D. *Int. J. Hydrogen Energy* **2007**, *32*, 1616; (d) Sherif, S. A.; Barbir, F.; Veziroglu, T. N. *Sol. Energy* **2005**, *78*, 647.
- 11) (a) Barbier, E. *Renew. Sust. Energ. Rev.* **1997**, *1*, 1; (b) Fridleifsson, I. B. *Renew. Sust. Energ. Rev.* **2001**, *5*, 299; (c) Lund, J. W.; Freeston, D. H. *Geothermics* **2001**, *30*, 29.
- 12) Bockris, J. O. M. *Science* **1972**, *176*, 1323.
- 13) Schlapbach, L.; Züttel, A. *Nature* **2001**, *414*, 353.
- 14) Carmo, M.; Fritz, D. L.; Mergel, J.; Stolten, D. *Int. J. Hydrogen Energy* **2013**, *38*, 4901.
- 15) Navarro, R. M.; Peña, M. A.; Fierro, J. L. G. *Chem. Rev.* **2007**, *107*, 3952.
- 16) Satyapal, S.; Petrovic, J.; Read, C.; Thomas, G.; Ordaz, G. *Catal. Today* **2007**, *120*, 246.
- 17) (a) Cheng, H.-M.; Yang, Q.-H.; Liu, C. *Carbon* **2001**, *39*, 1447; (b) Schimmel, H. G.; Kearley, G. J.; Nijkamp, M. G.; Visser, C. T.; de Jong, K. P.; Mulder, F. M. *Chem. Eur. J.* **2003**, *9*, 4764; (c) Yang, Z.; Xia, Y.; Mokaya, R. *J. Am. Chem. Soc.* **2007**, *129*, 1673.
- 18) Rosi, N. L.; Eckert, J.; Eddaoudi, M.; Vodak, D. T.; Kim, J.; O'Keeffe, M.; Yaghi, O. M. *Science* **2003**, *300*, 1127.
- 19) (a) Bowman, R. C.; Fultz, B. *MRS Bull.* **2002**, *27*, 688; (b) Ritter, J. A.; Ebner, A. D.; Wang, J.; Zidan, R. *Mater. Today* **2003**, *6*, 18; (c) Orimo, S.-i.; Nakamori, Y.; Eliseo, J. R.; Züttel, A.; Jensen, C. M. *Chem. Rev.* **2007**, *107*, 4111.
- 20) Bogdanović, B.; Schwickardi, M. *J. Alloy. Compd.* **1997**, *253–254*, 1.
- 21) (a) Marder, T. B. *Angew. Chem., Int. Ed.* **2007**, *46*, 8116; (b) Staubitz, A.; Robertson, A., P. M.; Manners, I. *Chem. Rev.* **2010**, *110*, 4079; (c) Stephens, F. H.; Pons, V.; Baker, R. T. *Dalton Trans.* **2007**, 2613.
- 22) (a) Chen, Y.; Fulton, J. L.; Linehan, J. C.; Autrey, T. *J. Am. Chem. Soc.* **2005**, *127*, 3254; (b) Clark, T. J.; Russell, C. A.; Manners, I. *J. Am. Chem. Soc.* **2006**, *128*, 9582; (c) Denney, M. C.; Pons, V.; Hebden, T. J.; Heinekey, D. M.; Goldberg, K. I. *J. Am. Chem. Soc.* **2006**, *128*, 12048; (d) Keaton, R. J.; Blackquiere, J. M.; Baker, R. T. *J. Am. Chem. Soc.* **2007**, *129*, 1844; (e) Friedrich, A.; Drees, M.; Schneider, S. *Chem. Eur. J.* **2009**, *15*, 10339; (f) Kaess, M.; Friedrich, A.; Drees, M.; Schneider, S. *Angew. Chem., Int. Ed.* **2009**, *48*, 905; (g) Marziale, A. N.; Friedrich, A.; Klopsch, I.; Drees, M.; Celinski, V. R.; Schmedt auf der Guenne, J.;

- Schneider, S. *J. Am. Chem. Soc.* **2013**, *135*, 13342; (h) Staubitz, A.; Sloan, M. E.; Robertson, A. P. M.; Friedrich, A.; Schneider, S.; Gates, P. J.; Schmedt auf der Gunne, J.; Manners, I. *J. Am. Chem. Soc.* **2010**, *132*, 13332; (i) Bhattacharya, P.; Krause, J. A.; Guan, H. *J. Am. Chem. Soc.* **2014**, *136*, 11153.
- 23) Stephens, F. H.; Baker, R. T.; Matus, M. H.; Grant, D. J.; Dixon, D. A. *Angew. Chem., Int. Ed.* **2007**, *46*, 746.
- 24) Hausdorf, S.; Baitalow, F.; Wolf, G.; Mertens, F. O. R. L. *Int. J. Hydrogen Energy* **2008**, *33*, 608.
- 25) Davis, B.; Dixon, D. A.; Garner, E. B.; Gordon, J. C.; Matus, M. H.; Scott, B.; Stephens, F. H. *Angew. Chem., Int. Ed.* **2009**, *48*, 6812.
- 26) Ramachandran, P. V.; Gagare, P. D. *Inorg. Chem.* **2007**, *46*, 7810.
- 27) Chen, G.; Zakharov, L. N.; Bowden, M. E.; Karkamkar, A. J.; Whittmore, S. M.; Garner, E. B.; Mikulas, T. C.; Dixon, D. A.; Autrey, T.; Liu, S.-Y. *J. Am. Chem. Soc.* **2014**.
- 28) Yadav, M.; Xu, Q. *Energy Environ. Sci.* **2012**, *5*.
- 29) Schirmann, J.-P.; Bourdaudicqo, P. In *Ullman's Encyclopedia of Industrial Chemistry*; Wiley-VCH: Weinheim, 2012.
- 30) (a) Cho, S. J.; Lee, J.; Lee, Y. S.; Kim, D. P. *Catal. Lett.* **2006**, *109*, 181; (b) Rees, N. V.; Compton, R. G. *Energy Environ. Sci.* **2011**, *4*, 1255; (c) Singh, S. K.; Iizuka, Y.; Xu, Q. *Int. J. Hydrogen Energy* **2011**, *36*, 11794; (d) Singh, S. K.; Xu, Q. *Inorg. Chem.* **2010**, *49*, 6148; (e) Singh, S. K.; Xu, Q. *Catal. Sci. Technol.* **2013**, *3*, 1889; (f) Wang, J.; Zhang, X.-B.; Wang, Z.-L.; Wang, L.-M.; Zhang, Y. *Energy Environ. Sci.* **2012**, *5*, 6885.
- 31) M. Zheng, R.; Cheng, X.; Chen, N.; Li, L.; Li, X.; Wang, X.; Zhang, T. *Int. J. Hydrogen Energy* **2005**, *30*, 1081.
- 32) Singh, S. K.; Zhang, X.-B.; Xu, Q. *J. Am. Chem. Soc.* **2009**, *131*.
- 33) Singh, S. K.; Xu, Q. *J. Am. Chem. Soc.* **2009**, *131*, 18032.
- 34) Singh, S. K.; Singh, A. K.; Aranishi, K.; Xu, Q. *J. Am. Chem. Soc.* **2011**, *133*, 19638.
- 35) Wang, H.-L.; Yan, J.-M.; Li, S.-J.; Zhang, X.-W.; Jiang, Q. *J. Mater. Chem. A* **2015**, *3*, 121.
- 36) Clot, E.; Eisenstein, O.; Crabtree, R. H. *Chem. Commun.* **2007**, 2231.
- 37) (a) Dobreiner, G. E.; Nova, A.; Schley, N. D.; Hazari, N.; Miller, S. J.; Eisenstein, O.; Crabtree, R. H. *J. Am. Chem. Soc.* **2011**, *133*, 7547; (b) Chakraborty, S.; Brennessel, W. W.; Jones, W. D. *J. Am. Chem.*

Soc. **2014**, *136*, 8564; (c) Yamaguchi, R.; Ikeda, C.; Takahashi, Y.; Fujita, K.-i. *J. Am. Chem. Soc.* **2009**, *131*, 8410; (d) Li, H.; Jiang, J.; Lu, G.; Huang, F.; Wang, Z.-X. *Organometallics* **2011**, *30*, 3131; (e) Zhang, X.-B.; Xi, Z. *Phys. Chem., Chem. Phys.* **2011**, *13*, 3997; (f) Wu, J.; Talwar, D.; Johnston, S.; Yan, M.; Xiao, J. *Angew. Chem., Int. Ed.* **2013**, *52*, 6983; (g) Luca, O.; Huang, D. L.; Takase, M. K.; Crabtree, R. H. *New J. Chem.* **2013**, *37*, 3402; (h) Tsuji, Y.; Kotachi, S.; Huh, K. T.; Watanabe, Y. *J. Org. Chem.* **1990**, *55*, 580; (i) Hara, T.; Mori, K.; Mizugaki, T.; Ebitani, K.; Kaneda, K. *Tetrahedron Lett.* **2003**, *44*, 6207; (j) Dean, D.; Davis, B.; Jessop, P. G. *New J. Chem.* **2011**, *35*, 417; (k) See Reference 37a for a complete list of homogeneous systems.

38) Williams, R.; Crandall, R. S.; Bloom, A. *Appl. Phys. Lett.* **1978**, *35*, 381.

39) Pokhodenko, V. D.; Koshechko, V. G.; Titov, V. E.; Sednev, D. V. *Theor. Exp. Chem.* **1993**, *28*, 85.

40) (a) Kang, P.; Chen, Z.; Brookhart, M.; Meyer, T. J. *Top. Catal.* **2014**, Ahead of Print; (b) Kang, P.; Cheng, C.; Chen, Z.; Schauer, C. K.; Meyer, T. J.; Brookhart, M. *J. Am. Chem. Soc.* **2012**, *134*, 5500; (c) Kang, P.; Meyer, T. J.; Brookhart, M. *Chem. Sci.* **2013**, *4*, 3497; (d) Kang, P.; Zhang, S.; Meyer, T. J.; Brookhart, M. *Angew. Chem., Int. Ed.* **2014**, *53*, 8709; (e) Zhang, S.; Kang, P.; Ubnoske, S.; Brennaman, M. K.; Song, N.; House, R. L.; Glass, J. T.; Meyer, T. J. *J. Am. Chem. Soc.* **2014**, *136*, 7845; (f) Zhang, S.; Kang, P.; Meyer, T. J. *J. Am. Chem. Soc.* **2014**, *136*, 1734; (g) Sullivan, B. P.; Bruce, M. R. M.; O'Toole, T. R.; Bolinger, C. M.; Megehee, E.; Thorp, H.; Meyer, T. J. *ACS Symp. Ser.* **1988**, *363*, 52.

41) (a) Tanaka, R.; Yamashita, M.; Chung, L. W.; Morokuma, K.; Nozaki, K. *Organometallics* **2011**, *30*, 6742; (b) Tanaka, R.; Yamashita, M.; Nozaki, K. *J. Am. Chem. Soc.* **2009**, *131*, 14168; (c) Jessop, P. G.; Ikarlya, T.; Noyori, R. *Nature* **1994**, *368*, 231; (d) Langer, R.; Diskin-Posner, Y.; Leitun, G.; Shimon, L. J. W.; Ben-David, Y.; Milstein, D. *Angew. Chem., Int. Ed.* **2011**, *50*, 9948; (e) Jeletic, M. S.; Mock, M. T.; Appel, A. M.; Linehan, J. C. *J. Am. Chem. Soc.* **2013**, *135*, 11533; (f) Schmeier, T. J.; Dobereiner, G. E.; Crabtree, R. H.; Hazari, N. *J. Am. Chem. Soc.* **2011**, *133*, 9274; (g) Federsel, C.; Boddien, A.; Jackstell, R.; Jennerjahn, R.; Dyson, P. J.; Scopelliti, R.; Laurenczy, G.; Beller, M. *Angew. Chem., Int. Ed.* **2010**, *49*, 9777; (h) Federsel, C.; Jackstell, R.; Beller, M. *Angew. Chem., Int. Ed.* **2010**, *49*, 6254.

42) (a) Xing, R.; Qi, W.; Huber, G. W. *Energy Environ. Sci.* **2011**, *4*, 2193; (b) Jin, F.; Enomoto, H. *Energy Environ. Sci.* **2011**, *4*, 382; (c) Fitzpatrick, D. J.; Hayes, S.; Hayes, M. H. B.; Ross, J. R. H. *Biorefineries-Industrial Processes and Products*; Wiley-VCH: Weinheim, 2010.

- 43) Grasemann, M.; Laurenczy, G. *Energy Environ. Sci.* **2012**, *5*, 8171.
- 44) Reutemann, W.; Kieczka, H. In *Ullmann's Encyclopedia of Industrial Chemistry*; Wiley-VCH Verlag GmbH & Co: Weinheim, 2012.
- 45) Enthaler, S.; von Langermann, J.; Schmidt, T. *Energy Environ. Sci.* **2010**, *3*, 1207.
- 46) Ojeda, M.; Iglesia, E. *Angew. Chem., Int. Ed.* **2009**, *48*, 4800.
- 47) Bulushev, D. A.; Beloshapkin, S.; Ross, J. R. H. *Catal. Today* **2010**, *154*, 7.
- 48) Coffey, R. S. *Chem. Commun.* **1967**, 923.
- 49) Gao, Y.; Kuncheria, J.; J. Puddephatt, R.; P. A. Yap, G. *Chem. Commun.* **1998**, 2365.
- 50) (a) Himeda, Y. *Green Chem.* **2009**, *11*, 2018; (b) Hull, J. F.; Himeda, Y.; Wang, W.-H.; Hashiguchi, B.; Periana, R.; Szalda, D. J.; Muckerman, J. T.; Fujita, E. *Nat. Chem.* **2012**, *4*, 383.
- 51) Manaka, Y.; Wang, W.-H.; Suna, Y.; Kambayashi, H.; Muckerman, J. T.; Fujita, E.; Himeda, Y. *Catal. Sci. Tech.* **2014**, *4*, 34.
- 52) (a) Loges, B.; Boddien, A.; Junge, H.; Beller, M. *Angew. Chem., Int. Ed.* **2008**, *47*, 3962; (b) Mellone, I.; Peruzzini, M.; Rosi, L.; Mellmann, D.; Junge, H.; Beller, M.; Gonsalvi, L. *Dalton Trans.* **2013**, *42*, 2495; (c) Loges, B.; Boddien, A.; Gärtner, F.; Junge, H.; Beller, M. *Top Catal* **2010**, *53*, 902.
- 53) Oldenhof, S.; de Bruin, B.; Lutz, M.; Siegler, M. A.; Patureau, F. W.; van der Vlugt, J. I.; Reek, J. N. H. *Chem. Eur. J.* **2013**, *19*, 11507.
- 54) Boddien, A.; Mellmann, D.; Gärtner, F.; Jackstell, R.; Junge, H.; Dyson, P. J.; Laurenczy, G.; Ludwig, R.; Beller, M. *Science* **2011**, *333*, 1733.
- 55) Zell, T.; Butschke, B.; Ben-David, Y.; Milstein, D. *Chem. Eur. J.* **2013**, *19*, 8068.
- 56) (a) Morris, D. J.; Clarkson, G. J.; Wills, M. *Organometallics* **2009**, *28*, 4133; (b) Barnard, J. H.; Wang, C.; Berry, N. G.; Xiao, J. *Chem. Sci.* **2013**, *4*, 1234.
- 57) Wagner, K. *Angew. Chem., Int. Ed.* **1970**, *9*, 50.
- 58) (a) Clarke, H. T. *J. Am. Chem. Soc.* **1933**, *55*, 4571; (b) Brieger, G.; Nestrick, T. J. *Chem. Rev.* **1973**, *74*, 567; (c) Linstead, R. P.; Braude, F. A.; Mitchell, P. W. D.; Wooldridge, K. R. H.; Jackman, L. M. *Nature* **1952**, *169*, 100.
- 59) Ott, J.; Gronemann, V.; Pontzen, F.; Fiedler, E.; Grossmann, G.; Kersebohm, D. B.; Weiss, G.; Witte, C. In *Ullmann's Encyclopedia of Industrial Chemistry*; Wiley-VCH: Weinheim, 2012.

- 60) Arapatsakos, C. *Biofuels Ethanol and Methanol in OTTO Engines*, 2013.
- 61) McFarlan, J. F. *Pharm. J. Trans.* **1855**, *15*, 310.
- 62) Kapur, B. M.; Vandenbroucke, A. C.; Adamchik, Y.; Lehotay, D. C.; Carlen, P. L. *Alcohol Clin. Exp. Res.* **2007**, *31*, 2114.
- 63) (a) Huff, C. A.; Sanford, M. S. *J. Am. Chem. Soc.* **2011**, *133*, 18122; (b) Wesselbaum, S.; vom Stein, T.; Klankermayer, J.; Leitner, W. *Angew. Chem., Int. Ed.* **2012**, *51*, 7499; (c) Balarman, E.; Gunanathan, C.; Zhang, J.; Shimon, L. J. W.; Milstein, D. *Nature Chem.* **2011**, *3*, 609; (d) Rezayee, N. M.; Huff, C. A.; Sanford, M. S. *J. Am. Chem. Soc.* **2015**.
- 64) (a) Itagaki, H.; Saito, Y.; Shinoda, S. *J. Mol. Catal.* **1987**, *41*, 209; (b) Shinoda, S.; Itagaki, H.; Saito, Y. *J. Chem. Soc., Chem. Commun.* **1985**, 860.
- 65) Rodríguez-Lugo, R. E.; Trincado, M.; Vogt, M.; Tewes, F.; Santiso-Quinones, G.; Grützmacher, H. *Nat. Chem.* **2013**, *5*, 342.
- 66) (a) Monney, A.; Barsch, E.; Sponholz, P.; Junge, H.; Ludwig, R.; Beller, M. *Chem. Commun.* **2014**, *50*, 707; (b) Nielsen, M.; Alberico, E.; Baumann, W.; Drexler, H.-J.; Junge, H.; Gladiali, S.; Beller, M. *Nature* **2013**, *495*, 85.
- 67) Hu, P.; Diskin-Posner, Y.; Ben-David, Y.; Milstein, D. *ACS Catal.* **2014**, *4*, 2649.
- 68) Alberico, E.; Sponholz, P.; Cordes, C.; Nielsen, M.; Drexler, H.-J.; Baumann, W.; Junge, H.; Beller, M. *Angew. Chem., Int. Ed.* **2013**, *52*, 14162.

Chapter 2: Synthesis and Spectroscopic Investigation of PNP Pincer-Supported Fe Compounds

I. Introduction

Over the last two decades pincer ligands have become some of the most versatile and important ligands for stabilizing reactive transition metal complexes.¹ In general, their straightforward and modular syntheses allow for relatively facile tuning of both the steric and electronic properties of the resulting pincer-supported complexes. Furthermore, the strong binding of these ligands to a variety of different metals often generates complexes with extremely high thermal stability. As a result, transition metal complexes supported by pincer ligands have been utilized for the activation of small molecules such as CO₂² and N₂³ and as catalysts for a variety of processes including alkane dehydrogenation,⁴ alkane metathesis,⁴ olefin polymerization⁵ and transfer hydrogenation.⁶ However, despite the impressive applications of pincer-supported complexes, the binding of pincer ligands to transition metals has not been explored to the same extent as the coordination of simple monodentate and bidentate ligands. Therefore, fundamental studies on the properties of pincer-supported transition metal complexes, which could provide insight for the design of the next generation of reactive species, are important.

In recent years, ^RPN^HP-type pincer ligands of the general formula HN{CH₂CH₂(PR₂)}₂ (R = alkyl or aryl) have received significant attention⁷ due to their ability to support transition metal catalysts and stabilize complexes in unusual geometries. For example, Beller and co-workers^{7ab,7ac} have demonstrated catalytic dehydrogenation of methanol to H₂ and CO₂ using both Fe and Ru complexes supported by a ^RPN^HP ligand, while Schneider and co-workers utilized this ligand to prepare the first examples of square planar Rh, Ru and Ir nitrides.^{7t,7w,7y} In almost all reported complexes supported by ^RPN^HP ligands, the ligand binds in a meridional fashion, as expected for a pincer ligand. Nevertheless, there are a handful of examples, particularly in dimeric complexes, where the ^RPN^HP ligand binds in a facial orientation.^{7d,7h,7i,7u} This has led to speculation that these ligands, especially those with alkyl linkers, are not only flexible, but also that reactive intermediates may lead to different products depending on whether the ligand is in a meridional or facial geometry.^{7d} However, at this stage, there are no examples of complexes supported by ^RPN^HP ligands which have been shown to exist in both meridional or facial geometries either in solution or the solid state. In general, this type of interconversion has rarely been demonstrated for pincer ligands.⁸ This chapter

describes a number of five coordinate Fe complexes supported by the $R^H\text{PN}^H\text{P}$ ligand, $\text{HN}\{\text{CH}_2\text{CH}_2(\text{PR}_2)\}_2$ ($R = i\text{Pr}$ ($i\text{Pr}^H\text{PN}^H\text{P}$), $t\text{Bu}$ ($t\text{Bu}^H\text{PN}^H\text{P}$) or cyclohexyl ($\text{Cy}^H\text{PN}^H\text{P}$)). A variety of techniques, including X-ray crystallography, Mössbauer, and magnetic circular dichroism (MCD) spectroscopy, show that these complexes exist as isomers in which the $R^H\text{PN}^H\text{P}$ ligand can be in a *pseudo*-meridional or a *pseudo*-facial geometry. These studies conclusively demonstrate that these ligands are flexible in solution, which could be a crucial factor in the reactivity of this important class of compounds. Below is presented a brief discussion of the flexible binding of these $R^H\text{PN}^H\text{P}$ -supported Fe compounds. A detailed explanation of the Mössbauer and MCD spectroscopy can be found in the Ph.D thesis of Kathlyn Fillman.⁹

II. Results and Discussion

This work has been previously published.¹⁰ Synthesis and crystallization conditions for **1a-c** were initially reported by Dr. Timothy Schmeier.¹¹

Using a modification of a procedure described by Milstein and co-workers,¹² the ligands $i\text{Pr}^H\text{PN}^H\text{P}$, $t\text{Bu}^H\text{PN}^H\text{P}$ and $\text{Cy}^H\text{PN}^H\text{P}$ were coordinated by heating the free ligand with anhydrous FeCl_2 in THF (Figure 2.01). The new pincer supported complexes **1a-c** are insoluble in THF and precipitate out of the reaction mixture as white solids. The reaction proceeded more slowly as the steric bulk of the phosphine substituent was increased. The coordination of the $i\text{Pr}^H\text{PN}^H\text{P}$ ligand required only two hours to reach completion, while the $t\text{Bu}^H\text{PN}^H\text{P}$ and $\text{Cy}^H\text{PN}^H\text{P}$ ligands required longer reaction times. The new complexes **1a-c** are paramagnetic and solution magnetic measurements using the Evans' NMR method, performed by Cassie Pan, were consistent with an $S = 2$ ground state for each complex.

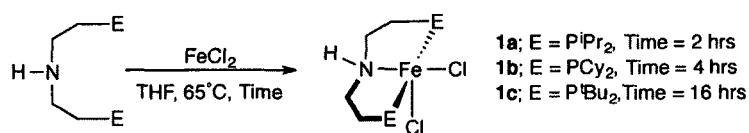
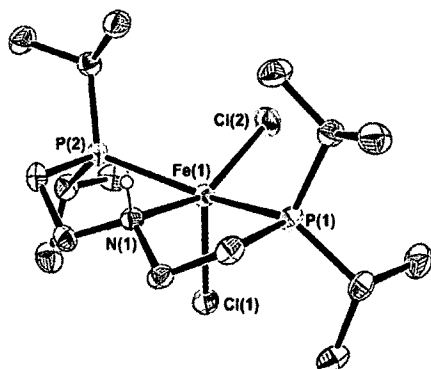


Figure 2.01. Synthesis of $R^H\text{PN}^H\text{P}$ -Supported Fe Compounds

Complexes **1a** and **1c** were characterized by X-ray crystallography. Interestingly, two different polymorphs of complex **1a** were crystallized, as shown in Figures 2.02a and 2.02b. In one polymorph the

Fe center is in a distorted square pyramidal geometry ($1a^{spy}$) with one acetonitrile molecule in the crystal lattice, whereas in the other polymorph the Fe is in a distorted trigonal bipyramidal geometry ($1a^{tbp}$). In $1a^{spy}$ the $iPrPN^H P$ ligand is coordinated in the expected meridional fashion and occupies positions around the base of the square pyramid, with one of the chloride ligands occupying the axial position. The P(1)-Fe(1)-P(2) bond angle is $151.60(4)^\circ$. The degree of distortion from square pyramidal was quantified by calculating the value τ .¹³ On the scale of 0 to 1, where 0 denotes idealized square pyramidal character and 1 idealized trigonal bipyramidal character, τ is 0.053. In contrast, in $1a^{tbp}$ the $iPrPN^H P$ ligand coordinates facially and the P(1)-Fe(1)-P(2) bond angle is $117.96(4)^\circ$, while the angle between the nitrogen atom of the $iPrPN^H P$ ligand, Fe(1) and Cl(2), which occupies one of the apical positions, is $170.19(8)^\circ$. Here, the value of τ is 0.79. Facial coordination of the $RPN^H P$ ligand has been observed mainly in dimeric species,^{7d,7h,7i,7u} although the structure of $(iPrPN^H P)CoCl_2$ is quite similar to $1a^{tbp}$.^{7h} The Fe(1)-N(1) bond distance is significantly elongated in $1a^{tbp}$ (2.372(4) Å) compared to $1a^{spy}$ (2.260(4) Å), while the Fe-P bond lengths are elongated in $1a^{spy}$ (2.5506(11) & 2.5853(11) Å) compared to $1a^{tbp}$ (2.4976(9) & 2.4857(9) Å). In both cases this is probably related to the *trans*-influence. In $1a^{tbp}$ the central nitrogen atom of the $iPrPN^H P$ ligand is directly opposite a chloride ligand, whereas in $1a^{spy}$ it is not directly opposite any ligand. However, in $1a^{spy}$ the two phosphorus atoms are *trans* to each other, whereas in $1a^{tbp}$ they are not *trans* to any ligand.

a)



b)

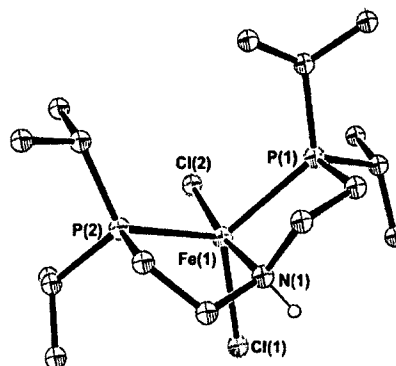


Figure 2.02. a) ORTEP¹⁴ of **1a^{spy}** (Selected hydrogen atoms and solvent of crystallization omitted for clarity). Selected bond lengths (Å) and angles (°): Fe(1)-Cl(1) 2.3678(10), Fe(1)-Cl(2) 2.3033(11), Fe(1)-N(1) 2.255(3), Fe(1)-P(1) 2.5506(11), Fe(1)-P(2) 2.5853(11), P(1)-Fe(1)-P(2) 151.60(4), P(1)-Fe(1)-Cl(1) 99.08(4), P(1)-Fe(1)-Cl(2) 96.56(4), P(1)-Fe(1)-N(1) 78.12(8), P(2)-Fe(1)-Cl(1) 99.77(4), P(2)-Fe(1)-Cl(2) 95.87(4), P(2)-Fe(1)-N(1) 77.93(8), Cl(1)-Fe(1)-Cl(2) 111.92(4), N(1)-Fe(1)-Cl(1) 99.66(8), N(1)-Fe(1)-Cl(2) 148.42(8). b) ORTEP¹⁴ of **1a^{tbp}** (Selected hydrogen atoms omitted for clarity). Selected bond lengths (Å) and angles (°): Fe(1)-Cl(1) 2.3390(8), Fe(1)-Cl(2) 2.3338(9), Fe(1)-N(1) 2.373(2), Fe(1)-P(1) 2.4976(9), Fe(1)-P(2) 2.4857(9), P(1)-Fe(1)-P(2) 118.03(3), P(1)-Fe(1)-Cl(1) 122.98(3), P(1)-Fe(1)-Cl(2) 94.78(3), P(2)-Fe(1)-N(1) 76.83(7), P(2)-Fe(1)-Cl(1) 109.49(3), P(2)-Fe(1)-Cl(2) 102.17(3), P(2)-Fe(1)-N(1) 77.82(7), Cl(1)-Fe(1)-Cl(2) 104.52(3), N(1)-Fe(1)-Cl(1) 84.58(6), N(1)-Fe(1)-Cl(2) 170.15(7).

In general, for simple five-coordinate (5C) transition metal compounds the potential energy surface is quite flat and the energy difference between trigonal bipyramidal and square pyramidal geometries can be small.¹⁵ The structures of **1a^{spy}** and **1a^{tbp}** are the first example where a complex containing the same ^RPN^HP ligand crystallizes in both meridional and facial geometries. Furthermore, this behavior has only been noted in three examples with any kind of pincer ligand.⁸ A potential cause for the different structures could be related to hydrogen bonding. In **1a^{spy}**, there is a weak hydrogen bonding interaction between the coordinated acetonitrile molecule and one of the chloride ligands, while in both structures there is hydrogen bonding between the N-H group of the ligand and one of the chloride ligands. However, DFT calculations in the gas phase (where there are no hydrogen bonding effects) at the M06L level, located two minimum energy structures, which gave reasonably good agreement with **1a^{spy}** and **1a^{tbp}** without the use of any constraints. The calculated structure of **1a^{spy}** is 0.73 kJ mol⁻¹ lower in energy than the calculated structure of **1a^{tbp}**, which is consistent with the observation of two different polymorphs. Similar results were obtained with the uB3LYP functional. This suggests that packing effects are not responsible for the observation of both isomers, although the packing between the two compounds is very different.

The crystal structure of **1c** (Figure 2.03a) is essentially isostructural with **1a^{spy}**. The ^tBuPN^HP ligand is coordinated in a meridional fashion (the P(1)-Fe(1)-P(2) angle is 150.33(4)°) and the Fe center is in a distorted square pyramidal geometry (the value of τ is 0.033). A structural overlay (Figure 2.03 b) of **1a^{spy}** and **1c** reveals that the extra methyl groups present on ^tBuPN^HP compared with ⁱPrPN^HP occupy space above the open coordination site of **1c**. This pushes Cl(2) away from the open site and the Cl(1)-Fe(1)-Cl(2) bond angle is more acute in **1c** (106.95(4)°) compared with **1a^{spy}** (111.97(5)°).

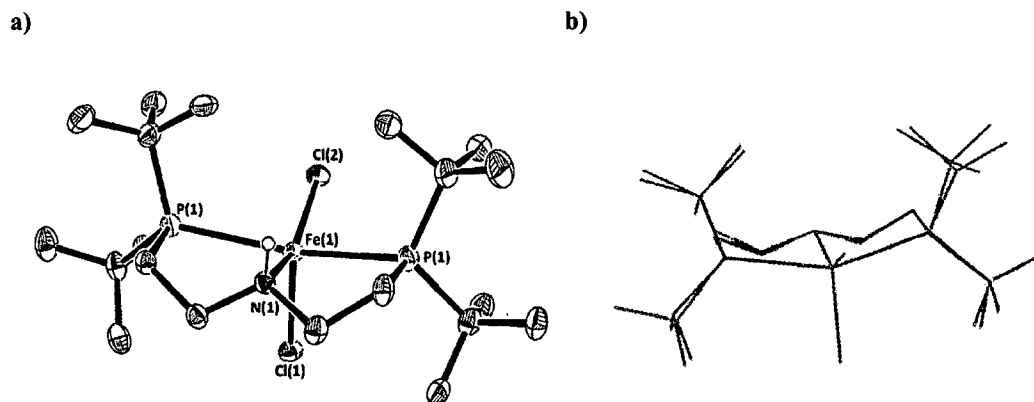


Figure 2.03. a) ORTEP¹⁴ of **1c** (Selected hydrogen atoms omitted for clarity). Selected bond lengths (Å) and angles (°): Fe(1)-Cl(1) 2.3334(14), Fe(1)-Cl(2) 2.3385(11), Fe(1)-N(1) 2.221(3), Fe(1)-P(1) 2.6144(15), Fe(1)-P(2) 2.6111(14), P(1)-Fe(1)-P(2) 150.33(4), P(1)-Fe(1)-Cl(1) 100.75(5), P(1)-Fe(1)-Cl(2) 97.81(4), P(1)-Fe(1)-N(1) 78.15(10), P(2)-Fe(1)-Cl(1) 100.02(5), P(2)-Fe(1)-Cl(2) 96.13(4), P(2)-Fe(1)-N(1) 77.35(10), Cl(1)-Fe(1)-Cl(2) 106.95(4), N(1)-Fe(1)-Cl(1) 100.70(11), N(1)-Fe(1)-Cl(2) 152.30(11). b) Structural overlay of **1a^{spy}** (green) with **1c** (red).

⁵⁷Fe Mössbauer spectroscopy, performed by Kathlyn Fillman, was used to investigate the electronic structures of as-isolated powder samples of **1a-1c** in the solid state (Figure 2.04). In all cases the samples were not exposed to acetonitrile. The 80 K Mössbauer spectrum of **1a** (Figure 2.04a) is well-fit to a single Fe species with $\delta = 0.86$ mm/s and $\Delta E_Q = 2.89$ mm/s. For **1b** (Figure 2.04b), the best fit to the 80 K Mössbauer data comprises a single major component with $\delta = 0.86$ mm/s and $\Delta E_Q = 2.98$ mm/s (~ 97 % of all Fe, red component). A minor species, which has parameters in the expected range for a potential Fe(III) impurity is also present ($\delta = 0.46$ mm/s, $\Delta E_Q = 0.69$ mm/s, ~ 3% of all Fe, blue component). The 80 K Mössbauer spectrum of **1c** (Figure 2.04c) is well-fit to a single Fe species with $\delta = 0.99$ mm/s and $\Delta E_Q = 2.69$ mm/s. The observed isomer shifts for the three (^RPN^HP)FeCl₂ complexes all fall in the range of 0.85-1.0 mm/s, consistent with the presence of high-spin, S = 2 Fe(II) species.¹⁶ By comparison, the high-spin S = 2 distorted square pyramidal (PN^{Py}P)FeCl₂ complex (PN^{Py}P = 2,6-C₅H₃N(CH₂PⁱPr₂)₂, where a pyridine

forms the central part of the pincer ligand) has Mössbauer parameters of $\delta = 0.80$ mm/s and $\Delta E_Q = 2.56$ mm/s.¹⁶ It is notable that while the Mössbauer parameters of **1a** and **1b** are very similar, **1c** exhibits a higher isomer shift (0.99 mm/s vs. 0.86 mm/s; error in δ is ± 0.02 mm/s) as well as a smaller quadrupole splitting (2.69 mm/s vs. 2.89 mm/s; error in $\Delta E_Q \pm 0.04$ mm/s). This variation suggests the possible presence of a different structural distortion for **1c** in the solid-state powder, which is more rigorously determined by direct evaluation of the observed differences in the d-d transitions of the powders in NIR MCD spectroscopy (*vide infra*). Lastly, no contributions of minor species corresponding to a second Fe(II) 5C species are observed in the solid-state spectra. Consistent with this, there is also no evidence of a second species from the d-d transitions observed of the same solid samples in NIR MCD (*vide infra*). If present, such a minor species is below our detectable limit and would represent $\sim < 1\text{-}2\%$ of all Fe present.

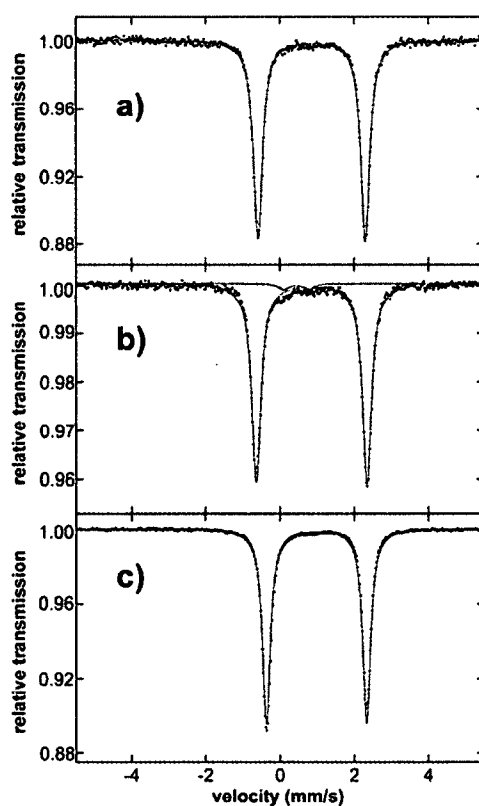


Figure 2.04. 80K ^{57}Fe Mössbauer data (black dots) and fit (black lines) of solid powders of **a)** $(^i\text{PrPN}^i\text{P})\text{FeCl}_2$; **1a**, **b)** $(^{\text{Cy}}\text{PN}^i\text{P})\text{FeCl}_2$; **1b** and **c)** $(^i\text{Bu}^i\text{PN}^i\text{P})\text{FeCl}_2$; **1c**. For **1b**, both major and minor components are present in the best fit as described in the text.

Near-infrared (NIR) MCD studies were performed on the solid-state powder samples used for Mössbauer spectroscopy, in order to further probe the electronic and geometric structures of **1a-1c** (Figure 2.05). The 5 K, 7T NIR MCD spectrum of a mull of **1a** (Figure 2.05a, blue) exhibits two ligand-field (LF) transitions at $< 5000 \text{ cm}^{-1}$ and 10560 cm^{-1} . A very similar set of LF transitions (bands at $< 5000 \text{ cm}^{-1}$ and 10770 cm^{-1}) are also observed in the 5K, 7T NIR MCD spectrum of a mull of **1b** (Figure 2.05a, green). In contrast, the 5K, 7T NIR MCD spectrum of **1c** exhibits only a single LF transition at 9260 cm^{-1} (Figure 2.05a, red). Importantly, the energies of the observed LF transitions can be directly related to the coordination number and geometry of the Fe(II) complexes.¹⁷ For a $S = 2$ Fe(II) 5C complex, the LF splittings have been previously quantified using both LF theory calculations and MCD measurements of well-defined coordination complexes with nitrogen and oxygen ligands. As shown in Figure 2.06, in distorted square pyramidal 5C Fe(II) ($S = 2$) complexes, the 5E state splits by $\sim 5000 \text{ cm}^{-1}$ resulting in two LF transitions at $> 10000 \text{ cm}^{-1}$ and $\sim 5000 \text{ cm}^{-1}$.^{17c-e} By comparison, distortion to a trigonal bipyramidal 5C structure leads to a smaller LF with transitions at $< 10000 \text{ cm}^{-1}$ and $< 5000 \text{ cm}^{-1}$.^{17c-e}

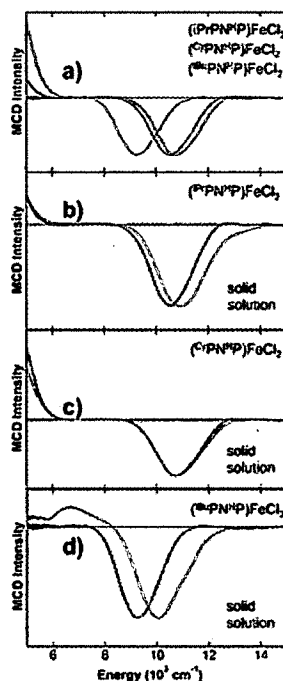


Figure 2.05. 5K, 7T NIR MCD spectra of ($^R\text{PN}^H\text{P}$)FeCl₂ complexes. NIR MCD of solid state mulls of a) ($^{i\text{Pr}}\text{PN}^H\text{P}$)FeCl₂; **1a**, ($^{\text{Cy}}\text{PN}^H\text{P}$)FeCl₂; **1b** and ($^{i\text{Bu}}\text{PN}^H\text{P}$)FeCl₂; **1c**. Comparison of solid-state mull and frozen solution glasses (1:1 DCM-d₂:toluene-d₈) NIR MCD spectra of b) ($^{i\text{Pr}}\text{PN}^H\text{P}$)FeCl₂; **1a**, c) ($^{\text{Cy}}\text{PN}^H\text{P}$)FeCl₂; **1b** and d) ($^{i\text{Bu}}\text{PN}^H\text{P}$)FeCl₂; **1c**.

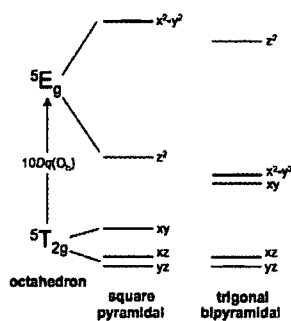


Figure 2.06. Ligand field energies in idealized 5C, high spin, $S = 2$ Fe (II) compounds in either square pyramidal or trigonal bipyramidal geometries

Importantly, the MCD model studies of 5C Fe(II) complexes also demonstrated that changes in bond lengths and/or distortions of square pyramidal structures can result in significant changes in the highest energy LF transition via stabilization/de-stabilization of the $d_{x^2-y^2}$ orbital.^{17c} For example, changes in the strength of axial M-L bonding (via substitution of Cl for Br) shifts Fe out of the xy-plane and stabilizes the $d_{x^2-y^2}$ orbital, resulting in an increase in highest energy LF transitions by $\sim 800 \text{ cm}^{-1}$ for $[\text{Fe}(\text{TMC})\text{Cl}]^+$ vs. $[\text{Fe}(\text{TMC})\text{Br}]^+$ (TMC = 1,4,8,11-tetramethyl-1,4,8,11-tetraazacyclotetradecane).^{17c} Furthermore, these studies demonstrated the sensitivity of the $d_{x^2-y^2}$ orbital to changes in the equatorial plane due to differences in LF strength, where differences of up to 1800 cm^{-1} were observed for Fe-O ligation in the equatorial plane by changing the bidentate oxygen donor across the series OAc (acetate), OBz (benzoyl) and acac (acetylacetonone). Differences in LF strengths can also occur due to changes in M-L bond distances. This LF analysis of geometries and structural distortions based on NIR MCD measurements has previously been successfully applied to several Fe(II) 5C species, including very low symmetry sites in non-heme Fe metalloenzymes.^{16d-f}

While direct measurements of LF transition energies in 5C high-spin $S = 2$ Fe complexes supported by PNP ligands have not been reported, the combination of equal numbers of stronger field phosphine ligands and weaker field chloride ligands would be anticipated to result in LF energies for the $(^R\text{PN}^H\text{P})\text{FeCl}_2$ complexes of comparable magnitude to those reported for the N/O- ligated model complexes previously reported^{16c} (as is observed from MCD in Figure 2.05). Thus, within a series of related $(^R\text{PN}^H\text{P})\text{FeCl}_2$ complexes, the extent of distortion towards a square pyramidal vs. a trigonal bipyramidal structure can be evaluated using the observed LF energies. The observed LF transitions for **1a** (Figure 2.05a, blue) at 10560

red), the solution NIR MCD spectrum indicates the presence of LF bands at $< 5000 \text{ cm}^{-1}$ and 10900 cm^{-1} and 12580 cm^{-1} . The presence of the weak transition at 12580 cm^{-1} is further demonstrated by variable-field MCD experiments (Figure 2.07). These results show that the higher energy band is present at all field strengths and shows behavior that is consistent with a real peak rather than an effect of baseline. Furthermore, this high-energy feature was seen in independently prepared samples.

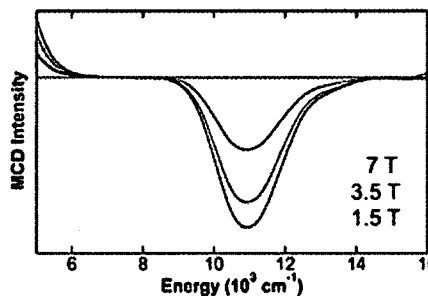


Figure 2.07. 5K, variable-field NIR MCD spectra of a frozen glass sample of $(iPrPN^H)FeCl_2$ (**1a**).

Since LF theory dictates that a single Fe(II) ($S = 2$) complex can exhibit only two LF transitions, the presence of three LF bands indicates the presence of two distinct structural distortions in solution. Based upon the energies of the two highest energy LF transitions, both species are consistent with distortion towards square pyramidal 5C species. Interestingly, the energies of these transitions (10900 cm^{-1} and 12580 cm^{-1}) are both increased compared to the solid state powder, consistent with an increased LF due to stronger Fe-L bonding interactions in solution and/or distortions of the complex to de-stabilize the $d_{x^2-y^2}$ orbital (for example, a more planar equatorial plane). Overall, these results suggest that the $iPrPN^H$ ligand is able to stabilize two different distorted 5C structures of **1a** in solution, although unlike the solid state results, where both *pseudo*-square pyramidal and *pseudo*-trigonal bipyramidal isomers are observed, it appears that only more square pyramidal species are present in solution. In contrast, the solution NIR MCD spectrum of **1b** (Figure 2.05c, red) contains only two LF transitions (at $< 5000 \text{ cm}^{-1}$ and 10770 cm^{-1}), identical to the energies observed for **1b** in the solid state mull indicating the presence of a single distorted square pyramidal species which is unchanged between the solution and solid states. Notably, the solution MCD spectrum of **1c** (Figure 2.05d, red) shows a dramatic change relative to the mull spectrum (Figure 2.05d, blue), with the presence of three distinct LF transitions indicating the presence of at least two

different Fe species in solution. This can be further substantiated by comparing peak-fit analysis of frozen glass samples of **1a** and **1c** (Figure 2.08).

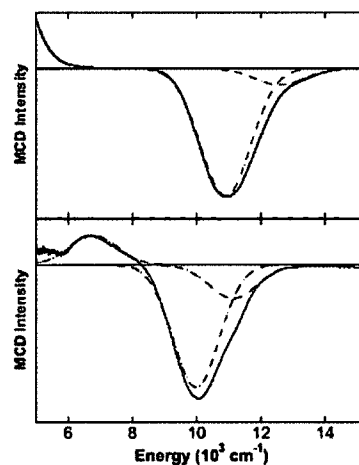


Figure 2.08. 5K, 7T NIR MCD peak fit analysis of frozen solution glass samples of $(iPr)PNHP)FeCl_2$, **1a** (blue) and $(tBu)PNHP)FeCl_2$, **1c** (red).

Two high energy transitions at 9980 cm^{-1} and 11140 cm^{-1} are present, both higher in energy than the transition observed in the mull at 9260 cm^{-1} . An additional LF band is also present in solution at 6770 cm^{-1} . The dramatic changes in the LF transition energies of **1c** in solution indicate significant structural perturbations of **1c** reflecting the flexibility of this $tBuPNHP$ complex. The Fe(II) species present in solution are best described as a distorted square pyramidal complex (11140 cm^{-1} band) as well as a species (9890 cm^{-1} band) with a reduced LF energy likely due to the potential distortions previously discussed for **1c** in the solid state (*vide supra*). Importantly, the NIR MCD data for **1c** demonstrates the significant structural changes that are possible in Fe(II) complexes supported by $RPNHP$ ligands between solid state and solution environments and indicates that the $tBuPNHP$ ligand in **1c** does not bind in the rigid fashion often invoked for pincer supported complexes.

III. Conclusions

For the first time, it has been demonstrated that $RPNHP$ -type pincer ligands are flexible both in solution and the solid state, providing further support for the hypothesis that the use of alkyl linkers in pincer ligands generates systems that are not rigid. It can be seen that solid-state structures of these compounds are

likely influenced by crystallization techniques, but solution-state structures appear similar across compounds regardless of preparation methods. Although more experiments must be performed to fully understand the link between the flexibility of the ligand and its substituents, these properties do appear to be linked. Future work will also aim to determine if there is a correlation between flexibility and reactivity.

IV. Experimental Details

General Methods

Experiments were performed under a dinitrogen or argon atmosphere in an M-Braun dry box or using standard Schlenk techniques unless otherwise noted. Under standard glovebox conditions purging was not performed between uses of pentane, diethyl ether, benzene, toluene and THF; thus when any of these solvents were used, traces of all these solvents were in the atmosphere. Moisture- and air-sensitive liquids were transferred by stainless steel cannula on a Schlenk line or in a dry box. The solvents for air- and moisture-sensitive reactions were dried by passage through a column of activated alumina followed by storage under dinitrogen or argon. All commercial chemicals were used as received except where noted. $^{iPr}PN^H P$,^{7c} $^{Cy}PN^H P$,¹⁸ and $^{iBu}PN^H P^{7m}$ were prepared using literature procedures. Anhydrous $FeCl_2$ was purchased from Aldrich and used as received. IR spectra were measured using a diamond smart orbit ATR on a Nicolet 6700 FT-IR instrument. Solution magnetic susceptibilities were determined by 1H NMR spectroscopy using the Evans method.¹⁹ Robertson Microlit Laboratories, Inc. performed the elemental analyses (inert atmosphere).

X-Ray Crystallography

Crystal samples were mounted in MiTeGen polyimide loops with immersion oil. Low-temperature diffraction data (ω -scans) were collected on either a Rigaku SCXMini diffractometer with a Rigaku CCD detector using filtered $MoK\alpha$ radiation ($\lambda = 0.71073 \text{ \AA}$) for $1a^{sp}$ and $1a^{tp}$ or a Rigaku MicroMax-007HF diffractometer coupled to a Saturn994+ CCD detector with $Cu K$. ($\lambda = 1.54178 \text{ \AA}$) for $1c$. All structures were solved by direct methods using SHELXS²⁰ and refined against F^2 on all data by full-matrix least squares with SHELXL-97²¹ using established refinement techniques.²² All hydrogen atoms were included into the model at geometrically calculated positions and refined using a riding model. The isotropic

displacement parameters of all hydrogen atoms were fixed to 1.2 times the U value of the atoms they are linked to (1.5 times for methyl groups).

⁵⁷Fe Mossbauer Spectroscopy

All solid samples for ⁵⁷Fe Mössbauer spectroscopy were run on non-enriched samples of the as-isolated samples. All samples were prepared in an inert atmosphere glove box equipped with a liquid nitrogen fill port to enable sample freezing to 77 K within the glove box. Each sample was loaded into a Delrin Mössbauer sample cup for measurements and loaded under liquid nitrogen. Low temperature Mössbauer measurements were performed using a See Co. MS4 Mössbauer spectrometer integrated with a Janis SVT-400T He/N₂ cryostat for measurements at 80 K with a 0.07 T applied magnetic field. Isomer shifts were determined relative to α -Fe at 298 K. All Mössbauer spectra were fit using the program WMoss (SeeCo). The errors for the Mössbauer parameters for the multi-component fits are the following: δ (± 0.02 mm/s), ΔE_Q (± 0.04 mm/s) and % contribution ($\pm 3\%$).

Magnetic Circular Dichroism Spectroscopy

All samples for MCD spectroscopy were prepared in an inert atmosphere glove box equipped with a liquid nitrogen fill port to enable sample freezing to 77 K within the glove box. MCD measurements of solid powders were performed on mulls prepared with fluorolube. Solution MCD samples were prepared in 1:1 (v:v) DCM-d₂:toluene-d₈ (to form low temperature optical glasses) in copper cells fitted with quartz disks and a 2 mm gasket. All solution measurements were performed on ~ 3 mM solutions of the corresponding (^RPN^HP)FeCl₂ complex. Low temperature Near-infrared (NIR) MCD data were collected with a Jasco J-730 spectropolarimeter and a liquid nitrogen cooled InSb detector. The MCD instrument utilizes a modified sample compartment incorporating focusing optics and an Oxford Instruments SM4000-7T superconducting magnet/cryostat. This set-up permits measurements from 1.6 K to 290 K with magnetic fields up to 7 T. A calibrated Cernox sensor directly inserted in the copper sample holder is used to measure the temperature at the sample to 0.001 K. All MCD spectra were baseline-corrected against zero-field scans.

Characterization of New Compounds

(^{iPr}PN^HP)FeCl₂ (1a)

To a suspension of 206 mg anhydrous FeCl₂ (1 eq, 1.6 mmol) in 7 ml THF was added 500 mg bis(diisopropylphosphinoethyl)amine (1 eq, 1.6 mmol) at 25°C. The solution was heated at reflux for 2 hours during which time **1a** precipitated as a white crystalline powder. The solution was allowed to cool to room temperature and the solid isolated by filtration. Crystals suitable for X-ray diffraction were grown from a saturated ACN solution at -30°C or a saturated THF solution at -30°C. Yield: 0.670 g (1.5 mmol, 93%).

Anal. found (calcd) for C₁₆H₃₇Cl₂FeNP₂: C, 44.50 (44.47); H, 8.81 (8.63); N, 3.44 (3.24). Magnetic susceptibility (CD₂Cl₂): 5.54 μ_B. IR (cm⁻¹): 3240, 2951, 2932, 2867, 1462, 1421, 1407, 1390, 1370, 1301, 1240, 1220, 1183, 1159, 1092, 1045, 929, 897, 821, 764, 692, 667, 640, 615, 549.

(^{Cy}PN^HP)FeCl₂ (1b)

To a solution of 740 mg of bis(dicyclohexylphosphinoethyl)amine (1 eq, 1.5 mmol) in 15 ml of THF was added 200 mg of anhydrous FeCl₂ (1 eq, 1.5 mmol) at 25°C. The solution was heated at reflux for 4 hours during which time **1b** precipitated as a white crystalline powder. The solution was allowed to cool to room temperature and **1b** was then isolated by filtration. Yield: 350 mg (0.5 mmol, 33%).

Anal. found (calcd): C, 56.14 (56.77); H, 8.61 (9.02); N, 2.26 (2.36). Magnetic susceptibility (CD₂Cl₂): 5.27 μ_B. IR (cm⁻¹): 3242, 2922, 2850, 1445, 1098, 1000, 884, 855, 800, 739, 672, 562, 511.

(^{tBu}PN^HP)FeCl₂ (1c)

To a solution of 1 g of bis(ditertbutylphosphinoethyl)amine (1 eq, 3.06 mmol) in 6ml of THF was added 386 mg (1 eq, 3.06 mmol) of anhydrous FeCl₂ at 25°C. The solution was heated at reflux for 16 hours during which time **1c** precipitated as a white crystalline powder. The solution was allowed to cool to room

temperature and the solid was then isolated by filtration. Crystals suitable for X-ray diffraction were grown from a saturated ACN/THF solution at -30°C. Yield: 1.00 g (2 mmol, 74%).

Anal. found (calcd) for $C_{20}H_{45}Cl_2FeNP_2$: C, 49.14 (49.20); H, 9.47 (9.29); N, 2.88 (2.87). Magnetic susceptibility (CD_2Cl_2): $5.34 \mu_B$. IR (cm^{-1}): 3216, 2937, 2863, 1479, 1467, 1389, 1369, 1176, 1129, 1076, 1054, 1020, 971, 933, 826, 813, 769, 690, 601, 577, 506.

V. Acknowledgements

I am very grateful to Dr. Timothy Schmeier for the original synthesis and crystallization conditions for compounds **1a-1c**. I am also grateful to Cassie Pan for conducting Evans' Method tests on these compounds. Finally, I am indebted to Professor Mike Neidig and his graduate student Kathlyn Fillman for their rigorous MCD and Mössbauer experiments, and for their patience in explaining these difficult techniques to me.

VI. References

- (a) Albrecht, M.; van Koten, G. *Angew. Chem., Int. Ed.* **2001**, *40*, 3750; (b) van der Boom, M. E.; Milstein, D. *Chem. Rev.* **2003**, *103*, 1759; (c) Leis, W.; Mayer, H. A.; Kaska, W. C. *Coord. Chem. Rev.* **2008**, *252*, 1787; (d) Benito-Garagorri, D.; Kirchner, K. *Acc. Chem. Res.* **2008**, *41*, 201; (e) Selander, N.; J. Szabó, K. *Chem. Rev.* **2010**, *111*, 2048; (f) Albrecht, M.; Lindner, M. M. *Dalton Trans.* **2011**, *40*, 8733.
- (a) McLoughlin, M. A.; Keder, N. L.; Harrison, W. T. A.; Flesher, R. J.; Mayer, H. A.; Kaska, W. C. *Inorg. Chem.* **1999**, *38*, 3223; (b) Tanaka, R.; Yamashita, M.; Nozaki, K. *J. Am. Chem. Soc.* **2009**, *131*, 14168; (c) Chakraborty, S.; Zhang, J.; Krause, J. A.; Guan, H. *J. Am. Chem. Soc.* **2010**, *132*, 8872; (d) Langer, R.; Diskin-Posner, Y.; Leitus, G.; Shimon, L. J. W.; Ben-David, Y.; Milstein, D. *Angew. Chem., Int. Ed.* **2011**, *50*, 9948.
- (a) Arashiba, K.; Miyake, Y.; Nishibayashi, Y. *Nat. Chem.* **2011**, *3*, 120; (b) Arashiba, K.; Sasaki, K.; Kuriyama, S.; Miyake, Y.; Nakanishi, H.; Nishibayashi, Y. *Organometallics* **2012**, *31*, 2035; (c) Hebden, T.; Schrock, R.; Takase, M.; Müller, P. *Chem. Commun.* **2012**, *48*, 1851.
- Choi, J.; MacArthur, A. H. R.; Brookhart, M.; Goldman, A. S. *Chem. Rev.* **2011**, *111*, 1761.

5) (a) McGuinness, D. S.; Gibson, V. C.; Wass, D. F.; Steed, J. W. *J. Am. Chem. Soc.* **2003**, *125*, 12716; (b) Britovsek, G. J. P.; Bruce, M.; Gibson, V. C.; Kimberley, B. S.; Maddox, P. J.; Mastroianni, S.; McTavish, S. J.; Redshaw, C.; Solan, G. A.; Stroemberg, S.; White, A. J. P.; Williams, D. J. *J. Am. Chem. Soc.* **1999**, *121*, 8728; (c) Small, B. L.; Brookhart, M.; Bennett, A. M. A. *J. Am. Chem. Soc.* **1998**, *120*, 4049.

6) Poyatos, M.; Mata, J. A.; Falomir, E.; Crabtree, R. H.; Peris, E. *Organometallics* **2003**, *22*, 1110.

7) (a) Danopoulos, A. A.; Edwards, P. G. *Polyhedron* **1989**, *8*, 1339; (b) Danopoulos, A. A.; Edwards, P. G.; Parry, J. S.; Wills, A. R. *Polyhedron* **1989**, *8*, 1767; (c) Danopoulos, A. A.; Wills, A. R.; Edwards, P. G. *Polyhedron* **1990**, *9*, 2413; (d) Bianchini, C.; Innocenti, P.; Peruzzini, M.; Romerosa, A.; Zanobini, F. *Organometallics* **1996**, *15*, 272; (e) Clarke, Z. E.; Maragh, P. T.; Dasgupta, T. P.; Gusev, D. G.; Lough, A. J.; Abdur-Rashid, K. *Organometallics* **2006**, *25*, 4113; (f) Choualeb, A.; Lough, A. J.; Gusev, D. G. *Organometallics* **2007**, *26*, 3509; (g) Bertoli, M.; Choualeb, A.; Lough, A. J.; Moore, B.; Spasyuk, D.; Gusev, D. G. *Organometallics* **2011**, *30*, 3479; (h) Rozenel, S. S.; Kerr, J. B.; Arnold, J. *Dalton Trans.* **2011**, *40*, 10397; (i) Rozenel, S. S.; Arnold, J. *Inorg. Chem.* **2012**, *51*, 9730; (j) McGuinness, D. S.; Wasserscheid, P.; Keim, W.; Hu, C.; Englert, U.; Dixon, J. T.; Grove, C. *Chem. Commun.* **2003**, 334; (k) McGuinness, D. S.; Wasserscheid, P.; Morgan, D. H.; Dixon, J. T. *Organometallics* **2005**, *24*, 552; (l) Schmeier, T. J.; Dobereiner, G. E.; Crabtree, R. H.; Hazari, N. *J. Am. Chem. Soc.* **2011**, *133*, 9274; (m) Meiners, J.; Friedrich, A.; Herdtweck, E.; Schneider, S. *Organometallics* **2009**, *28*, 6331; (n) Kaess, M.; Friedrich, A.; Drees, M.; Schneider, S. *Angew. Chem., Int. Ed.* **2009**, *48*, 905; (o) Friedrich, A.; Ghosh, R.; Kolb, R.; Herdtweck, E.; Schneider, S. *Organometallics* **2009**, *28*, 708; (p) Marziale, A. N.; Herdtweck, E.; Eppinger, J.; Schneider, S. *Inorg. Chem.* **2009**, *48*, 3699; (q) Friedrich, A.; Drees, M.; Schneider, S. *Chem. Eur. J.* **2009**, *15*, 10339; (r) Friedrich, A.; Drees, M.; auf der Günne, J. S.; Schneider, S. *J. Am. Chem. Soc.* **2009**, *131*, 17552; (s) Askevold, B.; Khusniyarov, M. M.; Herdtweck, E.; Meyer, K.; Schneider, S. *Angew. Chem., Int. Ed.* **2010**, *49*, 7566; (t) Askevold, B.; Nieto, J.; Tussupbayev, S.; Diefenbach, M.; Herdtweck, E.; Holthausen, M.; Schneider, S. *Nat. Chem.* **2011**, *3*, 532; (u) Friedrich, A.; Drees, M.; Käss, M.; Herdtweck, E.; Schneider, S. *Inorg. Chem.* **2010**, *49*, 5482; (v) Meiners, J.; Scheibel, M. G.; Lemee-Cailleau, M.-H.; Mason, S. A.; Boeddinghaus, M. B.; Faessler, T. F.; Herdtweck, E.; Khusniyarov, M. M.; Schneider, S. *Angew. Chem., Int. Ed.* **2011**, *50*, 8184; (w) Scheibel, M. G.; Askevold, B.; Heinemann, F. W.; Reijerse, E. J.; de Bruin, B.; Schneider, S. *Nat. Chem.* **2012**, *4*, 552; (x) Schneider, S.; Meiners, J.;

Askevold, B. *Eur. J. Inorg. Chem.* **2012**, 2012, 412; (y) Scheibel, M. G.; Wu, Y.; Stückl, A. C.; Krause, L.; Carl, E.; Stalke, D.; de Bruin, B.; Schneider, S. *J. Am. Chem. Soc.* **2013**, 135, 17719; (z) Marziale, A. N.; Friedrich, A.; Klopsch, I.; Drees, M.; Celinski, V. R.; auf der Günne, J. S.; Schneider, S. *J. Am. Chem. Soc.* **2013**, 135, 13342; (aa) Koehne, I.; Schmeier, T. J.; Bielinski, E. A.; Pan, C. J.; Lagaditis, P. O.; Bernskoetter, W. H.; Takase, M. K.; Würtele, C.; Hazari, N.; Schneider, S. *Inorg. Chem.* **2014**, 53, 2133; (ab) Nielsen, M.; Alberico, E.; Baumann, W.; Drexler, H.-J.; Junge, H.; Gladiali, S.; Beller, M. *Nature* **2013**, 495, 85; (ac) Alberico, E.; Sponholz, P.; Cordes, C.; Nielsen, M.; Drexler, H.-J.; Baumann, W.; Junge, H.; Beller, M. *Angew. Chem., Int. Ed.* **2013**, 52, 14162; (ad) Zhang, G.; Scott, B. L.; Hanson, S. K. *Angew. Chem., Int. Ed.* **2012**, 51, 11907; (ae) Zhang, G.; Vasudevan, K. V.; Scott, B. L.; Hanson, S. K. *J. Am. Chem. Soc.* **2013**, 135, 8668.

8) In fact to the best of our knowledge there are no conclusive examples of complexes with any pincer ligand being shown to exist as a mixture of meridional and facial isomers in solution under thermal control. There are two examples of complexes with pincer ligands being characterized by X-ray crystallography in both the meridional and facial configurations. For an example with an NNN ligand see Harkins, S.B.; Peters, J.C. *Inorg. Chem.* **2006**, 45, 4316, while for an example with an SPS ligand see Doux, M.; Mézailles, N.; Ricard, L.; Le Flock, P.; Vax, P.D.; Calhorda, M.J; Mahabiersing, T.; Hartl, F. *Inorg. Chem.* **2005**, 44, 9213. In both of these cases conversion between the isomers occurs photochemically. .

9) Fillman, K. Ph.D Thesis, University of Rochester, In Progress.

10) Fillman, K. L.; Bielinski, E. A.; Schmeier, T. J.; Nesvet, J. C.; Woodruff, T. M.; Pan, C. J.; Takase, M. K.; Hazari, N.; Neidig, M. L. *Inorg. Chem.* **2014**, 53, 6066.

11) Schmeier, T. J. Ph.D. Thesis, Yale University, 2013.

12) Langer, R.; Leitus, G.; Ben-David, Y.; Milstein, D. *Angew. Chem. Int. Ed.* **2011**, 50, 2120.

13) Addison, A. W.; Rao, T. N.; Reedijk, J.; van Rijn, J.; Verschoor, G. C. *J. Chem. Soc., Dalton Trans.* **1984**, 1349.

14) Farrugia, L. J. *J. Appl. Crystallogr.*, **45**, 849.

15) Crabtree, R. H., *The Organometallic Chemistry of the Transition Metals*. 5th ed.; Wiley, New York, **2009**.

- 16) Benito-Garagorri, D.; Alves, L. G.; Puchberger, M.; Mereiter, K.; Veiros, L. F.; Calhorda, M. J.; Carvalho, M. D.; Ferreira, L. P.; Godinho, M.; Kirchner, K. *Organometallics* **2009**, *28*, 6902.
- 17) (a) Solomon, E. I.; Pavel, E. G.; Loeb, K. E.; Campochiaro, C. *Coord. Chem. Rev.* **1995**, *144*, 369; (b) Whittaker, J. W.; Solomon, E. I. *J. Am. Chem. Soc.* **1988**, *110*, 5329; (c) Pavel, E. G.; Kitajima, N.; Solomon, E. I. *J. Am. Chem. Soc.* **1998**, *120*, 3949; (d) Solomon, E. I.; Brunold, T. C.; Davis, M. I.; Kemsley, J. N.; Lee, S.-K.; Lehnert, N.; Neese, F.; Skulan, A. J.; Yang, Y.-S.; Zhou, J. *Chem. Rev.* **2000**, *100*, 235; (e) Neidig, M. L.; Solomon, E. I. *Chem. Commun.* **2005**, 5843.
- 18) Abdur-Rashid, K.; Graham, T.; Tsang, C.-W.; Chen, X.; Guo, R.; Jia, W.; Amoroso, D.; Sui-Seng, C. (Kanata Chemical Technologies Inc., Canada). The Generation of Hydrogen from Ammonia Borane through Catalytic Hydrolysis. WO 2008141439 A1 20081127, **2008**.
- 19) Evans, D. F. *J. Chem. Soc.* **1959**, 2003.
- 20) Sheldrick, G. M. *Acta Crystallogr. A* **1990**, *A 46*, 467.
- 21) Sheldrick, G.M. *Acta Crystallogr. A* **2008**, *64*, 112.
- 22) Müller, P. *Crystallogr. Rev.* **2009**, *15*, 57.

Chapter 3: Lewis Acid-Assisted Formic Acid Dehydrogenation Using a Pincer-Supported Iron Compound

I. Introduction

The continued burning of fossil fuels for energy has contributed to the significant increase in atmospheric levels of CO₂ and global temperature.¹ As the world population and subsequent energy demands continue to increase, the search for alternative energy sources has become a growing area of research. Several approaches are currently under investigation to replace fossil fuels as energy vectors,² such as H₂ gas, which can be directly or electrochemically combusted within a proton-exchange membrane fuel cell, producing water as the only byproduct.³ However, as a result of problems with the storage of gaseous H₂ and its low volumetric energy density, chemical H₂ storage (CHS) based on the reversible (de)hydrogenation of small molecules is an attractive alternative.⁴ Formic acid (FA) can be obtained renewably from biomass oxidation or CO₂ hydrogenation and is a potential liquid CHS material.⁴ Several heterogeneous⁴⁻⁵ and homogeneous⁶ catalysts have been reported that can dehydrogenate FA to a mixture of H₂ and CO₂, which is directly suitable as a feed for fuel cells.⁷ The most active systems are based on expensive precious metals such as Ir,^{6d,6g,6h,6j,6m} Ru,^{6a,6b,6e,6i} Au,^{5b,5c} Ag,^{5a,5d,5f} and Pd.^{5c,5e} In addition, in order to achieve high turnover numbers (TON) many of the best homogeneous catalysts require either the addition of base or have a pendant base incorporated into the ligand framework.^{6a-k,6m} A more detailed discussion of highly active catalytic systems can be found in Chapter 1.

Recently, the first homogeneous Fe-based systems for FA dehydrogenation were reported.^{6f,6k,6o} Milstein and co-workers reported TONs of up to 100,000 using a pincer supported system, in the presence of 50 mol% NEt₃.^{6k} Additionally, Beller *et al.* described an Fe catalyst which requires extra equivalents of the tetradentate auxiliary ligand and gives approximately 92,000 TON.^{6o} Although these results with first row transition metal catalysts are promising, the TON and turnover frequencies (TOF) are still inferior to those achieved with precious metal catalysts, and the role of the additives in the catalytic reactions are unclear.

Previously, pincer ligands of the type HN{CH₂CH₂(PⁱPr₂)₂}₂ (ⁱPrPN^HP) were utilized to support Ir catalysts for CO₂ hydrogenation⁸ and Ru catalysts for ammonia borane dehydrogenation.⁹ Furthermore, the same ligand was used to support Fe complexes,¹⁰ which are related to catalysts for methanol dehydrogenation with strong base,¹¹ ester¹² and ketone¹³ hydrogenation and the de-/hydrogenation of N-heterocycles.¹⁴

Chapter 2 discussed the study of a related series of ($R\text{PN}^H\text{P}$)Fe¹⁵ compounds. This chapter outlines the synthesis and characterization of ($R\text{PN}^H\text{P}$)Fe compounds and their use as catalysts for FA dehydrogenation without additional base or ligand. Instead, the strong effect of Lewis Acid (LA) co-catalysts, which enabled TON of almost 1,000,000, is investigated.

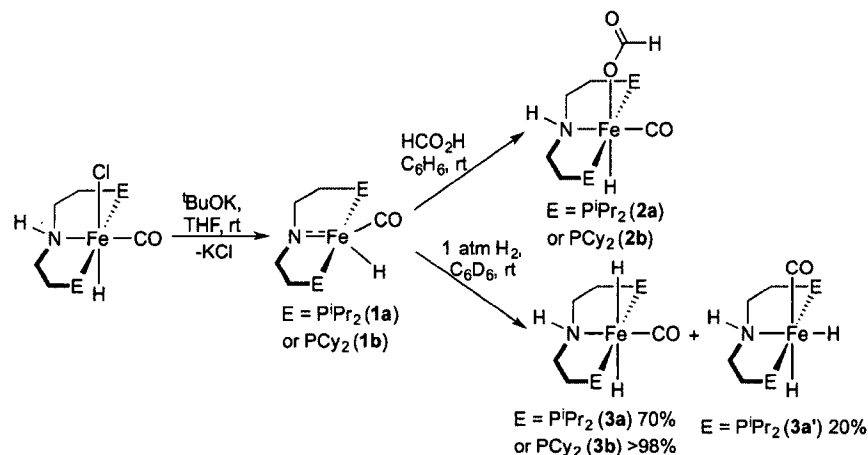
II. Results and Discussion

This work has been previously published.¹⁶ The synthesis of ($i\text{PrPN}^H\text{P}$)Fe(CO)H(Cl) was originally reported by Dr. Timothy Schmeier.¹⁵ Cassie Pan was integral in the development of the synthesis of (CyPN^HP)Fe(CO)H(Cl) ($\text{CyPN}^H\text{P} = \text{HN}\{\text{CH}_2\text{CH}_2(\text{PCy}_2)\}_2$). Dr. Paraskevi Lagaditis developed the synthesis of and provided characterization data for ($i\text{PrPNP}$)Fe(CO)H (**1a**) ($i\text{PrPNP} = \text{N}\{\text{CH}_2\text{CH}_2(\text{P}^i\text{Pr}_2)\}_2$).

The 5-coordinate amido complexes ($i\text{PrPNP}$)Fe(CO)H (**1a**) and (CyPNP)Fe(CO)H (**1b**; $\text{CyPNP} = \text{N}\{\text{CH}_2\text{CH}_2(\text{PCy}_2)\}_2$) were synthesized through the dehydrohalogenation of ($R\text{PN}^H\text{P}$)Fe(CO)H(Cl)^{10a} ($R = i\text{Pr}$ or Cy) with 1.2 eq. of $t\text{BuOK}$ (Scheme 3.01). The complexes are isolable as deep red solids and are indefinitely stable at room temperature under a nitrogen atmosphere. The molecular structures of **1a** and **1b** in the solid state are shown in Figure 3.01. The parameter τ can be used to describe the degree to which a five-coordinate compound deviates from either ideal square pyramidal ($\tau = 0$) or trigonal bipyramidal ($\tau = 1$) geometry.¹⁷ In both cases, the coordination of the metal ion can best be described as *pseudo*-trigonal bipyramidal with the phosphorus atoms in the apical position and $\tau = 0.31$ for **1a** and $\tau = 0.20$ for **1b**. The successful deprotonation of the N-H bond is also confirmed by the solid-state structures. The Fe(1)-N(1) bond length in **1a** is 1.884(2) Å, a significant contraction from 2.255(3) Å, as seen in ($i\text{PrPN}^H\text{P}$)Fe(Cl)₂, the analogous 5-coordinate compound in which the pincer N-H bond is retained.^{10b} The same contraction in bond length is seen for **1b**, where Fe(1)-N(1) is 1.8559(18) Å. Furthermore, there is a Y-shape distortion, as a consequence of strong $\text{N} \rightarrow \text{Fe}$ π -donation, which is typical for five-coordinate d^6 ions with one strongly π -donating ligand.¹⁸ Hence, **1a** and **1b** are 18 valence electron compounds with low spin ground states, which is a prerequisite for the formation of stable hydrides.¹⁹

The reaction of FA with both **1a** and **1b** results in 1,2-addition across the Fe amide bond to generate ($i\text{PrPN}^H\text{P}$)Fe(CO)H(COOH) (**2a**) and (CyPN^HP)Fe(CO)H(COOH) (**2b**) (Scheme 3.01). The ¹H NMR

resonances at 9.10 (**2a**) and 9.20 ppm (**2b**), respectively, are characteristic of coordinated formate ligands,^{8,21} while signals assignable to the hydride ligands are found at -25.71 (**2a**) and -25.82 ppm (**2b**), respectively.



Scheme 3.01. Synthesis and reactivity of 5-coordinate Fe amido species.

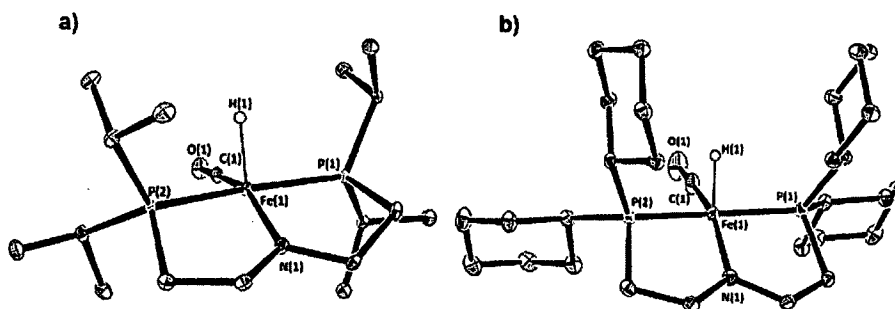


Figure 3.01. a) ORTEP²⁰ of (ⁱPrPNP)Fe(CO)H (**1a**). Hydrogen atoms (apart from Fe-H) are removed for clarity. Ellipsoids are shown at 30% probability. Selected bond lengths (Å) and angles (°): Fe(1)-C(1) 1.722(2), Fe(1)-N(1) 1.844(2), Fe(1)-P(1) 2.1800(5), Fe(1)-P(2) 2.1727(5), Fe(1)-H(1) 1.46(3), C(1)-O(1) 1.171(2), C(1)-Fe(1)-N(1) 151.70(8), C(1)-Fe(1)-P(1) 96.28(6), N(1)-Fe(1)-P(1) 85.73(5), C(1)-Fe(1)-P(2) 93.08(6), N(1)-Fe(1)-P(2) 85.57(5), P(1)-Fe(1)-P(2) 170.59(2), C(1)-Fe(1)-H(1) 84(1), N(1)-Fe(1)-H(1) 124(1), P(1)-Fe(1)-H(1) 92(1), P(2)-Fe(1)-H(1) 90(1), O(1)-C(1)-Fe(1) 177.5(3). b) ORTEP²⁰ of (^{Cy}PNP)Fe(CO)H (**1b**). Hydrogen atoms (apart from Fe-H) are removed for clarity. Ellipsoids are shown at 30% probability. Selected bond lengths (Å) and angles (°): Fe(1)-C(1) 1.715(3), Fe(1)-N(1) 1.8559(18), Fe(1)-P(1) 2.1713(6), Fe(1)-P(2) 2.1778(6), Fe(1)-H(1) 1.44(2), C(1)-O(1) 1.178(3), C(1)-Fe(1)-N(1) 153.11(11), C(1)-Fe(1)-P(1) 97.67(8), N(1)-Fe(1)-P(1) 85.40(6), C(1)-Fe(1)-P(2) 95.56(8), N(1)-Fe(1)-P(2) 85.88(6), P(1)-Fe(1)-P(2) 165.11(3), C(1)-Fe(1)-H(1) 83.2(9), N(1)-Fe(1)-H(1) 123.7(9), P(1)-Fe(1)-H(1) 88.6(9), P(2)-Fe(1)-H(1) 86.2(9), O(1)-C(1)-Fe(1) 177.6(2).

Both the amides (**1a/1b**) and the formate complexes (**2a/2b**) were tested for the catalytic dehydrogenation of FA under the reaction conditions described by Milstein, using 50 mol% NEt₃ as an additive. At a relatively high catalyst loading (0.1 mol%) and 80°C in dioxane **1a**, **1b**, **2a** and **2b** gave comparable activity to the Fe systems reported by Beller^{6o} and Milstein^{6k} (Table 3.01). In all cases, the gas mixture produced from catalysis was analyzed by Gas Chromatography (GC) and found to be a 1:1 mixture of H₂ and CO₂ with less than 0.5% CO. This is comparable to the amount of CO observed in Beller's best Fe system.^{6f}

Table 3.01. FA dehydrogenation using **1a**, **1b**, **2a** and **2b**.^a

$$\text{HCO}_2\text{H} \xrightarrow[\text{Temp, Solvent}]{\substack{0.1 \text{ mol\% cat} \\ 50 \text{ mol\% NEt}_3}} \text{H}_2 + \text{CO}_2$$

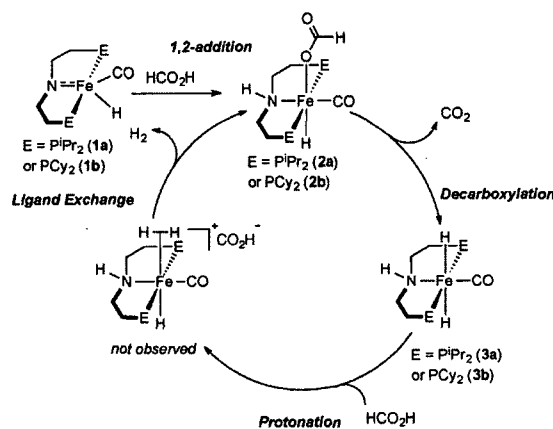
Catalyst	THF, 40°C		Dioxane, 80°C	
	TOF (hr ⁻¹) ^b	TON (Time) ^c	TOF (hr ⁻¹) ^b	TON (Time) ^c
1a	170	350 (5.5 hr)	530	910 (4.5 hr)
1b	220	270 (6 hr)	570	880 (2.5 hr)
2a	240	460 (6 hr)	620	>999 (3 hr)
2b	180	900 (7.5 hr)	740	990 (2.5 hr)

^aReaction conditions: FA (110 μL, 2.91 mmol), catalyst (2.91 μmol, 0.10 mol%), 50 mol% NEt₃, 5 mL solvent. ^bTOF was measured after the first hour. ^cTON was measured using a gas burette. All numbers are an average of two runs.

Further information about catalysis was obtained through stoichiometric reactions. The reactions of **1a/1b** with a 1:1 mixture of 1 atm H₂:CO₂ at room temperature resulted in clean formation of the formate compounds **2a/2b**. This reaction most likely proceeds via initial heterolytic cleavage of H₂, followed by CO₂ insertion into the Fe-H bond. Accordingly, in the absence of CO₂, **1a/1b** rapidly add H₂ (1 atm) to give the *trans*-dihydride complexes **3a/3b** as the main products (Scheme 3.01). This reaction is fully reversible, which prevents isolation of **3a/3b** due to facile H₂ loss. The *trans*-H₂ configuration is supported by the characteristic ¹H NMR chemical shifts (-9.57 & -9.69 ppm (**3a**); -9.29 & -9.37 ppm (**3b**)) and the mutual coupling constant of the hydride signals (²J_{HH} = 9.7 Hz for **3a** and 9.5 Hz for **3b**).¹³ In the case of **1a**, smaller amounts of the *cis*-H₂ complex **3a'** (Scheme 3.01) are also observed, based on the hydride chemical shifts (-8.63 and -21.13 ppm), hyperfine structure (²J_{HH} = 15 Hz) and NOESY spectrum.²² ¹H EXSY NMR spectroscopy, performed by Dr. Paraskevi Lagaditis, indicates intramolecular hydride exchange within **3a'** and intermolecular exchange of **3a** and **3a'**. Besides these main products, minor quantities of free ⁱPrPN^HP (7 %) and the Fe(0) complex (ⁱPrPN^HP)Fe(CO)₂^{10a} (3 %) are immediately formed. Over the course of several

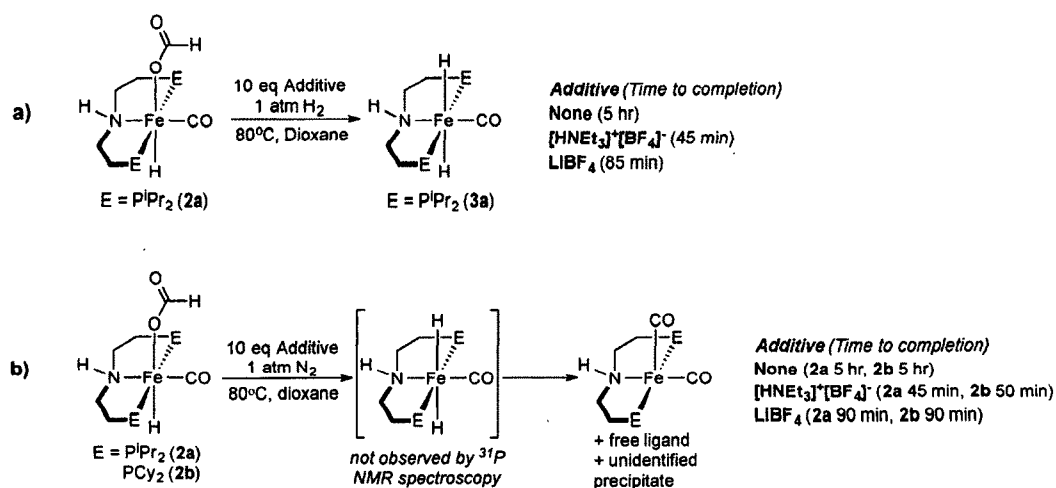
days, **3a** and **3a'** slowly convert to $(iPrPN^H P)Fe(CO)_2$, free $iPrPN^H P$ and an intractable precipitate. In contrast, presumably due to steric factors, the reaction of **1b** with H_2 results in the formation of only the *trans*-dihydride **3b** (Scheme 3.01). **3b** is also only moderately stable and slowly decomposes to free $CyPN^H P$, $(CyPN^H P)Fe(CO)_2$ and an intractable precipitate in solution.

Based on these results, a mechanism for FA dehydrogenation is proposed (Scheme 3.02). The 5-coordinate complexes **1a/1b** can enter the catalytic cycle through addition of FA (Scheme 3.01) to give the formate complexes **2a/2b**, which are part of the proposed cycle. Subsequent decarboxylation forms dihydrides **3a/3b**, in part the reverse of stoichiometric formation of **2a/2b** from **1a/1b** with H_2 and CO_2 . Accordingly, **3a/3b** are formed in high yield upon heating **2a/2b** at $80^\circ C$ in dioxane under H_2 (1 atm) (Scheme 3.03a). In the absence of H_2 , complete conversion to $(R^H PN^H P)Fe(CO)_2$ ($R = iPr$ or Cy), the appropriate free ligand and an unidentified precipitate was observed (Scheme 3.03b). These products are consistent with the initial formation of **3a/3b** and subsequent decomposition in the absence of H_2 . In the proposed cycle, regeneration of **2a/2b** and liberation of H_2 occurs through the reaction of **3a/3b** with FA, also confirmed stoichiometrically. This reaction may involve the formation of molecular H_2 complexes, but species of this type were not observed spectroscopically. The catalyst resting state was identified as the formate complexes **2a/2b** using *in situ* ^{31}P NMR spectroscopy. This observation is consistent with decarboxylation being the turnover-limiting step.



Scheme 3.02. Proposed mechanism of FA dehydrogenation.

The stoichiometric studies confirm the feasibility of each step in the absence of NEt_3 , yet the presence of base greatly increases catalyst activity (Table 3.03, Entry 1). A variety of other bases including pyridine and $^t\text{BuOK}$ also promote the catalytic reaction (Table 3.02). In the case of NEt_3 , this is presumably through the action of HNEt_3^+ formed under the catalytic conditions via the reaction of NEt_3 with excess FA. Accordingly, the rate of decarboxylation of **2a/2b**, the proposed turnover-limiting step, is significantly increased in the presence of $[\text{HNEt}_3]^+[\text{BF}_4]^-$ (Scheme 3.03).



Scheme 3.03. Effect of additives on the decarboxylation of **2** under a) H_2 and b) N_2 .

Table 3.02. Base Screening for FA dehydrogenation catalyzed by **2a** and **2b**.^a

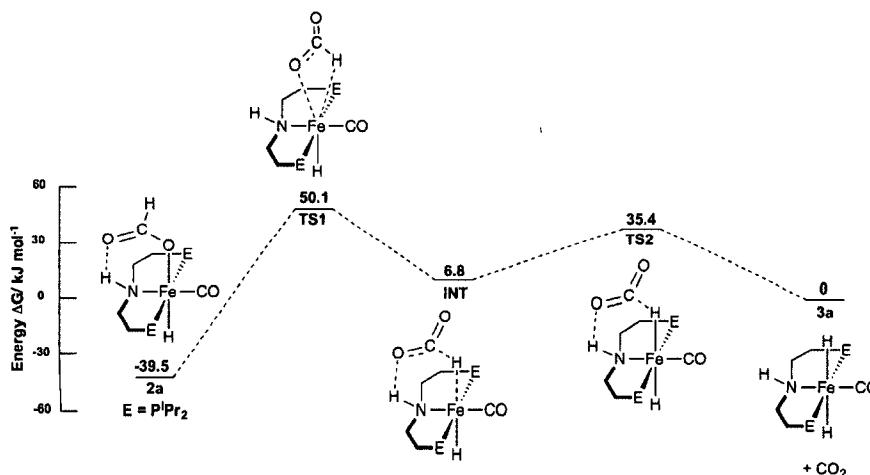
$$\text{HCO}_2\text{H} \xrightarrow[\text{50 mol\% Base, 80}^\circ\text{C, dioxane}]{\text{0.1 mol\% 2a or 2b}} \text{H}_2 + \text{CO}_2$$

Base	2a	2b
	TON ^b (Time) ^c	TON ^b (Time)
NEt_3	>999 (3 hr)	990 (2.5 hr)
KHMDs^d	890 (13 hr)	>999 (15 hr)
Pyridine	750 (16 hr)	940 (16 hr)
DBU^e	530 (10 hr)	550 (9 hr)
Cs_2CO_3	360 (4.5 hr)	480 (6 hr)
$^t\text{BuOK}$	800 (5.5 hr)	270 (8 hr)
MeCN	190 (1.5 hr)	100 (1 hr)

^aReaction conditions: FA (110 μL , 2.91 mmol), complex **2a** or **2b** (2.91 μmol , 0.10 mol%), 50 mol% base, 5 mL dioxane, 80°C. ^bTON measured by gas burette. All numbers are an average of two runs. ^cTime taken for reaction to reach completion or stop turning over. ^dKHMDs = Potassium bis(trimethylsilyl)amide. ^eDBU = 1,8-Diazabicyclo[5.4.0]undec-7-ene.

Although the decarboxylation is a formal β -hydride elimination reaction, the absence of a vacant coordination site on Fe requires an indirect pathway. Recently, Milstein and co-workers suggested that

decarboxylation in a related Fe pincer system proceeds via intramolecular rearrangement to an H-bound formate followed by CO₂ elimination.^{6k} DFT studies on **2a** support this mechanism (Scheme 3.04), with rate determining, initial rearrangement. Analysis of the transition state for intramolecular rearrangement and the H-bound formate intermediate indicates significant buildup of negative charge on the carboxylate group. Hence, Brønsted acids, like HNEt₃⁺, can presumably stabilize these species through hydrogen bonding. A pathway in which the formate ligand of **2a** rearranges to the H-bound formate via dissociation into solution was also calculated. This pathway would generate an unsaturated Fe complex and free formate in solution. However, this pathway can be discounted due to the extremely high energy (215 kJ mol⁻¹ higher than **3a**) of the intermediates.



Scheme 3.04. DFT calculated pathway for the decarboxylation of **2a**.

Recently, it was demonstrated that LAs facilitate β -hydride elimination in nickelalactones by stabilizing negatively charged carboxylate groups.²³ Similarly, addition of catalytic amounts of LA (10 mol%) promotes FA dehydrogenation with catalysts **2a/2b** (Table 3.03). A complete LA screen was performed for **2a**, the catalyst showing superior activity under conditions shown in Tables 3.02 and 3.03. However, **2b** was also tested using several LA and demonstrated comparable activity. In general, the highest TON and TOF are achieved with alkali or alkali earth metal salt co-catalysts. Importantly, the enhancement of activity correlates with the chemical affinity for carboxylate, with the best results obtained for Li⁺ (entries 7-12). Weakly coordinating anions, such as BF₄⁻, are preferred as anions (entries 3-7). LiBF₄ (entry 13) results in the most rapid completion of the reaction; however, full conversion is also obtained with much

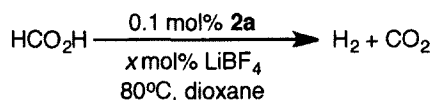
cheaper additives, such as NaCl. Additionally, the amount of LA affected the overall performance of the catalytic system, with the optimal loading of LA being 10 mol%. A decrease in efficiency is seen at both lower and higher loadings (Table 3.04).

Table 3.03. LA screening for FA dehydrogenation using **2a/2b**.^a

$$\text{HCO}_2\text{H} \xrightarrow[\text{80}^\circ\text{C, dioxane}]{\text{0.1 mol\% 2a or 2b, 10 mol\% LA}} \text{H}_2 + \text{CO}_2$$

Entry	LA	TOF (hr ⁻¹) ^b		TON (Time) ^c	
		2a	2b	2a	2b
1	No additive ^d	-	-	180 (48 hr)	-
2	B(C ₆ F ₅) ₃	230	200	640 (12.5 hr)	600 (13 hr)
3	HCOONa ^e	260	-	> 999 (7.5 hr)	-
4	NaPF ₆	150	150	450 (9 hr)	430 (9.5hr)
5	NaBAR ^f ₄	190	-	990 (8 hr)	-
6	NaBF ₄	320	-	> 999 (6.5 hr)	-
7	NaCl	260	250	> 999 (7.5 hr)	>999 (7.5 hr)
8	LiCl	270	-	> 999 (7 hr)	-
9	KCl	130	-	670 (8.5 hr)	-
10	CsCl	110	-	> 999 (7 hr)	-
11	CaCl ₂	130	-	390 (23 hr)	-
12	MgCl ₂	260	-	> 999 (8 hr)	-
13	LiBF ₄	230	190	> 999 (4 hr)	>999 (4.5 hr)

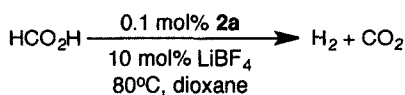
^aReaction conditions: FA (110 μL, 2.91 mmol), **2a/2b** (2.91 μmol, 0.10 mol%), LA (0.291 mmol, 10 mol%), 5mL dioxane, 80°C. ^bTOF were measured after the first hour. ^cTON were measured using a gas burette. All numbers are an average of two runs. ^dReaction performed in the absence of LA or base. ^e9:1 FA:HCOONa. ^fBAR₄^f = B{3,5-(CF₃)₂C₆H₃}₄.

Table 3.04. Effect of LA loading on FA dehydrogenation catalyzed by **2a**.^a

Entry	mol% LiBF ₄	TOF ^b (hr ⁻¹)	TON ^c (Time)
1	1	140	500 (10.5 hr)
2	5	180	>999 (16 hr)
3	10	230	>999 (4 hr)
4	20	230	>999 (4.5 hr)

^aReaction conditions: FA (110 μL , 2.91 mmol), complex **2a** (2.91 μmol , 0.10 mol%), LiBF₄, 5 mL dioxane, 80°C. ^bTOF measured after the first hour. ^cTON measured by gas burette. All numbers are an average of two runs.

A series of standard tests suggest that homogeneous catalysis is occurring.²⁴ During catalysis, the reaction maintained a pale yellow color, with no darkening of the solution or formation of precipitate. Furthermore, gas production began immediately with heating, indicating the active catalyst does not require an induction period. Mercury drop tests also indicated that the addition of elemental mercury did not affect the overall catalysts.²⁵ Finally, quantitative poisoning tests with PMe₃ (Table 3.05) indicate sub-stoichiometric amounts of PMe₃ do not affect catalysis (Table 3.05, entries 1 and 2). However, the addition of excess PMe₃ shuts down catalysis, indicating that poisoning of a homogeneous system is occurring upon irreversible binding of PMe₃ (Table 3.05, entry 3).²⁴

Table 3.05. Quantitative poisoning of FA dehydrogenation catalyzed by **2a**.^a

Entry	Equivalents PMe ₃	TOF ^b (hr ⁻¹)	TON ^c (Time)
1	0.10 (0.291 μmol)	250	>999 (4 hr)
2	1 (2.91 μmol)	240	>999 (4.5 hr)
3	20 (58.2 μmol)	230	230 (1 hr)

^aReaction conditions: FA (110 μL , 2.91 mmol), complex **2a** (2.91 μmol , 0.10 mol%), LiBF₄ (0.291 mmol, 10 mol%), PMe₃, 5 mL dioxane, 80°C. ^bTOF measured after the first hour. ^cTON measured by gas burette. All numbers are an average of two runs.

When NEt₃ is used as an additive with **2a/2b** at low catalyst loadings, low yields are obtained. Using 0.01 mol% **2a**/50 mol% NEt₃ gave a TON of only 2400 (6.5 hr). In contrast, complete substrate conversion was obtained using 0.01 mol% **2a**/10 mol% LA (NaCl, NaBF₄ or LiBF₄), with LiBF₄ again giving the fastest time to completion (Table 3.06). In fact, with catalyst loadings as low as 0.0001 mol% **2a**, a TON of >980,000 and TOF of 200,000 hr⁻¹ are obtained (Table 3.06, entry 6). These are comparable with the

highest TON^{6l} and TOF^{6d,6g,6h,6j} obtained with precious metal systems, without the need for a complicated ligand or external base (*vide infra*).

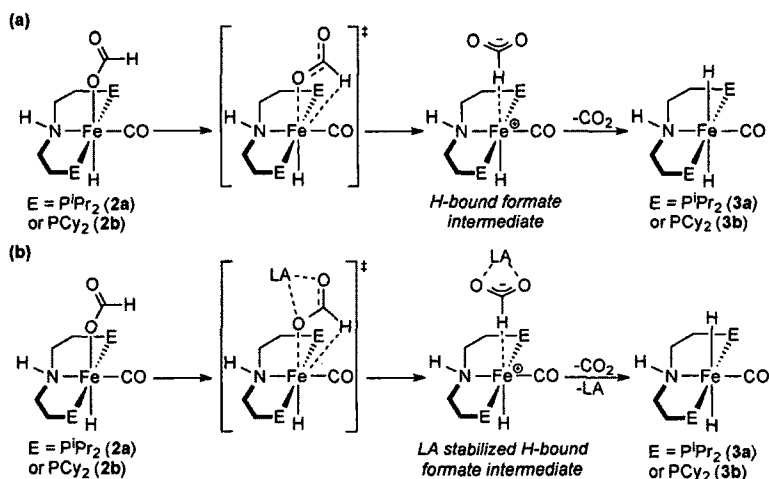
Table 3.06. Optimization of catalytic dehydrogenation of FA using **2a**.

$$\text{HCO}_2\text{H} \xrightarrow[\text{10 mol\% LiBF}_4, \text{80}^\circ\text{C, dioxane}]{\text{2a}} \text{H}_2 + \text{CO}_2$$

Entry	LA	mol% 2a	TOF (hr ⁻¹) ^b	TON (Time) ^c
1	CsCl	0.01	1440	7500 (15 hr)
2	NaCl	0.01	2200	> 9900 (7 hr)
3	NaBF ₄	0.01	1600	> 9900 (6 hr)
4	LiBF ₄	0.01	1800	> 9900 (5.5 hr)
5	LiBF ₄	0.001	21,000	93000 (6.5 hr)
6	LiBF ₄	0.0001	200,000 ^d	>980,000 (9.5 hr) ^d

^aReaction conditions: FA (110 μL , 2.91 mmol), **2a**, LA (0.291 mmol, 10 mol%), 5 mL dioxane, 80°C. ^bTOF were measured after the first hour. ^cTON were measured using a gas burette. All numbers are an average of two runs. ^dAverage of four runs.

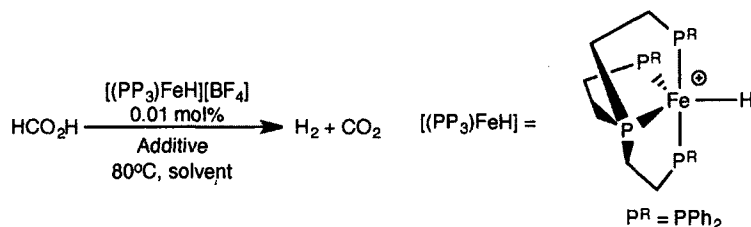
The LA effect was examined by monitoring the rate of decarboxylation of **2a/2b**, the proposed turnover-limiting step in catalysis, in the presence of 10 eq. of LiBF₄ (Scheme 3.03). A large increase in rate was observed compared to a reaction without an additive. However, a slightly slower rate was observed compared to when [HNEt₃]⁺[BF₄]⁻ was present, consistent with faster catalysis using NEt₃. It is proposed that the LA increases the rate by stabilizing the transition state to the H-bound formate (Scheme 3.05b).



Scheme 3.05. Proposed mechanism of β -hydride elimination a) in the absence of a LA and b) in the presence of a LA.

The utility of LA-promoted FA dehydrogenation for other catalysts was also examined. For example, with Beller's best catalyst, $[(PP_3)FeH][BF_4]^-$ ($PP_3 = P(CH_2CH_2PPh_3)_3$),^{6f} poor catalytic activity was obtained under the current conditions (80°C, dioxane) in the absence of a co-catalyst (Table 3.07). The addition of 10 mol% $LiBF_4$ or $NaBAR^F_4$ results in enhancement under both sets of conditions (80°C, propylene carbonate) and eliminates the need for excess ligand to achieve high activity.

Table 3.07. Application of LA assistance in FA dehydrogenation using Beller's system.



Solvent	No Additive		10 mol% $LiBF_4$		10 mol% $NaBAR^F_4$	
	TOF ^b (hr ⁻¹)	TON ^c (Time)	TOF ^b (hr ⁻¹)	TON ^c (Time)	TOF ^b (hr ⁻¹)	TON ^c (Time)
PC ^d	1000	>9900 (8.5 hr)	1500	>9900 (7 hr)	1900	>9900 (5 hr)
Dioxane	730	730 (1 hr)	1800	>9900 (6.5 hr)	2100	>9900 (5 hr)

^aReaction conditions: FA (110 μ L, 2.91 mmol), $[(PP_3)FeH][BF_4]$ (0.291 μ mol, 0.01 mol%), 10 mol% $LiBF_4$ or $NaBAR^F_4$, 5 mL solvent, 80°C. The catalyst $[(PP_3)FeH][BF_4]$ was synthesized according to literature methods.^{6f} ^bTOF measured after the first hour. ^cConversion measured by gas burette. All numbers are an average of two runs. ^dPC= propylene carbonate.

III. Conclusions

Previous systems for transition-metal catalyzed FA dehydrogenation have generally required the use of noble metal catalysts, often with expensive and complicated ligand frameworks. Furthermore, the requirement for an excess amount of added base was not understood from a mechanistic standpoint. For the first time, a first row transition metal catalyst is able to effect FA dehydrogenation in the absence of an added base. Additionally, mechanistic studies and stoichiometric reactivity have elucidated that the role of this base is to stabilize the transition state of a rate-limited decarboxylation. The replacement of this base with a LA has allowed for significant enhancement in not only catalyst stability, but also overall turnover number, and allowed nearly 1,000,000 turnovers for FA dehydrogenation using an Fe catalyst. Furthermore, this LA affect was found to be operative in not only this system, but also using Fe catalysts previously reported in the literature. In the future, understanding of the mechanism of this decarboxylation step will allow for better-designed catalysts and optimized systems for not only FA dehydrogenation, but also other acids and alcohols of interest for reversible hydrogen storage.

IV. Experimental Details

General Methods

Experiments were performed under a dinitrogen or argon atmosphere in a dry box or using standard Schlenk techniques, unless otherwise noted. Under standard dry box conditions, purging was not performed between uses of pentane, diethyl ether, benzene, toluene and THF; thus, when any of these solvents were used, traces of all these solvents were in the atmosphere and could be found intermixed in the solvent bottles. Moisture- and air-sensitive liquids were transferred by stainless steel cannula on a Schlenk line or in a dry box. Solvents were dried by passage through a column of activated alumina followed by storage under dinitrogen or argon. All commercial chemicals were used as received, except where noted. Anhydrous carbon dioxide, hydrogen, and a 1:1 mixture of carbon dioxide and hydrogen were purchased from Airgas, Inc and were used as received. Potassium *tert*-butoxide, potassium bis(trimethylsilyl)amide (KHMDS), tris(pentafluorophenyl)borane, sodium hexafluorophosphate, calcium chloride and magnesium chloride were purchased from Fisher Scientific Company. 1,8-Diazabicycloundec-7-ene (DBU) and pyridine were purchased from Fischer Scientific Company and degassed and distilled prior to use. Cesium carbonate and sodium formate were purchased from Alfa Aesar. Sodium chloride, lithium chloride, potassium chloride, cesium chloride and lithium tetraphenylborate were purchased from Acros. Formic acid was dried over phthalic anhydride, and triethylamine and 1,4-dioxane were dried over CaH₂ and distilled prior to use. Propylene carbonate was purchased from Sigma Aldrich and degassed prior to use. Deuterated solvents were obtained from Cambridge Isotope Laboratories or Euriso-Top GmbH. C₆D₆ was dried over sodium metal and vacuum-transferred prior to use. Literature procedures were used to prepare sodium tetrakis[(3,5-trifluoromethyl)phenyl]borate (NaBAr^F₄),²⁶ triethylammonium tetrafluoroborate,²⁷ (ⁱPrPN^HP)FeCl₂,^{10b} (^{Cy}PN^HP)FeCl₂,^{10b} (^tBuPN^HP)FeCl₂,^{10b} (ⁱPrPN^HP)Fe(CO)H(Cl),^{10a} (^{Cy}PN^HP)Fe(CO)H(Cl)^{10a} and (ⁱPrPN^HP)Fe(CO)H(BH₄).^{10a} NMR spectra were recorded on Bruker AMX-400, AMX-500, AMX-600, Avance III 300 or Avance 400 spectrometers at ambient probe temperatures, unless otherwise noted. Chemical shifts are reported in ppm with respect to residual internal protio solvent for ¹H and ¹³C{¹H} NMR spectra and to an external standard for ³¹P{¹H} (85% H₃PO₄ at 0.0 ppm); *J* values are given in Hz. Elemental analysis was performed by Robertson Microlit Laboratories, Inc or by the Analytical Laboratories at the Georg-August University (Göttingen, Germany). IR spectra were measured

using diamond smart orbit ATR on a Nicolet 6700 FT-IR instrument or as nujol mull between KBr plates on a Bruker Vertex 70 FT/IR Spectrometer. UV-vis spectra were measured using a Cary 50 spectrophotometer.

X-ray Crystallography

Crystal samples were mounted in a MiTeGen polyimide loop with immersion oil. The diffraction experiments were carried out on a Rigaku MicroMax-007HF diffractometer coupled to a Saturn994+ CCD detector with Cu K α radiation ($\lambda = 1.54178 \text{ \AA}$) (**1b**). For **1b** the data were processed using Rigaku CrystalClear²⁸ and corrected for Lorentz and polarization effects. The structure was solved by direct methods²⁹ and expanded using Fourier techniques.³⁰ The full-matrix least-squares refinement was carried out on F² using SHELXTL NT 6.12.³¹ All non-hydrogen atoms were refined with anisotropic displacement parameters. The C-H hydrogen atoms were refined isotropically on calculated positions by using a riding model with their U_{iso} values constrained to 1.5 U_{eq} of their pivot atoms for terminal sp³ carbon atoms and 1.2 times for all other carbon atoms. The Fe-H hydrogen atoms were found and isotropically refined.

Gas Chromatography

Gas chromatography experiments were performed on a Buck Scientific 910 Gas Chromatograph with FID/TCD and methanizer. The system uses N₂ as a carrier gas and allows for determination of the following gases at the detection limits:

H₂ \geq 100 ppm

CO \geq 1 ppm

CO₂ \geq 1 ppm

DFT Calculations

All geometry optimizations were performed using Gaussian 09 Revision A.02,³² using the m06l functional. The LANL2DZ basis set was used for Fe and the 6-31G++(d,p) basis set was used for all other atoms. The LANL2DZ pseudo-potential was used for Fe. Initial geometries were obtained using the coordinates from X-ray structures wherever possible and all of the optimized structures were verified using frequency

calculations to check that they did not contain any imaginary frequencies. The calculated transition states all showed one imaginary frequency with a motion connecting the reactant and product demonstrated using IRC calculations. Solvent was modeled using the IEPCM model (dioxane) as implemented in Gaussian 09. All energies presented are Gibbs Free Energies with solvent corrections.

Characterization of New Compounds

$(iPrPNP)Fe(CO)H$ (**1a**)

A vial was charged with $(iPrPN^H P)Fe(CO)H(Cl)$ (50.0 mg, 117 μ mol) and KO^tBu (14.6 mg, 130 μ mol). Upon addition of THF (10 mL) at room temperature an immediate color change from yellow to red was observed. The suspension was stirred for 15 minutes at room temperature and the solvent evaporated in vacuo. The red residue was extracted with pentanes, filtered and then the solvent was removed. This was repeated a second time. After evaporation of the solvent a red-purple residue remained which was lyophilized from benzene. Yield: 34.0 mg (75%).

Anal. found (calc) for $C_{17}H_{37}FeNOP_2$: C, 52.18 (52.45); H, 9.12 (9.58); N, 3.51 (3.60). 1H NMR (d_8 -THF, 400 MHz): -25.5 (t, $J = 53$ Hz, 1H, Fe- H), 1.08 (m, 3H, $CH(CH_3)_2$), 1.11 (m, 3H, $CH(CH_3)_2$), 1.25 (m, 3H, $CH(CH_3)_2$), 1.29 (m, 3H, $CH(CH_3)_2$), 1.91 (m, 2H, PCH_2), 2.00 (m, 2H, PCH_2), 2.21 (m, 2H, $CH(CH_3)_2$), 2.46 (m, 2H, $CH(CH_3)_2$), 3.01 (m, 2H, NCH_2), 3.13 (m, 2H, NCH_2). $^{13}C\{^1H\}$ NMR (d_8 -THF, 75 MHz): 221.8 (t, $J = 23$ Hz), 64.7 (t, $J = 10$ Hz), 27.9 (t, $J = 12$ Hz), 25.6 (indirectly determined by 1H - ^{13}C HSQC), 24.7 (t, $J = 12$ Hz), 19.8, 18.5, 18.3, 18.0. $^{31}P\{^1H\}$ NMR (d_8 -THF, 161 MHz): 116.1. IR (Nujol/KBr, ν (cm^{-1})): 1889 (CO), 1862 (CO).

X-ray quality single crystals of **1a** were obtained from a saturated solution of pentane at $-38^\circ C$.

$(CyPNP)Fe(CO)H$ (**1b**)

KO^tBu (12.0 mg, 107 μ mol) was added to a stirred solution of $(CyPN^H P)Fe(CO)H(Cl)$ (57.0 mg, 97.0 μ mol) in THF (10 mL) at room temperature. An immediate color change from yellow to deep magenta was observed. The solution was stirred for 2 hours at room temperature after which the solvent was evaporated

under vacuum to give a deep red residue. The residue was extracted with pentane (3 x 3 mL) and filtered. The solvent was evaporated under vacuum to give **1b** as a red-purple solid. Yield: 35.0 mg (65%).

Anal. found (calc) for $C_{29}H_{53}FeNOP_2$: C, 63.85 (63.88); H, 9.72 (9.72); N, 2.54 (2.55). 1H NMR (400 MHz, C_6D_6): -25.1 (t, $J = 53$ Hz, 1H, Fe- H), 1.19-1.31 (m, 22 H, Cy), 1.62-2.04 (m, 22 H, Cy), 2.37 (m, 4 H, PCH_2), 2.49 (m, 4H, NCH_2). $^{13}C\{^1H\}$ NMR (150 MHz, C_6D_6): 64.4 (t, $J = 10.4$ Hz), 37.0 (t, $J = 11.8$ Hz), 35.4 (t, $J = 10.0$ Hz), 29.5, 28.1, 27.7, 27.5 (t, $J = 3.8$ Hz), 27.3 (m), 26.8 (d, $J = 2.8$ Hz), 24.6 (t, $J = 6.4$ Hz), CO resonance not detected. $^{31}P\{^1H\}$ NMR (120 MHz, C_6D_6): 106.0. IR (ATR, ν (cm^{-1})): 1885 (CO). UV-vis [THF; λ , nm (ϵ , $L\ mol^{-1}\ cm^{-1}$): 530 (4974), 338 (16160).

X-ray quality single crystals of **1b** were obtained from a saturated solution of diethyl ether at $-30^\circ C$.

$(^{iPr}PN^H P)Fe(CO)H(COOH)$ (2a**)**

Formic acid (1.77 mg, 38.5 μ mol) was added to a solution of **1a** (15.0 mg, 38.5 μ mol) in 2 mL THF at room temperature. An immediate color change from deep magenta to yellow was observed. The solution was stirred for 10 min at room temperature after which the solvent was evaporated under vacuum. The yellow residue was recrystallized from pentane at $-30^\circ C$ to give **2a** as a yellow powder. Yield: 13.2 mg (78 %).

Alternately, a solution of **1a** (15.0 mg, 38.5 μ mol) was dissolved in 0.6 mL THF in a J. Young NMR tube. The solution was then subjected to three freeze-pump-thaw cycles and 1 atm of 1:1 $H_2:CO_2$ was introduced via a dual manifold Schlenk line. An immediate color change from deep magenta to yellow was observed and the solution was allowed to stand at room temperature for 10 min. The solvent was removed under vacuum and the yellow solid recrystallized from pentane at $-30^\circ C$. Yield: 15.0 mg (89%).

Anal. found (calc) for $C_{18}H_{39}FeNO_3P_2$: C, 50.10 (49.67); H, 8.96 (9.03); N, 3.14 (3.22). 1H NMR (C_6D_6 , 500 MHz): -25.8 (t, $J = 59$ Hz, 1H, Fe- H), 0.79-0.90 (m, 12H, $CH(CH_3)_2$), 1.13-1.19 (m, 12H, $CH(CH_3)_2$), 1.69-1.74 (m, 4H, $CH(CH_3)_2$), 1.81 (m, 2H, PCH_2), 1.97 (m, 2H, PCH_2), 2.30 (m, 2H, NCH_2), 2.81 (m, 2H,

NCH₂), 8.80 (s, 1H, N-H), 9.10 (s, 1H, COOH). ¹³C{¹H} NMR (C₆D₆, 150 MHz): 157.8, 67.8, 55.7 (t, J = 4.9 Hz), 26.4 (t, J = 8.9 Hz), 25.8 (t, J = 13.8 Hz), 23.3 (t, J = 4.0 Hz), 18.9 (d, J = 6.7), 18.8, 18.4, CO resonance not detected. ³¹P{¹H} NMR (C₆D₆, 125 MHz): 95.3. IR (ν (cm⁻¹)): 2969 (N-H), 1892 (CO), 1650 (CO₂), 1319 (CO₂). UV-vis [THF; λ, nm (ε, L mol⁻¹ cm⁻¹): 470 (2013), 321 (16707).

(^{Cy}P^{N^H}P)Fe(CO)H(COOH) (**2b**)

Formic acid (1.42 mg, 30.9 μmol) was added to a solution of **1b** (17.0 mg, 30.9 μmol) in 2 mL of THF at room temperature. An immediate color change from deep pink to yellow was observed. The solution was stirred for 10 min at room temperature after which the solvent was evaporated and the yellow residue recrystallized from pentane at -30°C to give **2b** as a yellow powder. Yield: 14.3 mg (77%).

Alternately, a solution of **1b** (15.0 mg, 27.3 μmol) was dissolved in 0.6 mL THF in a J. Young NMR tube. The solution was then subjected to three freeze-pump-thaw cycles and 1 atm of 1:1 H₂:CO₂ was introduced via a dual manifold Schlenk line. An immediate color change from deep pink to yellow was observed and the solution was allowed to stand at room temperature for 10 min. The solvent was removed under vacuum and the solid recrystallized from pentane at -30°C to give **2b** as a yellow solid. Yield: 14.0 mg (23.5 μmol, 86%).

Anal. found (calc) for C₃₀H₅₅FeNO₃P₂: C, 60.37 (60.50); H, 9.00 (9.31); N, 2.43 (2.35). ¹H NMR (C₆D₆, 500 MHz): -25.83 (t, J = 52.44, 1H, Fe-H), 1.19- 1.32 (m, 22H, Cy), 1.42-1.51 (m, 22H, Cy), 2.15 (m, 4H, PCH₂), 2.91 (m, 4H, NCH₂), 8.90 (s, 1H, N-H), 9.20 (s, 1H, COOH). ¹³C{¹H} NMR (C₆D₆, 150 MHz): 157.0, 55.9 (t, J = 5.1 Hz), 36.5 (t, J = 7.9 Hz), 36.2 (t, J = 15.4 Hz), 29.2, 28.1, 27.7 (t, J = 4.4 Hz), 27.6 (t, J = 5.5 Hz) 27.2 (t, J = 5.1 Hz), 27.0 (t, J = 4.2 Hz), 26.8, 26.5, 23.1 (t, J = 4.7 Hz), CO resonance not detected. ³¹P{¹H} NMR (C₆D₆, 125 MHz): 87.0. IR (ν (cm⁻¹)): 2851 (N-H), 1890 (CO), 1649 (CO₂), 1317 (CO₂). UV-vis [THF; λ, nm (ε, L mol⁻¹ cm⁻¹): 459 (5886), 347 (11784).

*In Situ Generation of (^{P^r}P^{N^H}P)Fe(CO)H₂ (**3a**) through the reaction of **1a** with H₂*

A J-Young NMR tube was charged with **1a** (5.0 mg, 12.8 μmol) and d₈-THF (0.7 mL). The NMR tube was degassed three times and back filled with H₂ gas (1 atm). The sample was shaken for 10 minutes by which

time the dark red solution turned pale pink. Four compounds were detected by $^3\text{P}\{^1\text{H}\}$ NMR spectroscopy, *trans*-($i\text{PrPN}^{\text{H}}\text{P}$)Fe(CO)H₂ (**3a**, 70%), *cis*-($i\text{PrPN}^{\text{H}}\text{P}$)Fe(CO)H₂ (**3a'**, 20%), ($i\text{PrPN}^{\text{H}}\text{P}$)Fe(CO)₂^{10a} (3%) and free $i\text{PrPN}^{\text{H}}\text{P}$ (7%). Selected NMR spectra of the mixture of are shown below.

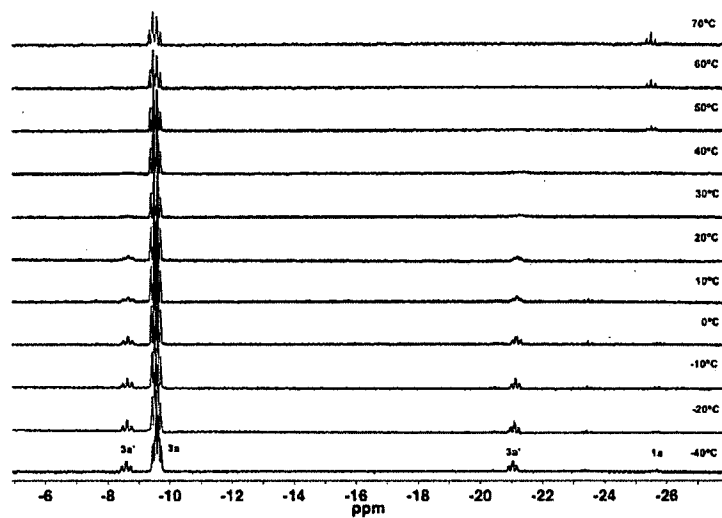


Figure 3.02. Variable temperature ^1H NMR spectra of the hydride region of the reaction between **1a** and H₂ (1 atm)

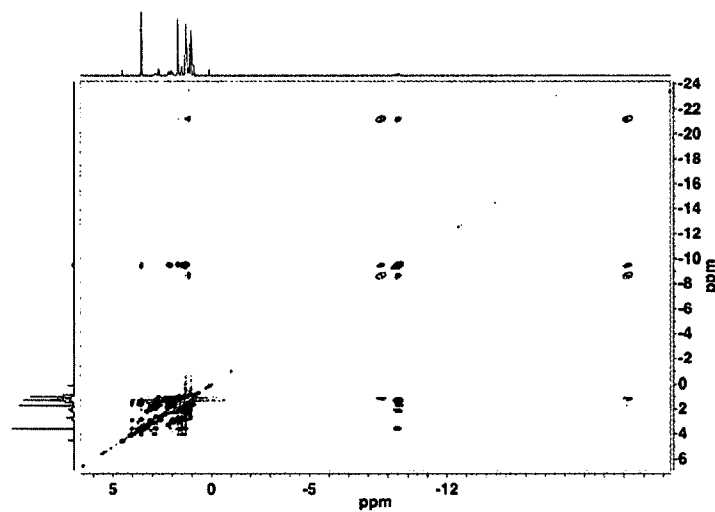


Figure 3.03. ^1H NOESY/EXSY NMR spectrum (400 MHz) of **3a/3a'** ($\tau = 1\text{s}$).

NMR data for 3a

^1H NMR (d_8 -THF, 400 MHz): -9.63 (td, $J = 9.0, 40$ Hz, 1H, Fe- H), -9.57 (td, $J = 9.0, 40$ Hz, 1H, Fe- H), 1.09 (m, 12H, CH(CH₃)₂), 1.29 (m, 12H, CH(CH₃)₂), 1.68 (m, 1H, NCH₂), 1.96 (m, 1H, NCH₂), 2.05 (m, 2H, PCH₂), 2.17 (m, 2H, PCH₂), 2.84 (m, 2H, NCH₂), 3.55 (1H, NH, determined from a 2D NOESY spectrum). $^{13}\text{C}\{^1\text{H}\}$ -NMR (d_8 -THF, 75 MHz): 221.8 (t, $J = 23$ Hz), 64.7 (t, $J = 10$ Hz), 27.9 (t, $J = 12$ Hz), 25.6 (indirectly determined by ^1H - ^{13}C HSQC), 24.7 (t, $J = 12$ Hz), 19.8, 18.5, 18.3, 18.0. $^{31}\text{P}\{^1\text{H}\}$ NMR (d_8 -THF, 161 MHz): 116.3.

Selected NMR data for 3a'

^1H NMR (d_8 -THF, 400 MHz, 263K): 21.13 (td, $J = 15, 40$ Hz, 1H, Fe- H), -8.63 (td, $J = 15, 57$ Hz, 1H Fe- H). $^{31}\text{P}\{^1\text{H}\}$ NMR (d_8 -THF, 400 MHz): 112.6.

*In Situ Generation of $(^{\text{Cy}}\text{PN}^{\text{H}}\text{P})\text{Fe}(\text{CO})\text{H}_2$ (**3b**) through the reaction of **1b** with H_2*

1b (10.0 mg, 18.2 μmol) was dissolved in 0.6 mL C_6D_6 in a J. Young NMR tube. The solution was subjected to 3 freeze-pump-thaw cycles and 1 atm H_2 was introduced via a dual manifold Schlenk line. The solution was allowed to stand at room temperature for 10 min, during which time the color changed from deep magenta to a pale orange. **3b** was characterized by ^1H and ^{31}P NMR spectroscopy, but decomposes too rapidly in solution, even under an H_2 atmosphere to record a ^{13}C NMR spectrum. The ^1H and ^{31}P NMR data are given below although both $(^{\text{Cy}}\text{PN}^{\text{H}}\text{P})\text{Fe}(\text{CO})_2$ and free $^{\text{Cy}}\text{PN}^{\text{H}}\text{P}$ are present in solution when **3b** is initially synthesized in an analogous fashion to the synthesis of **3a**.

^1H NMR (C_6D_6 , 500 MHz): -9.34 (m, 2H, Fe- H), 1.06-1.43 (m, 22H, Cy), 1.63-1.85 (m, 22H, Cy), 2.38 (m, 4H, PCH₂), 2.48 (m, 2H, NCH₂), 2.92 (m, 2H, NCH₂), 3.56 (t, $J = 6.1$ Hz, 1H, N- H). $^1\text{H}\{^{31}\text{P}\}$ NMR (C_6D_6): -9.37 (d, $J = 9.5$ Hz, 1H, Fe- H), -9.29 (d, $J = 9.5$ Hz, 1H, Fe- H). $^{31}\text{P}\{^1\text{H}\}$ NMR (C_6D_6 , 125 MHz): 105.0.

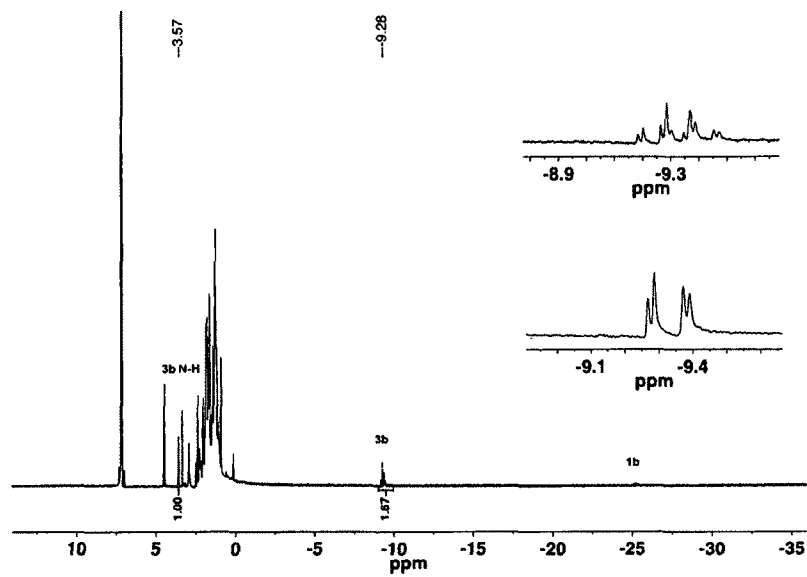


Figure 3.04. ^1H NMR spectrum of $(\text{CyPN}^{\text{H}}\text{P})\text{Fe}(\text{CO})\text{H}_2$ (**3b**). **1b** is present as a minor impurity.

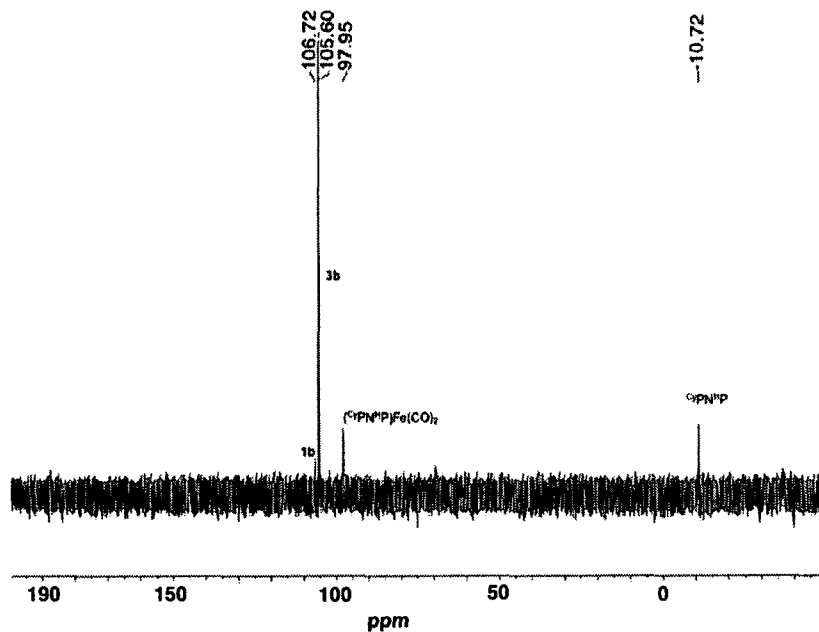


Figure 3.05. $^{31}\text{P}\{^1\text{H}\}$ NMR spectrum of $(\text{CyPN}^{\text{H}}\text{P})\text{Fe}(\text{CO})\text{H}_2$ (**3b**). Several impurities which are labeled in the spectrum are present.

Catalytic Reactions

General Methods for Catalytic FA Dehydrogenation Studies

In a dry box, a 50 mL Schlenk flask was loaded with the appropriate catalyst and additive (base/Lewis acid), if necessary, and dissolved in 1 mL of the appropriate solvent. A syringe was loaded with 4 mL of the appropriate solvent and formic acid. The Schlenk flask was sealed with a septum and removed from the dry box and attached to a gas burette setup. The gas burette and tubing was subjected to three vacuum/N₂ purge cycles. The Schlenk flask was then lowered into a preheated oil bath and allowed to equilibrate for 5 min. The solution of formic acid and solvent was then injected via syringe and the change in water level in the gas burette (V_{obs}) used to determine turnover using previously reported methods.⁶⁰ The turnover frequency (TOF) was determined to be the turnover number (TON) that occurred in the first hour. A blank reaction was run in which no catalyst was added to the solution. The volume of gas obtained from this reaction (trace solvent and FA) was recorded as V_{blank} .

$$\text{TON} = \frac{V_{\text{obs}} - V_{\text{blank}}}{n_{\text{cat}} \left(V(m, \text{H}_2, 25^\circ\text{C}) + V(m, \text{CO}_2, 25^\circ\text{C}) \right)}$$

n_{cat} = moles of catalyst

$$V(m, \text{H}_2, 25^\circ\text{C}) = \frac{RT}{p} + b - \frac{a}{RT} = 24.49 \text{ L/mol}$$

R: 8.3145 m³ Pa mol⁻¹ K⁻¹

T: 298.15 K

p: 101325 Pa

b: 26.7 10⁻⁶ m³ mol⁻¹

a: 2.49 10⁻¹⁰ Pa m³ mol⁻²

$$V(m, \text{CO}_2, 25^\circ\text{C}) = \frac{RT}{p} + b - \frac{a}{RT} = 24.42 \text{ L/mol}$$

R: 8.3145 m³ Pa mol⁻¹ K⁻¹

T: 298.15 K

p: 101325 Pa

b: 42.7 10⁻⁶ m³ mol⁻¹

a: 36.5 10⁻¹⁰ Pa m³ mol⁻²

General Methods for Decarboxylation Studies

Under N₂: In a dry box, a J. Young NMR tube was charged with catalyst (**2a** or **2b**) (8.4 μmol), triphenylphosphine oxide (2.3 mg, 8.4 μmol) and additive (10 eq). 1,4-dioxane (0.6 mL) was then added, the tube sealed, removed from the dry box and placed in an oil bath at 80°C. The conversion was measured by ³¹P NMR spectroscopy and integrated with respect to an internal standard (triphenylphosphine oxide).

Under H₂: In a dry box, a J. Young NMR tube was charged with catalyst (**2a** or **2b**) (8.4 μmol), triphenylphosphine oxide (2.3 mg, 8.4 μmol) and additive (10 eq). 1,4-dioxane (0.6 mL) was then added, the tube sealed, removed from the dry box. The tube was subjected to 3 freeze-pump-thaw cycles and 1 atm H₂ was introduced on a dual manifold Schlenk line. The tube was then placed in an oil bath at 80°C. The conversion was measured by ³¹P NMR spectroscopy and integrated with respect to an internal standard (triphenylphosphine oxide).

General Methods for Protonation Reactions

A solution of **2a** or **2b** (14.5 μmol) in 0.6 mL C₆D₆ in a J. Young NMR tube was subjected to three freeze-pump-thaw cycles. 1 atm of H₂ was introduced via a dual manifold Schlenk line and the tube was allowed to sit at room temperature for 10 min. The formation of **3a** or **3b** was confirmed using ³¹P NMR spectroscopy and the NMR tube was then pumped into a dry box. One equivalent of formic acid (14.5 μmol, as a stock solution in C₆D₆) was added and the tube was quickly sealed. A rapid color change from pale orange to bright yellow, as well as gas evolution, was observed. Conversion to **2a** or **2b** and concomitant release of H₂ was confirmed by ¹H and ³¹P NMR spectroscopy.

V. Acknowledgements

I am grateful to Dr. Brandon Mercado for X-ray crystallography, Dr. Paraskevi Lagaditis and Professor Sven Schneider for synthetic methods and characterization of **1a** and **3a**, and to Yuanyuan Zhang and Professor Wesley Bernskoetter for their continued input and helpful discussions. Finally, I would like to thank Professor Christoph Rose-Petruck for the use of his GC and Daniel Deciccio and Steven Ahn for their help in using the machine.

VI. References

- 1) (a) Crabtree, R. H. *Energy Environ. Sci.* **2008**, *1*, 134; (b) Li, Y.-N.; Ma, R.; He, L.-N.; Diao, Z.-F. *Catal. Sci. Tech.* **2014**, *4*, 1498.
- 2) (a) Bockris, J. O. M. *Science* **1972**, *176*, 1323; (b) Loges, B.; Boddien, A.; Gärtner, F.; Junge, H.; Beller, M. *Top. Catal.* **2010**, *53*, 902; (c) Staubitz, A.; Robertson, A. P. M.; Manners, I. *Chem. Rev.* **2010**, *110*, 4079; (d) Dalebrook, A. F.; Gan, W.; Grasmann, M.; Moret, S.; Laurenczy, G. *Chem. Commun.* **2013**, *49*, 8735.
- 3) Eberle, U.; Felderhoff, M.; Schüth, F. *Angew. Chem., Int. Ed.* **2009**, *48*, 6608.
- 4) Grasmann, M.; Laurenczy, G. *Energy Environ. Sci.* **2012**, *5*, 8171.
- 5) (a) Zhou, X.; Huang, Y.; Xing, W.; Liu, C.; Liao, J.; Lu, T. *Chem. Commun.* **2008**, 3540; (b) Ojeda, M.; Iglesia, E. *Angew. Chem., Int. Ed.* **2009**, *48*, 4800; (c) Bulushev, D. A.; Beloshapkin, S.; Ross, J. R. H. *Catal. Today* **2010**, *154*, 7; (d) Gu, X.; Lu, Z.-H.; Jiang, H.-L.; Akita, T.; Xu, Q. *J. Am. Chem. Soc.* **2011**, *133*, 11822; (e) Tedsree, K.; Li, T.; Jones, S.; Chan, C. W. A.; Yu, K. M. K.; Bagot, P. A. J.; Marquis, E. A.; Smith, G. D. W.; Tsang, S. C. E. *Nat. Nanotechnol.* **2011**, *6*, 302; (f) Bi, Q.-Y.; Du, X.-L.; Liu, Y.-M.; Cao, Y.; He, H.-Y.; Fan, K.-N. *J. Am. Chem. Soc.* **2012**, *134*, 8926.
- 6) (a) Gao, Y.; Kuncheria, J.; Puddephatt, R. J.; Yap, G. P. A. *Chem. Commun.* **1998**, 2365; (b) Fellay, C.; Dyson, P. J.; Laurenczy, G. *Angew. Chem., Int. Ed.* **2008**, *47*, 3966; (c) Loges, B.; Boddien, A.; Junge, H.; Beller, M. *Angew. Chem., Int. Ed.* **2008**, *47*, 3962; (d) Himeda, Y. *Green Chem.* **2009**, *11*, 2018; (e) Morris, D. J.; Clarkson, G. J.; Wills, M. *Organometallics* **2009**, *28*, 4133; (f) Boddien, A.; Mellmann, D.; Gärtner, F.; Jackstell, R.; Junge, H.; Dyson, P. J.; Laurenczy, G.; Ludwig, R.; Beller, M. *Science* **2011**, *333*, 1733; (g) Hull, J. F.; Himeda, Y.; Wang, W.-H.; Hashiguchi, B.; Periana, R.; Szalda, D. J.; Muckerman, J. T.; Fujita, E. *Nat. Chem.* **2012**, *4*, 383; (h) Barnard, J. H.; Wang, C.; Berry, N. G.; Xiao, J. *Chem. Sci.* **2013**, *4*, 1234; (i) Mellone, I.; Peruzzini, M.; Rosi, L.; Mellmann, D.; Junge, H.; Beller, M.; Gonsalvi, L. *Dalton Trans.* **2013**, *42*, 2495; (j) Oldenhof, S.; de Bruin, B.; Lutz, M.; Siegler, M. A.; Patureau, F. W.; van der Vlugt, J. I.; Reek, J. N. H. *Chem. Eur. J.* **2013**, *19*, 11507; (k) Zell, T.; Butschke, B.; Ben-David, Y.; Milstein, D. *Chem. Eur. J.* **2013**, *19*, 8068; (l) Sponholz, P.; Mellmann, D.; Junge, H.; Beller, M. *ChemSusChem* **2013**, *6*, 1172; (m) Manaka, Y.; Wang, W.-H.; Suna, Y.; Kambayashi, H.; Muckerman, J. T.; Fujita, E.; Himeda, Y. *Catal. Sci. Tech.* **2014**, *4*, 33; (n) Myers, T. W.; Berben, L. A. *Chem. Sci.* **2013**,

- 5, 3771; (o) Boddien, A.; Loges, B.; Gärtner, F.; Torborg, C.; Fumino, K.; Junge, H.; Ludwig, R.; Beller, M. *J. Am. Chem. Soc.* **2010**, *132*, 8924.
- 7) Boddien, A.; Loges, B.; Junge, H.; Beller, M. *ChemSusChem* **2008**, *1*, 751.
- 8) Schmeier, T. J.; Dobereiner, G. E.; Crabtree, R. H.; Hazari, N. *J. Am. Chem. Soc.* **2011**, *133*, 9274.
- 9) (a) Käss, M.; Friedrich, A.; Drees, M.; Schneider, S. *Angew. Chem., Int. Ed.* **2009**, *48*, 905; (b) Friedrich, A.; Drees, M.; Schneider, S. *Chem. Eur. J.* **2009**, *15*, 10339; (c) Staubitz, A.; Sloan, M. E.; Robertson, A. P. M.; Friedrich, A.; Schneider, S.; Gates, P. J.; auf der Günne, J. S.; Manners, I. *J. Am. Chem. Soc.* **2010**, *132*, 13332; (d) Marziale, A. N.; Friedrich, A.; Klopsch, I.; Drees, M.; Celinski, V. R.; auf der Günne, J. S.; Schneider, S. *J. Am. Chem. Soc.* **2013**, *135*, 13342.
- 10) (a) Koehne, I.; Schmeier, T. J.; Bielinski, E. A.; Pan, C. J.; Lagaditis, P. O.; Bernskoetter, W. H.; Takase, M. K.; Würtele, C.; Hazari, N.; Schneider, S. *Inorg. Chem.* **2014**, *53*, 2133; (b) Fillman, K. L.; Bielinski, E. A.; Schmeier, T. J.; Nesvet, J. C.; Woodruff, T. M.; Pan, C. J.; Takase, M. K.; Hazari, N.; Neidig, M. L. *Inorg. Chem.* **2014**, *53*, 6066.
- 11) Alberico, E.; Sponholz, P.; Cordes, C.; Nielsen, M.; Drexler, H.-J.; Baumann, W.; Junge, H.; Beller, M. *Angew. Chem., Int. Ed.* **2013**, *52*, 14162.
- 12) (a) Chakraborty, S.; Dai, H.; Bhattacharya, P.; Fairweather, N. T.; Gibson, M. S.; Krause, J. A.; Guan, H. *J. Am. Chem. Soc.* **2014**, *136*, 7869; (b) Werkmeister, S.; Junge, K.; Wendt, B.; Alberico, E.; Jiao, H.; Baumann, W.; Junge, H.; Gallou, F.; Beller, M. *Angew. Chem., Int. Ed.* **2014**, *53*, 8722.
- 13) Lagaditis, P. O.; Sues, P. E.; Sonnenberg, J. F.; Wan, K. Y.; Lough, A. J.; Morris, R. H. *J. Am. Chem. Soc.* **2014**, *136*, 1367.
- 14) Chakraborty, S.; Brennessel, W. W.; Jones, W. D. *J. Am. Chem. Soc.* **2014**, *136*, 8564.
- 15) Schmeier, T. J. Ph.D. Thesis, Yale University, 2014.
- 16) Bielinski, E. A.; Lagaditis, P. O.; Zhang, Y.; Mercado, B. Q.; Würtele, C.; Bernskoetter, W. H.; Hazari, N.; Schneider, S. *J. Am. Chem. Soc.* **2014**, *136*, 10234.
- 17) Addison, A. W.; Rao, T. N.; Reedijk, J.; van Rijn, J.; Verschoor, G. C. *J. Chem. Soc., Dalton Trans.* **1984**, 1349.
- 18) Friedrich, A.; Drees, M.; Käss, M.; Herdtweck, E.; Schneider, S. *Inorg. Chem.* **2010**, *49*, 5482.
- 19) Kubas, G. J. *Chem. Rev.* **2007**, *107*, 4152.

- 20) Farrugia, L. J. *J. Appl. Crystallogr.* **1997**, *30*, 565.
- 21) (a) Suh, H.-W.; Schmeier, T. J.; Hazari, N.; Kemp, R. A.; Takase, M. K. *Organometallics* **2012**, *31*, 8225; (b) Suh, H.-W.; M., G. L.; Hazari, N. *Chem. Sci.* **2014**, *5*, 3859.
- 22) Lehmkuhl, H.; Naeser, J.; Mehler, G.; Keil, T.; Danowski, F.; Benn, R.; Mynott, R.; Schroth, G.; Krueger, C.; Betz, P. *Chem. Ber.* **1991**, *124*, 441.
- 23) (a) Jin, D.; Schmeier, T. J.; Williard, P. G.; Hazari, N.; Bernskoetter, W. H. *Organometallics* **2013**, *32*, 2152; (b) Jin, D.; Williard, P. G.; Hazari, N.; Bernskoetter, W. H. *Chem. Eur. J.* **2014**, *20*, 3205.
- 24) Crabtree, R. H. *Chem. Rev.* **2012**, *112*, 1536.
- 25) Whitesides, G. M.; Hackett, M.; Brainard, R. L.; Lavalleye, J.-P. P. M.; Sowinski, A. F.; Izumi, A. N.; Moore, S. S.; Brown, D. W.; Staudt, E. M. *Organometallics* **1985**, *4*, 1819.
- 26) Yakelis, N. A.; Bergman, R. G. *Organometallics* **2005**, *24*, 3579.
- 27) Wang, C.; Guo, L.; Li, H.; Wang, Y.; Weng, J.; Wu, L. *Green Chem.* **2006**, *8*, 603.
- 28) *CrystalClear and CrystalStructure* Rigaku/MSK: The Woodlands, TX, 2010.
- 29) Altomare, A.; Casciarano, G.; Giacovazzo, C.; Guagliardi, A.; Burla, M. C.; Polidori, G.; Camalli, M. *J. Appl. Crystallogr.* **1994**, *27*, 435.
- 30) Sheldrick, G. M. *Acta Crystallographica* **2008**, *A64*, 112.
- 31) Müller, P. Hydrogen Atoms. In *Crystal Structure Refinement: A Crystallographer's Guide to SHELXL*; Müller, P., Ed.; Oxford University Press: Oxford, **2006**, p 26.
- 32) Gaussian 09, Revision A.02, Frisch, M. J.; Trucks, G. W.; Schlegel, H. B.; Scuseria, G. E.; Robb, M. A.; Cheeseman, J. R.; Scalmani, G.; Barone, V.; Mennucci, B.; Petersson, G. A.; Nakatsuji, H.; Caricato, M.; Li, X.; Hratchian, H. P.; Izmaylov, A. F.; Bloino, J.; Zheng, G.; Sonnenberg, J. L.; Hada, M.; Ehara, M.; Toyota, K.; Fukuda, R.; Hasegawa, J.; Ishida, M.; Nakajima, T.; Honda, Y.; Kitao, O.; Nakai, H.; Vreven, T.; Montgomery, Jr., J. A.; Peralta, J. E.; Ogliaro, F.; Bearpark, M.; Heyd, J. J.; Brothers, E.; Kudin, K. N.; Staroverov, V. N.; Kobayashi, R.; Normand, J.; Raghavachari, K.; Rendell, A.; Burant, J. C.; Iyengar, S. S.; Tomasi, J.; Cossi, M.; Rega, N.; Millam, N. J.; Klene, M.; Knox, J. E.; Cross, J. B.; Bakken, V.; Adamo, C.; Jaramillo, J.; Gomperts, R.; Stratmann, R. E.; Yazyev, O.; Austin, A. J.; Cammi, R.; Pomelli, C.; Ochterski, J. W.; Martin, R. L.; Morokuma, K.; Zakrzewski, V. G.; Voth, G. A.; Salvador, P.;

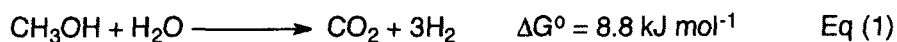
Dannenberg, J. J.; Dapprich, S.; Daniels, A. D.; Farkas, Ö.; Foresman, J. B.; Ortiz, J. V.; Cioslowski, J.;
Fox, D. J. Gaussian, Inc., Wallingford CT, 2009.

Chapter 4: Base-Free Methanol Dehydrogenation Using a Pincer-Supported Iron Compound and Lewis Acid Co-Catalyst

I. Introduction

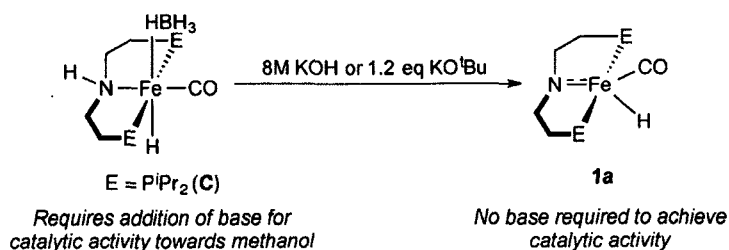
Homogeneous, transition metal-catalyzed methanol (MeOH) dehydrogenation was first reported in 1985 by Saito and co-workers. They showed that $\text{Ru}(\text{Cl})(\text{PR}_3)_3(\text{C}_2\text{H}_3\text{O}_2)$ ($\text{R} = \text{Ph}_2\text{Et}$) catalyzed the formation of methyl formate and H_2 from MeOH with a turnover number (TON) of 34.¹ Two years later, Cole-Hamilton and co-workers reported that $\text{Rh}(\text{bipy})_2\text{Cl}$ ($\text{bipy} = 2,2'$ -bipyridine) could also catalyze the dehydrogenation of MeOH to methyl formate, though with a TON of only 7.² It was more than 25 years later that Grützmacher³ and co-workers and Beller⁴ co-workers reported homogenous transition metal catalysts for the complete aqueous-phase dehydrogenation of MeOH to CO_2 and H_2 with the expressed purpose of use in hydrogen storage. In contrast, in the interim years, formic acid (FA) has received significant attention as a possible HSM and many highly active transition metal catalysts have been reported for its facile dehydrogenation⁵ (see Chapters 1 and 3 for a complete discussion). This disparity in attention is likely due to a variety of considerations, namely the challenges associated with regeneration of FA and MeOH from CO_2 and the demand for MeOH and FA in industrial applications. Much research has been devoted to the development of catalysts for the hydrogenation of CO_2 to FA^{5i,6} and many of these show high turnovers^{6b,6h} and use cheap, abundant first row transition metals.^{6f,6g} Research on the generation of MeOH from CO_2 has not seen the same success, and the few catalysts capable of this transformation show very low TONs and rely on expensive and rare noble metals.⁷ Both FA and MeOH are desired industrial chemicals, though on significantly different scales. FA is produced on a modest scale of 720,000 tons per year, most of which is used directly in industrial applications such as leather tanning, food preservation and polymerization catalysis.⁸ MeOH, however, is produced on a scale of 50 million metric tons per year, and 85% is further used for downstream chemical processes.⁹ As such, the renewable generation of MeOH, which is currently produced from steam reforming of fossil fuels, has received more attention than its related dehydrogenation for energy applications.¹⁰ In contrast, the more modest demand for FA has allowed for more varied research into both its production and other applications.¹¹ Despite the challenges associated with its production from CO_2 hydrogenation, renewable MeOH generation from biomass has seen recent success,^{10b} and MeOH is a

promising target for H₂ storage,^{10a,10b,12} as it has a high gravimetric H₂ content (12.6%) and can be dehydrogenated in the presence of water to release three equivalents of H₂ (Eq 1).



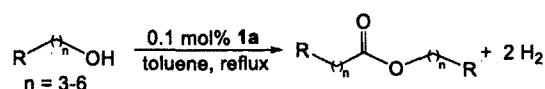
Heterogeneous catalysts are currently used for dehydrogenation in reformed MeOH fuel cells, which use the H₂ released from MeOH as a feedstock for the generation of electricity.^{10c,12-13} These catalysts operate at high temperatures and pressures and produce a significant amount of CO, which ultimately poisons the fuel cell.^{10c,12} Although there has been ongoing research into the development of homogeneous catalysts for MeOH dehydrogenation since the 1980s (*vide supra*),^{2,14} only recently have these systems been reported to operate at significantly lower temperatures than heterogeneous catalysts and produce less CO. However, the most active homogeneous catalysts to date are based on expensive precious metals such as Ru,⁴ and with the exception of Grützmacher's seminal Ru system,³ require either the use of a strong base or a precious metal co-catalyst.

The only first row transition metal catalyst for MeOH dehydrogenation was described by Beller and co-workers.¹⁵ This complex, (ⁱPrPN^HP)Fe(CO)H(HBH₃) (ⁱPrPNP = N(CH₂CH₂PⁱPr₂)₂, C),¹⁶ features a bifunctional PNP ligand and is able to achieve ~10,000 TONs in the presence of 8M KOH. Chapter 3 describes, in detail, the reaction of this compound with KO^tBu to generate the amido compounds (^RPNP)FeH(CO) (^RPNP = N{CH₂CH₂(PR₂)₂}; R = ⁱPr (**1a**) or Cy (**1b**)) (Scheme 4.01).^{51,17}

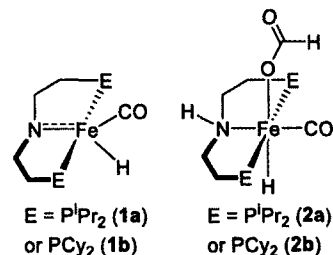
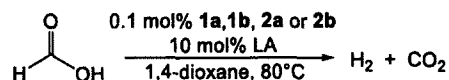


Scheme 4.01. Reaction of C with base to generate 1a.

i) Base Free Acceptorless Alcohol Dehydrogenation



ii) LA Assisted Formic Acid Dehydrogenation



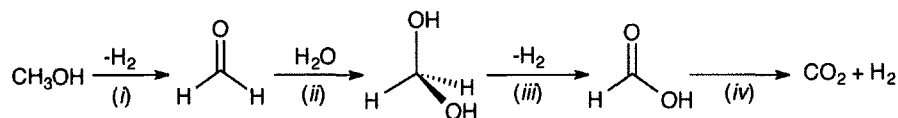
Scheme 4.02. Summary of selected previous reactions catalyzed by **1a**, **1b**, **2a** and **2b**.

Subsequently, Jones, Schneider and co-workers demonstrated the utility of these compounds as catalysts for alcohol dehydrogenation without the need for a base or terminal H₂ acceptor (Scheme 4.02).^{17d} Furthermore, work presented in Chapter 3 shows **1a** and **1b** can be used as highly efficient catalysts for base-free FA dehydrogenation, when combined with a Lewis acid (LA).⁵¹ Similarly, the related formate complexes **2a** and **2b** (^RPN^HP)Fe(CO)H(COOH) (^RPN^HP = HN{CH₂CH₂(PR₂)₂}; R = ⁱPr (**2a**) or Cy (**2b**)), which are proposed to generate **1a** and **1b** *in situ*, are also active catalysts for FA dehydrogenation in the presence of LA.⁵¹ Combining the reactivity of **1a**, **1b** towards alcohols with their action as FA dehydrogenation catalysts, it reasons that these compounds may be capable of affecting base-free MeOH dehydrogenation. This chapter describes the optimization of conditions for base-free MeOH dehydrogenation using **1a/1b** and **2a/2b** as well as preliminary mechanistic studies that suggest a connection between Beller's catalyst **C** and **1** due to the action of base

II. Results and Discussion

Previously it has been proposed that the complete aqueous-phase dehydrogenation of MeOH to CO₂ and H₂ occurs following the stepwise pathway shown in Scheme 4.03.³⁻⁴ Initial dehydrogenation of MeOH produces formaldehyde and releases one equivalent of H₂. Subsequently, the reaction of water with formaldehyde generates methanediol, which undergoes a second dehydrogenation to produce FA and a second equivalent of H₂. Finally, FA dehydrogenation results in the release of the third equivalent of H₂, along with CO₂. Given that **1a** and related Fe complexes catalyze both the dehydrogenation of primary alcohols such as 1-butanol to esters (analogous to steps i-iii in Scheme 4.03) and FA dehydrogenation (step iv in Scheme 4.03) without a base, it follows that they may be able to perform base-free aqueous-phase

MeOH dehydrogenation if compatible conditions for both reactions could be developed. To this end, first the dehydrogenation of MeOH in the absence of water (step i in Scheme 4.03) and then full aqueous-phase MeOH dehydrogenation were explored.



Scheme 4.03. Proposed stepwise pathway for aqueous-phase MeOH dehydrogenation to CO₂ and H₂.

MeOH Dehydrogenation in the Absence of Water

Although **1a** and **1b** have been used to dehydrogenate primary alcohols,^{17d} MeOH was not used as a substrate. Initially, conditions for the dehydrogenation of MeOH in the absence of water were screened (Table 4.01). The primary products of this reaction were methyl formate and H₂, which was identified using gas chromatography (GC). High yields of methyl formate were only obtained when the moderately polar solvents ethyl acetate and acetonitrile were utilized (Table 4.01). In contrast, excellent yields were previously obtained for the dehydrogenation of 1-butanol in non-polar toluene.^{17d} The exact reasons for the relatively low yield for MeOH dehydrogenation in non-polar solvents such as toluene are unclear. The dehydrogenation of MeOH was dependent not only on the identity of solvent, but also on the concentration (Table 4.02). Dilution studies indicate that the reaction fails at high concentrations. This is consistent with a bimolecular catalyst decomposition pathway. Accordingly, single crystals of the Fe(0) complex (CyPN^HP)Fe(CO)₂, which is proposed to form in a bimolecular fashion, were obtained from a catalytic reaction mixture (Figure 4.01). Similar to what was observed with the 5-coordinate (RPN^HP)FeCl₂ compounds described in Chapter 2, the 5-coordinate (RPN^HP)Fe(CO)₂ compounds are also isolable in either square pyramidal or trigonal bipyramidal geometries. Unlike the structure of (iPrPN^HP)Fe(CO)₂¹⁶ (obtained by Dr. Paraskevi Lagaditis) which is square pyramidal, (CyPN^HP)Fe(CO)₂ is trigonal bipyramidal in geometry, further highlighting the flexible nature of the RPN^HP ligand. However, this difference could also be attributed to the crystallization conditions, as (iPrPN^HP)Fe(CO)₂¹⁶ was crystallized via slow diffusion of pentane into a saturated solution in THF, while (CyPN^HP)Fe(CO)₂ resulted from a catalytic reaction.

Table 4.01. Solvent screen for MeOH dehydrogenation catalyzed by **1b**.^a

$$\text{CH}_3\text{OH} \xrightarrow[5 \text{ mL solvent, reflux}]{1 \text{ mol\% } \mathbf{1b}} \text{H}-\overset{\text{O}}{\parallel}{\text{C}}-\text{OCH}_3 + 2\text{H}_2$$

Solvent	Time (min) ^b	TON ^c	Yield (%)
Dioxane	20	53	26
Propylene carbonate	20	71	35
Chlorobenzene	10	80	40
Dimethylsulfoxide	11	96	48
Tetrahydrofuran	12	107	53
Cyclopentylmethylether	10	112	56
Toluene	15	116	58
Acetonitrile	10	170	85
Ethyl acetate	10	176	88

^aReaction conditions: MeOH (36 μL , 0.91 mmol), **1b** (9.1 μmol , 1 mol%) 5 mL solvent, reflux. ^bTime at which no further increase in TON was observed. ^cTON was measured using a gas burette. Each equivalent of H_2 generated is counted as a TON. All numbers are the average of two runs.

Table 4.02. Dilution study of MeOH dehydrogenation catalyzed by **1b**.^a

$$\text{CH}_3\text{OH} \xrightarrow[\text{Ethyl acetate, reflux}]{0.5 \text{ mol\% } \mathbf{1b}} \text{H}-\overset{\text{O}}{\parallel}{\text{C}}-\text{OCH}_3 + 2\text{H}_2$$

Volume ethyl acetate (mL)	Time (min) ^b	TON ^c	Yield (%)
1	15	25	6
2	20	200	48
5	20	300	77
10	25	380	93
15	25	320	80

^aReaction conditions: MeOH (36 μL , 0.91 mmol), **1b** (4.5 μmol , 0.5 mol%), ethyl acetate, reflux. ^bTime at which no further increase in TON was observed. ^cTON was measured using a gas burette. Each equivalent of H_2 generated is counted as a TON. All numbers are the average of two runs.

Under the optimized conditions shown in Table 4.03, **1a** and **1b** show nearly identical activity for MeOH dehydrogenation to methyl formate, giving 73% (1460 turnovers) and 71% yield (1420 turnovers), respectively. To the best of our knowledge these are the highest TONs reported to date for this reaction.^{2,14,18} Interestingly, the borohydride complex **C** is significantly less active, achieving only 19% yield (384 turnovers). This is consistent with recent observations by Guan and co-workers suggesting that the activation of **C** through loss of BH_3 results in increased catalytic activity for the hydrogenation of esters to alcohols, presumably due to rapid generation the active catalyst **1a**.¹⁹ In the current system there is no additive to facilitate the formation of the active species. Presumably, one of the roles of KOH in Beller's aqueous-phase dehydrogenation of MeOH using **C**,¹⁵ is to facilitate catalyst activation through the removal of BH_3 . The formate complexes **2a** and **2b** are also poor catalysts for MeOH dehydrogenation. This is most

likely due to the inability of these species to readily undergo decarboxylation and 1,2-elimination of H₂ to access catalytically active **1a** or **1b**, in the absence of base or LA.⁵¹

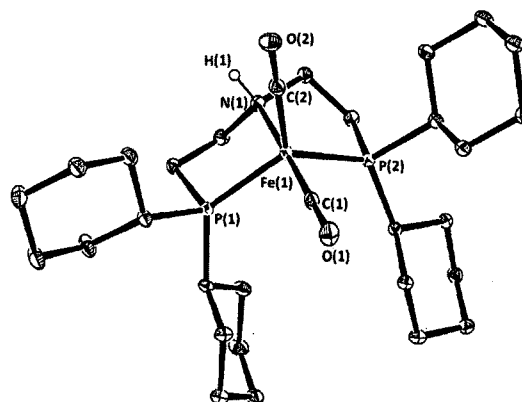


Figure 4.01. ORTEP²⁰ of (CyPNHP)Fe(CO)₂. Hydrogen atoms (apart from N-H) are removed for clarity. Ellipsoids are shown at 30% probability. Selected bond lengths (Å) and angles (°): Fe(1)-C(1) 1.761(2), Fe(1)-C(2) 1.738(2), Fe(1)-N(1) 2.1019(19), Fe(1)-P(1) 2.2179(6), Fe(1)-P(2) 2.2138(7), C(1)-O(1) 1.177(3), C(2)-O(2) 1.166(3), C(1)-Fe(1)-C(2) 93.48(11), C(1)-Fe(1)-N(1) 176.47(10), C(2)-Fe(1)-N(1) 90.04(9), C(1)-Fe(1)-P(2) 117.26(8), C(2)-Fe(1)-P(2) 93.94(8), N(1)-Fe(1)-P(2) 84.38(6), P(2)-Fe(1)-P(1) 124.64(3), N(1)-Fe(1)-P(1) 84.45(5).

Table 4.03. Catalyst optimization for MeOH dehydrogenation.^a

$$\text{CH}_3\text{OH} \xrightarrow[\text{10 mL Ethyl acetate, reflux}]{[\text{Fe}]} \text{H}-\text{C}(=\text{O})-\text{OCH}_3 + 2\text{H}_2$$

Catalyst	Mol% [Fe]	Time (min) ^b	TON ^c	Yield (%)
1a	0.1	50	1460	73
1b	0.1	45	1420	71
C	0.1	40	380	19
2a	0.1	25	260	12
2a + 10 mol% LiBF ₄	0.1	40	>1900	>99
2b	0.1	30	130	6
2b + 10 mol% LiBF ₄	0.1	45	1900	96
2a + 10 mol% LiBF ₄	0.01	260	>19000	>99
2a + 10 mol% LiBF ₄	0.001	340	12400	6

^aReaction conditions: MeOH (36 μL, 0.91 mmol), [Fe] (0.91 μmol, 0.1 mol%), 10mL ethyl acetate, reflux. ^bTime at which no further increase in TON was observed. ^cTON was measured using a gas burette. Each equivalent of H₂ generated is counted as a TON. All numbers are the average of two runs.

Chapter 3 outlines the use of LA co-catalysts to assist in the dehydrogenation of FA using **1a** and **1b**.⁵¹ However, the addition of 10 mol% LiBF₄ did not influence the yield or kinetic profile for the dehydrogenation of MeOH using **1b** (Figure 4.02), suggesting that the rate determining steps in MeOH dehydrogenation and FA dehydrogenation are not equivalent. Consistent with this proposal, the kinetic

isotope effect (KIE) for catalytic MeOH dehydrogenation (determined from rate constants for parallel reactions using MeOH and d_4 -MeOH and **1b**) is $k_H/k_D = 2.5(2)$. In contrast, for catalytic FA dehydrogenation using **1b** the KIE is $k_H/k_D = 4.2(3)$. Although the addition of LA co-catalysts did not enhance catalysis using **1a** and **1b**, a remarkable increase was observed in the cases of **2a** and **2b** (Table 4.03). In the presence of 10 mol% LiBF₄ complete conversion of MeOH to methyl formate was observed using 0.1 mol% **2a** and the catalyst loading could be decreased to 0.01 mol% without any loss in yield.²¹ This dramatic increase may occur because LiBF₄ facilitates the decarboxylation of the formate complexes, allowing access to the catalytically active species.⁵¹ The combination of **2** and a LA may provide an alternative strategy for dehydrogenating challenging organic substrates,^{17d} such as 1-cyclohexylmethanol, using low catalyst loading, as it appears to generate a more stable catalytic system than using **1** without any additives.

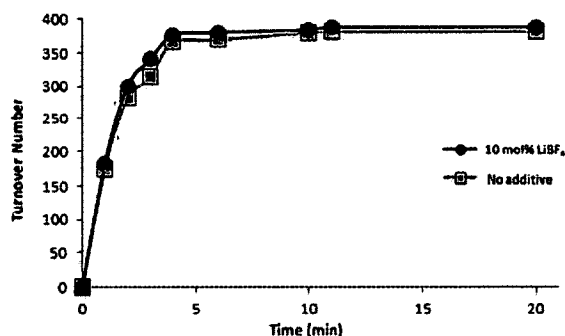
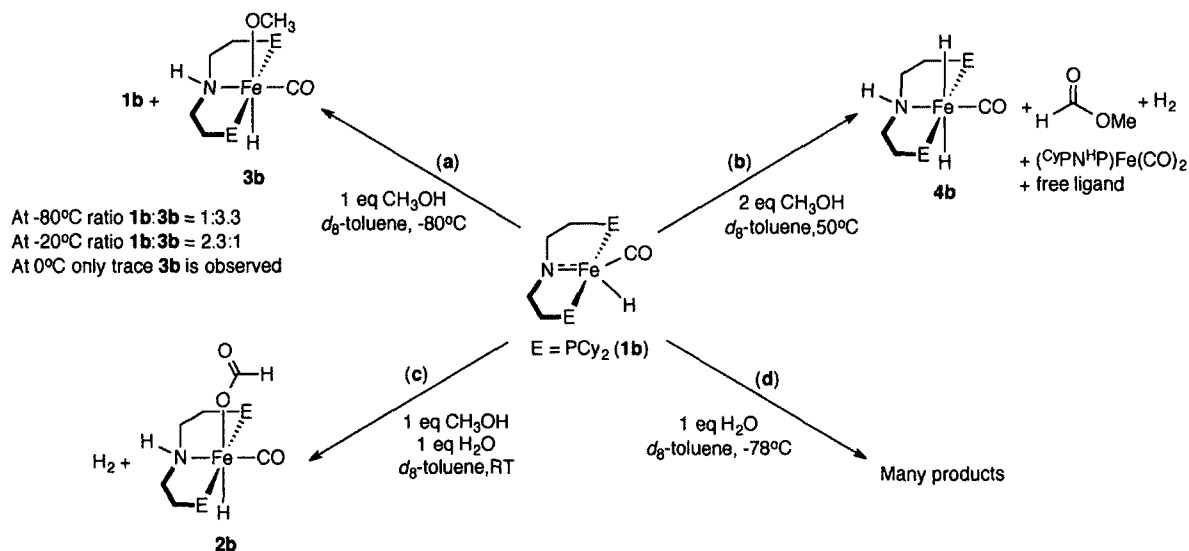


Figure 4.02. Effect of LA on MeOH dehydrogenation in the absence of water catalyzed by **1b**.

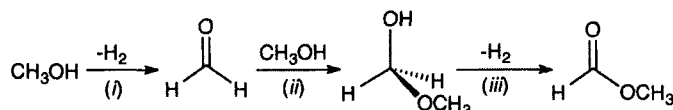
To further probe the mechanism of MeOH dehydrogenation, stoichiometric reactions were performed (Scheme 4.04). When one equivalent of MeOH was added to a d_8 -toluene solution of **1b** at low temperature (-80°C), a new PNP-supported Fe species **3b** was observed by ¹H and ³¹P NMR spectroscopy along with **1b** (Scheme 4.04a). Compound **3b** has a triplet resonance in the ¹H NMR spectrum at -23.95 ppm and a singlet resonance in the ³¹P{¹H} NMR spectrum at 84.8 ppm. It is assigned as (^{Cy}PN^HP)Fe(CO)(H)(OCH₃), which arises from 1,2-addition of MeOH to **1b**. Further evidence for this assignment was obtained through an experiment, performed by Yuanyuan Zhang, between CD₃OD and **1b** at -75°C. In this reaction, two resonances in a 3:1 ratio were observed at 3.57 and 2.04 ppm in the ²H NMR spectrum, along with the previously observed resonance at 84.8 ppm, in the ³¹P{¹H} NMR spectra. The resonances in the ²H NMR

spectrum are proposed to correspond to the OCD_3 ligand (3.57 ppm) bound to Fe and the N-D (2.04 ppm) moiety. Free CD_3OD was also observed in the ^2H NMR spectrum, which is consistent with the presence of unreacted **1b**. In both the experiments using CH_3OH and CD_3OD , the amount of **3b** decreased relative to the amount of **1b** as the temperature was increased. In fact, at 0°C only trace amounts of **3b** were observed by ^1H NMR or ^2H NMR spectroscopy and the predominant species is **1b**. Cooling the solutions back down to -80°C resulted in the conversion of **1b** and $\text{CH}_3\text{OH}/\text{CD}_3\text{OH}$ back to **3b**. These experiments suggest that **1b** and MeOH are in equilibrium with **3b** and that the 1,2-addition of MeOH is temperature dependent. It was not possible to isolate **3b**, as the removal of solvent resulted in the regeneration of **1b**, along with substantial amounts of free ligand and unidentified solid precipitate.

When the reaction between one equivalent of MeOH and **1b** in d_8 -toluene was performed at 50°C , there was no evidence for the formation of **3b**. Instead the major Fe containing products were the dihydride $(^{\text{Cy}}\text{PN}^{\text{H}}\text{P})\text{Fe}(\text{CO})\text{H}_2$ (**4b**), which we have previously characterized,⁵¹ and $(^{\text{Cy}}\text{PN}^{\text{H}}\text{P})\text{Fe}(\text{CO})_2$. Also present were a significant amount of free ligand, H_2 , methyl formate and MeOH. The analogous reaction between **1b** and two equivalents of MeOH (Scheme 4.04b), resulted in the formation of the same products, but no MeOH was observed. From these reactions, it is possible to propose a pathway for this reaction in which initial dehydrogenation of MeOH produces formaldehyde and H_2 followed by esterification of formaldehyde with MeOH to form methoxymethanol, which is subsequently dehydrogenated to generate methyl formate and the second equivalent of H_2 (Scheme 4.05). This is the same sequence of reactions previously proposed for butanol dehydrogenation^{17d} and is consistent with catalytic results. The observation of the dihydride complex **4b** suggests that release of H_2 to regenerate **1b** is slow and is in agreement with the observation that **4b** is the resting state during catalysis, as determined using $^{31}\text{P}\{^1\text{H}\}$ NMR spectroscopy.

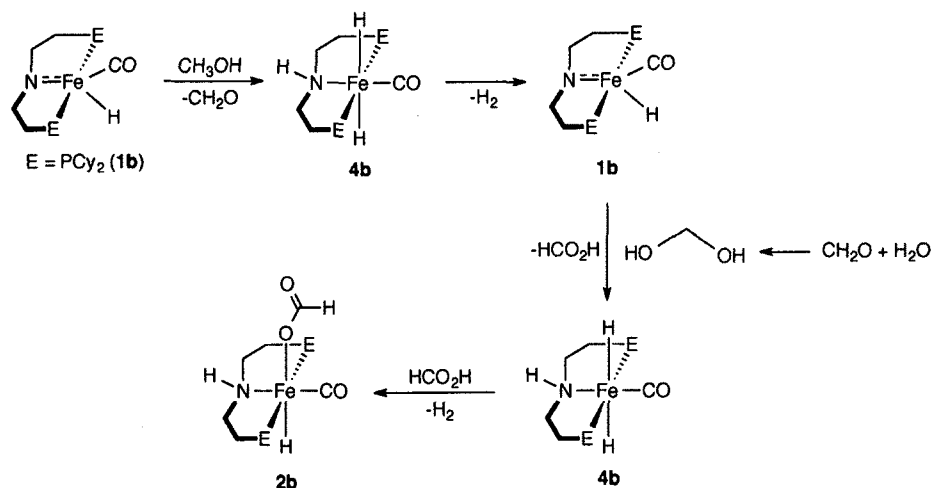


Scheme 4.04 Stoichiometric reactions of **1b** with MeOH and/or water.



Scheme 4.05. Proposed stepwise pathway for MeOH dehydrogenation in the absence of water.

In the reaction pathway shown in Scheme 4.03 water is necessary to fully dehydrogenate MeOH and generate three equivalents of H_2 . The stoichiometric reaction of **1b** with one equivalent of both MeOH and water, led to the formation of the previously characterized formate complex **2b** along with H_2 (Scheme 4.04c).⁵¹ A proposed pathway for this reaction is summarized in Scheme 4.06. Initially, MeOH is dehydrogenated by **1b** to generate formaldehyde and H_2 , via the dihydride intermediate **4b**. Subsequently, formaldehyde is trapped by water to form methanediol, which is dehydrogenated to form FA and **4b**. FA then protonates **4b** to form H_2 and the formate product **2b**. There is precedent for all of the steps in this reaction sequence.^{51,17d} In a control experiment, **1b** was treated with one equivalent of water (Scheme 4.04d). Even at low temperature a large number of different products were observed by ^{31}P NMR spectroscopy, none of which were identifiable. Furthermore, removal of the solvent led to almost complete decomposition of the complexes, with only a small amount of **1b** recovered, indicating that the addition of water is not reversible. This strongly suggests that when both water and MeOH are present, **1b** initially reacts with MeOH.



Scheme 4.06. Proposed pathway for stoichiometric reaction of one equivalent of MeOH and water with **1b**.

Aqueous-phase MeOH Dehydrogenation

Given the similarity of **1** to Beller's catalyst **C**, initial investigation of aqueous phase MeOH dehydrogenation focused on Beller's optimized conditions of 4:1 (molar ratio) MeOH:H₂O.¹⁵ In the absence of a base or other additive, **1b** catalyzes the generation of H₂ from an aqueous solution of MeOH in 58% yield, based on water as the limiting reagent (Table 4.04). However, methyl formate is also generated as a major product suggesting that complete MeOH dehydrogenation to H₂ and CO₂ is not occurring. When this reaction was monitored using ³¹P NMR spectroscopy the major Fe-containing product at the end of the reaction was the formate species **2b**. If **2b**, formed through 1,2 addition of FA to **1b** (*vide supra*), cannot undergo facile decarboxylation it represents a relatively inactive species in catalysis. In order to prevent the accumulation of **2b**, the catalytic reaction was performed in the presence of a variety of different LAs (Table 4.04). Several different LAs facilitate the complete aqueous phase dehydrogenation of MeOH, without formation of methyl formate. In general, the smaller, more oxophilic cations such as Li⁺ and Na⁺ are the most active. Additionally, non-coordinating anions are necessary, with PF₆⁻, BF₄⁻, and OTf giving the best results. It is possible to use LAs as simple as NaCl, but the poisoning effect of the chloride anion appears to be similar regardless of the cation, as there is little difference in activity between LiCl, NaCl and CsCl. Even in the presence of LAs, ³¹P NMR spectroscopy indicates that the formate complex **2b** is the resting state during catalysis, consistent with decarboxylation being the turnover-limiting step.

The six LAs that gave quantitative conversion of MeOH and water to H₂ and CO₂ were tested at lower catalyst loading to further explore the differences in their activities (Table 4.05). Despite their impressive performance at high catalyst loading, both LiOTf and NaOTf performed poorly under these conditions, while LiBF₄ was the most active, giving >99% yield in 12.5 hours. The gas produced from the reaction using LiBF₄ was analyzed by GC and found to contain a 3:1 ratio of H₂:CO₂ and <0.1% CO. This percentage of CO is significantly lower than that observed with the best heterogeneous catalysts^{10c,12} and comparable with state-of-the art precious metal homogeneous systems.³⁻⁴ Using LiBF₄ as the LA, the effect of changing the quantity of LA was explored (Table 4.06). When the catalyst loading of **1b** is 0.5 mol% the optimal LA loading is between 5-10 mol%, however at a lower loading of **1b** (0.1 mol%), a 10 mol% LA loading gives more efficient catalytic activity. The decrease in performance at both higher and lower LA loading is comparable to the LA effect that was observed in FA dehydrogenation using **1** and **2**.⁵¹

Table 4.04. LA screening for aqueous phase MeOH dehydrogenation using **1b**.^a

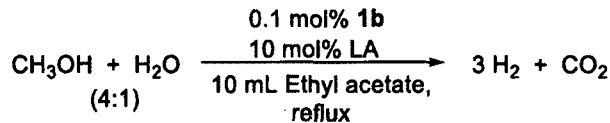
$$\text{CH}_3\text{OH} + \text{H}_2\text{O} \xrightarrow[\text{10 mL Ethyl acetate, reflux}]{\substack{0.5 \text{ mol\% } \mathbf{1b} \\ 10 \text{ mol\% LA}}} 3 \text{ H}_2 + \text{CO}_2$$

(4:1)

LA	TON ^b (Time, min) ^c	Yield (%) ^d	LA	TON ^b (Time, min) ^c	Yield (%) ^d
No additive	350 (20)	58 ^e	NaCl	500 (15)	82
			LiCl	500 (15)	83
LiPF ₆	>599 (30)	>99	KCl	500 (25)	82
NaPF ₆	420 (20)	70	CsCl	430 (15)	71
KPF ₆	>599 (35)	>99	CaCl ₂	300 (10)	49
LiBF ₄	>599 (25)	>99	NaBAR ₄ ^f	>599 (20)	>99
NaBF ₄	540 (20)	90	NaBPh ₄	400 (15)	68
KBF ₄	530 (30 min)	88	NaBF ₄	540 (20)	90
LiOTf	>599 (15)	>99			
NaOTf	>599 (35)	>99			
KOTf	390 (20)	65			

^aReaction conditions: Water (18 μ L, 1.0 mmol), MeOH (161 μ L, 4.0 mmol), **1b** (0.5 mol% with respect to water), LA (0.1 mmol, 10 mol% with respect to water), 10 mL ethyl acetate, reflux. ^bTON measured using a gas burette. Each equivalent of H₂ generated is counted as a TON. All numbers are the average of two runs. ^cTime at which no further increase in TON was observed. ^dBased on water as the limiting reagent. ^eMethyl formate was observed as a major product. ^fBAR₄^f = tetrakis[(3,5-trifluoromethyl)phenyl]borate

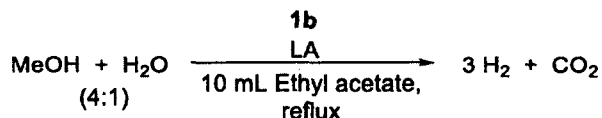
Table 4.05. Screening of LAs with low catalyst loading for MeOH dehydrogenation in the presence of water.^a



LA	Time (hr) ^b	TON ^c	Yield (%)
LiOTf	7	1500	52
NaOTf	6	620	20
LiBF ₄	10	>2900	>99
LiPF ₆	12.5	>2900	>99
KPF ₆	16	>2900	>99
NaBAR ₄ ^F	10	1900	63

^aReaction conditions: Water (18 μL , 1.0 mmol), MeOH (161 μL , 4.0 mmol), **1b** (0.1 mol% with respect to water), LA (0.10 mmol, 10 mol% with respect to water), 10 mL ethyl acetate, reflux. ^bTime at which no further increase in TON was observed. ^cTON measured using a gas burette. Each equivalent of H₂ generated is counted as a TON. All numbers are the average of two runs.

Table 4.06. Effect of amount of LA on MeOH dehydrogenation in the presence of water.^a



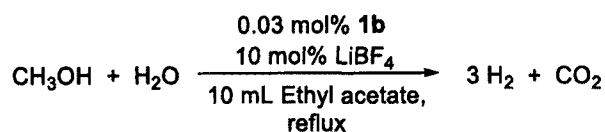
Mol% LA	Mol% 1b	Time (min) ^b	TON ^c	Yield (%)
1		25	350	58
2		25	380	62
5	0.5	20	>599	>99
10		25	>599	>99
20		60	>599	>99
5		320	980	32
10	0.1	600	>2900	>99
20		750	>2900	>99

^aReaction conditions: Water (18 μL , 1.0 mmol), MeOH (161 μL , 4.0 mmol), **1b** (x mol% with respect to water), LA (mol% with respect to water), 10 mL ethyl acetate, reflux. ^bTime at which no further increase in TON was observed. ^cTON measured using a gas burette. Each equivalent of H₂ generated is counted as a TON. All numbers are the average of two runs.

The effect of changing the ratio of MeOH:H₂O was explored using a catalyst system including **1b** and LiBF₄ (Table 4.07). A large excess of either MeOH or water afforded poor yields. More moderate ratios of 2:1 or 4:1 MeOH:H₂O gave significantly higher TON and yields, with a ratio of 4:1 giving a TON of 9500 (95% yield) in 41 hours. The significant decrease in catalytic activity at high water and/or MeOH concentrations may be related to the instability of **1b** in either neat MeOH or water. This is in contrast to the reaction of **1b** with one equivalent of a mixture of MeOH and water, which gave near quantitative

conversion to **2b**, with very little evidence of decomposition. Our optimal conditions are similar to those employed by Beller and co-workers to achieve a TON of approximately 10,000 in 43 hours using **C** and 8M KOH.¹⁵

Table 4.07. Effect of MeOH:H₂O ratio on MeOH dehydrogenation in the presence of water using **1b**.^a



MeOH:H ₂ O (molar)	Time (hr) ^b	TON ^c	Yield (%)
8:1	4	500	5
6:1	30	2800	28
4:1	41	9500	95
2:1	38	6000	60
1:1	5.5	5000	50
1:2	2.5	600	6

^aReaction conditions: Water (18 μ L, 1.0 mmol), appropriate molar quantity MeOH, **1b** (0.03 mol% with respect to water), LiBF₄ (0.10 mmol, 10 mol%), 10 mL ethyl acetate, reflux. ^bTime at which no further increase in TON was observed. ^cTON was measured using a gas burette. Each equivalent of H₂ generated is counted as a TON. All numbers are the average of two runs.

Finally, the catalytic activity of **1a**, **1b**, **2a**, **2b** and **C** were tested under optimized conditions (Table 4.08). In combination with LiBF₄, both the amido complexes **1a** and **1b** and the formate complexes **2a** and **2b** give yields greater than 80% (8000 turnovers) at 0.03 mol% catalyst loading. In an analogous fashion to the dehydrogenation of MeOH to methyl formate, **C** is not highly active under these base-free conditions, giving only 25% yield. Further optimization using **2a** at 0.01 mol% loading gave a TON of 30,000 and yield of greater than 99%. Lowering the catalyst loading to 0.006 mol% gave a TON of 51,000, but the yield was reduced to 50%. Overall, **2b** in combination with 10 mol% LiBF₄ represents the first example of base-free MeOH dehydrogenation by a first-row metal, giving five times greater turnover than previous Fe catalysts and twelve times better turnover than other base free systems.

Table 4.08. Screening of catalysts for MeOH dehydrogenation in the presence of water.^a

$$\text{CH}_3\text{OH} + \text{H}_2\text{O} \xrightarrow[\text{10 mL Ethyl acetate, reflux}]{\text{[Fe] 10 mol\% LiBF}_4} 3 \text{H}_2 + \text{CO}_2$$

(4:1)

Catalyst	Mol% [Fe]	Time (hr) ^b	TON ^c	Yield (%)
1a	0.03	42	8200	82
1b	0.03	41	9500	95
C	0.03	21	2500	25
2a	0.03	39	>9999	>99
2b	0.03	41	>9999	>99
2a	0.01	52	30,000	>99
2a	0.006	94	51,000	50

^aReaction conditions: Water (18 μL , 1.0 mmol), MeOH (160 μL , 4.0 mmol), [Fe], LiBF₄ (0.10 mmol, 10 mol%), 10 mL ethyl acetate, reflux. ^bTime at which no further increase in TON was observed. ^cTON measured using a gas burette. Each equivalent of H₂ generated is counted as a TON. All numbers are the average of two runs.

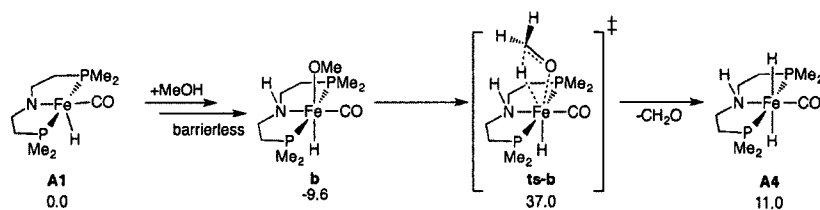
The superior catalytic activity of **2a** and **2b** compared to **1a** or **1b** appears surprising, given both the direct relationship between **2a/2b** and **1a/1b** via decarboxylation, and the assumption that **2a/2b** must convert to **1a/1b** before entering the catalytic cycle. A possible explanation for this disparity in reactivity lies in the nonproductive side reactions of five coordinate species with MeOH and water. Furthermore, it is important to note that these reactions are more prevalent at low temperature. For example, the 1,2-addition of MeOH to **1b**, which is not believed to lead to dehydrogenation, is more likely to occur at low temperature (*vide supra*). Thus, in catalysis using the five coordinate species, these unproductive side reactions deactivate some of the catalyst before MeOH dehydrogenation can occur. In contrast, in the case of the formate complexes, these side reactions are less likely to occur because the Fe center must first undergo decarboxylation, which typically only occurs at elevated temperature.⁵¹ Support for this hypothesis was obtained from the following experiment: the addition of an excess of a 4:1 molar mixture of MeOH:H₂O to an ethyl acetate solution containing **1b** and LiBF₄ at room temperature led to the formation of some free ligand, indicative of catalyst decomposition. In contrast, no reaction occurred when the same reaction was performed using **2b**. When **2a/2b** is used as a catalyst, in conjunction with a LA, decarboxylation occurs at a temperature that disfavors these nonproductive side reactions of **1a/1b** with MeOH and water. As such, the active catalytic species **1a/1b** are masked as **2a/2b** until they are activated by LA-assisted decarboxylation and react rapidly with MeOH to enter the catalytic cycle and generate

formaldehyde (Scheme 4.03*i*) rather than undergoing nonproductive reactions or decomposition via reactions outlined in Scheme 4.04, which are disfavored at such temperatures.

Mechanistic studies

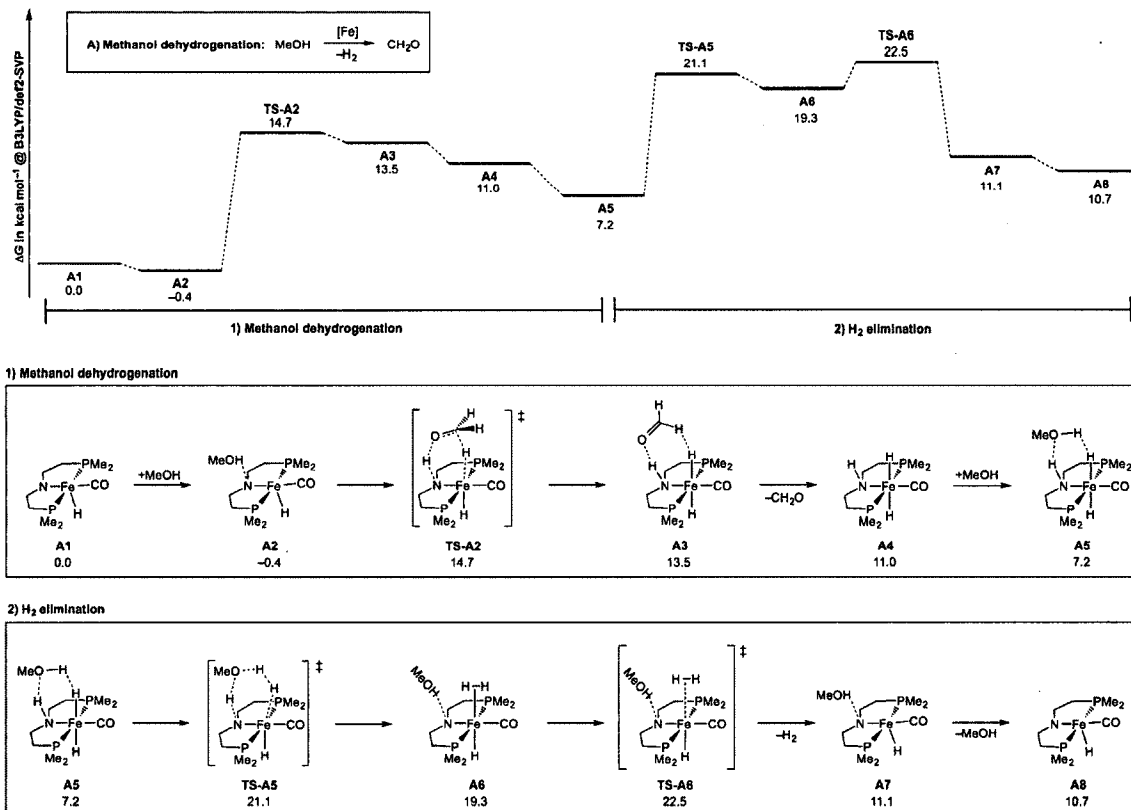
DFT calculations were performed by Moritz Förster to provide further insight into the mechanism of aqueous phase MeOH dehydrogenation using **1**. A smaller model Fe complex was used in the calculations by replacing the *iso*-propyl or cyclohexyl groups of the phosphine ligands with methyl substituents. It has previously been demonstrated that this change has only a minor effect on the energetics of PNP supported Fe complexes.^{17d} The relative free energies reported below were obtained at the B3LYP/def2-SVP level of DFT and relate to standard conditions (gaseous species at 298 K and 1 bar). The chosen level of DFT was validated by comparison to coupled-cluster single point results obtained at the extrapolated basis-set limit, CCSD(T)/CBS(T,Q), for a set of minima and transition structures representative of the system under study. The benchmarking study indicates sufficient agreement for a qualitative assessment of reaction pathways, but with a maximum deviation of about 6 kcal mol⁻¹ for relative electronic energies, expectations for a quantitative description are limited. This computational study explores pathways for full aqueous phase dehydrogenation of MeOH along the four-step reaction sequence depicted in Scheme 4.03. Accordingly, the four individual reaction steps are described as: **A**) MeOH dehydrogenation, **B**) hemi-acetal formation, **C**) methanediol dehydrogenation, and **D**) formate dehydrogenation. Stationary points identified along the individual routes are denoted correspondingly by preceding capital letters; please note that the numbering scheme deviates from that used in the experimental section above.

The first step in the dehydrogenation of MeOH is the formation of formaldehyde and one equivalent of H₂. A variety of possible mechanisms have been proposed for this step. Previously, Yang and co-workers^{18b} calculated a stepwise ionic pathway for the dehydrogenation of ethanol to acetaldehyde using **1a**.²² An alternative pathway for the reaction of MeOH and **A1** to generate formaldehyde and **A4** involves 1,2-addition of MeOH across the Fe-N bond to generate an alkoxide, followed by β -hydride elimination. The barrier to β -hydride elimination was calculated to be 46.6 kcal mol⁻¹ (Scheme 4.07)



Scheme 4.07. Possible pathway for MeOH dehydrogenation via 1,2-addition and β -hydride elimination

Despite this high barrier, initial 1,2-addition of MeOH was slightly energetically favored, consistent with our experimental observation of the alkoxide complex **3b** at low temperature (*vide supra*). However, it is more likely that the initial reaction to form formaldehyde occurs via lowest energy pathway shown in Scheme 4.08.

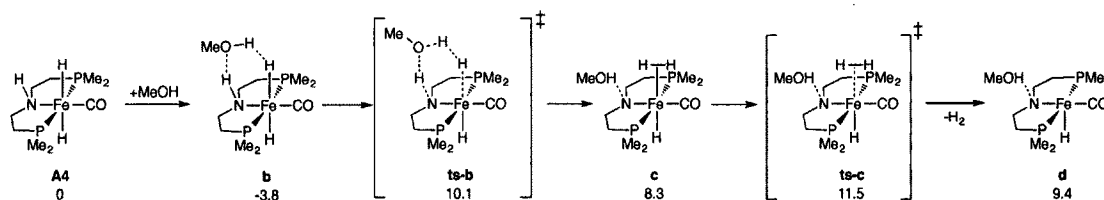


Scheme 4.08. Calculated lowest free energy pathway for MeOH dehydrogenation (A).

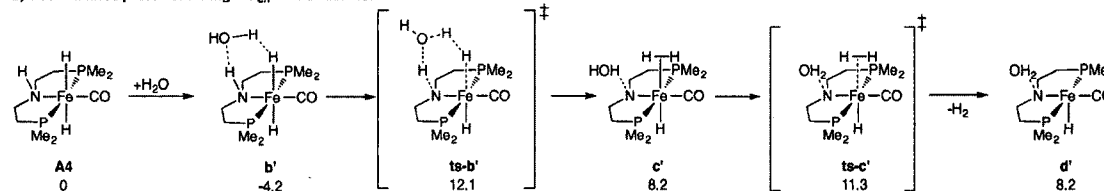
Initially, an encounter complex **A2** is formed via an N-H-O hydrogen bond between MeOH and the five coordinate amido species **A1**. Subsequently, concerted transfer of the hydrogen atoms associated with both the C-H and O-H bonds occurs to generate **A4** (corresponding to **4a** or **4b** discussed above) and formaldehyde, via an intermediate encounter complex **A3**. The barrier for this process via **TS-A2** is

relatively low (15 kcal mol⁻¹ relative to MeOH and A1) and this reaction sequence is analogous to the calculated first step in the conversion of alcohols to esters and two equivalents of H₂, which was previously reported.^{17d} The loss of dihydrogen from A4 to regenerate A1 is mediated by MeOH (Scheme 4.09 a). This step has a barrier of 23 kcal mol⁻¹ and represents the rate-determining step in the conversion of MeOH to formaldehyde and H₂. We have previously described this process for H₂ elimination in detail.^{17d} Scheme 4.09 shows possible pathways for the elimination of H₂ when mediated by MeOH (a) or water (b). The barrier for H₂ elimination is higher when mediated by water compared to MeOH. Furthermore, the barrier to H₂ elimination in the absence of a mediator is even higher and unlikely to occur (Scheme 4.09 c)

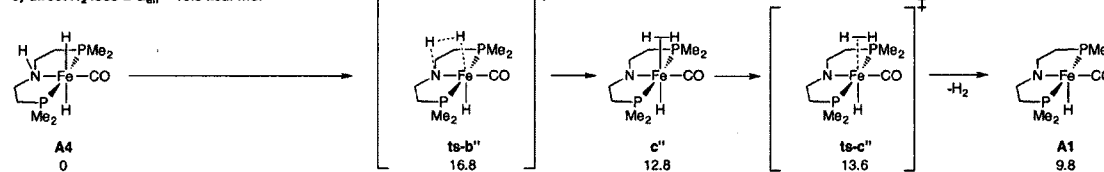
a) methanol assisted proton shuffling $\Delta^\ddagger G_{\text{eff}} = 15.3 \text{ kcal mol}^{-1}$



b) water assisted proton shuffling $\Delta^\ddagger G_{\text{eff}} = 16.3 \text{ kcal mol}^{-1}$



c) direct H₂ loss $\Delta^\ddagger G_{\text{eff}} = 16.8 \text{ kcal mol}^{-1}$



Scheme 4.09. Comparison of computed pathways for loss of H₂ from A4 a) MeOH assisted b) water assisted c) direct loss.

In line with expectation, the thermodynamic favorability of H₂ loss from A4 to form A1 varies as a function of the H₂ pressure (Figure 4.03), consistent with experimental results on the stability of 4a/4b.⁵¹

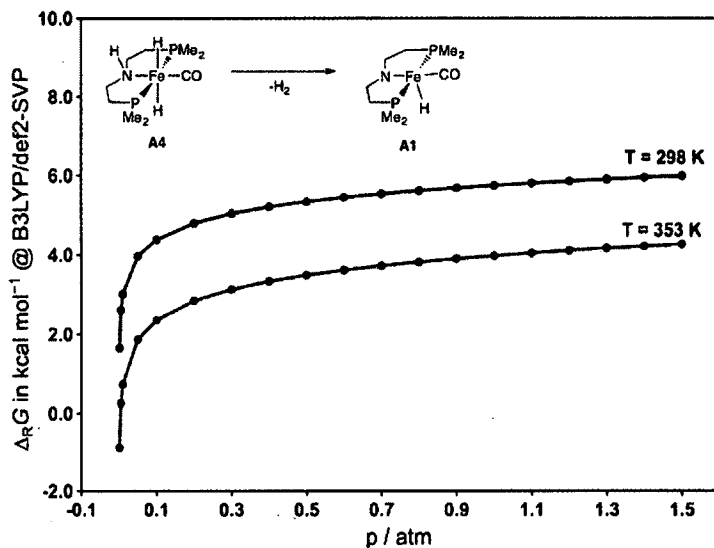
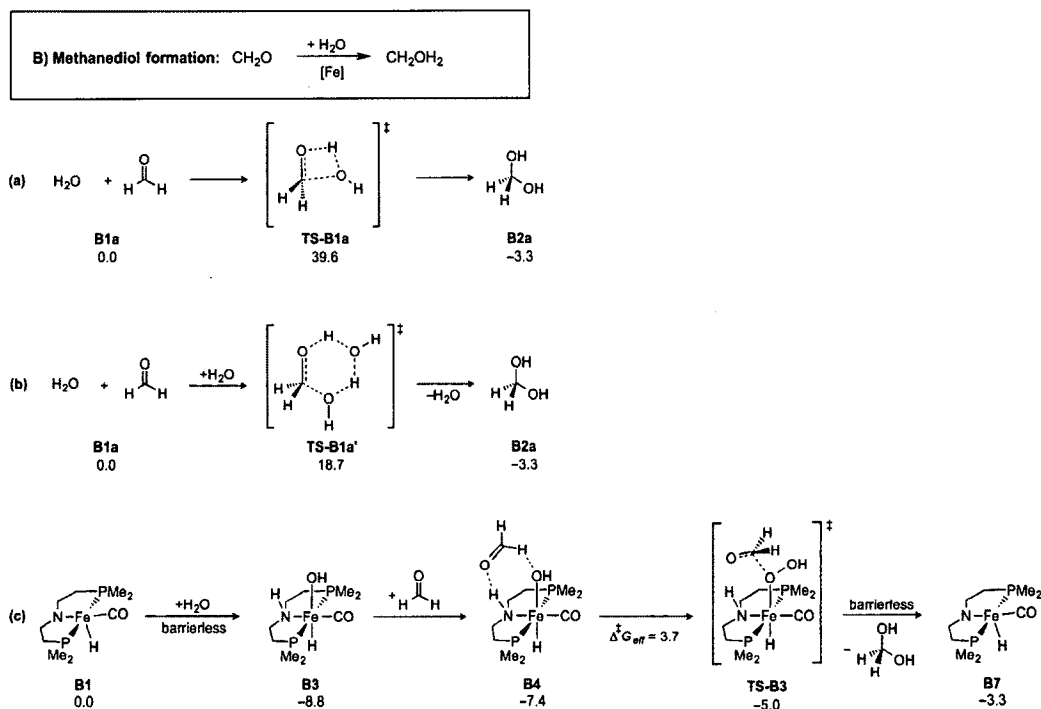


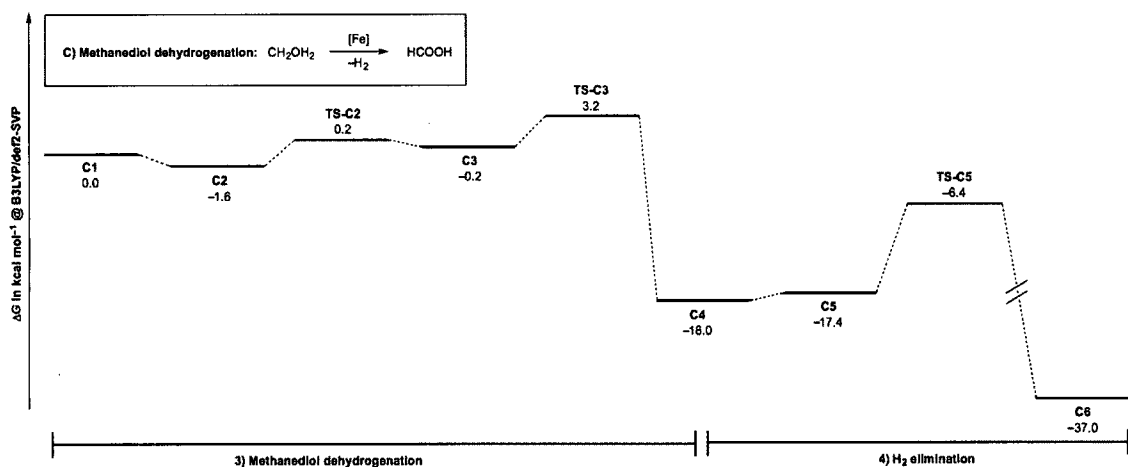
Figure 4.03. Impact of the applied pressure on the reaction free energy for the conversion of **A4** to **A1** and one equivalent H_2 at two temperatures.

The second step in MeOH dehydrogenation involves the reaction of formaldehyde with water to form methanediol. Recently both our group^{17d} and Azofra and co-workers²³ reported that there was a large barrier to uncatalyzed hemi-acetal formation from MeOH and formaldehyde. Similarly, the barrier to uncatalyzed methanediol formation from MeOH and water is also high (40 kcal mol⁻¹, Scheme 4.10a). A pathway in which a second molecule of water acts as a shuttle is significantly lower in energy, with a barrier of 19 kcal mol⁻¹ for the six-membered transition state (Scheme 4.10b). However, the lowest energy pathway for methanediol formation is mediated by **B1** (Scheme 4.10c) and involves initial 1,2-addition of water across the Fe-N bond to generate the hydroxide complex (**B3**, similar to **3b** discussed in the experimental section). This species forms an encounter complex with formaldehyde (**B4**), which facilitates the formation of the new C-O and O-H bonds, via a low energy transition state (**TS-B3**, 4 kcal mol⁻¹). The facile calculated pathway for 1,2-addition of water to **B1** is consistent with the experimental observation that **1** reacts rapidly with water (Scheme 4.04d), although no well-defined products were characterized in these experiments.

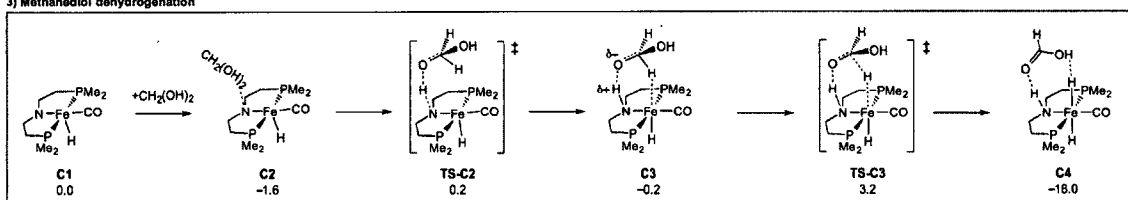


Scheme 4.10. Calculated pathways for conversion of formaldehyde and water into methanediol (**B**).

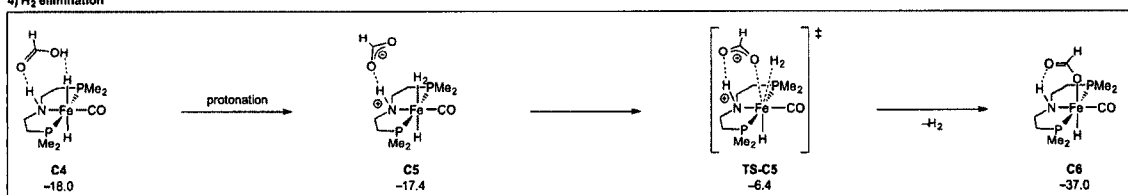
The third step in the overall process is the dehydrogenation of methanediol (Scheme 4.11). The initial approach of methanediol to **C1** is similar to that described for MeOH, with an encounter complex **C2**, formed via an N-H-O hydrogen bond. However, the subsequent dehydrogenation occurs through a stepwise rather than a concerted pathway. Initially, the amido ligand is protonated by methanediol to form intermediate **C3**. Subsequent transfer of the hydrogen atom associated with one of the C-H bonds of methanediol generates **C4**, an encounter complex between FA and the dihydride complex. FA, which is the strongest acid generated in the reaction cascade, then protonates an Fe-H bond in **C4** to form **C5**, a cationic molecular H_2 complex stabilized by a formate ion. The whole reaction cascade **C1** to **C5** occurs without significant activation barriers. The subsequent displacement of the coordinated H_2 ligand by formate to form **C6** has a small barrier (12 kcal mol⁻¹ via **TS-C5**). Overall, methanediol dehydrogenation represents a highly exergonic process (-37 kcal mol⁻¹ relative to **B1** or -26 kcal mol⁻¹ relative to **A1**).



3) Methanediol dehydrogenation



4) H₂ elimination

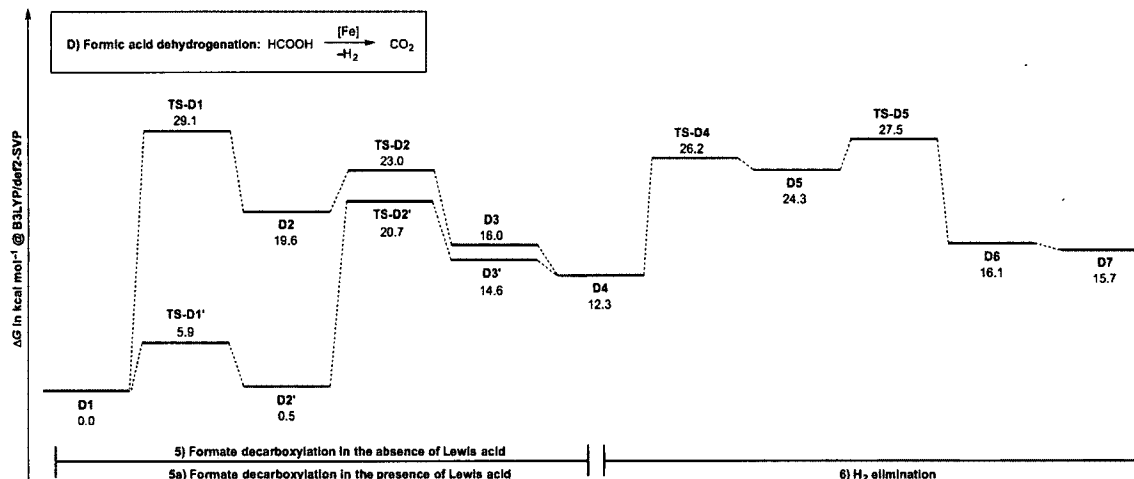


Scheme 4.11. Calculated lowest free energy pathway for methanediol dehydrogenation (C).

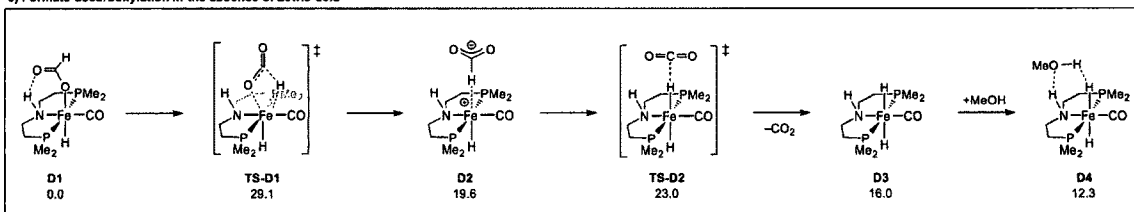
The final step in aqueous phase MeOH dehydrogenation is the decarboxylation of the formate complex **D1**, followed by release of H₂ to regenerate **D7** (Scheme 4.12). We have previously demonstrated that in the absence of LA the barrier for the decarboxylation of **D1** is high,⁵¹ consistent with the experimental observation that a LA is required for this process. As there is little relevant information on the nature of the Na⁺ coordination environment in the rather complex reaction mixture, Na(H₂O)₆⁺ was chosen as a model LA to study its influence on the formate decarboxylation in a qualitative fashion. The calculations predict that expulsion of one water ligand from the coordination sphere of Na⁺ and binding of Na(H₂O)₅⁺ to the formate ligand in **D1** is thermodynamically favored by -12 kcal mol⁻¹. This value is almost certainly an overestimation as no significant changes are observed in the NMR properties of the formate complexes when LAs are added and a species with a LA coordinated has never been isolated. In reality, it can be assumed that a LA adduct of the formate complex is approximately isoenergetic with the separated LA and

the formate in solution. Nevertheless as was previously hypothesized,⁵¹ Na⁺ coordination to the formate ligand stabilizes the negative charge that develops in the decarboxylation step, thereby significantly lowering its activation barrier. Correspondingly, both transition states, **TS-D1** and **TS-D2**, and the H-bound formate intermediate **D2** are substantially lowered by LA coordination (Scheme 4.12). Subsequent release of H₂ from **D3** to regenerate **D7** is then again facilitated by MeOH, as described before. In the presence of the LA, the latter step is overall rate limiting for the sequence **D1** to **D7**. In this scenario, there is a pre-equilibrium involving reversible CO₂ insertion/decarboxylation and the formate complex **D1** represents the resting state during catalysis, which is consistent with experimental observations.

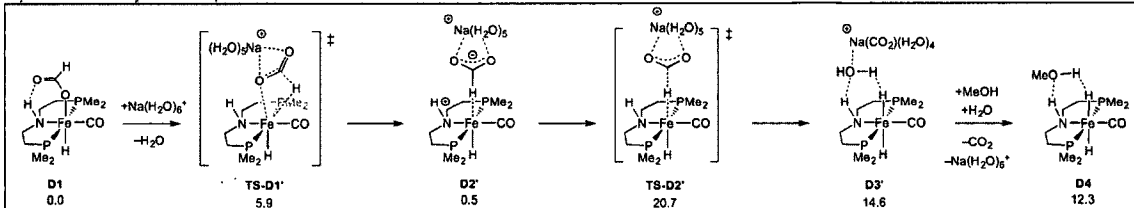
In summary, these calculations provide a qualitative picture of the elementary steps involved in aqueous phase MeOH dehydrogenation. Both the role of the LA in facilitating decarboxylation, and the difficulty associated in 1,2-elimination of H₂ from **4a/4b** have been identified. With this information it is clear that in order to design improved catalysts based on these Fe systems, it is crucial to reduce the barrier for H₂ elimination. This may result in systems which operate at lower temperature and are more stable, a necessary feature to achieving TONs which are comparable to the best precious metal systems.



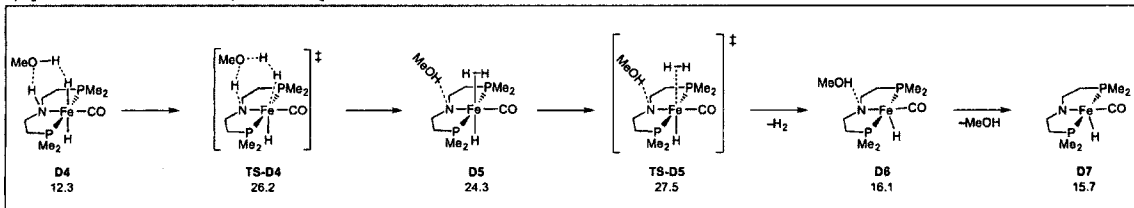
5) Formate decarboxylation in the absence of Lewis acid



5a) Formate decarboxylation in the presence of Lewis acid



6) H₂ elimination via a MeOH assisted proton shuffling mechanism



Scheme 4.12. FA dehydrogenation: Lowest free energy pathways in the absence (black) and presence of LA (red) (D).

III. Conclusions

A family of PNP-supported Fe complexes are highly active catalysts for the dehydrogenation of MeOH. In the absence of water, these catalysts rapidly convert MeOH to methyl formate and H₂. Although a LA is not required for this reaction, the catalytic system which gives the highest TON (approximately 20,000) requires a LA for activation. In the presence of water, the Fe complexes fully dehydrogenate MeOH to H₂ and CO₂, provided a LA co-catalyst is present. For this reaction the best Fe/LiBF₄ system gives a TON of

approximately 51,000, which is the highest reported to date for a homogeneous first row transition metal catalyst, or a system that does not require a Brønsted base. The mechanism of the reaction is proposed to involve four steps: (i) initial dehydrogenation of MeOH to formaldehyde; (ii) reaction of water with formaldehyde to form methanediol; (iii) dehydrogenation of methanediol to form an Fe formate species and H₂; and (iv) decarboxylation of the Fe formate species to release CO₂ and the final equivalent of H₂. The LA is required to facilitate the decarboxylation of the Fe formate species, while the ability of the PNP ligand to undergo bifunctional reactivity, such as 1,2-addition or elimination, is crucial to many of the elementary steps in the reaction pathway.

IV. Experimental Details

General Methods

Experiments were performed under a dinitrogen or argon atmosphere in a dry box or using standard Schlenk techniques, unless otherwise noted. Under standard dry box conditions, purging was not performed between uses of pentane, diethyl ether, benzene, toluene and THF; thus, when any of these solvents were used, traces of all these solvents were in the atmosphere and could be found intermixed in the solvent bottles. Moisture- and air-sensitive liquids were transferred by stainless steel cannula on a Schlenk line or in a dry box. Solvents were dried by passage through a column of activated alumina followed by storage under dinitrogen or argon. Ethyl acetate, propylene carbonate and dioxane were dried over CaH₂ and distilled before use. All commercial chemicals were used as received, except where noted. Lithium hexafluorophosphate, sodium hexafluorophosphate, potassium hexafluorophosphate, lithium triflate, sodium triflate, potassium triflate, and sodium tetraphenylborate were purchased from Fisher Scientific Company. Sodium chloride, lithium chloride, potassium chloride, cesium chloride, calcium chloride, lithium tetraphenylborate, sodium tetraphenylborate, and potassium tetraphenylborate were purchased from Acros. Deuterated solvents were obtained from Cambridge Isotope Laboratories. *d*₈-toluene was dried over sodium metal and vacuum-transferred prior to use. NMR spectra were recorded on Bruker AMX-400, AMX-500, AMX-600, spectrometers at ambient probe temperatures, unless otherwise noted. Literature procedures were used to prepare sodium tetrakis[(3,5-trifluoromethyl)phenyl]borate (NaBAr^F₄),²⁴ **1a**,⁵¹ **1b**,⁵¹ **2a**,⁵¹ **2b**,⁵¹ and **C**.¹⁶

X-ray Crystallography

X-ray diffraction experiments were carried out on a Rigaku R-AXIS RAPID diffractometer coupled to a R-AXIS RAPID imaging plate detector with graphite-monochromated Mo K α radiation ($\lambda = 0.71073 \text{ \AA}$) at -123°C . The crystals were mounted on MiTeGen polyimide loops with immersion oil. The data frames were processed using Rigaku CrystalClear and corrected for Lorentz and polarization effects. Using Olex2²⁵ the structure was solved with the XS²⁶ structure solution program by Patterson methods and refined with the XL²⁶ refinement package using least-squares minimization. The non-hydrogen atoms were refined anisotropically. Hydrogen atoms were refined using the riding model.

Computational Details

DFT calculations were performed using the Gaussian09 program package.²⁷ The B3LYP hybrid functional,²⁸ as implemented in Gaussian09, was used in combination with the def2-SVP basis set.²⁹ Unscaled zero-point vibrational energies as well as thermal and entropic corrections were obtained from computed Hessians using the standard procedures implemented in Gaussian09 and were used to obtain Gibbs free energies at 298.15 (1 bar atmospheric pressure).

Gas Chromatography

Gas chromatography experiments were performed on a Buck Scientific 910 Gas Chromatograph with FID/TCD and methanizer. The system uses N₂ as a carrier gas and allows for determination of the following gases at the detection limits: H₂ \geq 100 ppm, CO \geq 1 ppm and CO₂ \geq 1 ppm.

Representative Procedure for Catalytic MeOH Dehydrogenation in the Absence of Water

In a dry box, a 50 mL Schlenk flask was loaded with the appropriate catalyst, MeOH, and the desired solvent. The Schlenk flask was sealed with a glass stopper and removed from the dry box and attached to a gas burette setup and reflux condenser (*vide infra*). The gas burette and tubing was subjected to three vacuum/N₂ purge cycles and allowed to equilibrate. The solution flask was then lowered into an oil bath preheated to the desired temperature upon which gas evolution began immediately. The change in water

level in the gas burette (V_{obs}) was used to determine turnover using previously reported methods (*vide infra*).^{51,15} Each equivalent of H_2 produced was taken to be one turnover. A blank reaction was run in which no catalyst was added to the solution. The volume of gas obtained from this reaction (trace solvent and MeOH) was recorded as V_{blank} .

Representative Procedure for Catalytic Aqueous Phase MeOH Dehydrogenation

In a dry box, a 50 mL Schlenk flask was loaded with the appropriate catalyst, additive (LA), MeOH, water and desired solvent. The Schlenk flask was sealed with a glass stopper and removed from the dry box and attached to a gas burette setup and reflux condenser as shown below. The flask was then attached to a gas burette and reflux condenser (*vide infra*). The gas burette and tubing was subjected to three vacuum/ N_2 purge cycles and the U-tube trap was cooled with liquid nitrogen. The solution flask was then lowered into an oil bath preheated to desired temperature upon which gas evolution began immediately. The change in water level in the gas burette (V_{obs}) used to determine turnover using previously reported methods (*vide infra*).^{51,15} Each equivalent of H_2 produced was taken to be one turnover. Upon completion of reaction, the U-tube was removed from the liquid nitrogen bath and the CO_2 gas evolved was measured by the burette to be 1/3 of total turnover. A blank reaction was run in which no catalyst was added to the solution. The volume of gas obtained from this reaction (trace solvent, water and MeOH) was recorded as V_{blank} .

Experimental setup for measurement of H₂ in dehydrogenation reactions

H₂ was collected using the setup shown below in Figure 4.04

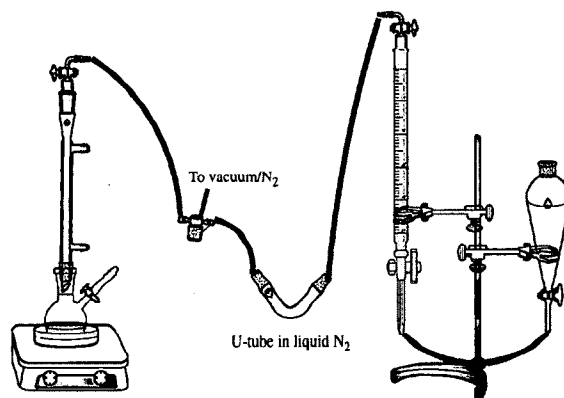


Figure 4.04. Burette set up used to collect H₂ for catalytic MeOH dehydrogenation.

Equation used to calculate TON

The TON was calculated using previously reported methods^{51,15} and as described in Chapter 3, with a few modifications.

Operating under the assumption that all gas produced in MeOH dehydrogenation to methyl formate is hydrogen, the equation below can be used to determine the volume per mol of H₂ at 298.15K. Each molecule of hydrogen is considered a turnover.

The TON was determined using the following expression:

TON = $n_{\text{prod}}/n_{\text{cat}}$ where n_{cat} is the molar quantity of the catalyst.

The following expression was used to determine the volume per mol of H₂ at 298.15K:

$$V_{\text{H}_2} = \frac{RT}{p} + b - \frac{a}{RT} = 24.49 \text{ L/mol}$$

$$R = 8.3145 \text{ m}^3 \text{ Pa mol}^{-1} \text{ K}^{-1}$$

$$T = 298.15 \text{ K}$$

$$p = 101325 \text{ Pa}$$

$$b = 26.7 \cdot 10^{-6} \text{ m}^3 \text{ mol}^{-1}$$

$$a = 2.49 \cdot 10^{-10} \text{ Pa m}^3 \text{ mol}^{-2}$$

In aqueous-phase MeOH dehydrogenation all of the CO₂ generated was trapped in the U-tube cooled by liquid N₂. This was verified by measuring the amount of gas produced when the U-tube was allowed to warm to room temperature and by GC.

Additional Stoichiometric Reactions

Addition of 1 eq MeOH to 1b at -80°C

In a nitrogen-filled glovebox, a J. Young NMR tube was charged with **1b** (15 mg, 27.3 μmol) and 0.3 mL *d*₈-toluene. The tube was then placed in a liquid nitrogen-cooled cold well until the solution was frozen. A solution of MeOH (27.3 μmol) in 0.1 mL *d*₈-toluene was then added to the tube and once again allowed to cool until frozen. The tube was then removed from the glovebox and immediately placed in a cold bath at -78°C. Once the solution had warmed to -78°C, the tube was inverted several times to ensure mixing and placed back in the cold bath. To perform the NMR study, the tube was placed in an NMR spectrometer that had been precooled to -80°C and spectra were obtained at the specified temperatures. The hydride region of the ¹H NMR spectrum (Figure 4.05) and selected ³¹P{¹H} NMR spectra (Figure 4.06) are shown below.

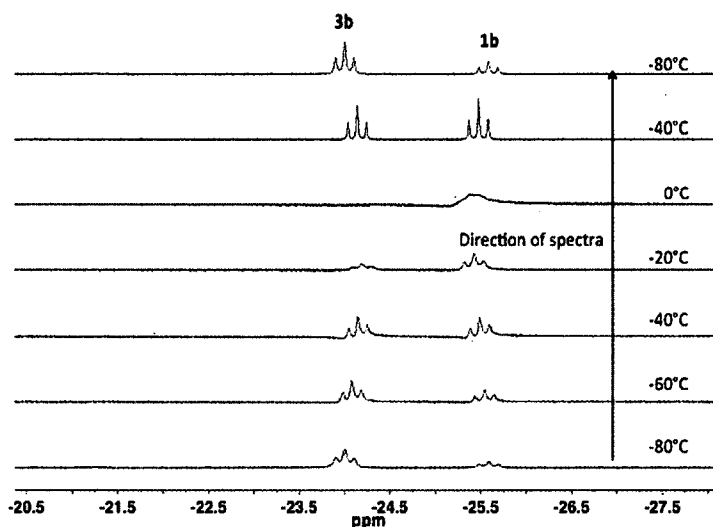


Figure 4.05. ¹H NMR spectra at different temperatures from the reaction of **1b** with 1 eq MeOH at -80°C.

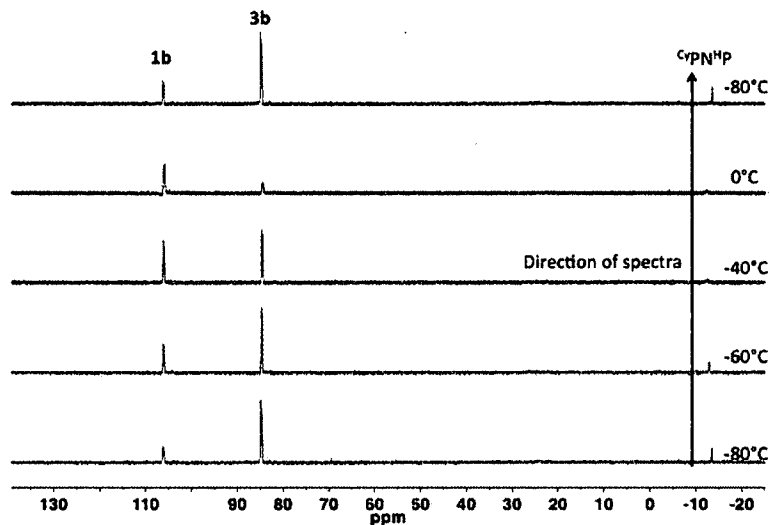


Figure 4.06. $^{31}\text{P}\{^1\text{H}\}$ NMR spectra at different temperatures from the reaction of **1b** with 1 eq MeOH at -80°C .

*Addition of 1 eq CD_3OD to **1b** at -75°C*

In a nitrogen-filled glovebox, an NMR tube was charged with **1b** (3.8 mg, 6.9 μmol), 0.4 mL toluene and 3 drops of d_6 -benzene (to enable locking and shimming of the NMR machine). The NMR tube was sealed with a Cajon compression fitting and attached to a vacuum line. The sample was frozen in liquid nitrogen and one equivalent of CD_3OD was added via calibrated gas bulb (11 torr in 10.91 mL). The tube was then flame sealed, removed from the liquid nitrogen bath and immediately placed in a cold bath at -78°C . Once the solution had warmed to -78°C , the tube was inverted several times to ensure mixing and placed back in the cold bath. To perform the NMR study, the tube was placed in an NMR spectrometer that had been precooled to -75°C and ^2H NMR spectra were obtained at the specified temperatures. These are shown below in Figure 4.07.

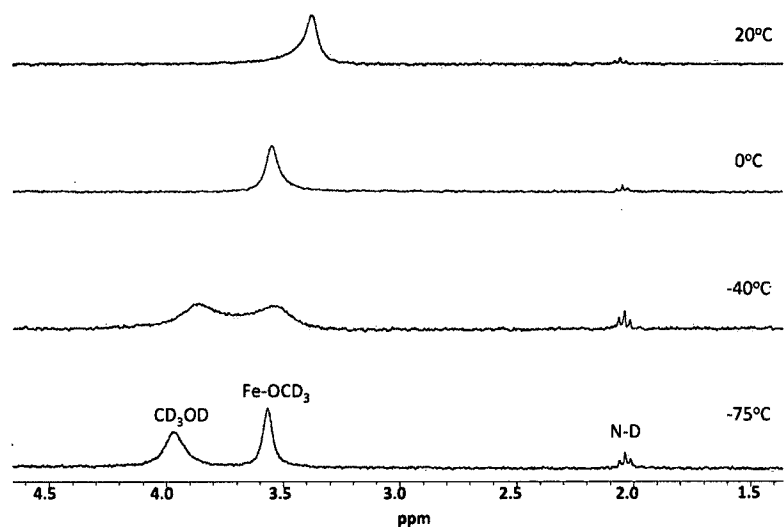


Figure 4.07. ^2H NMR spectra at different temperatures from the reaction of **1b** with 1 eq CD_3OD at -75°C .

Addition of 1 eq MeOH to 1b at 50°C

In a nitrogen-filled glovebox, a J. Young NMR tube was charged with **1b** (15 mg, $27.3\ \mu\text{mol}$) and 0.3 mL d_8 -toluene. A solution of MeOH ($27.3\ \mu\text{mol}$) in 0.1 mL d_8 -toluene was then added to the tube at room temperature. The tube was then sealed and removed from the glovebox and immediately placed in an oil bath preheated to 50°C . After heating for 40 min, the tube was removed from the oil bath and ^1H and $^{31}\text{P}\{^1\text{H}\}$ NMR spectra recorded. These spectra indicated the formation of **4b**, $(^{\text{C}}\text{yPN}^{\text{H}}\text{P})\text{Fe}(\text{CO})_2$, $^{\text{C}}\text{yPN}^{\text{H}}\text{P}$, and H_2 . The $^{31}\text{P}\{^1\text{H}\}$ NMR spectrum is shown below in Figure 4.08. The atmosphere of the J. Young NMR tube was then vacuum transferred to another J. Young NMR tube containing 0.4 mL degassed d_6 -benzene. The ^1H NMR spectrum of this solution contained resonances corresponding to methyl formate and MeOH and is shown below in Figure 4.09.

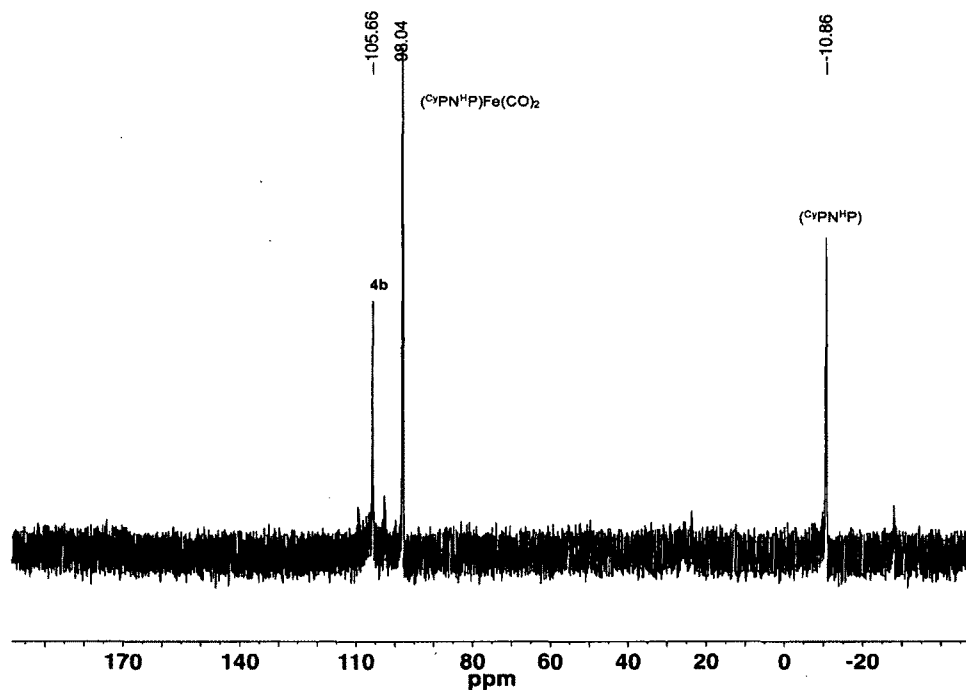


Figure 4.08. $^{31}\text{P}\{^1\text{H}\}$ NMR spectrum of crude mixture from the reaction of **1b** with 1 eq MeOH after heating at 50°C for 40 min.

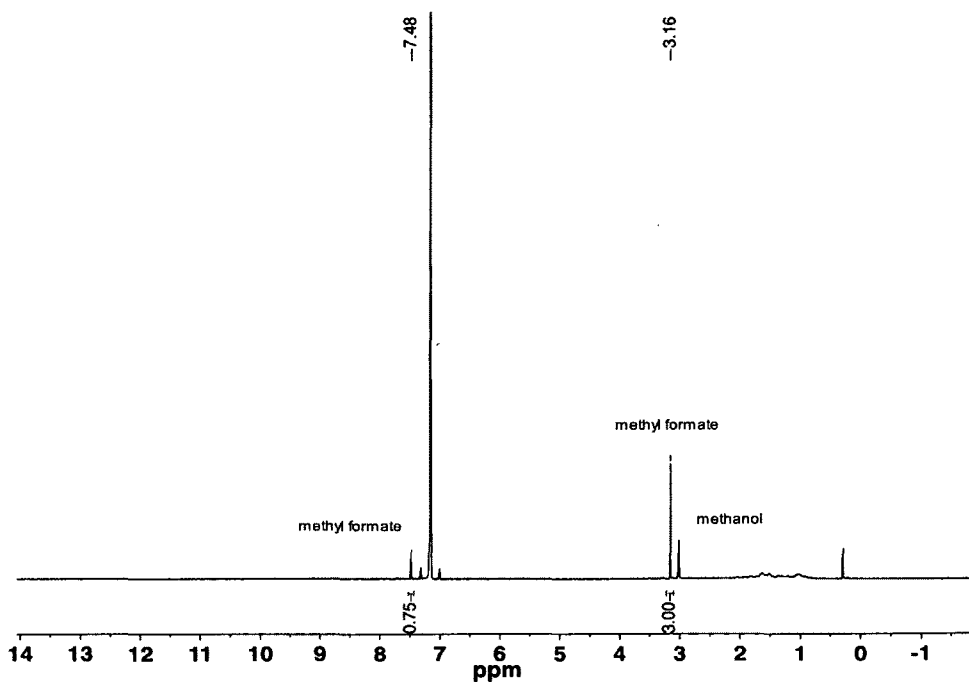


Figure 4.09. ^1H NMR spectrum of organic products vacuum transferred from reaction of **1b** with 1 eq MeOH.

Addition of 2 eq MeOH to 1b at 50°C

In a nitrogen-filled glovebox, a J. Young NMR tube was charged with **1b** (15 mg, 27.3 μmol) and 0.3 mL d_8 -toluene. A solution of MeOH (54.6 μmol) in 0.1 mL d_8 -toluene was then added to the tube at room temperature. The tube was then sealed and removed from the glovebox and immediately placed in an oil bath preheated to 50°C. After heating for 40 min, the tube was removed from the heat and ^1H and $^{31}\text{P}\{^1\text{H}\}$ NMR spectra were recorded, indicating formation of **4b**, $(^{\text{C}}\text{yPN}^{\text{H}}\text{P})\text{Fe}(\text{CO})_2$, $^{\text{C}}\text{yPN}^{\text{H}}\text{P}$, and H_2 . The atmosphere of the J. Young NMR tube was then vacuum transferred to another J. Young NMR tube containing 0.4 mL degassed d_6 -benzene. The ^1H NMR spectrum of this solution contained resonances corresponding to methyl formate.

Addition of 1 eq MeOH and 1 eq H₂O to 1b

In a nitrogen-filled glovebox, **1b** (10 mg, 18.2 μmol) was dissolved in 0.4 mL d_6 -benzene. Water (18.2 μmol) and MeOH (18.2 μmol) were added at room temperature and the tube was capped and shaken to fully mix. ^1H and $^{31}\text{P}\{^1\text{H}\}$ NMR spectroscopy (Figures 4.10 and 4.11) indicate the exclusive formation of **2b** and H_2 . There is no evidence for decomposition of the Fe containing starting material or product.

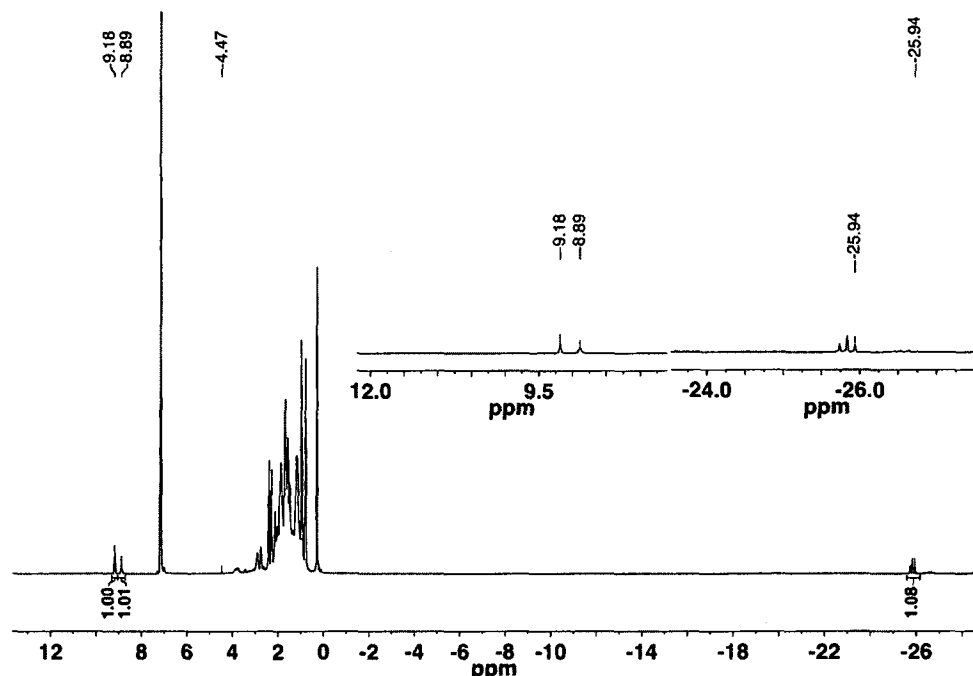


Figure 4.10. ^1H NMR spectrum from reaction of 1 eq of MeOH and 1 eq of H_2O with **1b**.

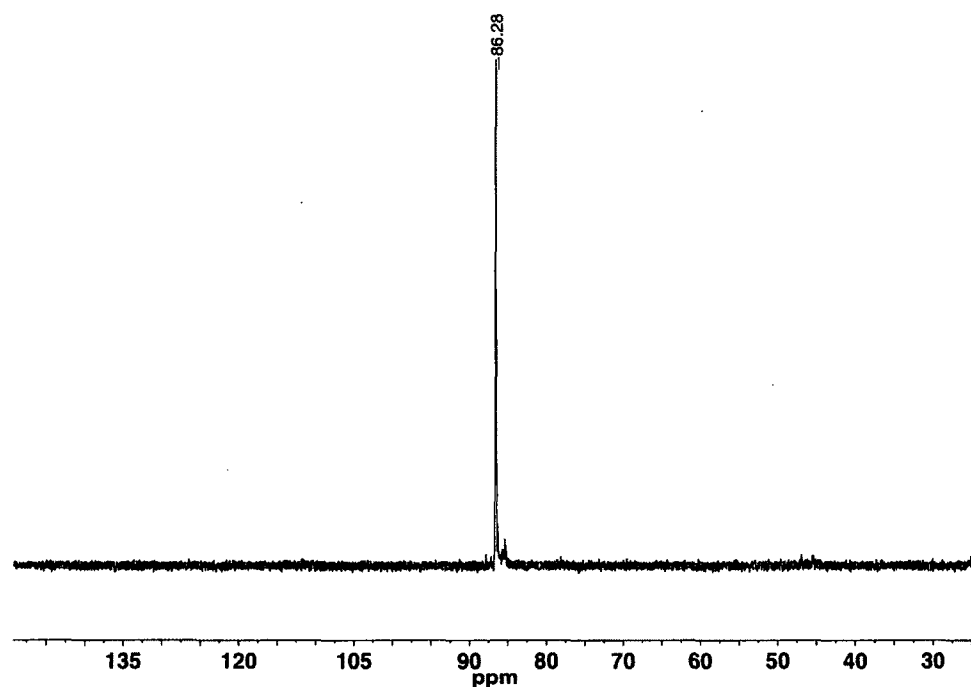


Figure 4.11. $^{31}\text{P}\{^1\text{H}\}$ NMR spectrum from reaction of 1 eq of MeOH and 1 eq of H_2O with **1b**.

Speciation of Fe at room temperature under catalytic conditions

1b

In a nitrogen-filled glovebox, a vial was charged with **1b** (10 mg, 18.2 μmol), LiBF_4 (10 mg, 10 mol% with respect to water), MeOH (161 μL , 4 mmol), water (18 μL , 1 mmol) and 10 mL ethyl acetate. The vial was agitated at room temperature for 30 minutes, after which a 400 μL aliquot was placed in a J. Young NMR tube. A $^{31}\text{P}\{^1\text{H}\}$ NMR spectrum was obtained and showed formation of free ligand as well as unidentified peaks between 30-40 ppm.

2b

In a nitrogen-filled glovebox, a vial was charged with **2b** (10 mg, 16.8 μmol), LiBF_4 (10 mg, 10 mol% with respect to water), MeOH (161 μL , 4 mmol), water (18 μL , 1 mmol) and 10 mL ethyl acetate. The vial was agitated at room temperature for 30 minutes, after which a 400 μL aliquot was placed in a J. Young NMR

tube. A $^{31}\text{P}\{^1\text{H}\}$ NMR spectrum was obtained and showed **2b** to be the only species in solution, with no formation of free ligand or unidentified products as with **1b**.

Measurement of Kinetic Isotope Effects

MeOH dehydrogenation in the absence of water catalyzed by 1b.

In a nitrogen-filled glovebox, MeOH (36 μL , 0.91 mmol), 10 mL ethyl acetate and **1b** (0.91 μmol , 0.1 mol%) were added to a Schlenk flask. The flask was sealed, removed from the glovebox and attached to the burette setup (*vide supra*). The system was evacuated and purged with N_2 three times and the flask then lowered into a oil bath preheated to 80°C at which point gas evolution began. The reaction rate (k_{H}) was determined using the method of initial rates. A similar reaction was run using d_4 -MeOH (37 μL , 0.91 mmol) to determine k_{D} . The KIE was determined using $\text{KIE} = k_{\text{H}}/k_{\text{D}}$.

Formic acid dehydrogenation catalyzed by 1b.

In a nitrogen-filled glovebox **1b** (2.91 μmol , 0.1 mol%), 9 mL ethyl acetate and 10 mol% LiBF_4 were added to a Schlenk flask. A syringe was loaded with formic acid (110 μL , 2.91 mmol) and 1 mL ethyl acetate. The flask was sealed with a rubber septum, the flask and syringe removed from the glovebox and attached to the burette setup as previously described (*vide supra*). The system was evacuated and purged with N_2 three times and the flask lowered into a preheated oil bath at 80°C . The formic acid/ethyl acetate solution was then injected via the rubber septum and gas evolution began. The reaction rate (k_{H}) was determined using the method of initial rates. A similar reaction was run using d_2 -formic acid (109 μL , 2.91 mmol) to determine k_{D} . The KIE was determined using $\text{KIE} = k_{\text{H}}/k_{\text{D}}$.

Crystallization Methods

Crystallization of $(^{\text{C}}\text{yPN}^{\text{H}}\text{P})\text{Fe}(\text{CO})_2$

In a nitrogen-filled glovebox, a Schlenk flask was loaded with MeOH (161 μL , 4.0 mmol), water (18 μL , 1.0 mmol), 10 mol% LiBF_4 (0.10 mmol, 9.4 mg), 10 mL ethyl acetate, and **1b** (0.1 mol% with respect to water). The flask was sealed and removed from the glovebox and attached to the burette system as described above. The system was evacuated and purged with N_2 three times and the flask lowered into an

oil bath preheated at 80°C, at which time gas evolution began. The reaction was allowed to run to completion (10 hours) and the flask was resealed and placed in a freezer at -30°C overnight after which time (^{Cy}PN^HP)Fe(CO)₂ was obtained as pale red crystals.

V. Acknowledgements

I am grateful to Dr. Brandon Mercado for X-ray crystallography of (^{Cy}PN^HP)Fe(CO)₂, to Dr. Wesley Bernksoetter and Yuanyuan Zhang for their continued insight and helpful discussions and assistance in running NMR reactions, to Dr. Christoph Rose-Petruck for the use of his GC and to Steven Ahn for help in operating the machine, and to Dr. Max Holthausen and Moritz Förster for their computational work. I am also grateful to Jocelyn Legere for her hard work over the summer of 2013, and for running many catalytic reactions as we worked to determine optimal conditions.

VI. References

- 1) Shinoda, S.; Itagaki, H.; Saito, Y. *J. Chem. Soc., Chem. Commun.* **1985**, 860.
- 2) Morton, D.; Cole-Hamilton, D. J. *J. Chem. Soc., Chem. Commun.* **1987**, 248.
- 3) Rodríguez-Lugo, R. E.; Trincado, M.; Vogt, M.; Tewes, F.; Santiso-Quinones, G.; Grützmacher, H. *Nat. Chem.* **2013**, *5*, 342.
- 4) Nielsen, M.; Alberico, E.; Baumann, W.; Drexler, H.-J.; Junge, H.; Gladiali, S.; Beller, M. *Nature* **2013**, *495*, 85.
- 5) (a) Fellay, C.; Dyson, P. J.; Laurency, G. *Angew. Chem., Int. Ed.* **2008**, *47*, 3966; (b) Manaka, Y.; Wang, W.-H.; Suna, Y.; Kambayashi, H.; Muckerman, J. T.; Fujita, E.; Himeda, Y. *Catal. Sci. Tech.* **2014**, *4*, 34; (c) Gao, Y.; Kuncheria, J.; J. Puddephatt, R.; P. A. Yap, G. *Chem. Commun.* **1998**, 2365; (d) Oldenhof, S.; de Bruin, B.; Lutz, M.; Siegler, M. A.; Patureau, F. W.; van der Vlugt, J. I.; Reek, J. N. H. *Chem. Eur. J.* **2013**, *19*, 11507; (e) Zell, T.; Butschke, B.; Ben-David, Y.; Milstein, D. *Chem. Eur. J.* **2013**, *19*, 8068; (f) Barnard, J. H.; Wang, C.; Berry, N. G.; Xiao, J. *Chem. Sci.* **2013**, *4*, 1234; (g) Mellone, I.; Peruzzini, M.; Rosi, L.; Mellmann, D.; Junge, H.; Beller, M.; Gonsalvi, L. *Dalton Trans.* **2013**, *42*, 2495; (h) Himeda, Y. *Green Chem.* **2009**, *11*, 2018; (i) Federsel, C.; Boddien, A.; Jackstell, R.; Jennerjahn, R.; Dyson, P. J.; Scopelliti, R.; Laurency, G.; Beller, M. *Angew. Chem., Int. Ed.* **2010**, *49*, 9777; (j) Hull, J. F.;

- Himeda, Y.; Wang, W.-H.; Hashiguchi, B.; Periana, R.; Szalda, D. J.; Muckerman, J. T.; Fujita, E. *Nat. Chem.* **2012**, *4*, 383; (k) Boddien, A.; Mellmann, D.; Gärtner, F.; Jackstell, R.; Junge, H.; Dyson, P. J.; Laurencyzy, G.; Ludwig, R.; Beller, M. *Science* **2011**, *333*, 1733; (l) Bielinski, E. A.; Lagaditis, P. O.; Zhang, Y.; Mercado, B. Q.; Würtele, C.; Bernskoetter, W. H.; Hazari, N.; Schneider, S. *J. Am. Chem. Soc.* **2014**, *136*, 10234.
- 6) (a) Tanaka, R.; Yamashita, M.; Chung, L. W.; Morokuma, K.; Nozaki, K. *Organometallics* **2011**, *30*, 6742; (b) Tanaka, R.; Yamashita, M.; Nozaki, K. *J. Am. Chem. Soc.* **2009**, *131*, 14168; (c) Boddien, A.; Gärtner, F.; Federsel, C.; Sponholz, P.; Mellmann, D.; Jackstell, R.; Junge, H.; Beller, M. *Angew. Chem., Int. Ed.* **2011**, *50*, 6411; (d) Federsel, C.; Jackstell, R.; Beller, M. *Angew. Chem., Int. Ed.* **2010**, *49*, 6254; (e) Federsel, C.; Jackstell, R.; Boddien, A.; Laurencyzy, G.; Beller, M. *ChemSusChem* **2010**, *3*, 1048; (f) Langer, R.; Diskin-Posner, Y.; Leitius, G.; Shimon, L. J. W.; Ben-David, Y.; Milstein, D. *Angew. Chem., Int. Ed.* **2011**, *50*, 9948; (g) Jeletic, M. S.; Mock, M. T.; Appel, A. M.; Linehan, J. C. *J. Am. Chem. Soc.* **2013**, *135*, 11533; (h) Jessop, P. G.; Ikarlya, T.; Noyori, R. *Nature* **1994**, *368*, 231; (i) Schmeier, T. J.; Dobreiner, G. E.; Crabtree, R. H.; Hazari, N. *J. Am. Chem. Soc.* **2011**, *133*, 9274; (j) Huff, C. A.; Sanford, M. S. *ACS Catal.* **2013**, *3*, 2412; (k) Kang, P.; Cheng, C.; Chen, Z.; Schauer, C. K.; Meyer, T. J.; Brookhart, M. *J. Am. Chem. Soc.* **2012**, *134*, 5500.
- 7) (a) Huff, C. A.; Sanford, M. S. *J. Am. Chem. Soc.* **2011**, *133*, 18122; (b) Rezayee, N. M.; Huff, C. A.; Sanford, M. S. *J. Am. Chem. Soc.* **2015**, *137*, 1028; (c) Wesselbaum, S.; vom Stein, T.; Klankermayer, J.; Leitner, W. *Angew. Chem., Int. Ed.* **2012**, *51*, 7499.
- 8) Reutemann, W.; Kieczka, H. In *Ullmann's Encyclopedia of Industrial Chemistry*; Wiley-VCH Verlag GmbH & Co: Weinheim, 2012.
- 9) Ott, J.; Gronemann, V.; Pontzen, F.; Fiedler, E.; Grossmann, G.; Kersebohm, D. B.; Weiss, G.; Witte, C. In *Ullmann's Encyclopedia of Industrial Chemistry*; Wiley-VCH: Weinheim, 2012.
- 10) (a) Olah, G. A. *Angew. Chem., Int. Ed.* **2005**, *44*, 2636; (b) Olah, G. A. *Angew. Chem., Int. Ed.* **2013**, *52*, 104; (c) Palo, D. R.; Dagle, R. A.; Holladay, J. D. *Chem. Rev.* **2007**, *107*, 3992.
- 11) (a) Dalebrook, A. F.; Gan, W.; Grasemann, M.; Moret, S.; Laurencyzy, G. *Chem. Commun.* **2013**, *49*, 8735; (b) Grasemann, M.; Laurencyzy, G. *Energy Environ. Sci.* **2012**, *5*, 8171; (c) Bockris, J. O. M. *Science* **1972**, *176*, 1323; (d) Loges, B.; Boddien, A.; Gärtner, F.; Junge, H.; Beller, M. *Top Catal* **2010**, *53*, 902.

- 12) Navarro, R. M.; Pena, M. A.; Fierro, J. L. *Chem. Rev.* **2007**, *107*, 3952.
- 13) (a) Gärtner, F.; Losse, S.; Boddien, A.; Pohl, M.-M.; Denurra, S.; Junge, H.; Beller, M. *ChemSusChem* **2012**, *5*, 530; (b) Okamoto, Y.; Ida, S.; Hyodo, J.; Hagiwara, H.; Ishihara, T. *J. Am. Chem. Soc.* **2011**, *133*, 18034.
- 14) Itagaki, H.; Saito, Y.; Shinoda, S. *J. Mol. Catal.* **1987**, *41*, 209.
- 15) Alberico, E.; Sponholz, P.; Cordes, C.; Nielsen, M.; Drexler, H.-J.; Baumann, W.; Junge, H.; Beller, M. *Angew. Chem., Int. Ed.* **2013**, *52*, 14162.
- 16) Koehne, I.; Schmeier, T. J.; Bielinski, E. A.; Pan, C. J.; Lagaditis, P. O.; Bernskoetter, W. H.; Takase, M. K.; Würtele, C.; Hazari, N.; Schneider, S. *Inorg. Chem.* **2014**, *53*, 2133.
- 17) (a) Chakraborty, S.; Dai, H.; Bhattacharya, P.; Fairweather, N. T.; Gibson, M. S.; Krause, J. A.; Guan, H. *J. Am. Chem. Soc.* **2014**, *136*, 7869; (b) Chakraborty, S.; Brennessel, W. W.; Jones, W. D. *J. Am. Chem. Soc.* **2014**, *136*, 8564; (c) Bornschein, C.; Werkmeister, S.; Wendt, B.; Jiao, H.; Alberico, E.; Baumann, W.; Junge, H.; Junge, K.; Beller, M. *Nat. Commun.* **2014**, *5*, 4111; (d) Chakraborty, S.; Lagaditis, P. O.; Förster, M.; Bielinski, E. A.; Hazari, N.; Holthausen, M. C.; Jones, W. D.; Schneider, S. *ACS Catal.* **2014**, *4*, 3994.
- 18) (a) Smith, T. A.; Aplin, R. P.; Maitlis, P. M. *J. Organomet. Chem.* **1985**, *291*, c13; (b) Yang, L.-C.; Ishida, T.; Yamakawa, T.; Shinoda, S. *J. Mol. Catal. A: Chem.* **1996**, *108*, 87; (c) Yamakawa, T.; Hiroi, M.; Shinoda, S. *J. Chem. Soc., Dalton Trans.* **1994**, 2265; (d) Shinoda, S.; Yamakawa, T. *J. Chem. Soc., Chem. Commun.* **1990**, 1511.
- 19) Qu, S.; Dai, H.; Dang, Y.; Song, C.; Wang, Z.-X.; Guan, H. *ACS Catal.* **2014**, 4377.
- 20) Farrugia, L. J. *J. Appl. Crystallogr.* **1997**, *30*, 565.
- 21) In the experiment using a low catalyst loading of **2a** (0.001 mol%) it was possible to reduce the amount of LiBF₄ from 10 mol% to 1 mol% with no decrease in catalytic activity.
- 22) For a more detailed discussion of the difference between Yang's proposed pathway and the current proposed pathway see reference 17d.
- 23) Azofra, L. M.; Alkorta, I.; Elguero, J.; Toro-Labbé, A. *J. Phys. Chem. A* **2012**, *116*, 8250.
- 24) Yakelis, N. A.; Bergman, R. G. *Organometallics* **2005**, *24*, 3579.

- 25) Dolomanov, O. V.; Bourhis, L. J.; Gildea, R. J.; Howard, J. A. K.; Puschmann, H. *J. Appl. Cryst.* **2009**, *42*, 339.
- 26) Sheldrick, G. *Acta Crystallogr., Sect. A: Found. Crystallogr.* **2008**, *64*, 112.
- 27) Gaussian 09, Revision A.02, Frisch, M. J.; Trucks, G. W.; Schlegel, H. B.; Scuseria, G. E.; Robb, M. A.; Cheeseman, J. R.; Scalmani, G.; Barone, V.; Mennucci, B.; Petersson, G. A.; Nakatsuji, H.; Caricato, M.; Li, X.; Hratchian, H. P.; Izmaylov, A. F.; Bloino, J.; Zheng, G.; Sonnenberg, J. L.; Hada, M.; Ehara, M.; Toyota, K.; Fukuda, R.; Hasegawa, J.; Ishida, M.; Nakajima, T.; Honda, Y.; Kitao, O.; Nakai, H.; Vreven, T.; Montgomery, Jr., J. A.; Peralta, J. E.; Ogliaro, F.; Bearpark, M.; Heyd, J. J.; Brothers, E.; Kudin, K. N.; Staroverov, V. N.; Kobayashi, R.; Normand, J.; Raghavachari, K.; Rendell, A.; Burant, J. C.; Iyengar, S. S.; Tomasi, J.; Cossi, M.; Rega, N.; Millam, N. J.; Klene, M.; Knox, J. E.; Cross, J. B.; Bakken, V.; Adamo, C.; Jaramillo, J.; Gomperts, R.; Stratmann, R. E.; Yazyev, O.; Austin, A. J.; Cammi, R.; Pomelli, C.; Ochterski, J. W.; Martin, R. L.; Morokuma, K.; Zakrzewski, V. G.; Voth, G. A.; Salvador, P.; Dannenberg, J. J.; Dapprich, S.; Daniels, A. D.; Farkas, Ö.; Foresman, J. B.; Ortiz, J. V.; Cioslowski, J.; Fox, D. J. Gaussian, Inc., Wallingford CT, 2009.
- 28) (a) Becke, A. D. *Phys. Rev. A: At., Mol., Opt. Phys.* **1988**, *38*, 3098; (b) Becke, A. D. *J. Chem. Phys.* **1993**, *98*, 5648; (c) Lee, C.; Parr, R. G.; Yang, W. *Phys. Rev. B.* **1988**, *37*, 785.
- 29) Weigend, F.; Ahlrichs, R. *Phys. Chem. Chem. Phys.* **2005**, *7*, 3297.

Chapter 5: Synthesis, Characterization and Reactivity of NHC-Supported Ni and Pd Compounds Bearing Combinations of Allyl, Cyclopentadienyl, and Indenyl Ligands

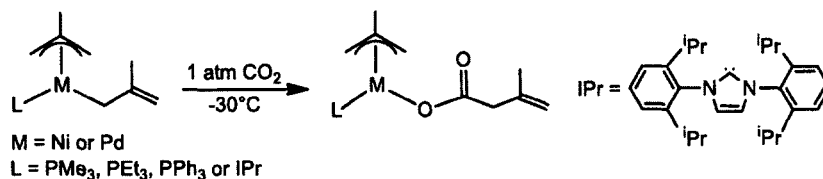
I. Introduction

Group 10 metal complexes containing allyl ligands play an important role in metal-mediated organic synthesis as catalysts¹ and precursors² for a variety of bond forming reactions. Additionally, they are interesting on a fundamental level as the bonding and subsequent reactivity of complexes with allyl ligands is heavily dependent on both the identity of the metal center and the nature of the ancillary ligands.³ In general, allyl ligands bind to transition metals in one of two different coordination modes. First, η^1 -allyls (Figure 5.01a) are nucleophilic and have been invoked as a key intermediate in many reactions with electrophiles⁴ such as CO_2 ,⁵ aldehydes⁶ and imines.^{6b,7} Conversely, η^3 -allyls (Figure 5.01b) are electrophilic and are crucial intermediates in the Tsuji-Trost reaction,⁸ as well as several other catalytic reactions involving attack on the η^3 -allyl ligand by a nucleophile.⁹



Figure 5.01. Depictions of the two most common binding modes of allyl ligands a) η^1 -allyl and b) η^3 -allyl.

We have previously synthesized highly unstable complexes of the type $(\eta^3\text{-allyl})(\eta^1\text{-allyl})\text{M}(\text{L})$ ($\text{M} = \text{Ni}$ or Pd ; $\text{L} = \text{PR}_3$ or IPr ; $\text{IPr} = 1,3\text{-bis}(2,6\text{-diisopropylphenyl})\text{-}1,3\text{-dihydro-}2\text{H-imidazol-}2\text{-ylidene}$).^{5a,5b} These complexes react readily with CO_2 to give carboxylated products in which one molecule of CO_2 inserts into the nucleophilic $\text{M}-\eta^1\text{-allyl}$ bond (Scheme 5.01). In the case of Pd , the bis(allyl) species are highly active catalysts for the carboxylation of allylstannanes^{5a,10} and allylboranes;^{10a} however, their poor thermal stability may limit the substrate scope. Mechanistic studies suggest that the η^3 -allyl ligand is simply a spectator and only the η^1 -allyl ligand is required to facilitate catalysis.^{5a,5b,10b,10c} Related work by Wendt and co-workers using $\text{Pd}-\eta^1\text{-allyl}$ complexes supported by tridentate pincer ligands is consistent with this proposal.^{5c} However, our attempts to use thermally stable $\text{Ni}-\eta^1\text{-allyl}$ complexes supported by pincer ligands¹¹ or Pd^{I} dimers with bridging allyl ligands¹² for catalytic carboxylation did not improve catalyst efficiency. Therefore, we wished to explore alternative ligand frameworks to support thermally stable Pd and Ni complexes containing η^1 -allyl ligands.



Scheme 5.01. Reaction of compounds of the type $(\eta^1\text{-2-methylallyl})(\eta^3\text{-2-methylallyl})\text{M}(\text{L})$ with CO_2 .

It is widely accepted that the allyl ligand is related to both cyclopentadienyl (Cp) and indenyl ligands through a similar method of bonding.¹³ However, despite the close similarities between Cp and indenyl ligands, they do not always bind in the same mode to a transition metal.¹⁴ This is primarily due to the “indenyl effect” which stabilizes the η^3 -binding mode of indenyl ligands relative to the η^5 -binding mode. Consequently, they are far more likely to bind in an η^3 -fashion than Cp ligands which generally bind in an η^1 - or η^5 -manner. Currently, a limited number of Pd and Ni complexes containing combinations of allyl and Cp ligands have been prepared.¹⁵ For example, as part of their studies towards the synthesis of Pd^I dimers with bridging Cp and allyl ligands,¹⁶ Werner and co-workers prepared the monomeric complex $(\eta^5\text{-Cp})(\eta^1\text{-2-chloroallyl})\text{Pd}\{\text{P}(\text{O-ortho-tolyl})_3\}$, as well as related species with different phosphine and allyl ligands.^{15c} In particular, they noted that $(\eta^5\text{-Cp})(\eta^1\text{-2-chloroallyl})\text{Pd}\{\text{P}(\text{O-ortho-tolyl})_3\}$ was stable at temperatures up to 50°C. Furthermore, Werner found that the related complexes $(\eta^5\text{-Cp})(\eta^1\text{-2-methylallyl})\text{Pd}(\text{PR}_3)$ ($\text{R} = \text{P}^i\text{Pr}_3, \text{PCy}_3$ or P^iBuPh_2)^{15a} showed unusual fluxional behavior in solution and at -60°C the $(\eta^5\text{-Cp})(\eta^1\text{-2-methylallyl})\text{Pd}(\text{PR}_3)$ isomer could also be observed. This species is a relatively rare example of a Pd complex with an η^1 -Cp ligand.^{15b,17} At this stage there is only one example of a Pd complex containing both an indenyl and allyl ligand,¹⁸ Ni species containing mixed Cp and allyl or indenyl and allyl ligand sets are unknown.

Given the stability of $(\eta^5\text{-Cp})(\eta^1\text{-2-chloroallyl})\text{Pd}\{\text{P}(\text{O-ortho-tolyl})_3\}$ and our desire to prepare complexes containing thermally stable η^1 -allyl ligands, we were interested in further exploring the synthesis and reactivity of Ni and Pd complexes with both Cp and allyl ligands. Ideally these complexes would be supported with a strongly donating ligand such as IPr,¹⁹ as this was the ancillary ligand for our most active bis(allyl)Pd systems for catalytic carboxylation.^{5a} In addition, given the close relationship between Cp and indenyl ligands,¹⁵ we wanted to prepare Pd and Ni complexes with indenyl and allyl ligands supported by

IPr. This chapter describes the synthesis, characterization and preliminary reactivity of the series of IPr supported Ni and Pd complexes with combinations of allyl, Cp and indenyl ligands, shown in Figure 5.02. The structures and reactivity of these systems have been compared to complexes of the type $(\eta^3\text{-allyl})(\eta^1\text{-allyl})\text{M}(\text{IPr})$ (M = Ni or Pd) that we recently studied.^{5a,5b}

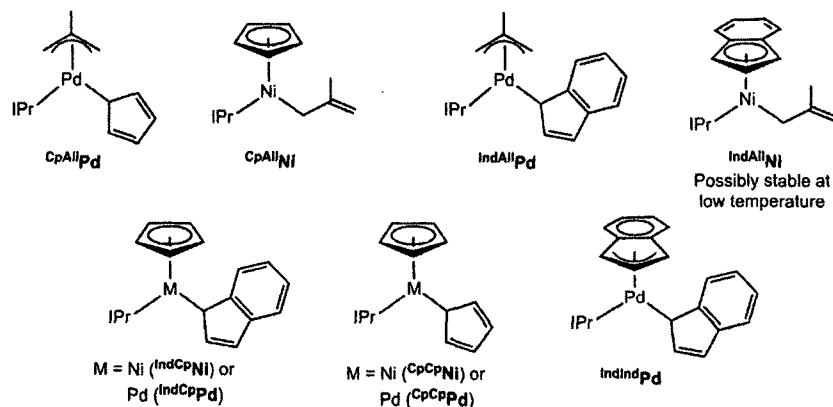


Figure 5.02. Ni and Pd complexes with combinations of allyl, Cp and indenyl ligands.

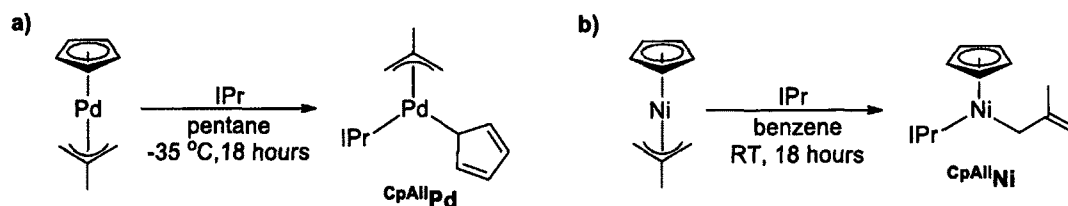
II. Results and Discussion

This work has been previously published.²⁰

A. Synthesis and structure of Ni and Pd complexes supported by both Cp and 2-methylallyl ligands

Previously, it has been demonstrated that the reaction of IPr with the homoleptic Ni and Pd complexes $(\text{allyl})_2\text{M}$ (M = Ni or Pd) generates $(\eta^3\text{-allyl})(\eta^1\text{-allyl})\text{M}(\text{IPr})$ in high yield.^{5a} Through the reaction of the previously prepared mixed ligand species $(\text{Cp})(2\text{-methylallyl})\text{Pd}$ ^{5b} with IPr at -35°C , it was possible to synthesize $(\eta^1\text{-Cp})(\eta^3\text{-2-methylallyl})\text{Pd}(\text{IPr})$ (**CpAllPd**) in moderate yield (Scheme 5.02a). Synthetic attempts at temperatures greater than -35°C gave mixtures of products and significant decomposition was observed if a toluene solution of **CpAllPd** was left at room temperature for longer than 48 hours. In addition, **CpAllPd** was unstable when stored in the solid state at room temperature; however, it could be stored indefinitely at -35°C in a nitrogen filled dry box. When the unsubstituted allyl complex $(\text{Cp})(\text{allyl})\text{Pd}$ was mixed with IPr, only the dimeric product $(\mu\text{-Cp})(\mu\text{-allyl})\text{Pd}_2(\text{IPr})_2$ was isolated.²¹ Similar dimers supported by phosphines have been studied by Werner and are proposed to form through the monomeric compound $(\eta^1\text{-$

$\text{Cp}(\eta^3\text{-allyl})\text{Pd}(\text{PR}_3)$.¹⁶ However, all attempts to spectroscopically characterize the related IPr-supported monomeric intermediate were unsuccessful.



Scheme 5.02. Synthesis of a) CpAllPd and b) CpAllNi .

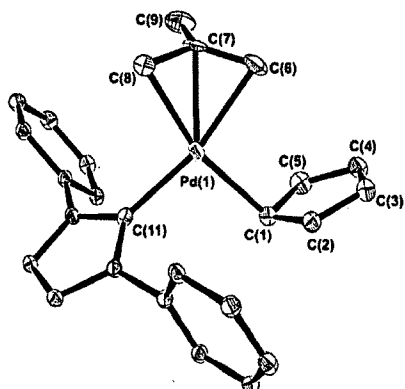
The solution state hapticities of the Cp and 2-methylallyl ligands in CpAllPd were determined using NMR spectroscopy. Sergeyev has demonstrated that the ^1H and ^{13}C NMR chemical shifts of the Cp ligand can be used as a diagnostic tool to determine the coordination mode of Cp ligands in transition metal complexes.²² Typically, the ^1H NMR chemical shift for the Cp resonance in complexes where the Cp ring forms a σ -bond (η^1) to the metal, ranges from 5.6-6.2 ppm, while in complexes where the Cp ring forms both σ - and π -bonds (η^5), the shift of the Cp resonance ranges from 4.0-4.8 ppm. In the case of ^{13}C NMR spectroscopy, chemical shifts for the Cp resonance ranging from 113-118 ppm are proposed to be indicative of η^1 -binding, while shifts ranging from 70-93 ppm are consistent with η^5 -binding.²² The ^1H NMR spectrum of CpAllPd at $-35\text{ }^\circ\text{C}$ showed a single peak for all five Cp protons at 6.13 ppm, which is consistent with η^1 -binding. This is further substantiated by the ^{13}C NMR shift of the Cp ligand at 108.9 ppm, which is also in the range proposed by Sergeyev for η^1 -binding. It should be noted that Sergeyev's ranges for the chemical shift of the Cp ligand are based only on data from η^1 - and η^5 -coordinated Cp ligands and at this stage no general trends have been determined for η^3 -bound Cp ligands, which are significantly less common.²³ As such, it is not possible to completely rule out the unlikely possibility of η^3 -binding of the Cp ligand in CpAllPd on the basis of NMR spectroscopy. However, X-ray crystallography (*vide infra*) is also consistent with an η^1 -bound Cp. The resonances for the 2-methylallyl ligand in the ^1H NMR spectrum of CpAllPd are typical of those expected for η^3 -binding of an allyl ligand in a C_1 symmetric complex.²⁴ Four distinct resonances are observed for the terminal protons, with each below 3.5 ppm.

Even at very low temperature, $-60\text{ }^\circ\text{C}$, only one sharp resonance was observed for the Cp ligand in the ^1H NMR spectrum of CpAllPd , suggesting that there is a low barrier for metallotropic rearrangement (a 1,2-

shift) which makes the Cp protons equivalent. Werner and co-workers have previously reported analogous NMR properties for compounds of the type $(\eta^1\text{-Cp})(\eta^3\text{-2-tert-butylallyl})\text{Pd}(\text{PR}_3)$ ($\text{R} = \text{P}^i\text{Pr}_3, \text{PCy}_3$ or P^tBuPh_2).^{15a} In contrast, low temperature ^1H NMR spectroscopy on complexes of the type $(\eta^1\text{-Cp})(\eta^3\text{-2-methylallyl})\text{Pd}(\text{PR}_3)$ ($\text{R} = \text{P}^i\text{Pr}_3, \text{PCy}_3$ or P^tBuPh_2) suggested that both the sixteen electron species $(\eta^1\text{-Cp})(\eta^3\text{-2-methylallyl})\text{Pd}(\text{PR}_3)$ and the eighteen electron species $(\eta^5\text{-Cp})(\eta^1\text{-2-methylallyl})\text{Pd}(\text{PR}_3)$ were present at low temperature,^{15b} although the sixteen electron species was the major isomer. It may be that the more electron donating NHC ligand in $\text{Cp}^{\text{All}}\text{Pd}$ exclusively favors the sixteen electron isomer. Alternatively, the sixteen and eighteen electron isomers may be in rapid equilibrium even at low temperature, and therefore indistinguishable by NMR spectroscopy.

The solid state structure of $\text{Cp}^{\text{All}}\text{Pd}$ was elucidated using X-ray crystallography and clearly contains an $\eta^1\text{-Cp}$ ligand and an $\eta^3\text{-2-methylallyl}$ ligand (Figure 5.03a). The Pd(1)-C(1) distance for the $\eta^1\text{-Cp}$ ligand is 2.186(4) Å, which is consistent with the bond lengths observed in the few other examples of Pd^{II} species containing $\eta^1\text{-Cp}$ ligands.^{17b} The Pd-C distances to all other carbon atoms of the $\eta^1\text{-Cp}$ ligand are greater than 2.85 Å. The C-C bond distances within the Cp ligand are also indicative of $\eta^1\text{-coordination}$. Two short bond distances of 1.363(6) and 1.381(8) Å are observed between C(2)-C(3) and C(4)-C(5), while three longer bond distances of 1.446(7), 1.416(9) and 1.439(7) Å are observed between C(1)-C(2), C(3)-C(4) and C(1)-C(5), respectively. The 2-methylallyl ligand is clearly bound in an $\eta^3\text{-fashion}$, although somewhat surprisingly the binding of the ligand is symmetric and the Pd(1)-C(6), Pd(1)-C(7), and Pd(1)-C(8) bond distances of 2.171(4), 2.178(5) and 2.173(5) Å, respectively, are equivalent. This suggests that both the IPr ligand and the $\eta^1\text{-Cp}$ ligand exert comparable *trans*-influences. Overall, the solid state structure of $\text{Cp}^{\text{All}}\text{Pd}$ is similar to that observed in closely related $(\eta^1\text{-Cp})(\eta^3\text{-2-tert-butylallyl})\text{Pd}(\text{P}^i\text{Pr})_3$.^{15b}

a)



b)

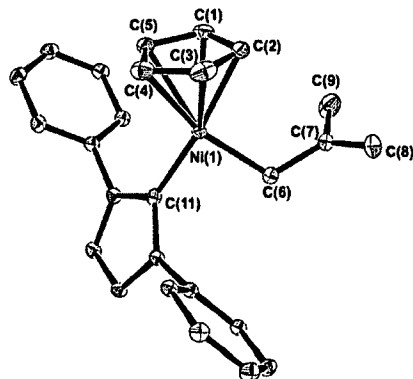


Figure 5.03. a) ORTEP²⁵ of $\text{Cp}^{\text{All}}\text{Pd}$. Hydrogen atoms, solvent in crystal lattice, and the isopropyl groups of IPr have been omitted for clarity. Ellipsoids are shown at 30%. Selected bond lengths (Å) and angles (°): Pd(1)-C(1) 2.186(4), Pd(1)-C(6) 2.174(5), Pd(1)-C(7) 2.171(5), Pd(1)-C(8) 2.171(5), Pd(1)-C(11) 2.043(4), C(1)-C(2) 1.446(7), C(2)-C(3) 1.363(6), C(3)-C(4) 1.416(9), C(4)-C(5) 1.381(8), C(1)-C(5) 1.439(7), C(6)-C(7) 1.382(8), C(7)-C(8) 1.420(7), C(7)-C(9) 1.506(9), C(1)-Pd(1)-C(6) 97.9(2), C(1)-Pd(1)-C(11) 98.0(2), C(8)-Pd(1)-C(11) 97.5(2), C(6)-Pd(1)-C(11) 163.0(2), C(1)-Pd(1)-C(6) 97.5(2). b) ORTEP²⁵ of $\text{Cp}^{\text{All}}\text{Ni}$. Hydrogen atoms and the isopropyl groups of IPr have been omitted for clarity. Ellipsoids are shown at 30%. Selected bond lengths (Å) and angles (°): Ni(1)-C(1) 2.203(5), Ni(1)-C(2) 2.075(6), Ni(1)-C(3) 2.111(7), Ni(1)-C(4) 2.158(9), Ni(1)-C(5) 2.217(6), Ni(1)-C(6) 1.971(2), Ni(1)-C(11) 1.870(2), C(1)-C(2) 1.42(1), C(2)-C(3) 1.40(1), C(3)-C(4) 1.405(9), C(4)-C(5) 1.42(1), C(1)-C(5) 1.383(8), C(6)-C(7) 1.474(3), C(7)-C(9) 1.496(4), C(7)-C(8) 1.336(3), C(2)-Ni(1)-C(6) 97.7(2), C(4)-Ni(1)-C(11) 108.2(2), C(6)-Ni(1)-C(11) 110.2(2), C(2)-Ni(1)-C(11) 172.6(2), C(4)-Ni(1)-C(6) 156.1(2).

The Ni analogue of $\text{Cp}^{\text{All}}\text{Pd}$, $(\eta^5\text{-Cp})(\eta^1\text{-2-methylallyl})\text{Ni}(\text{IPr})$ ($\text{Cp}^{\text{All}}\text{Ni}$), was prepared using a similar synthetic route as for the Pd complex (Scheme 5.02b). Initially, the precursor $(\text{Cp})(2\text{-methylallyl})\text{Ni}$ was synthesized through the reaction of $(\text{Cp})_2\text{Ni}$ with 2-methylallyl magnesium chloride in THF.²⁶ Subsequently, treatment of $(\text{Cp})(2\text{-methylallyl})\text{Ni}$ with one equivalent of IPr in benzene at room temperature gave $\text{Cp}^{\text{All}}\text{Ni}$ in good yield. In contrast to $\text{Cp}^{\text{All}}\text{Pd}$, the ^1H and ^{13}C NMR chemical shifts for the resonances associated with the Cp ligand in $\text{Cp}^{\text{All}}\text{Ni}$, 4.64 and 91.6 ppm respectively, are consistent with an η^5 -bound Cp.²² Furthermore, in the ^1H NMR spectrum the resonances associated with the 2-methylallyl ligand are consistent with an η^1 -binding mode for the allyl ligand. Two signals, both integrating to one proton, at 4.55 and 4.59 ppm, are assigned as the terminal protons of the non-coordinated olefin, while a resonance at 1.24 ppm, integrating to two protons, is assigned as the protons of the metal bound CH_2 group. Their NMR shifts are similar to those observed for the η^1 -2-methylallyl ligand in Pd complexes of the type

(η^3 -2-methylallyl)(η^1 -2-methylallyl)Pd(L) (L = PR₃ or IPr)^{5a} and those that Werner noted for (η^5 -Cp)(η^1 -2-methylallyl)Pd(PⁱPr)₃.^{15b} At room temperature the resonances associated with the 2-methylallyl ligand are not fluxional, which indicates that no exchange processes involving an η^3 -2-methylallyl ligand are occurring. This stands in contrast to the previously reported compound (η^3 -2-methylallyl)(η^1 -2-methylallyl)Ni(IPr), where rapid interconversion between η^1 - and η^3 -2-methylallyl ligands is observed at 80°C by ¹H NMR spectroscopy.^{5b}

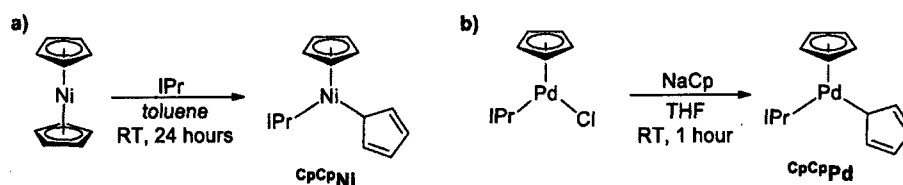
The η^5 -binding of the Cp ligand in ^{CpAll}Ni means that the total valence electron count around the Ni is eighteen electrons, whereas in ^{CpAll}Pd, there are only sixteen electrons around Pd. This is in agreement with results for (allyl)₂M(L) complexes (M = Ni or Pd, L = PR₃ or NHC), where Ni systems are more likely to adopt an eighteen electron structure with two η^3 -allyl ligands, and Pd systems prefer sixteen electron structures with one η^1 -allyl and one η^3 -allyl ligand.^{5a,5b} In the bis(allyl) systems the preference for Pd complexes to have a lower total valence electron count is proposed to be related to the fact that Pd forms stronger metal-ligand bonds and therefore an extra π -type bond from the ligand is not required.¹³ This explanation is also plausible for explaining the difference between ^{CpAll}Ni and ^{CpAll}Pd, although in mixed ligand systems alternative explanations are also possible. Presumably, due to the difficulty of full ring slippage from η^5 -Cp to η^3 -Cp, ^{14b} ^{CpAll}Ni forms the eighteen electron structure through η^5 -binding of the Cp ligand and η^1 -binding of the 2-methylallyl ligand, rather than η^3 -binding of both ligands. Most likely due to its eighteen electron configuration, ^{CpAll}Ni is stable as both a solid and in solution at room temperature, although it does decompose to Ni⁰ when heated at 40°C in solution for longer than twenty-four hours.

The solid state structure of ^{CpAll}Ni clearly contains an η^5 -bound Cp ligand (Figure 5.03b). The Ni-C bond lengths for the Cp ligand range from 2.075(6) to 2.217(6) Å, with the longest Ni-C bond length being observed for the carbon atom opposite the 2-methylallyl ligand. The C-C bond lengths within the Cp ligand are quite similar, ranging from 1.382(5) to 1.418(6) Å. It does not appear that a diene distortion of the Cp ligand, which was observed by Crabtree and co-workers²⁷ in complexes of the type (η^5 -Cp)Ni(NHC)Cl, is present in ^{CpAll}Ni. However, in complexes of the type (η^5 -Cp)Ni(PR₃)Cl, Bergman and co-workers²⁸ have previously described an ene-allyl distortion of the Cp ligand, in which there is slight ring slippage.^{14a} In ^{CpAll}Ni there is some evidence for an ene-allyl distortion of the Cp ligand, as the shortest C-C bond distance

inside the Cp ring (C(1)-C(5) is 1.383(8) Å) involves the carbon atoms which form the longest Ni-C bonds (Ni(1)-C(1) is 2.203(5) Å and Ni(1)-C(5) is 2.217(6) Å). However, the magnitude of the distortion is small and it is reasonable to describe $\text{Cp}^{\text{All}}\text{Ni}$ as an eighteen electron complex. The 2-methylallyl ligand is bound in an η^1 -fashion, with the C(6)-C(7) bond length of 1.474(3) Å, being significantly longer than the C(7)-C(8) bond length of 1.336(3) Å. The Ni-C bond length for the η^1 -bound 2-methylallyl ligand (Ni(1)-C(6) is 1.971(2) Å) is similar to that observed in $(\eta^3\text{-2-methylallyl})(\eta^1\text{-2-methylallyl})\text{Ni}(\text{IPr})$,^{5b} while the Ni-NHC bond distance is also consistent with those previously reported in the literature.²⁹ Overall, $\text{Cp}^{\text{All}}\text{Ni}$ exhibits a classic piano-stool geometry with a *pseudo* five-coordinate arrangement around Ni.

B. Synthesis and structure of Ni and Pd complexes supported by two Cp ligands

For the purpose of comparison with $\text{Cp}^{\text{All}}\text{Ni}$, the eighteen electron complex $(\eta^5\text{-Cp})(\eta^1\text{-Cp})\text{Ni}(\text{IPr})$ ($\text{Cp}^{\text{Cp}}\text{Ni}$), which was stable at room temperature as both a solid and in solution, was prepared through the reaction of $(\text{Cp})_2\text{Ni}$ and IPr in toluene (Scheme 5.03a). Two different resonances, at 5.65 and 4.11 ppm, were observed for the Cp ligands in the ^1H NMR spectrum of $\text{Cp}^{\text{Cp}}\text{Ni}$. This suggests the presence of both η^1 - and η^5 -bound Cp ligands and also indicates that there is a relatively high barrier for interconversion between the Cp ligands. Upon warming to 60°C, the resonances associated with the two Cp ligands began to broaden and at 80°C no Cp resonances were observed, presumably because they had broadened into the baseline. At temperatures above 80°C, the compound decomposed. The room temperature ^1H NMR spectrum did not change upon cooling to -60°C, indicating that the barrier for metallotropic rearrangement in the η^1 -Cp ligand is low. At temperatures below -60°C the compound lacked sufficient solubility to obtain NMR spectra. In the room temperature $^{13}\text{C}\{^1\text{H}\}$ NMR spectrum, two sharp peaks at 108.8 and 92.8 ppm were observed for the Cp ligands, consistent with both η^1 - and η^5 -binding of the two Cp ligands. X-ray crystallography confirmed this assignment (Figure 5.04a). To the best of our knowledge there is only one other example of a Ni complex containing both η^1 - and η^5 -bound Cp ligands and it displays similar NMR properties to $\text{Cp}^{\text{Cp}}\text{Ni}$.²⁹



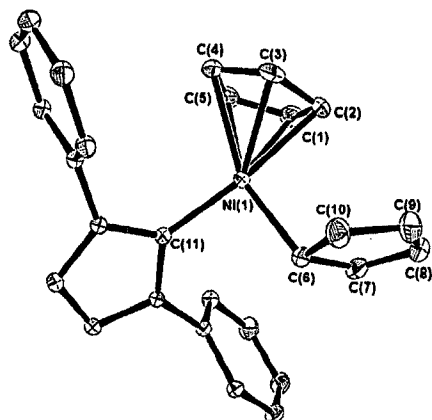
Scheme 5.03. Synthesis of a) CpCpNi and b) CpCpPd .

The Pd complex ($\eta^5\text{-Cp})(\eta^1\text{-Cp})\text{Pd}(\text{IPr})$ (CpCpPd) was synthesized from the reaction of $(\text{Cp})\text{Pd}(\text{IPr})\text{Cl}^{30}$ and sodium cyclopentadienyl (NaCp) in THF (Scheme 5.03b). It is unstable in solution at room temperature and decomposes to give the dimeric product $(\mu\text{-Cp})_2\text{Pd}_2(\text{IPr})_2$.²¹ Furthermore, unlike CpCpNi , the room temperature ^1H NMR spectrum of CpCpPd showed one broad resonance at approximately 5.24 ppm for the Cp ligands. When the spectrum was recorded at -40°C , the single broad resonance split into one sharp resonance at 4.69 ppm and one broad resonance at 5.90 ppm, which suggests the presence of both $\eta^1\text{-}$ and $\eta^5\text{-}$ bound Cp ligands. Further evidence for these hapticities was obtained from the $^{13}\text{C}\{^1\text{H}\}$ NMR spectrum at room temperature, which showed two broad resonances at 98.7 and 107.6 ppm for the Cp ligands that become sharper at lower temperature. The structure was confirmed by X-ray crystallography (Figure 5.04b). Cooling the sample further resulted in significant loss of solubility and as a result it was not possible to record spectra at lower temperatures. In the ^1H NMR spectrum at 60°C both Cp signals broaden and decrease in intensity, similar to what was seen with CpCpNi . However, formation of the dimeric product $(\mu\text{-Cp})_2\text{Pd}_2(\text{IPr})_2$ was accelerated at higher temperatures and precluded us from obtaining spectra above 60°C , where two Cp peaks would coalesce. Overall, the ^1H NMR data for CpCpPd suggest that two fluxional processes are occurring: i) an $\eta^5/\eta^1\text{-}$ exchange of the two Cp ligands most likely through an intermediate structure which contains either two $\eta^1\text{-}$ or one $\eta^3\text{-}$ and one $\eta^1\text{-Cp}$ ligands, and ii) a lower energy metallotropic rearrangement, which makes the protons of the $\eta^1\text{-Cp}$ ligand equivalent. Process (i) appears to be more facile for CpCpPd than for CpCpNi , probably because it is more favorable for Pd to form a structure with a lower total valence electron count around the metal. Similar fluxional behavior has been observed by Werner in compounds of the type $(\eta^5\text{-Cp})(\eta^1\text{-Cp})\text{Pd}(\text{PR}_3)$.^{17b}

The solid-state structures of CpCpNi and CpCpPd are isomorphous (Figure 5.04). In both structures, the presence of both an $\eta^5\text{-}$ and $\eta^1\text{-Cp}$ ligand is confirmed by comparison of the M-C and C-C bond lengths associated with the Cp ligands. In the $\eta^5\text{-}$ bound Cp ligand, all the C-C bond lengths are similar (between

1.381(4) and 1.426(3) Å), whereas in the η^1 -bound Cp ligand there are three long C-C bonds (between 1.426(4) and 1.448(4) Å) and two short C-C bonds (between 1.335(2) and 1.363(4) Å). The M-C bond lengths for the η^5 -bound Cp ligand range from 2.077(2) to 2.179(2) Å for Ni and from 2.233(2) to 2.380(2) Å for Pd, with the shorter bond lengths for Ni reflecting its smaller size. The η^5 -Cp ligands in both complexes display a small ene-allyl distortion with the shortest C-C bond in the ring corresponding to the atoms which form the longest Pd-C or Ni-C bonds. In $\text{Cp}^{\text{Cp}}\text{Pd}$, the bond lengths between the Pd and the η^5 -Cp ligand are considerably longer than those observed between the Pd and the η^3 -2-methylallyl ligand in $\text{Cp}^{\text{All}}\text{Pd}$. This implies that the Pd-C interactions in the η^5 -Cp ligand are weaker than those between Pd-C in the η^3 -2-methylallyl ligand. The M-C bond length for the η^1 -bound Cp ligand is 2.115(2) Å for Pd and 2.026(1) Å for Ni. Although examples of crystallographically characterized Ni and Pd complexes containing η^1 -Cp ligands are rare, these bond distances are comparable to those previously reported.^{17b,29,31} The overall 'piano stool' geometry for both molecules is analogous to that observed for $\text{Cp}^{\text{All}}\text{Ni}$.

a)



b)

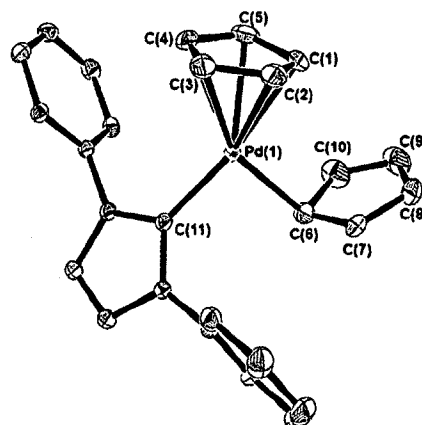
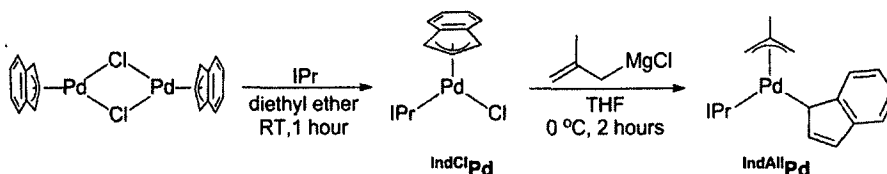


Figure 5.04. a) ORTEP²⁵ of CpCpNi . Hydrogen atoms, solvent in crystal lattice and the isopropyl groups of IPr have been omitted for clarity. Ellipsoids are shown at 30%. Selected bond lengths (Å) and angles (°): Ni(1)-C(1) 2.152(2), Ni(1)-C(2) 2.077(2), Ni(1)-C(3) 2.175(2), Ni(1)-C(4) 2.179(2), Ni(1)-C(5) 2.142(2), Ni(1)-C(6) 2.026(2), Ni(1)-C(11) 1.887(1), C(1)-C(2) 1.406(3), C(2)-C(3) 1.426(3), C(3)-C(4) 1.389(2), C(4)-C(5) 1.426(3), C(1)-C(5) 1.397(2), C(6)-C(7) 1.457(2), C(7)-C(8) 1.336(2), C(8)-C(9) 1.434(3), C(9)-C(10) 1.335(2), C(6)-C(10) 1.457(2), C(2)-Ni(1)-C(11) 172.04(6), C(5)-Ni(1)-C(6) 152.70(6), C(6)-Ni(1)-C(2) 93.96(6), C(6)-Ni(1)-C(11) 93.91(5), C(11)-Ni(1)-C(4) 109.26(6). b) ORTEP²⁵ of CpCpPd . Hydrogen atoms, solvent in crystal lattice and isopropyl groups of IPr have been omitted for clarity. Ellipsoids are shown at 30%. Selected bond lengths (Å) and angles (°): Pd(1)-C(1) 2.233(2), Pd(1)-C(2) 2.348(3), Pd(1)-C(3) 2.364(3), Pd(1)-C(4) 2.380(3), Pd(1)-C(5) 2.373(3), Pd(1)-C(6) 2.115(2), C(1)-C(2) 1.402(4), C(2)-C(3) 1.381(4), C(3)-C(4) 1.423(5), C(4)-C(5) 1.391(4), C(1)-C(5) 1.425(4), C(6)-C(7) 1.458(4), C(7)-C(8) 1.363(4), C(8)-C(9) 1.426(6), C(9)-C(10) 1.359(5), C(6)-C(10) 1.468(4), C(1)-Pd(1)-C(11) 170.38(9), C(3)-Pd(1)-C(6) 148.4(1), C(6)-Pd(1)-C(2) 114.45(9), C(6)-Pd(1)-C(11) 92.18(8), C(11)-Pd(1)-C(4) 112.18(9).

C. Synthesis and structure of Ni and Pd complexes supported by both indenyl and 2-methylallyl ligands

Indenyl and Cp ligands are often compared because of their ability to bind to metal centers in η^1 -, η^3 - and η^5 -fashions, although their reactivity can differ significantly due to the “indenyl effect”.^{14b} We were interested in exploring the consequences of replacing the Cp ligand of $\text{Cp}^{\text{All}}\text{Ni}$ and $\text{Cp}^{\text{All}}\text{Pd}$ with an indenyl ligand. Unfortunately, the Pd and Ni complexes (Ind)(2-methylallyl)M (M = Ni or Pd) have not been reported, and attempts to prepare them as part of this work resulted in extremely unstable products, which could not be used as precursors for direct reaction with IPr. We postulated that treatment of the unknown Pd complex $(\eta^3\text{-Ind})\text{Pd}(\text{IPr})\text{Cl}$ ($^{\text{IndCl}}\text{Pd}$) and the known Ni species $(\eta^3\text{-Ind})\text{Ni}(\text{IPr})\text{Cl}$ ($^{\text{IndCl}}\text{Ni}$)³² with 2-methylallyl magnesium chloride could generate the desired $\text{Cp}^{\text{All}}\text{Ni}$ and $\text{Cp}^{\text{All}}\text{Pd}$ complexes. Previously, Zargarian³³ and co-workers reported the syntheses of $(\eta^3\text{-Ind})\text{Pd}(\text{PR}_3)\text{Cl}$ (R = Ph, Cy and Me) through the

reaction of $\{(\eta^3\text{-Ind})\text{Pd}(\mu\text{-Cl})\}_2$ with the appropriate free phosphine. The reaction of two equivalents of IPr with $\{(\eta^3\text{-Ind})\text{Pd}(\mu\text{-Cl})\}_2$ in diethyl ether generated $^{\text{IndCl}}\text{Pd}$ as a bench stable orange solid, which served as the starting material for our further studies with indenyl-supported Pd complexes (Scheme 5.04).



Scheme 5.04. Synthesis of $^{\text{IndCl}}\text{Pd}$ and $^{\text{IndAll}}\text{Pd}$.

The coordination mode of the indenyl ligand in $^{\text{IndCl}}\text{Pd}$ was determined by analysis of the $^{13}\text{C}\{^1\text{H}\}$ NMR spectrum. While η^1 -indenyl ligands have their own characteristic ^1H NMR pattern, more sophisticated analysis is required to differentiate between η^3 - and η^5 -indenyl ligands. Baker³⁴ and Marder³⁵ have shown that indenyl binding modes (η^3 - or η^5 -) mode can be differentiated by comparing the average ^{13}C NMR chemical shifts of the hinge carbons (labeled 3a and 7a in Figure 5.05) of the indenyl ligand with those of sodium indenyl. The magnitude of this difference, defined as $\Delta\delta_{\text{av}}$ ($\Delta\delta_{\text{av}} = \delta_{\text{av}}(\text{C}(3\text{a}),\text{C}(7\text{a}))$ of M-Ind - $\delta_{\text{av}}(\text{C}(3\text{a}),\text{C}(7\text{a}))$ of Na^+Ind^-) is related to the solution hapticity of the indenyl ligand. A value of $\Delta\delta_{\text{av}} \ll 0$ is indicative of η^5 -coordination and a value of $\Delta\delta_{\text{av}} \gg 0$ is indicative of η^3 -coordination. Values of $\Delta\delta_{\text{av}}$ close to zero indicate intermediate hapticity between η^3 - and η^5 -coordination. For $^{\text{IndCl}}\text{Pd}$, $\Delta\delta_{\text{av}}$ was equal to 8.7, a value consistent with η^3 -coordination.^{14b}



Figure 5.05. Numbering scheme of indenyl ligand.

In the solid state, $^{\text{IndCl}}\text{Pd}$ also contains an η^3 -bound indenyl ligand (Figure 5.06). The bond distances between Pd and C(1), C(2), and C(3) are 2.270(2), 2.167(2), and 2.173(2) Å, respectively. All of these values are comparable with those observed in similar complexes.^{14b,36} The Pd-C distances to the hinge carbons of the indenyl ligand are significantly longer, 2.608(2) and 2.643(2) Å. As a result, the $\Delta\text{M-C}$ value which is defined as $\Delta\text{M-C} = \text{average distance (M-C}(3\text{a}),\text{C}(7\text{a})) - \text{average distance (M-C}(1),\text{C}(3))$ is 0.40(2) Å.³⁴⁻³⁵ The disparity in the Pd(1)-C(1) and Pd(1)-C(3) bond distances is likely due to the difference in *trans*

influence between the Cl and IPr ligands, with the shorter Pd-C bond distance observed for the carbon opposite the Cl ligand. This asymmetry has also been observed in related phosphine supported indenyl Ni complexes.^{33,37} The coordination of indenyl ligands to transition metals can be further described by the hinge and fold angles, which quantify the degree to which the indenyl ring has slipped from the idealized η^5 -coordination. The hinge angle is defined as the angle between the planes formed by C(1), C(2), C(3) and C(1), C(3), C(3a) and C(7a), while the fold angle defines the angle between the planes formed by C(1), C(2), C(3) and C(3a) C(4), C(5), C(6), C(7) and C(7a), with numbering consistent with Figure 5.06.³³ $^{IndCl}Pd$ has a hinge angle of 14.83° and a fold angle of 12.53° . These values along with the $\Delta M-C$ value are consistent with other examples of η^3 -indenyl compounds.^{14b,33} A similar solid state structure has been described for the analogous compound $^{IndCl}Ni$, although in this case the hapticity of the indenyl ligand is more ambiguous and is proposed to be in between η^3 - and η^5 -binding.³⁸

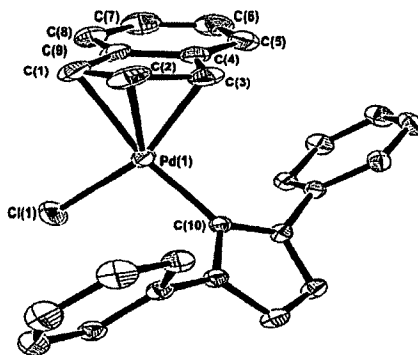


Figure 5.06. ORTEP²⁵ of $^{IndCl}Pd$. Hydrogen atoms and the isopropyl groups of IPr have been omitted for clarity. Ellipsoids are shown at 30%. Selected bond lengths (Å) and angles ($^\circ$): Pd(1)-Cl(1) 2.3265(7), Pd(1)-C(1) 2.270(2), Pd(1)-C(2) 2.167(2), Pd(1)-C(3) 2.173(2), Pd(1)-C(4) 2.608(2), Pd(1)-C(9) 2.643(2), Pd(1)-C(10) 2.007(2), C(1)-C(2) 1.468(8), C(2)-C(3) 1.34(1), C(3)-C(4) 1.415(9), C(4)-C(5) 1.406(1), C(5)-C(6) 1.36(1), C(6)-C(7) 1.38(1), C(7)-C(8) 1.41(1), C(8)-C(9) 1.391(9), C(1)-C(9) 1.451(8), C(4)-C(9) 1.411(8), Cl(1)-Pd(1)-C(1) 100.64(7), Cl(1)-Pd(1)-C(3) 160.12(6), C(1)-Pd(1)-C(10) 166.95(8), Cl(1)-Pd(1)-C(10) 92.05(5), C(3)-Pd(1)-C(10) 106.66(8).

The reaction of one equivalent of 2-methylallyl magnesium chloride with $^{IndCl}Pd$ in THF generated $^{IndAll}Pd$ in good yield. $^{IndAll}Pd$ is stable at room temperature in the solid state for up to three weeks and stable in solution at room temperature overnight. Significant formation of Pd^0 was observed when a benzene solution of $^{IndAll}Pd$ was heated above $50^\circ C$ overnight. The 1H NMR spectrum of $^{IndAll}Pd$ shows 2-methylallyl resonances similar to $^{CpAll}Pd$ with four signals below 3.5 ppm integrating to one proton each.

This is consistent with an η^3 -2-methylallyl ligand.^{24a,24b} The ^1H NMR spectrum indicates that the indenyl ligand is coordinated in an η^1 -fashion. The aromatic region shows four resonances above 7.0 ppm, which correspond to the protons of the benzene ring of the indenyl ligand. An apparent triplet at 6.57 ppm and two broad resonances at 5.97 and 5.90 ppm are associated with the five membered ring of the indenyl ligand. These resonances are consistent with literature examples of η^1 -indenyl complexes.^{14b,36a} When the sample is cooled to -40°C in toluene, the broad resonances separate into two unique signals at 6.00 and 5.64 ppm, each integrating to one proton. The apparent triplet at 6.57 ppm does not change upon cooling. Loss of solubility below -40°C prevented analysis at lower temperatures. X-ray crystallography confirmed the presence of both an η^1 -indenyl and an η^3 -2-methylallyl ligand (Figure 5.07). The Pd-C bond distances for the 2-methylallyl ligand are 2.188(5), 2.171(5) and 2.132(5) Å, respectively. The longest Pd-C bond is *trans* to the η^1 -indenyl ligand. This bond is slightly longer than the Pd-C bond to the 2-methylallyl ligand for the carbon atom *trans* to the η^1 -Cp ligand in $\text{Cp}^{\text{All}}\text{Pd}$, suggesting that the η^1 -indenyl ligand is a stronger donor than the η^1 -Cp ligand. The Pd only interacts with one carbon of the indenyl ligand and the Pd(1)-C(1) bond length is 2.162(6) Å. This is longer than the Pd-C bond length in other reported η^1 -indenyl complexes, presumably due to the increased *trans* influence of the allyl ligand as compared to Cl, the most common *trans* ligand in reported structures.^{36a} The C-C bond distances within the five membered ring of the indenyl ligand are also suggestive of η^1 -coordination. The C(2)-C(3) bond distance of 1.34(1) Å is consistent with a double bond, while the C(1)-C(9) distance of 1.451(8) Å is significantly longer.

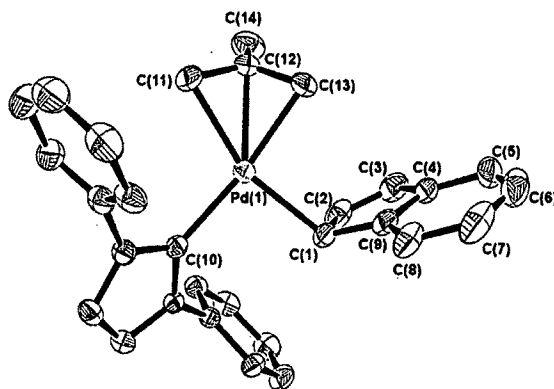
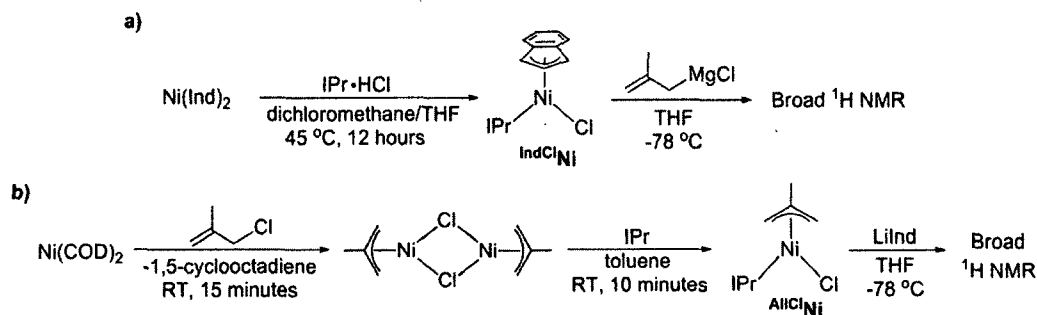


Figure 5.07. ORTEP²⁵ of $\text{IndAl}^{\text{II}}\text{Pd}$. Hydrogen atoms and the isopropyl groups of IPr have been omitted for clarity. Ellipsoids are shown at 30%. Selected bond lengths (Å) and angles (°): Pd(1)-C(1) 2.162(6), Pd(1)-C(10) 2.073(5), Pd(1)-C(11) 2.188(5), Pd(1)-C(12) 2.171(5), Pd(1)-C(13) 2.132(5), C(1)-C(2) 1.468(8), C(2)-C(3) 1.34(1), C(3)-C(4) 1.415(9), C(4)-C(5) 1.40(1), C(5)-C(6) 1.36(1), C(6)-C(7) 1.38(1), C(7)-C(8) 1.41(1), C(8)-C(9) 1.391(9), C(1)-C(9) 1.451(8), C(4)-C(9) 1.411(8), C(11)-C(12) 1.400(8), C(12)-C(13) 1.400(8), C(12)-C(14) 1.495(9), C(1)-Pd(1)-C(13) 93.0(2), C(1)-Pd(1)-C(10) 95.7(2), C(10)-Pd(1)-C(11) 104.6(2), C(1)-Pd(1)-C(11) 159.7(2), C(10)-Pd(1)-C(13) 167.3(2).

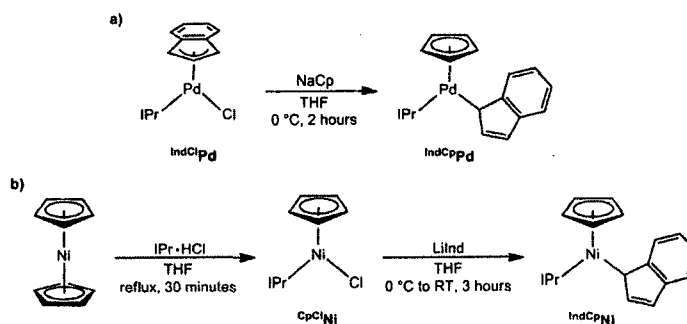
Unfortunately, the Ni compound $\text{IndAl}^{\text{II}}\text{Ni}$ was not successfully isolated. Two different routes were attempted as summarized in Scheme 5.05. The reaction of 2-methylallyl magnesium chloride with $\text{IndCl}^{\text{I}}\text{Ni}$ (synthesized using a literature route)^{38,39} at low temperature (-78°C) gave a product which displayed broad signals in the ¹H NMR spectrum (Scheme 5.05a). We were unable to characterize this product as when the solution was raised above -78°C rapid decomposition to Ni^0 occurred. An alternative route using $\text{Al}^{\text{II}}\text{Cl}^{\text{I}}\text{Ni}$ as the starting material was attempted. Initially, the dimeric compound $\{(\eta^3\text{-2-methylallyl})\text{Ni}(\mu\text{-Cl})\}_2$ was synthesized *in situ* from the reaction of $\text{Ni}(\text{COD})_2$ and 2-methylallyl chloride (Scheme 5.05b).⁴⁰ Subsequent addition of IPr generated $\text{Al}^{\text{II}}\text{Cl}^{\text{I}}\text{Ni}$. The addition of lithium indenyl to $\text{Al}^{\text{II}}\text{Cl}^{\text{I}}\text{Ni}$ at both room temperature and -35°C gave a mixture of products. Performing the reaction at -78°C gave a deep red solution that showed broad ¹H NMR signals. These signals were the same as those observed in the reaction between 2-methylallyl magnesium chloride and $\text{IndCl}^{\text{I}}\text{Ni}$. The sample quickly decomposed to Ni^0 when the solution was raised even slightly above -78°C. Although both routes resulted in the same species we cannot say with certainty that this is our desired $\text{IndAl}^{\text{II}}\text{Ni}$ product due to the extreme thermal instability of the complex, which prevented further characterization.



Scheme 5.05. Attempted synthesis of a) IndClNi and b) IndAllNi .

D. Synthesis and structure of Ni and Pd complexes supported by both indenyl and Cp ligands

The mixed Cp/indenyl complex IndCpPd was synthesized through the reaction of IndClPd with NaCp in THF at 0°C (Scheme 5.06). While low temperature was required during the synthesis to avoid the formation of multiple products, IndCpPd is stable for up to one week in solution at room temperature under a nitrogen atmosphere and indefinitely stable as a solid. ^1H NMR spectroscopy indicates IndCpPd has an η^1 -indenyl ligand and an η^5 -Cp ligand. In a similar fashion to IndAllPd , IndCpPd shows four aromatic resonances above 6.8 ppm associated with the benzene ring of the indenyl ligand. Of these four resonances, two are coincident with the aryl protons of the IPr ligand. The remaining resonances appear as a doublet at 7.54 ppm and a doublet at 6.88 ppm. The proton bound to the η^1 -carbon of the five membered indenyl ring appears as a singlet at 4.54 ppm. The two olefinic protons of this ring appear as an apparent triplet at 6.40 ppm and a broad resonance at 6.74 ppm. These shifts are consistent with what has been reported for η^1 -indenyl complexes of Pt, Pd.^{14b,41} Furthermore, the ^1H NMR spectrum shows a single resonance at 4.63 ppm for the five Cp protons, well within the range cited by Sergeyev for η^5 -bound Cp rings.²²

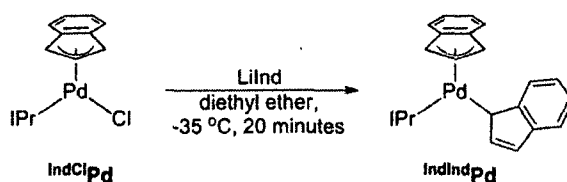


Scheme 5.06. Synthesis of a) IndCpPd and b) IndCpNi .

For unknown reasons we were unable to synthesize a pure sample of the analogous Ni complex $^{\text{IndCp}}\text{Ni}$ through the reaction of $^{\text{IndCl}}\text{Ni}$ with sodium cyclopentadienyl. However, $^{\text{IndCp}}\text{Ni}$ was synthesized through the reaction of $(\eta^5\text{-Cp})\text{Ni}(\text{IPr})\text{Cl}^{42}$ ($^{\text{CpCl}}\text{Ni}$) with lithium indenyl in THF at -40°C (Scheme 5.06b). $^{\text{IndCp}}\text{Ni}$ is stable as a solid at room temperature under a nitrogen atmosphere and slowly decomposes to Ni^0 in solution over the course of three days at room temperature. The ^1H and $^{13}\text{C}\{^1\text{H}\}$ NMR shifts for the Cp ring, 4.17 ppm and 92.5 ppm, respectively, confirm that the Cp is η^5 -bound. ^1H NMR spectroscopy suggests that like $^{\text{IndAll}}\text{Pd}$ and $^{\text{IndCp}}\text{Pd}$, the indenyl ligand is η^1 -bound. A singlet at 3.82 ppm corresponds to the proton on the η^1 -bound carbon of the indenyl ring. The two olefinic protons for the five-membered ring appear at 6.56 ppm as an apparent triplet and as complex multiplet coincident with an indenyl aryl peak at 6.79 ppm.

E. Synthesis and structure of Ni and Pd complexes supported by two indenyl ligands

The Pd species with two indenyl ligands, $^{\text{IndInd}}\text{Pd}$, was synthesized through the reaction of $^{\text{IndCl}}\text{Pd}$ with lithium indenyl at -35°C in diethyl ether (Scheme 5.07). The dark pink solid is not stable at room temperature and decomposes to give $(\mu\text{-Ind})_2\text{Pd}_2(\text{IPr})_2$ as the major product with a minor amount of $\text{Pd}(\text{IPr})_2$.²¹ The ^1H NMR spectrum at -40°C displays fourteen unique indenyl resonances. The eight aromatic resonances appear above 6.31 ppm and the remaining six protons on the five membered rings appear below 6.25 ppm. Attempts to prepare the Ni analogue of $^{\text{IndInd}}\text{Pd}$ either through the reaction of $(\text{Ind})_2\text{Ni}$ with IPr or the treatment of $^{\text{IndCl}}\text{Ni}$ with lithium indenyl were unsuccessful and resulted in complex mixtures of products.



Scheme 5.07. Synthesis of $^{\text{IndInd}}\text{Pd}$.

X-ray quality crystals of $^{\text{IndInd}}\text{Pd}$ were grown from a concentrated solution of diethyl ether at -35°C (Figure 5.08). The solid state structure clearly shows two different coordination modes for the two indenyl ligands. One indenyl ligand is bound in a η^1 -fashion, with a $\text{Pd}(1)\text{-C}(1)$ bond distance of 2.115(4) Å. All other Pd-C distances to this indenyl ligand are greater than 2.9 Å. The other indenyl ring is coordinated in an η^3 -

fashion, similar to that seen in IndClPd . The Pd(1)-C(11) and Pd(1)-C(12) bond lengths are similar at 2.217(5) and 2.220(5) Å, respectively, while the Pd(1)-C(19) distance is considerably longer at 2.345(4) Å, indicating the increased *trans* influence of the η^1 -indenyl ligand compared to IPr. The Pd-C distances to the hinge carbons are 2.610(4) and 2.674(5) Å, resulting in a $\Delta\text{M-C}$ value of 0.36(4) Å.^{34,35} As with IndClPd , the hinge and fold angles of 12.53° and 13.53° for the η^3 -indenyl ligand of IndIndPd are consistent with previous examples for η^3 -indenyl complexes.^{36a,43} The Pd(1)-C(1) bond distance to the η^1 -indenyl ligand is shorter than that in IndAllPd , presumably because the η^3 -allyl ligand exerts a stronger *trans* influence than the η^3 -indenyl ligand. It is noteworthy that IndIndPd is a sixteen electron species, with one η^1 -indenyl ligand and one η^3 -indenyl ligand, whereas the related species CpCpPd is an eighteen electron species with one η^1 -Cp ligand and one η^5 -Cp ligand. This highlights the “indenyl effect”^{14b} with the indenyl ligand adopting an η^3 -binding mode, while the Cp ligand prefers an η^5 -binding mode.

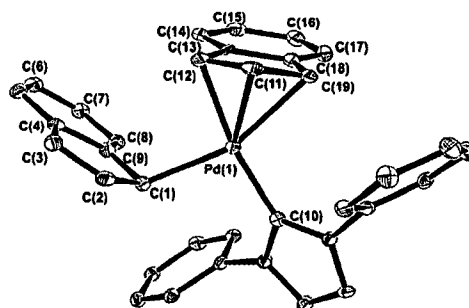


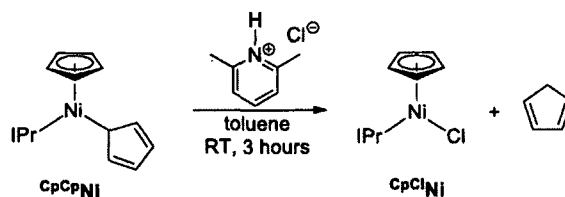
Figure 5.08. ORTEP²⁵ of IndIndPd . Hydrogen atoms and the isopropyl groups of IPr have been omitted for clarity. Ellipsoids are shown at 30%. Selected bond lengths (Å) and angles (°): Pd(1)-C(1) 2.115(4), Pd(1)-C(10) 2.017(4), Pd(1)-C(11) 2.217(5), Pd(1)-C(12) 2.220(5), Pd(1)-C(13) 2.610(4), Pd(1)-C(19) 2.345(4), C(1)-C(2) 1.468(8), C(2)-C(3) 1.348(7), C(3)-C(4) 1.453(6), C(4)-C(5) 1.396(6), C(5)-C(6) 1.391(7), C(6)-C(7) 1.397(8), C(7)-C(8) 1.381(6), C(8)-C(9) 1.383(7), C(1)-C(9) 1.480(6), C(4)-C(9) 1.417(8), C(11)-C(12) 1.406(5), C(12)-C(13) 1.450(7), C(13)-C(14) 1.403(6), C(14)-C(15) 1.391(8), C(15)-C(16) 1.399(7), C(16)-C(17) 1.390(6), C(17)-C(18) 1.394(8), C(13)-C(18) 1.435(6), C(18)-C(19) 1.443(6), C(11)-C(19) 1.420(8), C(10)-Pd(1)-C(12) 169.7(2), C(1)-Pd(1)-C(12) 97.3(2), C(1)-Pd(1)-C(10) 92.8(2), C(10)-Pd(1)-C(19) 109.6(2), C(1)-Pd(1)-C(19) 157.3(2), C(12)-Pd(1)-C(19) 60.2(2).

F. Reactivity of Ni and Pd compounds with electrophiles

Previously, it has been proposed that in complexes of the type $(\eta^3\text{-allyl})(\eta^1\text{-allyl})\text{M(L)}$ (M = Ni or Pd; L = PR_3 or IPr), electrophiles such as Brønsted acids, aldehydes and CO_2 react with the nucleophilic η^1 -allyl

ligand.^{1a,2c,4,6a,44} In comparison, relatively little is known about the reactivity of η^1 -Cp and η^1 -indenyl ligands bound to Pd and Ni with these substrates.⁴⁵ As a result we were interested in probing the reactivity of the mixed compounds prepared as part of this work with simple electrophiles. Table 5.01 summarizes our results for the reactions of $\text{Cp}^{\text{All}}\text{Pd}$, $\text{Cp}^{\text{All}}\text{Ni}$, $\text{Ind}^{\text{All}}\text{Pd}$, $\text{Ind}^{\text{Cp}}\text{Pd}$ and $\text{Ind}^{\text{Cp}}\text{Ni}$ with 2,6-lutidinium chloride, a solid source of HCl. Although different reaction conditions were needed depending on the specific reaction to obtain clean conversion, in all cases with mixed ligands selective protonation at the η^1 -ligand was observed and high yields of the organic product were detected by ^1H NMR spectroscopy. For example, in the case of $\text{Cp}^{\text{All}}\text{Pd}$, which contains an η^1 -Cp ligand and an η^3 -2-methylallyl ligand the sole product of protonation was $(\eta^3$ -2-methylallyl)Pd(IPr)Cl (AllClPd), whereas for $\text{Cp}^{\text{All}}\text{Ni}$, which contains an η^5 -Cp ligand and an η^1 -2-methylallyl ligand the only product was $(\eta^5$ -Cp)Ni(IPr)Cl (CpClNi). From the results of these reactions we believe that two conclusions can be drawn: i) in the case of acid, where reaction is proposed to proceed directly with the carbon bound to the metal center, η^1 -allyl, η^1 -Cp and η^1 -indenyl ligands all display similar reactivity, and ii) protonation with acid can almost certainly be used as a general technique to confirm the identity of the ligand bound in an η^1 -fashion in mixed ligand complexes of the type described here.

Table 5.01. Summary of reactivity of species prepared in this work with acid (2,6-lutidinium chloride). Representative reaction shown below.

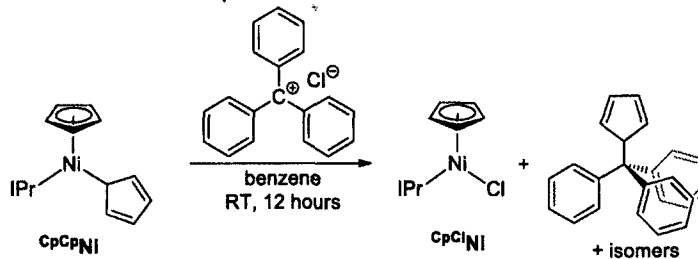


Compound	Conditions	Metal product ^a	Organic product ^a
$\text{Cp}^{\text{All}}\text{Pd}$	Toluene, -35 °C, 4 hours	AllClPd	Cyclopentadiene
$\text{Cp}^{\text{All}}\text{Ni}$	Toluene, RT, 4 hours	CpClNi	2-methylpropene
$\text{Ind}^{\text{All}}\text{Pd}$	Toluene, 0 °C to RT, 2 hours	AllClPd	Indene
$\text{Ind}^{\text{Cp}}\text{Pd}$	Toluene, 0 °C to RT, 2 hours	CpClPd	Indene
$\text{Ind}^{\text{Cp}}\text{Ni}$	Toluene, 0 °C to RT, 2 hours	CpClNi	Indene
CpCpPd	Benzene, RT, 1 hour	CpClPd	Cyclopentadiene
CpCpNi	Toluene, RT, 3 hours	CpClNi	Cyclopentadiene

^aProducts determined using ^1H NMR spectroscopy. See experimental section for more information.

The above reactions with a Brønsted acid led us to investigate reactivity with non-acidic electrophiles. In 2009, Legzdins and co-workers reported the reaction of tungsten compounds supported by both η^5 -pentamethylcyclopentadienyl and η^3 -allyl ligands with triphenylcarbenium tetrafluoroborate to give allylated triphenylmethyl products.⁴⁶ The first step in these reactions was proposed to be the isomerization of the allyl ligand from an η^3 - to an η^1 -binding mode, followed by nucleophilic attack of the terminal carbon of the η^1 -allyl ligand (as opposed to the metal bound carbon) on triphenylcarbenium tetrafluoroborate to form a new C-C bond. In our systems, the reaction of $\text{Cp}^{\text{All}}\text{Ni}$ with one equivalent of triphenylcarbenium chloride gave quantitative conversion to the new organic compound 2-methylallyltriphenylmethane and $\text{Cp}^{\text{Cl}}\text{Ni}$. The organic compound was isolated using column chromatography. The reaction with $\text{Cp}^{\text{All}}\text{Pd}$ showed orthogonal reactivity, giving $\text{All}^{\text{Cl}}\text{Pd}$ and several isomers of the organic product, cyclopentadienyltriphenylmethane, which have previously been characterized by Werner.⁴⁷ Similar reactions were performed on the remaining compounds of the series, as shown in Table 5.02. In contrast to the reactions with $\text{Cp}^{\text{All}}\text{Pd}$ and $\text{Cp}^{\text{All}}\text{Ni}$, the reactions with indenyl ligands did not give quantitative conversion. Multiple organic and metal containing products were seen by ^1H NMR spectroscopy, however the metal containing product reported in Table 5.02 was the major product. Similarly, the major organic product was indenyltriphenylmethane.⁴⁸ It is noteworthy that although these reactions were not clean; there was no evidence to support a reaction taking place at either the η^3 -2-methylallyl ligand in the case of $\text{Ind}^{\text{All}}\text{Pd}$ or the η^5 -Cp ligand in the case of $\text{Ind}^{\text{Cp}}\text{Pd}$ or $\text{Ind}^{\text{Cp}}\text{Ni}$. Overall, the reactions described in Table 5.02 suggest that in an analogous fashion to η^1 -allyl ligands, η^1 -Cp and η^1 -indenyl ligands can also act as nucleophiles with substrates where the initial point of attack of the electrophile is not proposed to be the metal bound carbon. However, the exact pathway for the reaction of triphenylcarbenium chloride with the η^1 -Cp and η^1 -indenyl species studied in this work still needs to be determined.

Table 5.02. Summary of reactivity of species prepared in this work with triphenylcarbenium chloride. Representative reaction shown below.



Compound	Conditions	Metal product ^a	Organic product ^a
^{CpAll} Pd	Toluene, -35 °C to RT, 24 hours	^{AllCl} Pd	Cyclopentadienyltriphenylmethane ^b
^{CpAll} Ni	Benzene, RT, 12 hours	^{CpCl} Ni	2-methylallyltriphenylmethane
^{IndAll} Pd	Toluene, 0 °C to RT, 24 hours	^{AllCl} Pd	Indenyltriphenylmethane ^b
^{IndCp} Pd	Toluene, 0 °C to RT, 24 hours	^{CpCl} Pd	Indenyltriphenylmethane ^b
^{IndCp} Ni	Toluene, 0 °C to RT, 24 hours	^{CpCl} Ni	Indenyltriphenylmethane ^b
^{CpCp} Pd	Benzene, RT, 12 hours	^{CpCl} Pd	Cyclopentadienyltriphenylmethane ^b
^{CpCp} Ni	Benzene, RT, 12 hours	^{CpCl} Ni	Cyclopentadienyltriphenylmethane ^b

^aProducts determined using ¹H NMR spectroscopy. See experimental section for more information. ^bSeveral different isomers were formed.

III. Conclusions

A family of Pd and Ni complexes containing combinations of 2-methylallyl, Cp and indenyl ligands, as well as an ancillary IPr ligand, has been synthesized. Unfortunately, a single general synthetic route cannot be used to access the family of complexes due to differences in the stability of the precursors. For example, ^{CpAll}Pd and ^{CpAll}Ni can be prepared through the reaction of IPr with (Cp)(2-methylallyl)Pd and (Cp)(2-methylallyl)Ni, respectively. However, because (Cp)₂Pd does not exist, an alternative strategy was used to synthesize ^{CpCp}Pd.

In general, the hapticities of the 2-methylallyl, Cp and indenyl ligands in the complexes synthesized in this work can be explained by the following two observations: i) Cp ligands prefer to adopt either an η⁵- or an η¹-binding mode as opposed to an η³-binding mode, and ii) Ni complexes prefer to be eighteen electron, whereas Pd complexes prefer to be sixteen electron.⁴⁹ As a result in ^{CpAll}Pd, the Cp ligand binds in an η¹-fashion and the 2-methylallyl ligand in an η³-fashion to give a complex with sixteen electrons around Pd. In the corresponding Ni complex ^{CpAll}Ni, the Cp ligand binds in an η⁵-fashion and the 2-methylallyl ligand in an η¹-fashion so that Ni is eighteen electrons. Normally, observation (i) takes priority over (ii). Therefore, ^{CpCp}Pd is an eighteen electron species with one η¹- and one η⁵-bound Cp ligand. An exception to our

observations is $^{IndCp}Pd$, an eighteen electron species with one η^1 -bound indenyl ligand and one η^5 -bound Cp ligand, whereas we would predict a 16 electron species with one η^1 -bound Cp ligand and one η^3 -bound indenyl ligand. In contrast to the Cp ligand, due to the indenyl effect, the indenyl ligand can bind in an η^1 -, η^3 - or η^5 -fashion to satisfy observation ii, although the structure of $^{IndCp}Pd$ suggests that even for the indenyl ligand η^3 -binding is not favored. In this work, the only compound isolated with both indenyl and allyl ligands was $^{IndAll}Pd$, so at this stage there are not enough data to evaluate the preferred hapticity of the allyl ligand compared to the indenyl ligand. Overall, we believe that the trends observed here will be general for related Pd and Ni complexes with combinations of allyl, Cp and indenyl ligands.

Preliminary reactivity studies of our new complexes with electrophiles, indicate that the η^1 -ligand reacts selectively, regardless of whether it is an allyl, Cp or indenyl ligand. Therefore, whereas acid protonates the Cp ligand in $^{CpAll}Pd$, it protonates the 2-methylallyl ligand in $^{CpAll}Ni$. Similar reactivity is observed using the non-acidic electrophile triphenylcarbenium chloride. Although it is well known that Pd and Ni complexes with η^1 -allyl ligands will act as nucleophiles, comparable reactions with η^1 -Cp and η^1 -indenyl ligands are significantly less common. Further work will look to explore the reactivity of these species with less activated electrophiles such as aldehydes and CO_2 .

IV. Experimental Details

General methods

Experiments were performed under a dinitrogen atmosphere in an M-Braun dry box or using standard Schlenk techniques, unless otherwise noted. (Under standard glovebox conditions, purging was not performed between uses of pentane, diethyl ether, benzene, toluene and THF; thus, when any of these solvents were used, traces of all these solvents were in the atmosphere and could be found intermixed in the solvent bottles.) Moisture- and air-sensitive liquids were transferred by stainless steel cannula on a Schlenk line or in a dry box. Solvents were dried by passage through a column of activated alumina followed by storage under dinitrogen. All commercial chemicals were used as received, except where noted. $(Cp)_2Ni$ was purchased from Alfa Aesar and triphenylcarbenium chloride from Fisher Scientific Company. Deuterated solvents were obtained from Cambridge Isotope Laboratories. C_6D_6 and d_8 -toluene were dried over sodium metal and vacuum-transferred prior to use. NMR spectra were recorded on Bruker AMX-400

and -500 spectrometers at ambient probe temperatures, unless otherwise noted. Chemical shifts are reported in ppm with respect to residual internal protio solvent for ^1H and $^{13}\text{C}\{^1\text{H}\}$ NMR spectra; J values are given in Hz. Robertson Microlit Laboratories, Inc., performed the elemental analyses. Literature procedures were used to prepare the following compounds: $(\text{Cp})(2\text{-methylallyl})\text{Pd}$,⁵⁰ 1,3-bis(2,6-diisopropylphenyl)-1,3-dihydro-2*H*-imidazol-2-ylidene (IPr),⁵¹ 2-methylallyl magnesium chloride,⁵² $(\eta^5\text{-Cp})\text{Pd}(\text{IPr})\text{Cl}$,³⁰ sodium cyclopentadienyl,⁵³ $\{(\eta^3\text{-Ind})\text{Pd}(\mu\text{-Cl})\}_2$,⁵⁴ $(\eta^5\text{-Cp})\text{Ni}(\text{IPr})\text{Cl}$,⁴² AlCl_3Ni ,⁴⁰ lithium indenyl⁵⁵ and 2,6-lutidinium chloride.⁵⁶

X-ray crystallography

Low-temperature diffraction data (ω -scans) were collected on either a Rigaku SCXmini diffractometer coupled to a Mercury275R CCD detector with Mo *K*. radiation ($\lambda = 0.71073 \text{ \AA}$), a Rigaku R-AXIS RAPID diffractometer coupled to a R-AXIS RAPID imaging plate detector with Mo *K*. radiation ($\lambda = 0.71073 \text{ \AA}$) or a Rigaku MicroMax-007HF diffractometer coupled to a Saturn994+ CCD detector with Cu *K*. ($\lambda = 1.54178 \text{ \AA}$). All structures were solved by direct methods using SHELXS⁵⁷ and refined against F^2 on all data by full-matrix least squares with SHELXL-97⁵⁸ using established refinement techniques.⁵⁹ All non-hydrogen atoms were refined anisotropically. All hydrogen atoms were included into the model at geometrically calculated positions and refined using a riding model. The isotropic displacement parameters of all hydrogen atoms were fixed to 1.2 times the U value of the atoms to which they are linked (1.5 times for methyl groups). All disorders were refined with the help of similarity restraints on the 1,2- and 1,3-distances and displacement parameters as well as rigid bond restraints for anisotropic displacement parameters.

Characterization of New Compounds

$(\eta^1\text{-Cp})(\eta^3\text{-2-methylallyl})\text{Pd}(\text{IPr})$ ($\text{Cp}^{\text{All}}\text{Pd}$)

A solution of $(\text{Cp})(2\text{-methylallyl})\text{Pd}$ (0.025 g, 0.110 mmol) in 5 mL pentane was added to a solution of IPr (0.042 g, 0.110 mmol) in 5 mL pentane at -35°C . The solution was stirred at -35°C for 14 hours. The volatiles were removed under reduced pressure at -35°C to give a pale yellow solid. The solid was washed three times with 5 mL portions of cold pentane and dried under vacuum at -35°C to give $\text{Cp}^{\text{All}}\text{Pd}$ as a pale

yellow solid. Yield: 0.040 g, 53%. Due to the thermal instability of this compound elemental analysis was not performed. X-ray quality crystals were grown by slow diffusion of pentane into a saturated toluene solution at -35°C.

^1H NMR (d_8 -toluene, -35 °C, 400 MHz): 7.19 (t, $J = 6.6$ Hz, 2H, *para*-H Ar_{IPr}), 7.12 (d, $J = 6.6$ Hz, 4H, *meta*-H Ar_{IPr}), 6.55 (s, 2H, HCCH), 6.13 (s, 5H, Cp), 3.36 (sept, $J = 6.3$ Hz, 2H, $(\text{CH}_3)_2\text{CH}$), 3.03 (s, 1H, CH_2 allyl), 2.91 (sept, $J = 6.3$ Hz, 2H, $(\text{CH}_3)_2\text{CH}$), 2.30 (s, 1H, CH_2 allyl), 1.51 (s, 1H, CH_2 allyl), 1.28 (d, $J = 6.3$ Hz, 12H, $(\text{CH}_3)_2\text{CH}$), 1.22 (s, 3H, CH_3 allyl), 1.04 (d, $J = 6.3$ Hz, 12H, $(\text{CH}_3)_2\text{CH}$), 0.77 (s, 1H, CH_2 allyl). $^{13}\text{C}\{^1\text{H}\}$ NMR (d_8 -toluene, -35 °C, 126 MHz): 191.7, 145.8, 145.4, 109.1, 87.6, 47.2, 28.7, 26.2, 25.5, 25.0, 23.5, 23.4, 22.7, 22.4.

(Cp)(2-methylallyl)Ni

There is a literature procedure for the synthesis of (Cp)(2-methylallyl)Ni,⁶⁰ however the procedure described below represents an improved protocol.

A solution of (Cp)₂Ni (0.250 g, 1.32 mmol) in 10 mL THF was cooled to 0°C and 2-methylallyl magnesium chloride (2.09 mL of a 0.657 M solution in diethyl ether, 1.32 mmol) was added dropwise with stirring. The resulting solution was allowed to warm to room temperature and stirred for twelve hours to give a dark purple solution. The solvent was removed at 30 torr and the resulting residue extracted three times with 10 mL portions of pentane. The filtrate was concentrated at 30 torr to give (Cp)(2-methylallyl)Ni as a dark purple oil. Yield: 0.200 g, 84.7%. The ^1H NMR data were consistent with that previously reported in the literature.⁶⁰

(η^5 -Cp)(η^1 -2-methylallyl)Ni(IPr) ($\text{Cp}^{\text{All}}\text{Ni}$)

A solution of (Cp)(2-methylallyl)Ni (0.183 g, 1.02 mmol) was dissolved in 5 mL benzene and added to a solution of IPr (0.397 g, 1.02 mmol) in 5 mL benzene. The solution was stirred at room temperature for 12 hours and the solvent removed under reduced pressure. The residue was washed three times with 10 mL

portions of cold pentane and dried under vacuum to give $\text{Cp}^{\text{All}}\text{Ni}$ as a pale green solid. Yield: 0.350 g, 60%. X-ray quality crystals were grown from a concentrated pentane solution at -35°C .

Anal. Calcd (found) for $\text{C}_{36}\text{H}_{48}\text{N}_2\text{Ni}$: C, 76.06 (76.23); H, 8.69 (8.41); N, 4.93 (4.83). ^1H NMR (d_8 -toluene, 400 MHz): 7.25 (t, $J = 7.3$ Hz, 2H, *para*-H Ar_{IPr}), 7.16 (d, $J = 7.6$ Hz, 4H, *meta*-H Ar_{IPr}), 6.50 (s, 2H, *HCCH*), 4.64 (s, 5H, *Cp*), 4.59 (d, $J = 2.6$ Hz, 1H, CH_2 allyl), 4.55 (d, $J = 1.9$ Hz, 1H, CH_2 allyl), 3.06 (sept, $J = 6.8$ Hz, 4H, $(\text{CH}_3)_2\text{CH}$), 1.45 (s, 3H, CH_3 allyl), 1.40 (d, $J = 6.8$ Hz, 12H, $(\text{CH}_3)_2\text{CH}$), 1.24 (s, 2H, CH_2 allyl), 0.98 (d, $J = 6.8$ Hz, 12H, $(\text{CH}_3)_2\text{CH}$). $^{13}\text{C}\{^1\text{H}\}$ NMR (d_8 -toluene, 126 MHz): 188.0, 158.7, 146.1, 138.0, 129.8, 124.1, 101.6, 91.6, 28.9, 25.8, 24.0, 22.4, 1.0.

$(\eta^5\text{-Cp})(\eta^1\text{-Cp})\text{Ni}(\text{IPr})$ ($\text{Cp}^{\text{Cp}}\text{Ni}$)

$(\text{Cp})_2\text{Ni}$ (0.010 g, 0.052 mmol) was dissolved in 2 mL benzene at room temperature. A 3 mL benzene solution of IPr (0.020 g, 0.052 mmol) was added and the resulting suspension stirred at room temperature for 10 hours to give a dark red solution. The solvent was removed under reduced pressure. The residue was extracted in 5 mL pentane and dried under vacuum to give $\text{Cp}^{\text{Cp}}\text{Ni}$ as a dark red solid. Yield: 0.025 g, 82%. X-ray quality crystals were grown by layering pentane on top of a saturated toluene solution at -35°C .

Anal. Calcd (found) for $\text{C}_{37}\text{H}_{46}\text{N}_2\text{Ni}$: C, 76.82 (76.92); H, 8.19 (7.92); N, 4.84 (4.58). ^1H NMR (d_8 -toluene, 400 MHz): 7.26 (t, $J = 7.6$ Hz, 2H, *para*-H Ar_{IPr}), 7.15 (d, $J = 7.6$ Hz, 4H, *meta*-H Ar_{IPr}), 6.48 (s, 2H, *HCCH*), 5.65 (s, 5H, *Cp*), 4.11 (s, 5H, *Cp*), 3.20 (s, br, 4H, $(\text{CH}_3)_2\text{CH}$), 1.31 (d, $J = 6.6$ Hz, 12H, $(\text{CH}_3)_2\text{CH}$), 0.98 (d, $J = 6.5$ Hz, 12H, $(\text{CH}_3)_2\text{CH}$). $^{13}\text{C}\{^1\text{H}\}$ NMR (d_8 -toluene, 126 MHz): 182.6, 145.8, 137.4, 130.0, 124.1, 108.8, 92.3, 28.8, 28.4, 25.6, 24.5.

$(\eta^5\text{-Cp})(\eta^1\text{-Cp})\text{Pd}(\text{IPr})$ ($\text{Cp}^{\text{Cp}}\text{Pd}$)

$(\text{Cp})\text{Pd}(\text{IPr})\text{Cl}^{30}$ (0.019 g, 0.032 mmol) was dissolved in 2 mL THF at room temperature. A 2.0 M THF solution of sodium cyclopentadienyl (0.016 mL, 0.032 mmol) was added and the resulting solution stirred at room temperature for one hour to give a dark green solution. The solvent was removed under reduced pressure and the residue was extracted twice in 5 mL of pentane. The combined extracts were dried under

vacuum to give Cp^*Pd as a dark green solid. Yield: 0.014 g, 71%. X-ray quality crystals were grown by layering pentane on a saturated solution of diethyl ether at -35°C .

Anal. Calcd (found) for $\text{C}_{37}\text{H}_{46}\text{N}_2\text{Pd}$: C, 71.08 (71.15); H, 7.42 (7.66); N, 4.48 (4.26). ^1H NMR (C_6D_6 , 400 MHz): 7.25 (m, $J = 7.5$ Hz, 2H, *para*-H Ar_{IPr}), 7.13 (d, $J = 7.6$ Hz, 4H, *meta*-H Ar_{IPr}), 6.56 (s, 2H, *HCCCH*), 5.51 (br s, 5H, *Cp*), 5.07 (br s, 5H, *Cp*), 3.08 (sept, $J = 6.5$ Hz, 4H, $(\text{CH}_3)_2\text{CH}$), 1.30 (d, $J = 6.8$ Hz, 12H, $(\text{CH}_3)_2\text{CH}$), 0.98 (d, $J = 6.9$ Hz, 12H, $(\text{CH}_3)_2\text{CH}$). ^1H NMR (d_8 -toluene, 400 MHz, -30°C): 7.23 (t, $J = 7.5$ Hz, 2H, *para*-H Ar_{IPr}), 6.47 (s, 2H, *HCCCH*), 5.86 (s, 5H, *Cp*), 4.64 (s, 5H, *Cp*), 3.04 (m, 4H, $(\text{CH}_3)_2\text{CH}$), 1.28 (d, $J = 6.4$ Hz, 12H, $(\text{CH}_3)_2\text{CH}$), 0.97 (d, $J = 6.8$ Hz, 12H, $(\text{CH}_3)_2\text{CH}$). The *meta*-H Ar_{IPr} protons are under the solvent resonances. $^{13}\text{C}\{^1\text{H}\}$ NMR (d_8 -toluene, 100 MHz): 181.1, 146.4, 137.6, 130.5, 124.6, 124.4, 109.7 (br), 100.2 (br), 29.5, 26.1, 22.9.

$(\eta^3\text{-Ind})\text{Pd}(\text{IPr})\text{Cl}$ ($^{\text{IndCl}}\text{Pd}$)

$\{(\eta^3\text{-Ind})\text{Pd}(\mu\text{-Cl})\}_2$ (0.060 g, 0.116 mmol) and IPr (0.090 g, 0.232 mmol) were suspended in 15 mL diethyl ether and stirred at room temperature for one hour. The resulting orange suspension was filtered and the filtrate concentrated to approximately 5 mL under reduced pressure. 20 mL of cold pentane was added to the concentrated filtrate and an orange solid precipitated out of solution. The solid was isolated via filtration, washed three times with 5 mL portions of cold pentane, and dried under vacuum to give $^{\text{IndCl}}\text{Pd}$ as a dark orange solid. Yield: 0.113 g, 75%. X-ray quality crystals were grown by slow diffusion of pentane into a saturated toluene solution at room temperature.

Anal. Calcd (found) for $\text{C}_{36}\text{H}_{43}\text{N}_2\text{PdCl}$: C, 66.87 (65.09); H, 6.86 (5.69); N, 4.33 (4.12). ^1H NMR (C_6D_6 , 400 MHz): 7.37 (t, $J = 7.7$ Hz, 2H, *para*-H Ar_{IPr}), 7.26 (d, $J = 7.7$ Hz, 2H, *meta*-H Ar_{IPr}), 7.08 (d, $J = 7.7$ Hz, 2H, *meta*-H Ar_{IPr}), 6.97 (s, 2H, *HCCCH*), 6.78 (d, $J = 7.4$ Hz, 1H, Ar_{Ind}), 6.60 (t, $J = 7.4$ Hz, 1H, Ar_{Ind}), 6.21 (m, 2H, Ar_{Ind}); 5.66 (d, $J = 7.4$ Hz, 1H, Cp_{Ind}), 5.48 (t, $J = 2$ Hz, 1H, Cp_{Ind}), 5.22 (t, $J = 2$ Hz, 1H, Cp_{Ind}), 3.03 (sept, $J = 6.8$ Hz, 2H, $(\text{CH}_3)_2\text{CH}$), 2.57 (sept, $J = 6.8$ Hz, 2H, $(\text{CH}_3)_2\text{CH}$), 1.36 (d, $J = 6.7$ Hz, 6H, $(\text{CH}_3)_2\text{CH}$), 1.10 (d, $J = 6.7$ Hz, 6H, $(\text{CH}_3)_2\text{CH}$), 0.97 (d, $J = 6.7$ Hz, 6H, $(\text{CH}_3)_2\text{CH}$), 0.85 (d, $J = 6.7$

Hz, 6H, (CH₃)₂CH). ¹³C{¹H} NMR (C₆D₆, 126 MHz): 177.9, 146.3, 138.6, 137.7, 136.8, 130.2, 124.8, 118.4, 116.3, 110.2, 86.1, 69.5, 28.8, 28.7, 26.4, 25.7, 23.7, 22.4.

(η^1 -Ind)(η^3 -2-methylallyl)Pd(IPr) (^{IndAll}Pd)

^{IndCl}Pd (0.050 g, 0.077 mmol) was dissolved in 3 mL of THF and the solution was cooled to 0°C. 2-methylallyl magnesium chloride (0.117 mL of a 0.657 M THF solution, 0.077 mmol) was added dropwise with stirring and the resulting solution was stirred at 0°C for 90 minutes to give a bright yellow solution. The solvent was removed under reduced pressure and the resulting residue extracted twice with 5 mL portions of pentane. The combined extracts were dried under vacuum to give ^{IndAll}Pd as a bright yellow solid. Yield: 0.037 g, 68%. X-ray quality crystals were grown from a saturated pentane solution at -35°C.

Anal. Calcd (found) for C₄₀H₅₁N₂Pd: C, 72.11 (70.89); H, 7.72 (7.66); N, 4.20 (4.20). ¹H NMR (C₆D₆, 500 MHz): 7.46 (d, J = 6.5 Hz, 1H, Ar_{Ind}), 7.24 (t, J = 7.7 Hz, 2H, *para*-H Ar_{IPr}), 7.21 (d, J = 1.3 Hz, 1H, Ar_{Ind}), 7.19 (d, J = 1.6 Hz, 1H, Ar_{Ind}), 7.14 (d, J = 7.7 Hz, 2H, *meta*-H Ar_{IPr}), 7.10 (d, J = 7.7 Hz, 2H, *meta*-H Ar_{IPr}), 6.64 (s, 2H, HCCH), 6.56 (t, J = 3.2 Hz, 1H, Cp_{Ind}), 5.97 (br, 1H, Cp_{Ind}), 5.90 (br, 1H, Cp_{Ind}), 3.38 (sept, J = 6.8 Hz, 2H, (CH₃)₂CH), 3.01 (sept, J = 6.8 Hz, 2H, (CH₃)₂CH), 2.31 (d, J = 3.2 Hz, 1H, CH₂ allyl), 2.13 (s, 1H, CH₂ allyl), 1.50 (s, 1H, CH₂ allyl), 1.30 (d, J = 6.8 Hz, 6H, (CH₃)₂CH), 1.21 (d, J = 6.7 Hz, 6H, (CH₃)₂CH), 1.05 (d, J = 6.8 Hz, 6H, (CH₃)₂CH), 1.01 (d, J = 6.8 Hz, 6H, (CH₃)₂CH), 1.00 (s, 3H, CH₃ allyl), 0.95 (d, J = 2.8 Hz, 1H, CH₂ allyl), one Ar_{Ind} peak is coincidental with solvent. ¹³C{¹H} NMR (C₆D₆, 75 MHz): 191.8, 146.4, 146.2, 138.6, 137.8, 130.5, 124.8, 124.6, 124.5, 121.2, 120.1, 119.9, 78.5, 51.3, 29.3, 29.2, 26.7, 25.9, 23.8, 23.2, 23.1, 1.77.

(η^1 -Ind)(η^5 -Cp)Pd(IPr) (^{IndCp}Pd)

^{IndCl}Pd (0.050 g, 0.077 mmol) was dissolved in 3 mL of THF and the solution was cooled to 0°C. A solution of sodium cyclopentadienyl (0.038 mL of a 2 M THF solution, 0.077 mmol) was added dropwise with stirring and the resulting solution stirred at 0°C for 90 minutes. The solvent was removed under reduced pressure and the residue extracted twice with 5 mL portions of pentane. The solvent from the combined extracts was removed under vacuum to give ^{IndCp}Pd as an orange solid. Yield: 0.040 g, 71%.

Anal. Calcd (found) for $C_{41}H_{49}N_2Pd$: C, 72.82 (73.09); H, 7.30 (7.11); N, 4.14 (4.13). 1H NMR (C_6D_6 , 400 MHz): 7.53 (d, $J = 7.1$ Hz, 1H, Ar_{Ind}), 7.26 (t, $J = 7.7$ Hz, 2H, *para-H* Ar_{IPr}), 7.20-7.11 (m, 6H, Ar_{Ind} and Ar_{IPr}), 6.89 (d, $J = 7.2$ Hz, 1H, Ar_{Ind}), 6.74 (br, 1H, Cp_{Ind}), 6.56 (s, 2H, *HCCCH*), 6.40 (m, 1H, Cp_{Ind}), 4.63 (s, 5H, *Cp*), 4.54 (br, 1H, Cp_{Ind}), 3.19 (sept, $J = 6.8$ Hz, 2H, $(CH_3)_2CH$), 3.06 (sept, $J = 6.8$ Hz, 2H, $(CH_3)_2CH$), 1.32 (d, $J = 7.0$ Hz, 6H, $(CH_3)_2CH$), 1.25 (d, $J = 6.8$ Hz, 6H, $(CH_3)_2CH$), 1.01 (d, $J = 7.0$ Hz, 6H, $(CH_3)_2CH$), 0.99 (d, $J = 7.0$ Hz, 6H, $(CH_3)_2CH$). $^{13}C\{^1H\}$ NMR (C_6D_6 , 75 MHz): 181.5, 146.5, 146.3, 141.8, 137.8, 130.6, 124.9, 124.8, 124.6, 124.2, 122.9, 121.9, 121.1, 118.1, 99.2, 34.9, 29.4, 26.3, 22.8, 23.0, 14.6.

$(\eta^1-Ind)(\eta^5-Cp)Ni(IPr)$ ($^{IndCp}Ni$)

$(\eta^5-Cp)Ni(IPr)Cl$ (0.050 g, 0.091 mmol) was dissolved in 2 mL THF and cooled to $-40^\circ C$. Lithium indenyl (0.0012 g, 0.100 mmol) in 1 mL THF was added dropwise with stirring. The solution was allowed to warm to room temperature over one hour and stirred for an additional two hours at room temperature. The solvent was removed under vacuum and the residue extracted twice with 5 mL portions of pentane to give a red solution. The solvent was removed from the combined extracts to give $^{IndCp}Ni$ as a red solid. Yield: 0.045g, 75%.

Anal. Calcd (found) for $C_{41}H_{49}N_2Ni$: C, 78.35 (78.07); H, 7.86 (8.01); N, 4.46 (4.47). 1H NMR (C_6D_6 , 500 MHz): 7.51 (d, $J = 7.2$ Hz, 1H, Ar_{Ind}), 7.30 (t, $J = 7.7$ Hz, 3H, Ar_{Ind} and *para-H* Ar_{IPr}), 7.21-7.19 (m, 5H, Ar_{Ind} and *meta-H* Ar_{IPr}), 6.79 (m, 2H, Ar_{Ind} and Cp_{Ind}), 6.56 (t, $J = 3.3$ Hz, 1H, Cp_{Ind}), 6.55 (m, 1H, Cp_{Ind}), 6.52 (s, 2H, *HCCCH*), 4.17 (s, 5H, *Cp*), 3.82 (br, 1H, Cp_{Ind}), 3.43 (br, 2H, $(CH_3)_2CH$), 3.08 (br, 2H, $(CH_3)_2CH$), 1.38 (d, $J = 6.5$ Hz, 6H, $(CH_3)_2CH$), 1.20 (d, $J = 6.5$ Hz, 6H, $(CH_3)_2CH$), 0.98 (d, $J = 6.8$ Hz, 12H, $(CH_3)_2CH$). $^{13}C\{^1H\}$ NMR (C_6D_6 , 126 MHz): 184.0, 158.9, 146.5, 146.4, 146.2, 146.0, 142.3, 138.3, 138.1, 130.6, 130.5, 125.4, 124.7, 124.1, 122.2, 121.6, 120.9, 120.0, 117.1, 97.5, 34.7, 29.4, 26.3, 26.1, 22.8, 19.8.

$(\eta^3\text{-Ind})(\eta^1\text{-Ind})\text{Pd}(\text{IPr})$ ($^{\text{IndInd}}\text{Pd}$)

$^{\text{IndCl}}\text{Pd}$ (0.018 g, 0.028 mmol) was dissolved in 5 mL of diethyl ether at -35°C . The solution was added to lithium indenyl (0.003 g, 0.028 mmol) in 5 mL diethyl ether at -35°C and stirred at this temperature for 20 minutes to give a cloudy, dark pink solution. The precipitate was removed by quickly filtering the mixture through a celite plug. The solvent was removed from the filtrate under reduced pressure to give $^{\text{IndInd}}\text{Pd}$ as dark pink solid. Due to the thermal instability of this compound elemental analysis was not performed, nor was a ^{13}C NMR spectrum recorded. X-ray quality crystals were grown in a concentrated solution of diethyl ether at -35°C . Yield: 0.016 g, 80%.

^1H NMR (d_8 -toluene, -40°C , 500 MHz): 7.78 (d, $J = 6.8$ Hz, 1H, Ar_{Ind}), 7.47 (t, $J = 7.7$ Hz, 1H, Ar_{Ind}), 7.34 (t, $J = 7.7$ Hz, 1H, Ar_{Ind}), 6.86 (d, $J = 4.8$ Hz, 1H, Ar_{Ind}), 6.71 (t, $J = 7.4$ Hz, 1H, Ar_{Ind}), 6.61 (m, 2H, Ar_{Ind}), 6.35 (d, $J = 6.61$ Hz, 1H, Ar_{Ind}), 6.30 (s, 1H, HCCH), 6.22 (t, $J = 3$ Hz, 1H, Cp_{Ind}), 6.13 (t, $J = 3$ Hz, 1H, Cp_{Ind}), 6.06 (br, 1H, Cp_{Ind}), 5.69 (d, $J = 7.6$ Hz, 1H, Cp_{Ind}), 4.94 (br, 1H, Cp_{Ind}), 4.54 (br, 1H, Cp_{Ind}), 3.01 (br, 4H, $(\text{CH}_3)_2\text{CH}$), 0.94 (br, 24H, $(\text{CH}_3)_2\text{CH}$).

Reactivity Studies

General procedure for the reaction of Pd and Ni compounds with 2,6-lutidinium chloride

A solution of 2,6-lutidinium hydrochloride (0.010g, 0.006 mmol) in 0.25 mL d_8 -toluene was added to a solution of the metal complex (0.006 mmol) in 0.25 mL d_8 -toluene at the desired temperature in an NMR tube. The solution was allowed to stand at the desired temperature for the specified time (see Table 5.01 for specific temperatures and reaction times). Quantitative formation of the known complexes $(\eta^3\text{-2-methylallyl})\text{Pd}(\text{IPr})\text{Cl}^{1b}$ and $(\eta^5\text{-Cp})\text{Pd}(\text{IPr})\text{Cl}^{61}$ was observed by ^1H NMR spectroscopy. $(\eta^5\text{-Cp})\text{Ni}(\text{IPr})\text{Cl}^{42}$ precipitated out of solution and was isolated by filtration and then identified using ^1H NMR spectroscopy.

Reaction between $^{\text{CpAll}}\text{Pd}$ and triphenylcarbenium chloride

Triphenylcarbenium chloride (0.002 g, 0.008 mmol) was added to a solution of $^{\text{CpAll}}\text{Pd}$ (0.005 g, 0.008 mmol) in toluene at -35°C in an NMR tube. The solution was allowed slowly to come to room temperature over three hours and left at room temperature for twenty-four hours. Quantitative conversion to $(\eta^3\text{-2-$

methylallyl)Pd(IPr)Cl⁶² and three non-isolable isomers of cyclopentadienyltriphenylmethane were observed by ¹H NMR spectroscopy.⁴⁷ Independent synthesis of cyclopentadienyltriphenylmethane through the reaction of sodium cyclopentadienyl with triphenylcarbenium chloride provided confirmation of product identity.

Reaction between Cp^{All}Ni and triphenylcarbenium chloride

Triphenylcarbenium chloride (0.002 g, 0.008 mmol) was added to a solution of Cp^{All}Ni (0.005 g, 0.008 mmol) in 0.5 mL C₆D₆ in an NMR tube. The mixture was allowed to stand at room temperature for 12 hours. The solvent was removed under reduced pressure and the residue dissolved in a minimal amount of chloroform and loaded onto a silica gel plug. Cp^{All}Ni was isolated as a bright pink solid (0.003 g, 0.005 mol) and identified by ¹H NMR spectroscopy.⁴² 2-methylallyltriphenylmethane was isolated as a white solid (0.002 g, 0.006 mol) and characterized by ¹H and ¹³C NMR spectroscopy. Yield: 0.002 g, 75%.

¹H NMR (CDCl₃, 400 MHz): 7.29-7.15 (m, 15H, *phenyl*), 4.66 (s, 1H, terminal allyl CH₂), 4.26 (s, 1H, terminal allyl CH₂), 3.37 (s, 2H, allyl CH₂), 1.42 (s, 3H, allyl CH₃). ¹³C{¹H} NMR (CDCl₃, 126 MHz): 147.3, 142.2, 130.6, 129.7, 127.7, 125.9, 115.9, 48.6, 25.6.

V. Acknowledgements

I am grateful to Dr. Wei Dai for the synthesis of ^{Ind}IndPd, to Dr. Mike Takase for X-ray crystallography, and to Dr. Damian Hruszkewycz and Matthew Chalkey for helpful discussions and synthetic insights.

VI. References

- 1) (a) Nakamura, H.; Iwama, H.; Yamamoto, Y. *J. Am. Chem. Soc.* **1996**, *118*, 6641; (b) Marion, N.; Navarro, O.; Mei, J.; Stevens, E. D.; Scott, N. M.; Nolan, S. P. *J. Am. Chem. Soc.* **2006**, *128*, 4101.
- 2) (a) Chartoire, A.; Lesieur, M.; Falivene, L.; Slawin, A. M. Z.; Cavallo, L.; Cazin, C. S. J.; Nolan, S. P. *Chem. Eur. J.* **2012**, *18*, 4517; (b) Fortman, G. C.; Nolan, S. P. *Chem. Soc. Rev.* **2011**, *40*, 5151; (c) Iglesias, M. J.; Prieto, A.; Nicasio, M. C. *Adv. Synth. Catal.* **2010**, *352*, 1949.

- 3) (a) Akermark, B.; Zetterberg, K. *Tetrahedron Lett.* **1975**, 3733; (b) Baker, R. *Chem. Rev.* **1973**, *73*, 487; (c) Trost, B. M. *Tetrahedron* **1977**, *33*, 2615.
- 4) Kurosawa, H.; Urabe, A. *Chem. Lett.* **1985**, 1839.
- 5) (a) Wu, J.; Green, J. C.; Hazari, N.; Hruszkewycz, D. P.; Incarvito, C. D.; Schmeier, T. J. *Organometallics* **2010**, *29*, 6369; (b) Wu, J.; Hazari, N.; Incarvito, C. D. *Organometallics* **2011**, *30*, 3142; (c) Johnson, M. T.; Johansson, R.; Kondrashov, M. V.; Steyl, G.; Ahlquist, M. S. G.; Roodt, A.; Wendt, O. F. *Organometallics* **2010**, *29*, 3521.
- 6) (a) Barczak, N. T.; Grote, R. E.; Jarvo, E. R. *Organometallics* **2007**, *26*, 4863; (b) Solin, N.; Kjellgren, J.; Szabo, K. J. *J. Am. Chem. Soc.* **2004**, *126*, 7026.
- 7) Solin, N.; Wallner, O. A.; Szabo, K. J. *Org. Lett.* **2005**, *7*, 689.
- 8) Tsuji, J.; Takahashi, H.; Morikawa, M. *Tetrahedron Lett.* **1965**, 4387.
- 9) (a) Szabo, K. J. *Chem. Eur. J.* **2000**, *6*, 4413; (b) Aranyos, A.; Szabo, K. J.; Castano, A. M.; Bäckvall, J.-E. *Organometallics* **1997**, *16*, 1058.
- 10) (a) Wu, J.; Hazari, N. *Chem. Commun.* **2011**, *47*, 1069; (b) Johansson, R.; Wendt, O. F. *Dalton Trans.* **2007**, 488; (c) Shi, M.; Nicholas, K. M. *J. Am. Chem. Soc.* **1997**, *119*, 5057.
- 11) Schmeier, T. J.; Hazari, N.; Incarvito, C. D.; Raskatov, J. A. *Chem. Commun.* **2011**, *47*, 1824.
- 12) (a) Hruszkewycz, D. P.; Wu, J.; Hazari, N.; Incarvito, C. D. *J. Am. Chem. Soc.* **2011**, *133*, 3280; (b) Hruszkewycz, D. P.; Wu, J.; Green, J. C.; Hazari, N.; Schmeier, T. J. *Organometallics* **2012**, *31*, 470.
- 13) Crabtree, R. H. *The Organometallic Chemistry of the Transition Metals*; 4th ed.; John Wiley & Sons: Hoboken, N.J., 2005.
- 14) (a) O'Connor, J. M.; Casey, C. P. *Chem. Rev.* **1987**, *87*, 307; (b) Zargarian, D. *Coord. Chem. Rev.* **2002**, *233-234*, 157.
- 15) (a) Werner, H.; Kuhn, A. *Angew. Chem., Int. Ed.* **1979**, *18*, 416; (b) Werner, H.; Kuhn, A.; Burschka, C. *Chem. Ber.* **1980**, *113*, 2291; (c) Lehmkuhl, H.; Danowski, F.; Benn, R.; Mynott, R.; Schroth, G. *Chem. Ber.* **1986**, *119*, 2542; (d) Lehmkuhl, H.; Naydowski, C.; Danowski, F.; Bellenbaum, M.; Benn, R.; Ruffńska, A.; Schroth, G.; Mynott, R.; Pasynkiewicz, S. *Chem. Ber.* **1984**, *117*, 3231; (e) Tune, D. J.; Werner, H. *Helv. Chim. Acta* **1975**, *58*, 2240.
- 16) Werner, H. *Adv. Organomet. Chem.* **1981**, *19*, 155.

- 17) (a) Werner, H.; Kraus, H. J. *Angew. Chem., Int. Ed.* **1979**, *18*, 948; (b) Werner, H.; Kraus, H. J.; Schubert, U.; Ackermann, K.; Hofmann, P. *J. Organomet. Chem.* **1983**, *250*, 517.
- 18) Werlé, C.; Hamdaoui, M.; Bailly, C.; Le Goff, X.-F.; Brelot, L.; Djukic, J.-P. *J. Am. Chem. Soc.* **2013**, *135*, 1715.
- 19) Arduengo, A. J., III; Harlow, R. L.; Kline, M. *J. Am. Chem. Soc.* **1991**, *113*, 361.
- 20) Bielinski, E. A.; Dai, W.; Guard, L. M.; Hazari, N.; Takase, M. K. *Organometallics* **2013**, *32*, 4025.
- 21) Dai, W.; Chalkley, M. J.; Brudvig, G. W.; Hazari, N.; Melvin, P. R.; Pokhrel, R.; Takese, M. K. *Organometallics* **2013**, *32*, 5114.
- 22) Sergeev, N. M. *Prog. Nucl. Magn. Reson. Spectrosc.* **1975**, *9*, 71.
- 23) (a) Jordan, M.; Saak, W.; Haase, D.; Beckhaus, R. *Eur. J. Inorg. Chem.* **2007**, 5168; (b) Huttner, G.; Brintzinger, H. H.; Bell, L. G.; Friedrich, P.; Bejenke, V.; Neugebauer, D. *J. Organomet. Chem.* **1978**, *145*, 329; (c) Kowaleski, R. M.; Rheingold, A. L.; Trogler, W. C.; Basolo, F. *J. Am. Chem. Soc.* **1986**, *108*, 2460.
- 24) (a) Scrivanti, A.; Carturan, G.; Crociani, B. *Organometallics* **1983**, *2*, 1612; (b) Carmona, E.; Palma, P.; Poveda, M. L. *Polyhedron* **1990**, *9*, 757; (c) Chernyshova, E. S.; Goddard, R.; Poerschke, K.-R. *Organometallics* **2007**, *26*, 3236; (d) Filipuzzi, S.; Pregosin, P. S.; Albinati, A.; Rizzato, S. *Organometallics* **2008**, *27*, 437.
- 25) Farrugia, L. J. *J. Appl. Crystallogr.*, *45*, 849.
- 26) Lehmkuhl, H.; Naeser, J.; Mehler, G.; Keil, T.; Danowski, F.; Benn, R.; Mynott, R.; Schroth, G.; Krueger, C.; Betz, P. *Chem. Ber.* **1991**, *124*, 441.
- 27) Luca, O. R.; Thompson, B. A.; Takase, M. K.; Crabtree, R. H. *J. Organomet. Chem.* **2013**, *730*, 79.
- 28) Holland, P. L.; Smith, M. E.; Andersen, R. A.; Bergman, R. G. *J. Am. Chem. Soc.* **1997**, *119*, 12815.
- 29) Abernethy, C. D.; Clyburne, J. A. C.; Cowley, A. H.; Jones, R. A. *J. Am. Chem. Soc.* **1999**, *121*, 2329.
- 30) Jin, Z.; Gu, X.-P.; Qiu, L.-L.; Wu, G.-P.; Song, H.-B.; Fang, J.-X. *J. Organomet. Chem.* **2011**, *696*, 859.
- 31) Schaub, T.; Backes, M.; Radius, U. *Eur. J. Inorg. Chem.* **2008**, 2680.
- 32) Liu, Z.-h.; Xu, Y.-C.; Xie, L.-Z.; Sun, H.-M.; Shen, Q.; Zhang, Y. *Dalton Trans.* **2011**, *40*, 4697.
- 33) Huber, T. A.; Belanger-Gariepy, F.; Zargarian, D. *Organometallics* **1995**, *14*, 4997.

- 34) Baker, R. T.; Tulip, T. H. *Organometallics* **1986**, *5*, 839.
- 35) Westcott, S. A.; Kakkar, A. K.; Stringer, G.; Taylor, N. J.; Marder, T. B. *J. Organomet. Chem.* **1990**, *394*, 777.
- 36) (a) Sui-Seng, C.; Enright, G. D.; Zargarian, D. *Organometallics* **2004**, *23*, 10; (b) Groux, L. F.; Belanger-Gariepy, F.; Zargarian, D.; Vollmerhaus, R. *Organometallics* **2000**, *19*, 1507.
- 37) Calhorda, M. J.; Veiros, L. F. *Coord. Chem. Rev.* **1999**, *185-186*, 14.
- 38) Xie, L.-Z.; Sun, H.-M.; Hu, D.-M.; Liu, Z.-H.; Shen, Q.; Zhang, Y. *Polyhedron* **2009**, *28*, 2585.
- 39) Koehler, F. H. *Chem. Ber.* **1974**, *107*, 570.
- 40) Dible, B. R.; Sigman, M. S. *J. Am. Chem. Soc.* **2003**, *125*, 872.
- 41) O'Hare, D. *Organometallics* **1987**, *6*, 1766.
- 42) Cooke, J.; Lightbody, O. C. *J. Chem. Educ.* **2011**, *88*, 88.
- 43) Fontaine, F.-G.; Dubois, M.-A.; Zargarian, D. *Organometallics* **2001**, *20*, 5156.
- 44) (a) Solin, N.; Kjellgren, J.; Szabo, K. J. *Angew. Chem., Int. Ed.* **2003**, *42*, 3656; (b) Szabo, K. J. *Chem. Eur. J.* **2004**, *10*, 5268.
- 45) (a) Baya, M.; Crochet, P.; Esteruelas, M. A.; Onate, E. *Organometallics* **2001**, *20*, 240; (b) Kerber, R. C.; Garcia, R.; Nobre, A. L. *Organometallics* **1996**, *15*, 5756.
- 46) Semproni, S. P.; Graham, P. M.; Buschhaus, M. S. A.; Patrick, B. O.; Legzdins, P. *Organometallics* **2009**, *28*, 4480.
- 47) Werner, H.; Mattmann, G.; Salzer, A.; Winkler, T. *J. Organomet. Chem.* **1970**, *25*, 461.
- 48) Meurling, L. *Acta Chem Scand B* **1974**, *28*, 295.
- 49) Navarro, R. M.; Pena, M. A.; Fierro, J. L. *Chem. Rev.* **2007**, *107*, 3952.
- 50) Tatsuno, Y.; Yoshida, T.; Seiyotsuka; Al-Salem, N.; Shaw, B. L. *Inorg. Synth.* **1991**, *19*, 220.
- 51) Arduengo III, A. J.; Krafczyk, R.; Schmutzler, R.; Craig, H. A.; Goerlich, J. R.; Marshall, W. J.; Unverzagt, M. *Tetrahedron* **1999**, *55*, 14523.
- 52) O'Brien, S.; Fishwick, M.; McDermott, B.; Wallbridge, M. G. H.; Wright, G. A. *Inorg. Synth.* **1971**, *13*, 73.
- 53) Panda, T. K.; Gamer, M. T.; Roesky, P. W. *Organometallics* **2003**, *22*, 877.
- 54) Nakasuji, K.; Yamaguchi, M.; Murata, I.; Tatsumi, K.; Nakamura, A. *Organometallics* **1984**, *3*, 1257.

- 55) Christopher, J. N.; Diamond, G. M.; Jordan, R. F.; Petersen, J. L. *Organometallics* **1996**, *15*, 4038.
- 56) Grönberg, K. L. C.; Henderson, R. A.; Oglieve, K. E. *Dalton Trans.* **1998**, 3093.
- 57) Sheldrick, G. M. *Acta Crystallogr. Sect. A* **1990**, *A 46*, 467.
- 58) Sheldrick, G. M. *Acta Crystallogr. Sect. A* **2008**, *A64*, 112.
- 59) Müller, P. *Crystallogr. Rev.* **2009**, *15*, 57.
- 60) Lehmkuhl, H.; Rufinska, A.; Mehler, K.; Benn, R.; Schroth, G. *Liebigs Ann.* **1980**, 744.
- 61) Jin, Z.; Guo, S.-X.; Gu, X.-P.; Qiu, L.-L.; Song, H.-B.; Fang, J.-X. *Adv. Synth. Catal.* **2009**, *351*, 1575.
- 62) Navarro, O.; Oonishi, Y.; Kelly, R. A.; Stevens, E. D.; Briel, O.; Nolan, S. P. *J. Organomet. Chem.* **2004**, *689*, 3722.